WIDE-FIELD IMAGING FROM SPACE

PROCEEDINGS OF THE CONFERENCE HELD AT LAWRENCE BERKELEY NATIONAL LABORATORY, BERKELEY, CA, 16–18 MAY 2004

edited by

Tim McKAY
Andrew FRUCHTER

ELSEVIER

Amsterdam • Boston • Jena • London • New York • Oxford • Paris • Philadelphia • San Diego • St Louis

ISSN 1387-6473

New Astronomy Reviews

Editors

Jean Audouze
Institut d'Astrophysique, Paris

Alfonso G. Cavaliere
Università di Roma "Tor Vergata"

Philip A. Charles
South African Astronomical Observatory

Peter S. Conti
University of Colorado

Jack J. Lissauer
NASA Ames Research Center

Ken'ichi Nomoto
University of Tokyo

Ralph A.M.J. Wijers
University of Amsterdam

Also available on
SCIENCE DIRECT®
www.sciencedirect.com

http://www.elsevier.com/locate/newastrev

Volume 49, Numbers 7–9, November 2005

Wide Field Imaging from Space
editors: T. McKay, A. Fruchter

Available online at www.sciencedirect.com
SCIENCE DIRECT®
New Astronomy Reviews 49 (2005) v–vi
New Astronomy Reviews
www.elsevier.com/locate/newastrev

Contents

Volume 49, Numbers 7–9, November 2005

A.S. Fruchter
An introduction to a conference and a field 335

D.H. Weinberg
Dark energy: The observational challenge 337

G. Aldering
Exploring dark energy with SNAP 346

T.R. Lauer
DESTINY: The dark energy space telescope 354

D.J. Eisenstein
Dark energy and cosmic sound 360

R.S. Somerville
Why we need wide-field imaging from space to understand galaxy formation 366

K. Glazebrook, I. Baldry, W. Moos, J. Kruk and S. McCandliss
Monster redshift surveys through dispersive slitless imaging: The Baryon Oscillation Probe 374

D.W. Hogg
Galaxy evolution with future wide-field space missions 379

P. Marshall, R. Blandford and M. Sako
The SNAP strong lens survey 387

C. Heymans, M.L. Brown, M. Barden, J. Caldwell, B. Häußler, K. Jahnke, H.-W. Rix, S. Beckwith, E.F. Bell, A. Borch, S. Jogee, D.H. McIntosh, K. Meisenheimer, C. Peng, S. Sánchez, R. Somerville, A.N. Taylor, L. Wisotzki and C. Wolf
Weak lensing studies from space with GEMS 392

K. Stapelfeldt, C. Beichman and M. Kuchner
General astrophysics with the optical terrestrial planet finder mission 396

doi:10.1016/S1387-6473(05)00140-5

P.G. van Dokkum
Observing cluster galaxies and their progenitors with JDEM 400

E.L. Wright
The infrared sky 407

S.E. Zepf
Wide-field imaging from space of early-type galaxies and their globular clusters 413

W. Zheng
Probing the universe at redshift 10 and beyond 417

L. Yan
Spitzer 24 μm observations of optical/near-IR selected extremely red galaxies: Evidence for assembly of massive galaxies at $z\sim$1–2? 420

A. Gould
Microlensing search for planets 424

W.N. Brandt
X-ray surveys and wide-field optical/near-infrared imaging with JDEM 430

J.E. Grindlay
EXIST: All-sky hard X-ray imaging and spectral–temporal survey for black holes 436

M. Giavalisco
Lessons from the GOODS 440

H.J. Newberg
Galactic structure from wide-field surveys 447

E.D. Skillman
Star formation histories in local group dwarf galaxies 453

A.M. Koekemoer and N.Z. Scoville
The COSMOS 2-degree HST/ACS survey 461

R.M. Rich
Wide field imaging from space: Galaxy formation from nearby stellar populations 465

T.M. Brown
Star formation histories in the Local Group 474

G. Basri, W.J. Borucki and D. Koch
The Kepler Mission: A wide-field transit search for terrestrial planets 478

Available online at www.sciencedirect.com
SCIENCE DIRECT®
New Astronomy Reviews 49 (2005) 335–336
New Astronomy Reviews
www.elsevier.com/locate/newastrev

An introduction to a conference and a field

Abstract

An introduction to the conference is presented. Some of the opportunities and difficulties for the future of wide-field imaging from space are discussed.
© 2005 Published by Elsevier B.V.

Keywords: Wide-field imaging; Space-based imaging; Space telescope

Astrophysical conferences have many purposes. They may celebrate and review the achievements of a rapidly expanding scientific field. They can spur collaborations. Some of the best produce new syntheses of scientific ideas. But this conference, if successful, may help create and direct a new field.

There is much to be gained from wide-field instruments in space. However, space-based optical and near-infrared imagers have generally had narrow fields of view – primarily because the detectors and data handling required for larger fields exceeded the available technology. Yet this is changing. A number of instruments now in design and development, typically for specific scientific goals, may have the capability to also serve as wide-field imagers in space. This would, however, require the community to reserve part of their operations for general science, as opposed to the more targeted original goals of these programs. In this conference, we hope to explore the science that a wide-field imager could do, and thus better inform discussions over whether it would indeed be worthwhile to either dedicate time on otherwise targeted missions to general surveys, or perhaps start a mission dedicated solely to general-purpose wide-field imaging.

The SNAP satellite – discussed later in this conference by Greg Aldering – would be capable of imaging a substantial fraction of M31 in a single pointing. Could this instrument, proposed and most likely largely funded for another purpose (the Joint Dark Energy Mission, JDEM, of NASA and DOE), provide the astronomical community with a powerful new means of obtaining wide-field images from space? If so, are there small modifications to the basic design that could substantially enlarge its impact as a general service instrument without compromising its ability to perform as a dark energy experiment?

Or does the field have a different DESTINY (see Tod Lauer's talk)? Would a wide-field instrument whose sole filters were grisms provide a large variety of ancillary science, or would the addition of pass-band filters be strongly desired by the community (if not required for the main mission)? Would the lack of optical detectors further substantially reduce the science that might be done, or would the wide-field near-IR grism capability prove strongly attractive to the astronomical community?

1387-6473/$ - see front matter © 2005 Published by Elsevier B.V.
doi:10.1016/j.newar.2005.08.001

Finally, could the Terrestrial Planet Finder find a place in wide-field imaging surveys? Might an ancillary off-axis instrument on this new probe allow some astronomers to survey large-fields while their colleagues hunt for planets? Will the optical requirements of the primary mission allow a sufficiently wide field to satisfy many astronomers? Might a TPF and a JDEM function in happy symbiosis, with the former providing a moderately wide-field with excellent resolution, and the latter providing an extremely large field with somewhat more limited resolution?

Or, will a wide-field imager result from the now nascent Origins Probe program?

While it is clear this is a time of great intellectual and technological ferment, it is also a time of danger for the field. JDEM has virtually no funding in the NASA budget. TPF has advanced outside the standard NASA mechanisms and reviews. And perhaps most importantly the NASA science program is itself in crisis.

There is a claim much beloved by self-help gurus that in ancient Chinese the two characters that combine to produce the word "crisis" can be separately translated as "danger" and "opportunity". Although I do not speak Chinese, a bit of research into this subject suggests that the better translation of the character pair might be "danger, danger".

Nonetheless in this crisis there is certainly opportunity. The technology for a wide-field imager in space appears feasible. There are several (largely unfunded) missions in the queue capable of producing wide-field science. And the very turmoil that threatens space science may allow new ideas to move to the fore. It should therefore be our goal to evaluate the science that a wide-field imager in space might do, and if we find it compelling, as I believe a reader of these proceedings will, then we must seize this opportunity. If we do our work well, we can hope that this conference and its proceedings will be remembered as an introduction to a new field – wide-field imaging from space.

Andrew S. Fruchter
Space Telescope Science Institute
3700 San Martin Dr., Balitmore, MD 21218
United States
E-mail address: fruchter@stsci.edu

Available online 21 September 2005

Available online at www.sciencedirect.com
SCIENCE DIRECT®
New Astronomy Reviews 49 (2005) 337–345
New Astronomy Reviews
www.elsevier.com/locate/newastrev

Dark energy: The observational challenge

David H. Weinberg

Department of Astronomy, Ohio State University, Columbus, OH 43210, United States

Available online 5 October 2005

Abstract

Nearly all proposed tests for the nature of dark energy measure some combination of four fundamental observables: the Hubble parameter $H(z)$, the distance-redshift relation $d(z)$, the age-redshift relation $t(z)$, or the linear growth factor $D_1(z)$. I discuss the sensitivity of these observables to the value and redshift history of the equation of state parameter w, emphasizing where these different observables are and are not complementary. Demonstrating time-variability of w is difficult in most cases because dark energy is dynamically insignificant at high redshift. Time-variability in which dark energy tracks the matter density at high redshift and changes to a cosmological constant at low redshift is *relatively* easy to detect. However, even a sharp transition of this sort at $z_c = 1$ produces only percent-level differences in $d(z)$ or $D_1(z)$ over the redshift range $0.4 \leqslant z \leqslant 1.8$, relative to the closest constant-w model. Estimates of $D_1(z)$ or $H(z)$ at higher redshift, potentially achievable with the Lyα forest, galaxy redshift surveys, and the CMB power spectrum, can add substantial leverage on such models, given precise distance constraints at $z < 2$. The most promising routes to obtaining sub-percent precision on dark energy observables are space-based studies of Type Ia supernovae, which measure $d(z)$ directly, and of weak gravitational lensing, which is sensitive to $d(z)$, $D_1(z)$, and $H(z)$.
© 2005 Elsevier B.V. All rights reserved.

Contents

1. Introduction . . . 338
2. Constraining dark energy . . . 339
3. Considerations for a space-based dark energy experiment . . . 344
Acknowledgments . . . 345
References . . . 345

E-mail address: dhw@astronomy.ohio-state.edu.

1387-6473/$ - see front matter © 2005 Elsevier B.V. All rights reserved.
doi:10.1016/j.newar.2005.08.003

1. Introduction

The acceleration of the universe should come as a surprise to anyone who has ever thrown a ball into the air and watched it fall back to earth. What goes up must come down. Gravity sucks.

Repulsive gravity is possible in General Relativity, but it requires the energy density of the universe to be dominated by a substance with an exotic equation of state, having negative pressure $p < -\rho c^2/3$. Alternatively, one can modify GR itself, so that cosmic acceleration arises even with "normal" gravitating components like pressureless matter and radiation. In this article I will adopt the language of "dark energy" solutions in which GR is preserved and a new component drives acceleration, but at present I think that a modification of the theory of gravity must be considered almost equally plausible.

Given the theoretical difficulty of explaining cosmic acceleration, it is worth emphasizing that the observational evidence for it is impressively robust. The results of the high-redshift supernova campaigns published in the late 1990s (Riess et al., 1998; Perlmutter et al., 1999) provided the first direct evidence for acceleration, but they were accepted quickly in part because studies of large scale structure and CMB anisotropies already argued indirectly in favor of a cosmological constant (e.g., Efstathiou et al., 1990; Krauss and Turner, 1995; Ostriker and Steinhardt, 1995). The supernova evidence has become much stronger on its own terms (Riess et al., 2004), and measurements of the first acoustic peak in the CMB power spectrum (de Bernardis et al., 2000; Hanany et al., 2000; Bennett et al., 2003) greatly strengthen the overall case for dark energy by showing that the *total* energy density of the universe is close to critical. This rules out the nearly empty open models that might otherwise be marginally compatible with the supernova data, and in combination with dynamical evidence for a low density of clustered matter ($\Omega_m \sim 0.2-0.4$), it demonstrates that there must be some additional entry in the cosmic energy budget. Unless this new component has negative pressure, the inferred ages of globular cluster stars conflict with the most convincing recent estimates of the Hubble constant (Freedman et al., 2001). We thus have three largely independent lines of argument for dark energy: the supernova Hubble diagram, the dynamical evidence for low matter density, and the age of the universe. In addition, we have the astonishing success of the inflationary cold dark matter paradigm in explaining high-precision measurements of CMB anisotropy, galaxy clustering, the Lyα forest, gravitational lensing, and other phenomena (see Seljak et al., 2004 for an up-to-date discussion), a success that vanishes if there is no dark energy component.

From a theoretical point of view, there are three different aspects of the dark energy puzzle. The first is the "old" cosmological constant problem: a naive application of quantum field theory suggests that the energy density associated with vacuum zero-point fluctuations should be of order one Planck mass per cubic Planck length, which exceeds the observational bound by $\sim$120 orders of magnitude. Since the only natural number that is $\sim 10^{-120}$ is zero, it is usually assumed that a correct calculation will someday show that the true value of the fundamental vacuum energy is exactly zero or vanishingly small. This leaves us with the second problem: what *is* causing the universe to accelerate? Finally, there is the coincidence problem: why is the dark energy density comparable to the matter density today, when most models predict that they were very different in the past and will be very different in the future?

Faced with these conundra, theorists have proposed an impressive variety of possible solutions. The most common class introduces a new energy component, typically a scalar field, and associates dark energy with the field's potential energy or kinetic degrees of freedom. These solutions do not address the "old" cosmological constant problem, so some other mechanism must set the fundamental vacuum energy to zero. Alternatively, the dark energy really could be the fundamental vacuum energy, and it has its remarkably small value as a consequence of not-yet-understood aspects of quantum gravity, or because it varies widely throughout an inflationary "multiverse" and anthropic selection restricts life to regions where it is small enough to allow structure formation (Weinberg, 1987; Efstathiou, 1995; Garriga and Vilenkin, 2000), or because gravitational back

reaction causes it to oscillate in time producing alternating phases of acceleration and deceleration (Brandenberger and Mazumdar, 2004). Finally, there is the possibility that GR itself must be modified, perhaps pointing the way to extra spatial dimensions or testable consequences of string theory. No matter what, the existence of cosmic acceleration implies a fundamental revision to our understanding of the cosmic energy contents, or particle physics, or gravity, or all of the above. The combination of theoretical importance and observational difficulty make the dark energy problem a worthy science driver for an ambitious wide field imaging mission in space.

2. Constraining dark energy

If dark energy is not a simple cosmological constant, then it is generically expected to have spatial inhomogeneities that affect CMB anisotropies and large scale structure. However, unless we are lucky (i.e., dark energy properties are just what is required to produce large inhomogeneities), these effects are too weak to detect in the face of cosmic variance. If cosmic acceleration is a consequence of modified gravity, then laboratory measurements or tests for intermediate-range forces could also turn up clues. But again, we would have to be lucky.

The only generic method of studying dark energy is to measure its influence on cosmic expansion history, described by the Friedmann equation

$$H(z) = H_0\left[\Omega_{\rm m}(1+z)^3 + \Omega_k(1+z)^2 + \Omega_\phi\frac{\rho_\phi(z)}{\rho_{\phi,0}}\right]^{1/2}. \tag{1}$$

Here the Ω_x refer to densities at the present day ($z=0$) in units of the critical density, and $\Omega_k \equiv 1-\Omega_{\rm m}-\Omega_\phi$. I have ignored the radiation term $\Omega_{\rm r}(1+z)^4$, which becomes important only at high redshifts. A "fluid" with equation of state $p = w\rho c^2$ has $\rho_\phi(z) = \rho_{\phi,0}(1+z)^{3(1+w)}$, so a true cosmological constant with $\rho_\phi(z) = \rho_{\phi,0}$ has $w=-1$. The effects of modified gravity solutions that change the Friedmann equation itself may be well approximated by a dark energy model with some $\rho_\phi(z)$, but perhaps not in all cases.

There have been many proposed tests of dark energy based on supernovae, radio galaxies, the virial masses, X-ray properties, or Sunyaev–Zel'dovich decrements of galaxy clusters, large scale structure traced by galaxies, clusters, or the Lyα forest, galaxy ages, or various aspects of strong or weak gravitational lensing (see Kujat et al., 2002 for an extensive but not exhaustive list). Nearly all of these tests depend on some combination of four fundamental observables: the Hubble parameter $H(z)$, the distance-redshift relation $d(z)$, the age-redshift relation $t(z)$, or the linear growth factor of mass fluctuations $D_1(z)$. The evolution of $H(z)$ is governed by the Friedmann Eq. (1). The comoving line-of-sight distance to an object at redshift z is

$$d(z) = \frac{c}{H_0}\int_0^z {\rm d}z'\,\frac{H_0}{H(z')}. \tag{2}$$

In a flat ($\Omega_k = 0$) universe, the angular diameter and luminosity distances measured with standard rulers or candles are related to $d(z)$ by cosmology-independent powers of $(1+z)$. In a curved universe, they are proportional instead to the transverse comoving distance,

$$d_{\rm M}(z) = \frac{c}{H_0}|\Omega_k|^{-1/2}S_k\left(|\Omega_k|^{1/2}\frac{H_0}{c}d(z)\right), \tag{3}$$

where $S_k(x) = \sin x$ or $\sinh x$ for $k = +1,\ -1$ (Hogg, 1999). The age of the universe at redshift z is

$$t(z) = \int_z^\infty \frac{{\rm d}z'}{(1+z')H(z')}. \tag{4}$$

The linear growth factor is the solution to the differential equation

$$\ddot{D}_1 + 2H(z)\dot{D}_1 - \frac{3}{2}\Omega_{\rm m}H_0^2(1+z)^3 D_1 = 0. \tag{5}$$

The solution can be written as a simple integral only for special values of w (including $w=-1$), but one can gain intuition using the approximation ${\rm d}\log D_1/{\rm d}\log a \equiv f(\Omega_{\rm m}) \approx \Omega_{\rm m}^{4/7}$, implying

$$\log D_1(z) = -\int_0^z \frac{{\rm d}z}{1+z}[\Omega_{\rm m}(z)]^{4/7}, \tag{6}$$

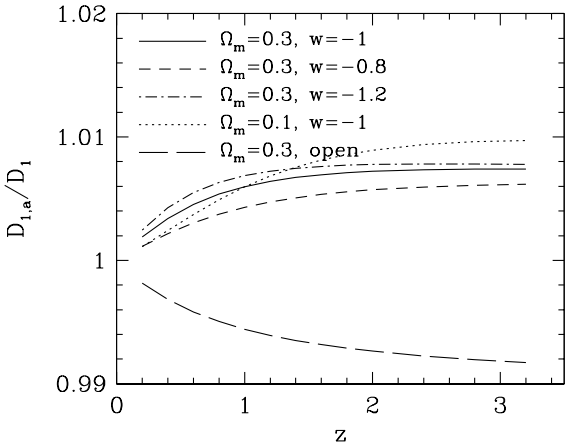

Fig. 1. Ratio of the approximate growth factor $D_1(z)$ calculated by Eq. (6) to the exact value for various combinations of Ω_m and w, including an open universe model with $\rho_\phi = 0$.

where $\Omega_m(z) = \Omega_m(1+z)^3/[\Omega_m(1+z)^3 + \Omega_k(1+z)^2 + \Omega_\phi\rho_\phi(z)/\rho_{\phi,0}]$ is the matter density parameter at redshift z. Here I have normalized $D_1(z=0) \equiv 1$ and used the index 4/7 that is accurate for $\Omega_m(z) \approx 1$ (Lightman and Schechter, 1990) instead of the value 0.6 that is more accurate for low Ω_m (Peebles, 1980). Fig. 1 shows that the approximation (6) is accurate to better than 1% for a wide range of models; the accuracy degrades to ~3% using $f(\Omega_m) = \Omega_m^{0.6}$.

The virtue of discussing dark energy tests in terms of these observables is that one can see whether and how different observational strategies complement each other. For example, Type Ia supernovae and other standard candle or standard ruler methods measure $d(z)$ directly, while the abundance of clusters as a function of redshift depends on both $D_1(z)$ and the volume element $dV \propto d^2(z)/H(z)$. Weak lensing observables depend on $D_1(z)$, $d(z)$, and $H(z)$, depending on just what properties (power spectrum, skewness, etc.) are measured. The Alcock and Paczyński anisotropy test (Alcock and Paczyński, 1979) measures the product $d(z)H(z)$.

Current observational evidence demonstrates that $\rho_\phi \neq 0$, and it is compatible with a model having $\Omega_m = 0.3$, $\Omega_\phi = 0.7$, $\Omega_k = 0$, and $w = -1$. To show that dark energy is not a cosmological constant, one must show that the data are incompatible with constant $\rho_\phi(z)$. To show that the equation of state parameter w is time-variable, one must show that the data are incompatible with $\rho_\phi(z) \propto (1+z)^n$ for any choice of n. Let us begin with the first, much less demanding problem, and make the further simplifying assumption that $\Omega_k = 0$. While CMB measurements provide a precise value of the angular diameter distance to the surface of last scattering, they do not demonstrate that $\Omega_k = 0$ at the level of precision of interest here (see, e.g., Tegmark et al., 2004), so exact spatial flatness is a theoretically motivated assumption rather than an observational constraint.

With these assumptions, the parameters to be constrained are w and $\Omega_m = 1 - \Omega_\phi$. The decelerating effect of matter is proportional to Ω_m, and the accelerating effect of dark energy is proportional to Ω_ϕ but also depends on the pressure-to-density ratio w. For any given redshift and observable, there is a contour in the Ω_m–w plane along which the value of the observable is constant. Fig. 2 shows such contours at $z = 0.5$, 1, 1.5, and 3 for the Hubble parameter $H(z)$, the distance $d(z)$, the linear growth factor $D_1(z)$, and the Alcock–Pacyzński (AP) parameter $H(z)d(z)$, assuming a fixed value of H_0. Error bars on the $z = 1$ curves show the impact of a 1% error on the corresponding observable. I have not included plots for $t(z)$ because I think it unlikely that the systematic errors on absolute age measurements can be brought low enough to teach us anything we do not already know about dark energy.

There are several lessons to be drawn from Fig. 2. First, interesting ($\Delta w \sim 0.1$) constraints on w typically require ~1–2% measurements at a given redshift, if Ω_m is known independently. Second, measurements of different observables, or of the same observable at different redshifts, can break the degeneracy between Ω_m and w. Combinations of $D_1(z)$ with $d(z)$ or $H(z)$ are especially useful in this regard, because Ω_m changes have opposite effects. Applications of the AP test at $z \sim 2$–3, which may be possible with the Lyα forest (Hui et al., 1999; McDonald and Miralda-Escudé, 1999; McDonald, 2001), would yield Ω_m constraints that are nearly independent of w, also helping to break degeneracies. The AP test is inde-

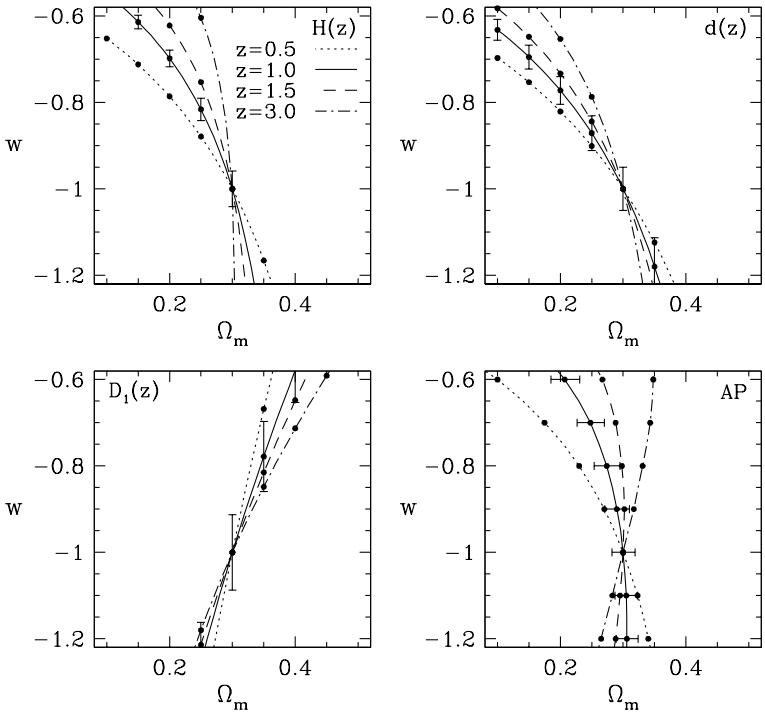

Fig. 2. Contours in the Ω_m–w plane along which the values of expansion history observables are constant, assuming $\Omega_k = 0$, constant w, and fixed H_0. The four line types correspond to four redshifts, as indicated. Error bars show the uncertainty in w or Ω_m associated with a $\pm 1\%$ uncertainty in the observable, at $z = 1$.

pendent of uncertainties in H_0, as are measurements of $d(z)$ that use candles or rulers calibrated in the local Hubble flow and measurements of $H(z)$ that compare a velocity scale measured at high redshift to a lengthscale measured from local galaxy redshift surveys. However, the CMB provides a standard ruler in absolute Mpc, so tests that use this standard ruler also require a precise determination of H_0 (see Hu, 2004 for an excellent discussion of this point).

Constraining w becomes substantially more difficult if we drop the assumption that $\Omega_k = 0$, since Ω_m and Ω_ϕ can now vary independently. Most error forecasting papers do not investigate this case in detail, and I have not done so myself. Curvature affects all observables through the $\Omega_k(1+z)^2$ term in the Friedmann equation, and it additionally affects the distance-redshift relation (and thus also the AP parameter) through geometrical effects. Thus, complementary studies using distance/AP measurements and growth factor/$H(z)$ measurements would be especially valuable for this case, as would precise independent measurements of Ω_m from large scale structure. The CMB determines the combination $\Omega_m h^2$ very well, but a tight CMB constraint on Ω_m again requires a precise measurement of H_0.

Demonstrating time-variation of w is in general very difficult. If the effective value of w is close to -1 today, as the observations imply, then the ratio of the matter density to the dark energy density scales as $\sim(1+z)^3$. Dark energy is therefore dynamically unimportant even at moderate redshift ($z \sim 2$), leaving little leverage to show that the scaling of $\rho_\phi(z)$ is *not* adequately described by a power law $(1+z)^n$ as expected for constant w. While quintessence models generically predict that w varies in time, the effects of that variation are much too weak to detect in typical cases (Kujat et al., 2002).

Fig. 3 illustrates examples from a class of models in which

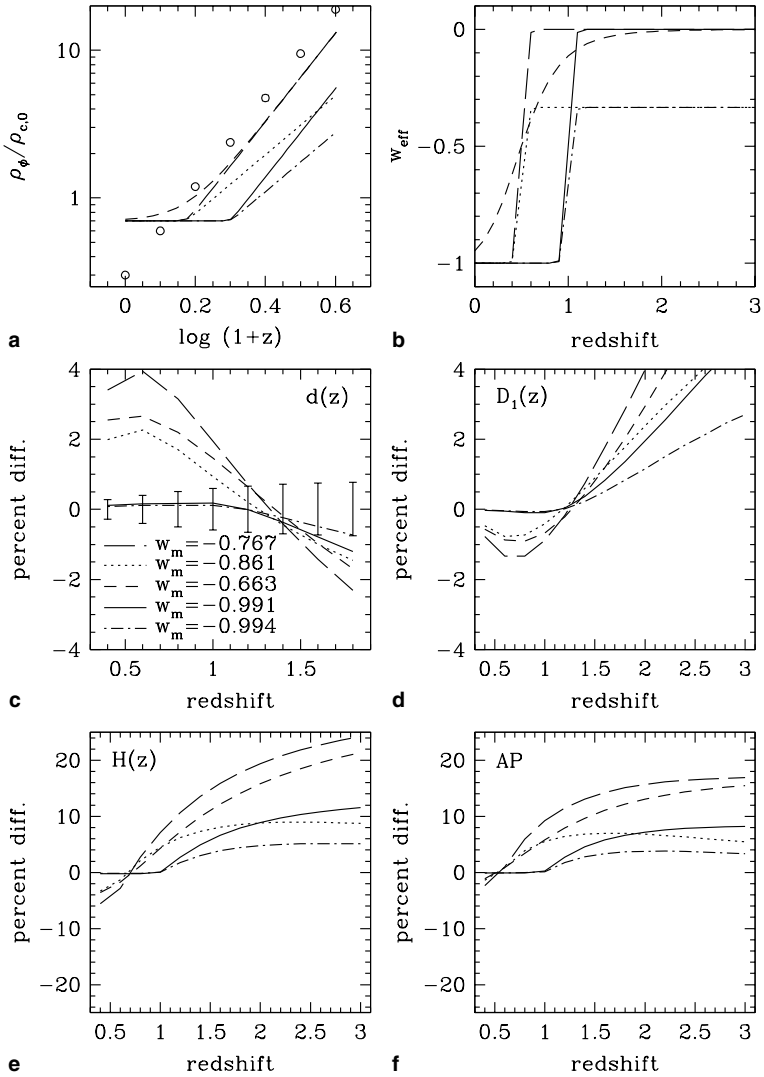

Fig. 3. Time-varying w models, with the parameterization of Eq. (7). Panels a and b show the evolution of $\rho_\phi(z)$ and $w_{\rm eff} \equiv \frac{1}{3}\mathrm{d}\log\rho_\phi/\mathrm{d}\log(1+z) - 1$ for five different parameter combinations. Circles in panel a show the matter density. Panel c plots the percentage difference between the time-variable model and the constant-w model that best matches its distance predictions over the range $0.4 \leqslant z \leqslant 1.8$. For reference, error bars show the percentage difference caused by changing $\Omega_{\rm m}$ by ± 0.01. Panels d–f show percentage differences in other observables relative to the same constant-w models. Note changes in horizontal and vertical axis scales.

$$\rho_\phi(z) = \rho_{\phi,0}(1+z)^n \left[1 + \left(\frac{1+z}{1+z_c}\right)^\alpha\right]^{(m-n)/\alpha}, \qquad (7)$$

so that $\rho_\phi \propto (1+z)^n$ at $z \ll z_{\rm c}$ and $\rho_\phi \propto (1+z)^m$ at $z \gg z_{\rm c}$. Kujat et al. (2002) considered a similar class of models, but the additional parameter α allows the transition in scaling behavior at $z_{\rm c}$ to be arbitrarily sharp, instead of necessarily occurring over an interval $\Delta z \sim z_{\rm c}$. Long-dashed lines show a model that I consider maximally optimistic from the point of view of detecting time variations of w: the energy scaling changes from $\rho_\phi \propto (1+z)^3$ to $\rho_\phi = \text{constant}$ at $z_{\rm c} = 0.5$, and the transition is nearly instantaneous. One can argue that $m = 3$ is a "natural" (or at least interesting) choice because a model in which ρ_ϕ scales like the matter

density during the matter dominated era has a better chance of solving the coincidence problem (Albrecht and Skordis, 2000; Doran et al., 2001). However, the low redshift and sharpness of the transition make it as easy as possible to detect, and there is no obvious reason that nature should be so kind to us. The short-dashed lines show a case with a smooth transition at $z_c = 0.5$, and solid lines show a sharp transition at $z_c = 1$. Dotted and dot-dashed lines show sharp transitions at $z_c = 0.5$ and 1, but with high-redshift energy scaling $\rho_\phi \propto (1+z)^2$ instead of $(1+z)^3$.

Fig. 3(c) shows the key result, focusing on the redshift range $z = 0.4-1.8$ where a space-based Type Ia supernova survey is likely to produce its tightest constraints. For each of the time-variable models, I have identified the constant-w model that most nearly matches its $d(z)$ relation, minimizing the summed absolute fractional differences over the range $0.4 \leqslant z \leqslant 1.8$. The quantity plotted is the percentage difference of $d(z)$ between the time-variable model and the "matched" constant-w model.

For the maximally optimistic model, the prospects look quite good. There is a 6% variation in distance between this model and the matched constant-w model, and a mission like SNAP or DESTINY could reasonably expect to measure such a variation at high significance. For a smooth transition (short-dashed line) or high-redshift scaling $m = 2$ (dotted line), the variation is $\sim$3%, still plausibly within reach. However, if the transition redshift is $z_c = 1$, then the maximum difference in distance is $\leqslant$1%, and this is reached only in the highest redshift bin.

Following Fig. 2, one might hope that measurements of the growth factor would complement distance measurements, yielding combined tests of time variation of w that are much more powerful than either measure alone. Unfortunately, the complementarity in the $\Omega_m - w$ space does not translate to complementarity for this new problem, at least at $z < 2$. Fig. 3(d) shows percentage differences in $D_1(z)$ relative to the *same* constant-w models that best match the distance measurements. [I have been lazy and used the approximation (6).] The differences in $D_1(z)$ are smaller than those in $d(z)$, even though the values of w were chosen to match the latter not the former. The discriminatory power of $D_1(z)$ does increase at higher redshifts, especially for $m = 3$, because in this case ρ_ϕ freezes in at a constant fraction of ρ_m (Fig. 3(a)), so $d\log D_1/d\log(1+z) \approx \Omega_m^{4/7}$ is always depressed below unity. The Lyα forest might eventually allow a measurement of D_1 at $z \sim 3$ with enough precision to be interesting in this regard (Croft et al., 1998; McDonald et al., 2004). The comparison of CMB anisotropy amplitude to the matter power spectrum amplitude at low redshift would be more powerful still, if the latter can be measured precisely enough and the effects of dark energy variation can be separated from those of the reionization optical depth and tensor fluctuations, both of which affect the relative amplitudes of CMB and matter power spectra.

The high-redshift behavior of $\rho_\phi(z)$ has a stronger impact on $H(z)$ because there is no integrated contribution from low redshift like those in Eqs. (2) and (6). Thus observations that directly constrain $H(z)$ at $z > z_c$ can add discriminatory power even if they are much less precise than the distance measurements at $z < 2$. Because the $H(z)$ variations are much larger than the $d(z)$ variations, the AP test effectively serves the same role as an $H(z)$ measurement at high redshift. The Lyα forest and redshift surveys of Lyman-break galaxies both offer possible routes to inferring these quantities at the few percent level (Weinberg et al., 1997; Hui et al., 1999; McDonald and Miralda-Escudé, 1999; McDonald, 2001; Blake and Glazebrook, 2003; Seo and Eisenstein, 2003; Weinberg et al., 2003), though it is not yet clear that systematic errors in these approaches can indeed be controlled to this level of accuracy.

The experiment in Fig. 3 is similar to that carried out by Kujat et al. (2002). If my conclusions here seem a bit more optimistic, it is mainly because I have zeroed in on the subset of models for which time variation of w is easiest to detect, and partly because the prospect of a wide-field imager in space makes the idea of percent-level distance measurements seem worthy of serious discussion, not simply pie in the sky. Note also that Fig. 3 is restricted to flat models. Evidence for strong time-variation of w would be surprising enough that one would want to consider

observationally allowed values of $\Omega_k \neq 0$, thus giving more freedom to reproduce the data with a constant-w model.

3. Considerations for a space-based dark energy experiment

The discovery of dark energy has profound implications for cosmology and particle physics, even if we do not yet understand what all of those implications are. A demonstration that the dark energy density has changed over time (i.e., that $w \neq -1$) would be an achievement of comparable magnitude. A precise measurement of w would rule out many models of dark energy and provide a clear target for predictive models that might emerge from fundamental physics. A demonstration that the effective value of w has changed with time would be much more remarkable still, eliminating most models and providing a strong clue to the physics of dark energy.

While $w = -1$ has history on its side, it has no particular claim to physical plausibility in the absence of a successful theory of fundamental vacuum energy. I thus see no reason to conclude that w is likely to be -1 just because current data are consistent with this value, and improved observations that restricted it to, say, $w = -1.0 \pm 0.1$ would not change this situation. If $|w + 1|$ is $\sim$0.15 or more, then there are good prospects for detecting this departure with the few percent level of precision that can be obtained by ground-based experiments, especially as different approaches can provide complementary constraints and independent tests (Fig. 2). However, a demonstration that $w = -0.95$ would be just as profound as a demonstration that $w = -0.85$, and a demonstration that $w = -1.05$ would be still more striking, implying physics even weirder than that we are currently forced to accept. The level of precision and control of systematics required to detect such small departures from $w = -1$ can only be achieved from space.

Detecting time-variation of w would almost certainly require a space-based investigation, since the complementarity of different methods is largely lost, and the measurements must probe the largest possible redshift range to achieve maximum leverage. Even with the capabilities of a mission like SNAP or DESTINY, I think one must deem a convincing detection of time-variation unlikely, because for slow variations there will always be a constant-w model that produces nearly identical results over the redshift range where dark energy is dynamically important. There is one class of "generic" models in which time variation is *relatively* easy to detect: dark energy scales like matter during the matter-dominated era and transitions to a constant density when $\Omega_{\rm m}$ falls significantly below one. However, even in this class the transition must occur quickly and at low redshift to be observable.

Because I consider a detectable value of $|w + 1|$ to be a priori much more plausible than a detectable level of time-variation, I think that one should not sacrifice precision on the former to gain leverage on the latter. If one assumes that supernova distance measurements in redshift bins at $z \leqslant 1$ will be limited by systematic uncertainty rather than by statistics, then there is no reason not to pursue higher redshift objects in the quest for time variability. This is the attitude of the SNAP team, and it seems to me entirely reasonable. However, if cost constraints force consideration of a descoped mission, then the choice between precision on w and leverage on time-variation may become unavoidable.

The very fact that a space-based dark energy mission will be much more capable than any ground-based experiment raises the stakes, since any discovery made by this mission would be unrepeatable for many years to come. Everyone will have slightly different views on what statistical confidence level is needed for an "interesting" result on dark energy. In my view, satisfying evidence for $w \neq -1$ would require one result with $>3\sigma$ significance or two consistent results with $>2\sigma$ significance, along with convincing tests for systematic effects. Time-variation of w demands a higher standard because of its lower prior probability, maybe one $>4\sigma$ result or two $>3\sigma$.

To my mind, the great advantage of the SNAP concept for a dark energy mission relative to the DESTINY concept is that the Type Ia supernova experiment and the weak lensing experiment look capable of achieving similar statistical precision, with largely independent systematic uncertainties.

With DESTINY, there is no obvious backup method that comes close to the precision of the supernova search, making it harder to show that an unexpected result on dark energy is actually correct. The comparison is not entirely fair, since DESTINY would likely be much less expensive than SNAP, and it is no surprise that it has narrower scope. Either of these missions would be a great step forward in our efforts to unravel the most intriguing cosmic mystery of our time, and, as we heard throughout this workshop, either would enable a vast array of other fascinating investigations.

Acknowledgments

I am indebted to my collaborators on this subject, Jens Kujat, Angela Linn, and Robert Scherrer. I also thank the organizers for inviting me to discuss this topic and for patience in awaiting my proceedings contribution.

References

Albrecht, A., Skordis, C., 2000. PRL 84, 2076.
Alcock, C., Paczyński, B., 1979. Nature 281, 358.
Bennett, C.L. et al., 2003. ApJS 148, 1.
Blake, C., Glazebrook, K., 2003. ApJ 594, 665.
Brandenberger, R., Mazumdar, A., 2004. JCAP 8, 15.
Croft, R.A.C., Weinberg, D.H., Katz, N., Hernquist, L., 1998. ApJ 495, 44.
de Bernardis, P. et al., 2000. Nature 404, 955.
Doran, M., Schwindt, J.-M., Wetterich, C., 2001. PhRvD 64, 123520.
Efstathiou, G., Sutherland, W.J., Maddox, S.J., 1990. Nature 348, 705.
Efstathiou, G., 1995. MNRAS 274, L73.
Freedman, W.L. et al., 2001. ApJ 553, 47.
Garriga, J., Vilenkin, A., 2000. PhRvD 61, 083502.
Hanany, S. et al., 2000. ApJ 545, L5.
Hogg, D.W., 1999. astro-ph/9905116.
Hu, W., 2004. astro-ph/0407158.
Hui, L., Stebbins, A., Burles, S., 1999. ApJ 511, 5.
Krauss, L.M., Turner, M.S., 1995. Gen Rel & Grav 27, 1137.
Kujat, J., Linn, A.M., Scherrer, R.J., Weinberg, D.H., 2002. ApJ 572, 1.
Lightman, A.P., Schechter, P.L., 1990. ApJS 74, 831.
McDonald, P., Miralda-Escudé, J., 1999. ApJ 518, 24.
McDonald, P., et al., 2004. astro-ph/0407377.
McDonald, P., 2001. ApJ 585, 383.
Ostriker, J.P., Steinhardt, P.J., 1995. Nature 377, 600.
Peebles, P.J.E., 1980. The Large Scale Structure of the Universe. Princeton University Press, Princeton.
Perlmutter, S. et al., 1999. ApJ 517, 565.
Riess, A.G. et al., 1998. AJ 116, 1009.
Riess, A.G. et al., 2004. ApJ 607, 665.
Seljak, U., et al., 2004. astro-ph/0407372.
Seo, H., Eisenstein, D.J., 2003. ApJ 598, 720.
Tegmark, M. et al., 2004. PRD 69, 103501.
Weinberg, D.H., Hernquist, L., Katz, N., Croft, R., Miralda-Escude, J., 1997. In Petitjean, P., Charlot, S., Proceedings of the 13th IAP Colloquium, Structure and Evolution of the IGM from QSO Absorption Line Systems (Paris: Nouvelles Frontières), p. 133, astro-ph/9709303.
Weinberg, D.H., Davé, R., Katz, N., Kollmeier, J.A., 2003. AIP Conference Proceedings 666: The Emergence of Cosmic Structure, 666, p. 157, astro-ph/0301186.
Weinberg, S., 1987. Phys Rev Lett 59, 2607.

Available online at www.sciencedirect.com
SCIENCE DIRECT®
New Astronomy Reviews 49 (2005) 346–353
New Astronomy Reviews
www.elsevier.com/locate/newastrev

Exploring dark energy with SNAP

G. Aldering

Physics Division, Lawrence Berkeley National Laboratory, Berkeley, CA, United States

Available online 13 September 2005

Abstract

The accelerating expansion of the Universe is one of the most surprising and potentially profound discoveries of modern cosmology. Measuring the acceleration well enough to meaningfully constrain interesting physical models requires improvements an order of magnitude beyond on-going and near-term experiments. The Supernova/Acceleration Probe has been conceived as a powerful yet simple experiment to use Type Ia supernovae and weak gravitational lensing to reach this level of accuracy. As fundamentally different causes for the acceleration map into very small differences in observational parameters for all relevant cosmological methods, control of systematics is especially important and so has been built into the SNAP mission design from the very beginning.

Though focused on the study of the accelerating Universe, the overall SNAP instrument suite is quite general and able to make unique contributions to a wide variety of astronomical studies. The baseline satellite consists of a 2-m anastigmat telescope, with a 0.7 square degree focal plane paved with optical and NIR imaging arrays. Spectroscopy can be obtained using a high-throughput low-resolution optical + NIR integral field spectrograph. The baseline science programs will result in a 15 square degree "deep field" having temporal coverage every 4 days and summing to $m_{AB} \sim 30.3$ in all colors – to be used for discovery and follow-up of some 2000 Type Ia supernova in the range $0.1 < z < 1.7$ – and a wide area survey spanning 1000 square degrees and reaching $m_{AB} \sim 27.7$ in all colors – to be used to measure the weak lensing power spectrum well into the non-linear regime. A panoramic survey covering 10,000 square degrees to $m_{AB} \sim 26.7$ in all colors is also possible. This baseline dataset represents a gold mine for archival astronomical research and follow-up with JWST, while guest observer survey programs will substantially broaden the impact that *SNAP* will have.
© 2005 Elsevier B.V. All rights reserved.

Contents

1. Introduction 347
2. Cosmology with supernova from the ground and space 347

E-mail address: galdering@lbl.gov.

1387-6473/$ - see front matter © 2005 Elsevier B.V. All rights reserved.
doi:10.1016/j.newar.2005.08.002

3. Enabling better type Ia standardization . . . 348
4. From science objectives to project design . . . 350
5. The power of weak lensing from space . . . 350
6. SNAP instrument concept . . . 352
7. Conclusion . . . 353
Acknowledgements . . . 353
References . . . 353

1. Introduction

SNAP[1] is a space telescope mission concept aimed at measuring the time variation in the equation of state of the dark energy responsible for the accelerating expansion of the universe. SNAP initially focused on the use of Type Ia supernovae as a means of measuring the expansion history of the universe through the luminosity–distance relation. However, the *SNAP* instrument suite proved to be quite generic, allowing, for example, the inclusion of gravitational weak lensing as another means of constraining the properties of dark energy. Indeed, SNAP's very powerful wide-field imager and the interest in using it for complementary science has in many ways motivated and shaped this "Wide-Field Imaging from Space" conference.

2. Cosmology with supernova from the ground and space

Before looking at the exciting discoveries that SNAP holds for the future, it is worthwhile to consider recent past and on-going work to constrain the nature of dark energy. In the six years since the discovery of the accelerating expansion of the universe, a wealth of new observations have confirmed and further refined the initial discovery. In concert with newer data from Type Ia supernovae (including constraints on flatness from the CMB and on Ω_M from large-scale structure and clusters), the statistical significance of the acceleration is now $>10\sigma$. Just as importantly, the equation of state of the dark energy is now constrained to be $w < -0.7$ (assuming the equation of state is constant).

Space-based observations have played an increasing role in cosmological measurements of Type Ia supernovae. This is simply due to the much smaller sky noise present in a point-source photometry aperture in space compared with the ground – especially at redder optical wavelengths. The discovery papers (Perlmutter et al., 1999; Riess et al., 1998) contained just four supernovae measured with HST. Samples totaling 39 Type Ia supernovae, segregated into early, middle and late host-galaxy morphologies from an HST Snapshot survey, were shown to support an accelerating expansion (Sullivan et al., 2003). Precise corrections for dust extinction of 11 more supernovae made possible by accurate HST photometry were shown to support the accelerating expansion and provided tighter constraints on the dark energy equation of state (Knop et al., 2003). A sample of high-redshift supernovae reaching $z \sim 1.6$ has shown that the supernovae follow the transition from deceleration to acceleration expected as the universe goes from matter domination to dark energy domination (Riess et al., 2004; Knop et al., 2003; Tonry et al., 2003). These space-based measurements have significantly bolstered both the case for dark energy and the efficacy of Type Ia supernovae as distance indicators. Accordingly, today the most precise and highest-redshift supernova measurements – several dozen so far – are most often obtained with HST.

An example of the state of the art in space-based supernova cosmology is a joint endeavor involving the Supernova Cosmology Project (SCP[2]) and the Higher-Z Supernova Search Team (HZSST) which around the time of this conference was conducting a search spanning four epochs,

[1] snap.lbl.gov; see also (Aldering et al., 2004).

[2] supernova.lbl.gov.

each covering 15 pointings covering the northern GOODS field. The searches are separated by 45 days – roughly equal to the time from explosion to maximum light in the restframe of $z > 1$ Type Ia supernovae. The search uses the Advanced Camera for Surveys (ACS) with the 850 nm long-pass filter in order to reach redward of the restframe UV cut-off exhibited by Type Ia supernovae. A short exposure in the F775W filter is added in order to reject some fraction of Type II supernovae, which in the first 10 days have much more UV flux than Type Ia supernovae. The depth of the GOODS field at optical (HST) and infrared (ground-based) wavelengths means that photometric redshifts are known for many supernova host galaxies. In addition, the galaxy colors at the location of the supernovae provide a handle on whether or not star-formation is likely to be ongoing, which can help eliminate likely core-collapse supernovae. All of this advance information is used to help select one or two likely Type Ia supernovae suitable for follow-up. Each team has three target-of-opportunity triggers and 60 orbits for near-infrared follow-up observations with NICMOS and slitless spectroscopy with ACS. For these searches each supernova lightcurve and its associated search costs roughly 30 HST orbits (see Fig. 1).

At the time of this conference the SCP had netted a probable $z \sim 1.7$ Type Ia supernova from the first of the four search epochs. The discovery image is shown in Fig. 2. Since then, several more supernova have been found as part of this program. Unfortunately, all of these supernovae have just the bare minimum of data needed to place them on the Hubble diagram, leaving little extra information for testing for systematic effects in the measurement. A satellite such as SNAP will increase the number of such supernovae by orders of magnitude, but will also have much higher data quality and systematics controls (see Fig. 3).

3. Enabling better type Ia standardization

While Type Ia supernovae have shown tremendous value in revealing the presence of dark energy and exploring its nature, we should be concerned that this purely empirical technique will reach a systematics floor. The single-parameter light-curve width correction method (plus extinction correction) reduces the scatter in Type Ia supernovae at peak to somewhere in the range 0.10–0.15 mag (Tripp, 1998; Phillips et al., 1999). However, there is nothing special about the physical conditions in a supernova when it appears its

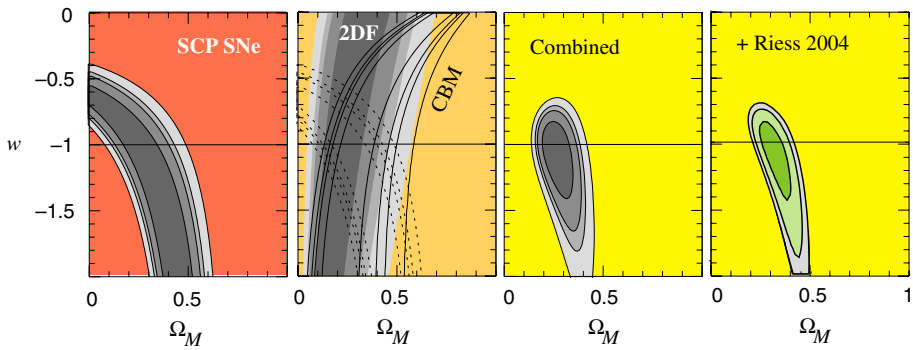

Fig. 1. The most recent constraints on the dark energy equation of state, w. A constant equation of state and flat topology are assumed. Inner and outer contours delimit 68% and 99% confidence, respectively. On the left, the constraints from the Supernova Cosmology Project sample (Perlmutter et al., 1997, 1998, 1999; Knop et al., 2003) are shown. These include 11 supernovae with very well-measured colors from HST. The next panel shows independent constraints from WMAP (Spergel et al., 2003) and from the 2dF redshift survey (Percival et al., 2002). The third panel shows the results of combining these independent measurements. The right-most panel shows the effect of the improved constraints on Ω_M from the Type Ia supernovae in the deceleration epoch resulting from the addition of supernovae from the Higher-Z Supernova Search Team (Riess et al., 2004).

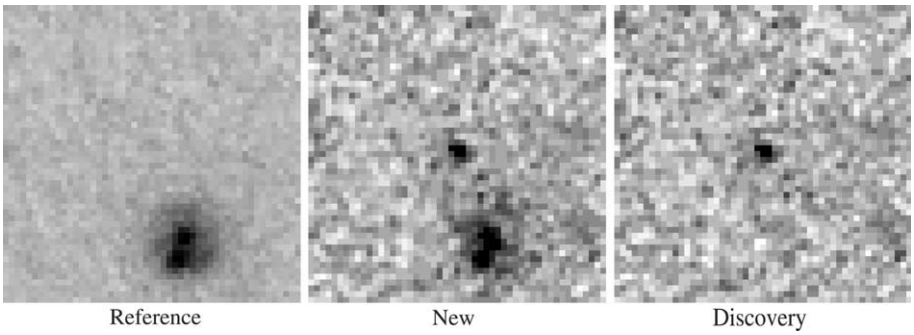

Fig. 2. Discovery image of a candidate $z \sim 1.7$ Type Ia supernova from a search of the HDF-N with HST by the SCP. The image on the left is the reference image constructed from the GOODS program. The central panel shows the discovery image, obtained in one HST orbit in the F850LP filter. The image on the right is the difference of the discovery and reference images, isolating the new supernova. The redshift is based on photometric redshifts kindly provided by GOODS. HST F775W images and follow-up ACS slitless spectra do not show blue light that would be expected if the supernova were of Type II.

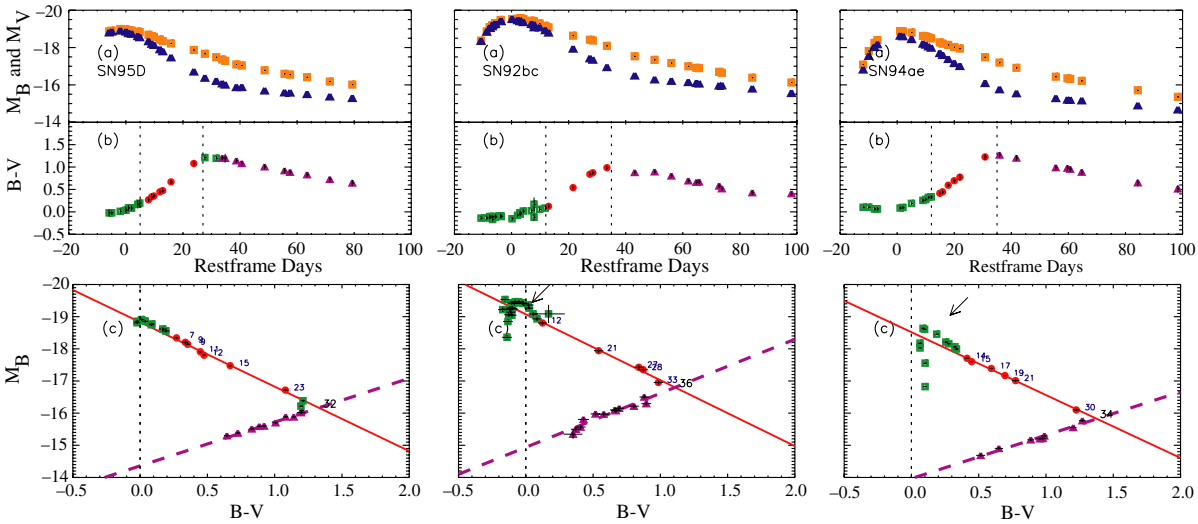

Fig. 3. Illustration of the CMAGIC Type Ia supernova standardization technique for three well-observed Type Ia SNe. The upper row shows the B and V lightcurves, the middle row shows the B–V color curves, and the bottom row shows B versus B–V color. Classical techniques (stretch, Δm_{15}, MLCS) use the lightcurves and color curves versus time, whereas CMAGIC uses brightness versus color, which has an amazingly linear region starting about a week after maximum light. (There is also a linear region at late times, during the nebular phase.) The brightness when B–$V = 0.6$ is an excellent standard candle (Wang et al., 2003).

brightest. Indeed, a newly developed technique, CMAGIC, standardizes Type Ia supernovae using the color and magnitude roughly 15 days after maximum, when the supernova reaches a color of B–$V = 0.6$ (Wang et al., 2003). This method has been shown to reduce the scatter to below 0.10 mag. Thus, it is possible that Type Ia supernovae are more homogeneous at a given color rather than at a given lightcurve epoch. Many more observations of nearby supernovae, focusing on accurate colors with well-determined uncertainties will be a great boon in improving the standardization of Type Ia supernovae. By lowering the remaining scatter, stronger limits

are also set on any possible remaining systematics in the Type Ia methodology.

4. From science objectives to project design

The objective of the SNAP mission is to provide the best possible constraint on the time-evolution of the dark energy equation of state. The only demonstrated experimental techniques are astronomical, and of these, the luminosity distance from Type Ia supernovae is by far the most mature. Therefore, it was natural to design a mission focused on supernovae, but as we shall see, the resulting design is sufficiently general to perform exceptionally well for gravitational weak lensing.

Pushing the Type Ia supernova method to its limit requires thousands of supernovae spanning a wide range in redshift. The present SNAP design targets 2000 normal Type Ia supernovae from redshift 0.1 to 1.7. It is extremely critical that the photometry be of high quality continuously from low to high redshift, not only to realize the statistical power of the sample but to avoid introduction of systematics errors (Kim et al., 2004). Due to the increasing brightness of the terrestrial night sky at redder wavelengths where higher redshift Type Ia supernovae must be observed, coupled with increasing atmospheric water absorption at redder wavelengths, the necessary data quality can be obtained only from space. The broad redshift coverage needed to control systematics further requires detectors at both optical and infrared wavelengths. Telescope optical design and spacecraft size and mass constraints point to a dedicated 2-m telescope[3] with a field of view several hundred times larger than that possessed by HST, populated with visible and near-infrared detectors. Further, in order to determine the supernova type, and possible sub-class, a sensitive low-resolution spectrograph is required. Systematics control enabled by spectrophotometric spectra, as well as allowance for spacecraft pointing margin, call for an integral field unit spectrograph.

[3] For diffraction-limited photometry of faint point sources, exposure time goes as the 4th power of the telescope aperture.

5. The power of weak lensing from space

Gravitational weak lensing measurements have become increasingly robust over the past decade. Long viewed as a means of constraining Ω_M, more detailed theoretical studies – several developed within the SNAP collaboration – indicate that precision weak lensing measurements have the capability to place constraints on the dark energy equation of state similar to those possible with Type Ia supernovae. In particular, weak lensing cross-correlation cosmography – measuring the association between foreground template mass distributions and background weak lensing shear using galaxies located using photometric redshifts – appears to be the most powerful weak lensing approach (Bernstein and Jain, 2004).

Atmospheric turbulence results in poor spatial resolution for high-redshift galaxies observed from the ground. Furthermore, ground-based telescope and camera optics are far from being diffraction-limited. So great care must be taken in removing the effects of seeing, tracking errors, and optical aberrations. Stars provide the reference for removing these effects, but the number of usable stars is limited, due to both the limited size of the isoplanatic patch within which seeing is correlated and difficulty in distinguishing the few stars from the large number of galaxies at faint magnitudes. Errors in these corrections set a limit on the quality that ground-based weak lensing will be able to achieve.

In comparison, space-based wide-field observations resolve many more sources and the remaining corrections for tracking and telescope aberrations are much smaller relative to the sizes of the sources. Fig. 4 illustrates the dramatic gain in the number of resolved galaxies in going from ground- to space-based observations. Moreover, in contrast to HST, SNAP will be placed in a stable thermal environment so that any corrections can be determined using many spatially uncorrelated images. Moreover, the deep optical and infrared photometry from SNAP will provide high-quality photometric redshifts as needed to implement the cross-correlation cosmography method. Therefore, SNAP can provide excellent

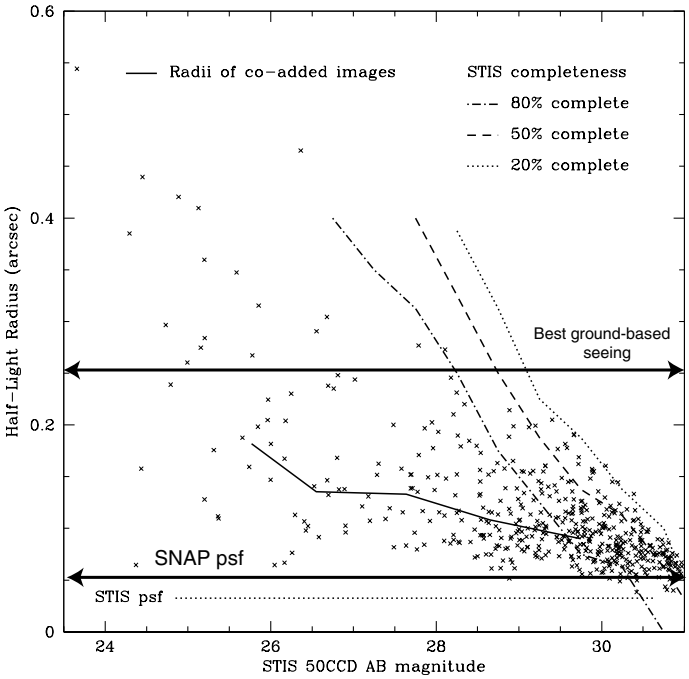

Fig. 4. Measurements of the sizes of galaxies versus magnitude (Gardner and Satyapal, 2000), illustrating the large reservoir of faint, distant galaxies which can be spatially resolved from space but not from the ground.

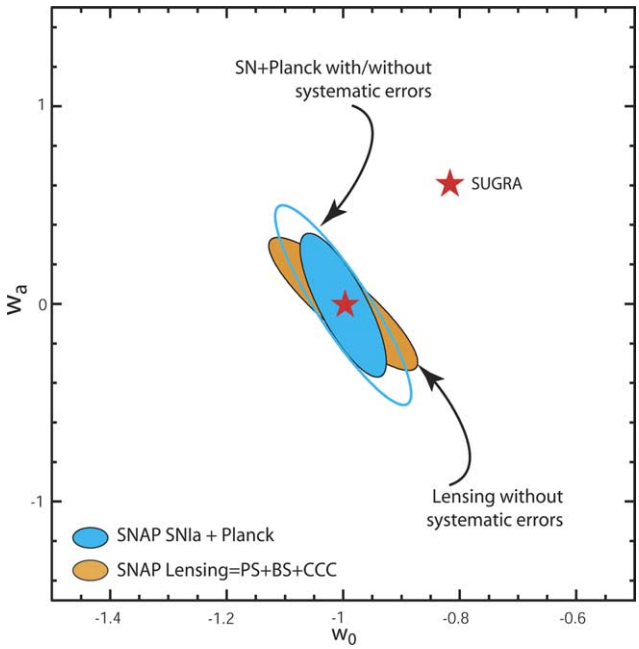

Fig. 5. Individual constraints on the dark energy equation of state and its derivative from the SNAP Type Ia SN program and the weak gravitational lensing program, demonstrating the comparable and complementary power of these two methods when executed with SNAP.

weak lensing data for constraining changes in the dark energy equation of state (Rhodes et al., 2004) (see Fig. 5).

6. SNAP instrument concept

In detail, the SNAP telescope design is a three-mirror anastigmat with a 2-m primary mirror (Lampton et al., 2002b). The optics are silver-coated to maximize the optical and near-infrared throughput and minimize the thermal emissivity. The imager consists of 0.34 square degrees paved with red-sensitive CCDs and a scale of 0.10″/pixel, and 0.34 square degrees paved with HgCdTe near-infrared detectors with a scale of 0.18″/pixel (Lampton et al., 2002a). The sizes of the detectors are identical and those made of HgCdTe have a long-wavelength cutoff which reduces the dark current (and sensitivity to thermal emission). These features allow the CCD and HgCdTe detectors to be mounted in the same focal plane, simplifying the imager construction, mounting, and alignment. Each detector has its own filter, so a large filter wheel which would otherwise be needed is avoided. Detailed simulations show that photometry of sufficient quality and redshift range is not possible from the ground even under optimistic assumptions (see Fig. 6).

The SNAP spectrograph has a prism as its dispersing element, providing resolution $R \sim 100$ across optical and near-infrared wavelengths (Prieto et al., 2002). Higher resolution is unnecessary due to the velocity broadening intrinsic to the spectra of Type Ia supernovae. Again, the optical detector is a red-sensitive CCD while the near-infrared detector is HgCdTe with a long-wavelength cut-off near 1.7 μm. The spectrograph is fed by an image slicer integral field unit. The field is $6'' \times 3''$, with the latter dimension being divided into 40 slices. Detailed simulations show quite dramatically that spectroscopy of comparable quality

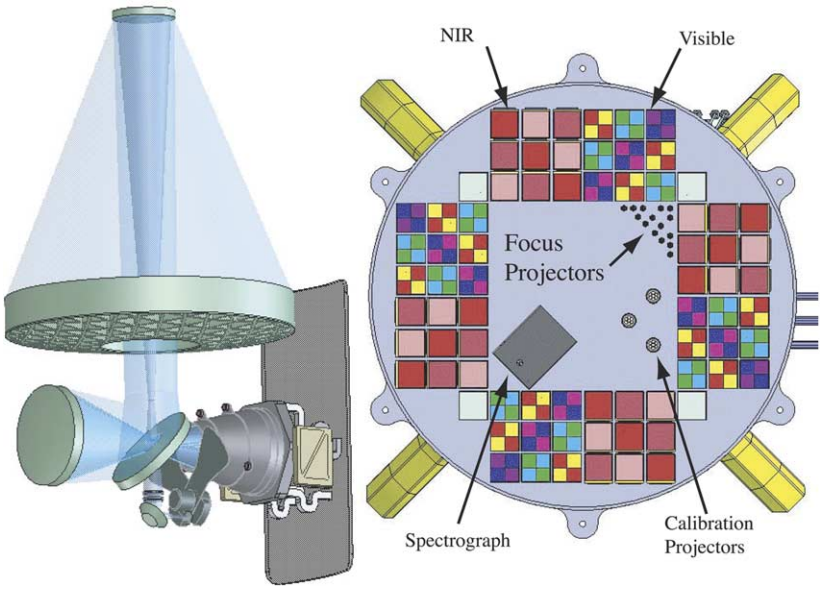

Fig. 6. Left: Layout of the SNAP optical telescope assembly (OTA) (Lampton et al., 2002b). The telescope, shutter, camera (shielded by the cone), electronics, and passive radiator are shown. Right: Layout of the SNAP focal plane (Lampton et al., 2002a). NIR and visible detectors populate a single focal plane. Each detector has its own filter. The filters (and hence detectors) are laid out so that as SNAP passes over a field, each location is observed in all filters. The SNAP spectrograph is mounted behind the imaging focal plane, and is fed by an IFU in the imaging focal plane (Prieto et al., 2002). Detectors for guiding populate each quadrant, and projectors for focus and calibration are also integrated into the focal plane.

Table 1
Nominal parameters of the SNAP surveys

Survey mode	Areal coverage (square degrees)	Depth (AB Mag)	Resolved galaxy surface density (# arcmin^{-2})	Number of resolved galaxies
Deep SNe	15	30.3	250	$10^{7.0}$
Wide	300–1000	27.7	100	$10^{8.5}$
Panoramic	7000–10000	26.7	40–50	$10^{9.0}$

is not possible from the ground, even with a 30 m telescope with adaptive optics.

7. Conclusion

The nature of dark energy is a fundamental question, which astronomical observations can address. Type Ia supernova and weak lensing are the most powerful techniques yet developed for studying dark energy. Reaching the requisite statistical and systematics accuracy with these techniques requires a widefield imager in space. SNAP represents a very advanced concept for such a widefield imager, having an instrument suite which is both powerful and versatile. Table 1 details this power for the Type I supernova survey, a nominal wide-field weak lensing survey, and a possible panoramic weak lensing survey. The planned dark energy program for the Joint Dark Energy Mission (JDEM) will produce a treasure trove of data for archival study. Guest Observer programs that could further exploit such a powerful instrument are envisioned in the JDEM concept. The following conference presentations describe many of the scientific lines of inquiry which would be greatly advanced with a facility such as SNAP.

Acknowledgements

The work described here is supported by the DOE Office of Science and by NASA. The author thanks his collaborators in SNAP and the SCP for their valuable contributions to this work.

References

Aldering, G. et al. 2004, astro-ph/0405232.
Bernstein, G., Jain, B., 2004. ApJ 600, 17.
Gardner, J.P., Satyapal, S., 2000. AJ 119, 2589.
Kim, A.G., Linder, E.V., Miquel, R., Mostek, N., 2004. MNRAS 347, 909.
Knop, R.A. et al., 2003. ApJ 598, 102.
Lampton, M.L. et al., 2002a. Proc. SPIE 4854, 632.
Lampton, M.L. et al., 2002b. Proc. SPIE 4849, 215.
Percival, W.J. et al., 2002. MNRAS 337, 1068.
Perlmutter, S. et al., 1997. ApJ, 483.
Perlmutter, S. et al., 1998. Nature, 391.
Perlmutter, S. et al., 1999. ApJ 517, 565.
Phillips, M.M. et al., 1999. AJ 118, 1766.
Prieto, E. et al., 2002. Proc. SPIE, 4850.
Rhodes, J. et al., 2004. APh 20, 377.
Riess, A.G. et al., 1998. AJ 116, 1009.
Riess, A.G. et al., 2004. ApJ 600, L163.
Spergel, D.N. et al., 2003. ApJS 148, 175.
Tonry, J.L. et al., 2003. ApJ 594, 1.
Tripp, R. et al., 1998. A&A 331, 815.
Sullivan, M. et al., 2003. MNRAS 340, 1057.
Wang, L., Goldhaber, G., Aldering, G., Perlmutter, S., 2003. ApJ 590, 944.

Available online at www.sciencedirect.com
SCIENCE DIRECT®
New Astronomy Reviews 49 (2005) 354–359
New Astronomy Reviews
www.elsevier.com/locate/newastrev

DESTINY: The dark energy space telescope

Tod R. Lauer

NOAO, P.O. Box 26732, Tucson, AZ 85726, United States

The Destiny Science Team (Jon Morse (PI), Chris Fryer, Robert Kirshner, Tod Lauer, Philip Pinto, Marc Postman, Adam Riess, David Spergel, Tom Vestrand, Mike Warren, and Robert Woodruff.)
Available online 22 September 2005

Abstract

The Dark Energy Space Telescope (DESTINY) is an all-grism NIR 1.8 m survey camera optimized to return richly sampled Hubble diagrams of Type Ia and Type II supernovae (SN) over the redshift range $0.5 < z < 1.7$, for determining cosmological distances, measuring the expansion rate of the universe as a function of time, and characterizing the nature of the so-called "dark energy" component of the universe. SN will be discovered by repeated imaging of a 7.5 square-degree area located at the north ecliptic poles. Grism spectra with resolving power $\lambda/\Delta\lambda = R \sim 75$ will provide broad-band spectrophotometry, redshifts, SN classification, as well as valuable time-resolved diagnostic data for understanding the SN explosion physics. This methodology features only a single mode of operation with no time-critical interactions, a single detector technology, and a single instrument. Although grism spectroscopy is slow compared to SN detection in any single broad-band filter for photometry, or to conventional slit spectra for spectral diagnostics, the multiplex advantage of being able to observe a large field-of-view simultaneously over a full octave in wavelength makes this approach highly competitive.
© 2005 Elsevier B.V. All rights reserved.

Keywords: Supernovae; Dark energy

Contents

1. Introduction . . . 355
2. The DESTINY concept . . . 356
3. The survey design . . . 356
References . . . 359

E-mail address: tlauer@noao.edu.

1387-6473/$ - see front matter © 2005 Elsevier B.V. All rights reserved.
doi:10.1016/j.newar.2005.08.004

1. Introduction

The startling discovery that the expansion rate of the universe is accelerating rather than slowing with time was made through the construction of Hubble diagrams of the distances and redshifts to a sample of relatively low-redshift SN Ia (Riess et al., 1998; Perlmutter et al., 1999). Identifying the driver of this acceleration, presumed to be some form of "dark energy," has motivated no shortage of observational programs to provide a richer, and presumably revealing, description of the expansion history of the universe. SN Ia observations will continue to play a leading role in this task, and several ground-based observational programs are now underway that should provide over an order or magnitude gain in the richness of the SN Ia Hubble diagram at low redshift. At the same time, it is clear that knowledge of the past Hubble flow must extend to higher redshifts than can be explored by ground-based SN Ia observations, in order to offer any serious constraints on the dark energy equation of state (Linder and Huterer, 2003). Observation of SN Ia at $z > 0.8$ essentially requires a space telescope with near-IR (NIR) instrumentation.

The case for a space-based dark energy probe has already been made strongly by the team that has been developing the SNAP mission concept (Aldering et al., 2004), of course. This in turn has motivated the Joint Dark Energy Mission (JDEM) concept, in which both NASA, and the Department of Energy would partner to develop and operate a such a facility. As part of this process, however, NASA issued a call under its "Beyond Einstein" program for competitive ideas for JDEM; we proposed DESTINY (the Dark Energy Space Telescope) in response to this call.

The DESTINY concept is defined by the following precepts: (1) *Do only from space what must be done from space.* This means, as above, focusing only on high-z SN and the NIR instrumentation required to provide accurate distances and redshifts; leave the low-z SN and weak-lensing to ground-based programs. (2) *Build on the work likely to be done prior to the launch of JDEM.* The dark energy problem is of such criticality that the required low-z work indeed is already being pursued and should be close to maturity by the time that JDEM can be launched. (3) *Spectra are critical to obtaining SN redshifts and classification, as well as probing the explosion physics.* Obtaining SN spectra to follow-up the SN imaging detections and photometry has been the "bottle-neck" that most strongly limits existing SN surveys. DESTINY, however, would obtain spectra of all SN events at all times throughout its field-of-view. Such spectral coverage not only addresses the need for SN redshifts and classification, but offers substantial advantages over programs that can obtain only one SN spectrum per SN event. (4) *Keep it as simple as possible.* "Better" is the enemy of "good enough." Not only is the DESTINY instrument design simple, but mission operations would also minimize complexity.

DESTINY will provide observational data at the high redshift, $0.5 < z < 1.7$, end of the SN Ia Hubble diagram. A key aspect of our approach is to coordinate the space-based observations with a vigorous ground-based effort to hone the SN Ia Hubble diagram at low redshifts. One example of such an observational program is the ESSENCE project at CTIO, co-led by one of us (N.S.), to find and measure 200 SN Ia in the redshift range $0.15 < z < 0.7$. Part of our study will be to design an intensive follow-up program specifically tied to the DESTINY observing strategy that will provide full redshift coverage out to $z \sim 1.7$ and to cross-calibrate the photometric data in the overlapping redshift range between $0.5 < z < 1$. Our SN Ia results will also be combined with large-scale structure and lensing studies directed at exploring the nature of dark matter and dark energy, such as 2dFGRS (Percival et al., 2002) or those being considered for LSST and future Gemini instrumentation. From the DESTINY observations, we will obtain time-resolved grism spectra of all supernovae in our survey fields. Thus we will gather large datasets on both SN Ia and SN II events (plus other rarer SN types). We will make use of the SN II data in order to provide independent luminosity-based distance measurements (Hamuy and Pinto, 2002). While at this time the use of SN II as distance indicators is considerably less mature than the SN Ia methodologies, we will

obtain rich SN II datasets for no extra mission cost. We can thus be prepared to capitalize on the state-of-the-art SN II methodology at mission time.

2. The DESTINY concept

DESTINY is a 1.8-m aperture, grism-mode imaging system operating over the 0.9–1.7 μm bandpass. The telescope is a three-mirror anastigmat with a rectangular field of view (FOV) of $0.25 \times 1°$ feeding a $6K \times 24K$ mosaic of hybridized HgCdTe Rockwell H-2RG focal plane arrays. The pixel scale is $\sim 0.13''$. The mission will focus on detecting and characterizing SN Ia and SN II at redshifts $z > 0.5$, which are increasingly difficult to study from the ground for $z > 0.8$; despite the emphasis on the truly high-z SN, we will have substantial overlap with ground-based observations. We will combine our results with complementary ground-based surveys, some of which are already underway under the direction of our team members. The survey design also reflects well-grounded predictions for the number of objects that we will detect and their redshift distributions. Our goals in this mission concept study are to achieve the science objectives with high efficiency, while minimizing instrumentation requirements, operating modes, telemetry, costs, and complexity. DESTINY contrasts with SNAP (Aldering et al., 2004) in the following ways: it (1) eliminates one detector technology and reduces the total pixel count by a factor of four; (2) eliminates the need for a separate spectrograph; (3) restricts the number and complexity of operational modes; (4) reduces the required simultaneous FOV; (5) uses on-board processing to reduce telemetry requirements; and (6) eliminates the need for separate spectroscopic observations of transient targets.

We employ an academic/industry/national center partnership. There are significant and meaningful roles to be played by NASA, DoE, and NSF supported institutions in the DESTINY concept. In general, NASA funding will be used to construct the observing facility and launch it; DoE funding will be used for mission operations, flight software development, and data storage; NSF funds will be used to support the ground-based coordinated observing program. DESTINY provides an excellent opportunity for synergistic interagency cooperation toward a common scientific goal that leverages expertise and experience of each agency.

3. The survey design

The design of the grism survey is dictated by the basic exposure sequence, plus the need to resample the survey area at regular intervals to track the luminosity evolution of the SN events. The fiducial exposure time is 4 h for each 0.25 square-degree DESTINY field. Exposures of this length are advantageous; the spacecraft pointing would be fixed during this time, minimizing the overhead associated with acquiring guide stars, repointing, etc. By minimizing such overheads, and adopting an orbit (at Sun–Earth L2) that allows continuous observation of the survey area at an ecliptic pole, 1.5 square-degrees can be imaged per day. Because our proposed mission focuses on SN Ia at $z > 0.5$, the corresponding time dilation eases the cadence of repeat visits over that required for a mission that also observes SN Ia at low redshifts. Our initial expectation, based on Monte Carlo simulations of $z > 0.5$ SN light curves for LSST, is that a 5-day sampling interval is sufficient. The implied total survey area is thus 7.5 square-degrees composed of 30 separate fields. Adopting a local SN Ia rate of $5.2 \times 10^{-5}\ \mathrm{Mpc}^{-3}\ \mathrm{yr}^{-1}$ (Tonry et al., 2003), for $\Omega_0 = 1$, $\Omega_\Lambda = 0.7$, and $H_0 = 72$, then $\sim$2500 SN Ia within $0.5 < z < 1.7$ should be observed in a nominal two-year mission, assuming that aside from time dilation, the supernovae rate does not evolve significantly with lookback time. At $z = 0.5$, $\sim$150 SN Ia are expected in a $z = 0.1$ bin in two years. The yield reaches $\sim$230 events at $z = 1.0$, declining only slightly to $\sim$190 events at $z = 1.7$. A two-year mission should thus yield a Hubble diagram accurate to 1% on the $\Delta z = 0.1$ scale, given the 0.1 mag dispersion in SN Ia peak luminosity, after correcting for the lightcurve decay rate. For w constant with z, Linder and Huterer Linder and Huterer (2003) show that $\sigma_w < 0.05$ should be readily achieved. Allowing for the possibility that w varies

with z, covariance between w_0 and w' makes the errors on each a strong function of the limiting redshift of the survey. With SN Ia observations limited to $z < 0.7$, it is essentially impossible to separate the two terms. With observations over $0 < z < 1.7$, and a Hubble diagram accuracy quoted above, the 1σ error in w_0 is $\sim$0.05, with a corresponding error in w' of $\sim$0.2.

The traditional approach to photometric observations of a distant SN is to obtain a time series of broad-band images through several different filters over its lifetime. Photometry in any filter at any epoch is measured by fitting a point-source model to the light of the SN left over after a reference image of its host galaxy has been subtracted. This procedure is straightforward and is optimal, if the overall goal is limited to the detection and photometric observation of SN Ia events *in a single band.* A complete scientific program to obtain a calibrated Hubble diagram of cosmologically distant SN events, however, additionally requires that spectra be obtained of the SN candidates to cull SN Ia events from other SN types, to obtain the redshift of the SN (or their host galaxies), as well as to obtain other potentially useful spectral diagnostics. Accurate use of the broad-band photometry also requires deriving complex k-corrections to correct for the fact the SN Ia occur over a wide range of redshifts but are observed in fixed filter bandwidths. Lastly, the program design must reflect a temporal cadence for observing a large enough area of the sky within a short enough time span to achieve a statistically interesting sample of SN Ia.

Our approach is to meld the spectroscopy and photometry into a program of spectrophotometric grism observations. While it is obvious that the observing time required to obtain a given S/N cratio by integrating over any single band within the grism spectrum will be substantially longer than that required to obtain a satisfactory image through an equivalent broad-band filter, a simple analysis suggests that the total time required to obtain a complete suite of multiple-band observations and spectra with a grism camera allows for a competitive and completely adequate survey to be conducted. If one factors in simplicity of the instrument and its operational modes, then we believe that this can be a superior approach. We sketch this out below.

The grism is specified to have $R = 100$ at $\sim$1.2 μm, an implied spectral scale of 60 Å/pixel. The survey area will be located at the north ecliptic pole to minimize zodiacal background; the spacecraft orbit and baffling design will minimize other external background sources such as earthshine or scattered sunlight. The total background is thus the integral of the zodiacal light over the bandpass plus the dark current of the detector. We use the ecliptic pole zodiacal background as a function of wavelength provided by Giavalisco et al. Giavalisco et al. (2002). For reference, bracketing values of the background are $f_\lambda = 1.81 \times 10^{-22}$ erg s^{-1} cm^{-2} μm^{-1} arcsec^{-2} at 0.5 μm, dropping to $f_\lambda = 1.26 \times 10^{-23}$ at 2.2 μm. With an assumed total DQE = 50%, and a detector dark current of 0.1 e^{-1} s^{-1} pixel^{-1}, the total (detected) background is 0.55 e^{-1} s^{-1} pixel^{-1}. In Fig. 1, we calculate S/N per spectral bin in 4-h exposures for SN Ia at various redshifts, assuming $\Omega_0 = 1$, $\Omega_\Lambda = 0.7$, and $H_0 = 72$. The input spectrum is a theoretical model of an SN Ia at peak luminosity (Nugent

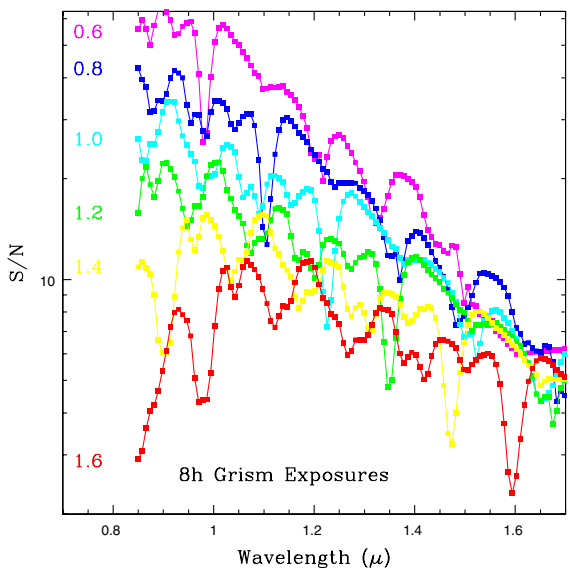

Fig. 1. S/N ratios per spectral pixel (60 Å) are shown for SN Ia spectra at redshifts 0.6, 0.8, 1.0, 1.2, 1.4, and 1.6. A 4-h exposure is assumed. The template spectrum corresponds to the time of peak luminosity.

et al., 2002). We also assume that at redshifts $z > 1$, the host galaxies will be compact and dominated in the grism images by the zodiacal background, and that at lower redshifts the host galaxy will dominate. The strong absorption feature is the Si II 6150 Å line, which is a type Ia diagnostic, and will be used to provide the SN redshift. $R \sim 75$ resolution is clearly adequate to characterize the broad spectral features. At the highest redshifts, one can smooth the spectra to boost the S/N over that shown. Time dilation also allows us to co-add spectra from multiple visits, while maintaining the same time resolution as $z \sim 0.5$ events. We conclude that a 4-h exposure with the proposed instrument is about right for obtaining the needed spectral information.

As a "proof of concept," we note that the HST/ACS grism mode has already been used to observe SN Ia at $z > 0.5$ (Blakeslee et al., 2003).

Fig. 2 shows an HST/ACS grism spectrum of an SN Ia at $z \sim 1.3$ (kindly provided by Adam Riess) obtained in 4 h. The broad features in the spectrum are well matched by an SN Ia template spectrum; the same features are not seen in a 4-h spectrum of clearly poorer quality obtained with the Keck telescope. Simply integrating the grism spectra over broad wavelength intervals provides broad-band photometry. The wavelength coverage of 0.9 μm < λ < 1.7 μm can be roughly divided into 4 contiguous $R \sim 5$ bands.

Fig. 3 shows the resulting S/N in these bands. Given the native dispersion in the peak luminosity of SN Ia of 0.1 mag, again 4-h exposures are sufficient to obtain adequate broad-band photometry at all redshifts. In practice the intervals of the bands would track the SN Ia redshift, completely eliminating the need for k-corrections. The time required to obtain a given S/N for the bandpasses shown in Fig. 3 can be compared directly to that required for traditional direct images obtained in the same $R = 5$ bands. Intriguingly, while the grism is on average ~4× slower, since one obtains all four bands in a single exposure, a grism camera is roughly equivalent to the traditional approach of imaging the field in one filter at a time.

The dataset collected by DESTINY will also be profoundly valuable, at no additional mission

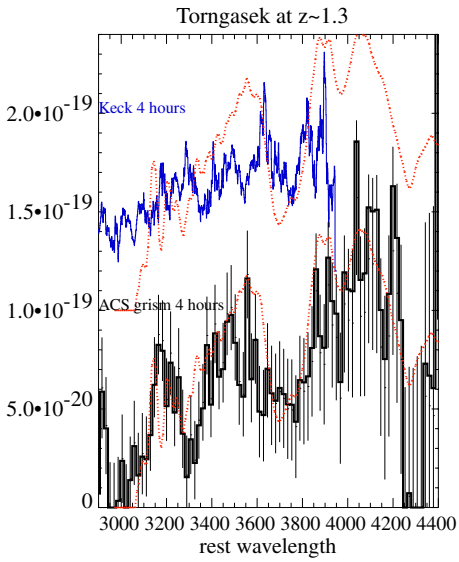

Fig. 2. Spectra on an SN Ia at $z \approx 1.3$, comparing 4-h exposures with the Keck (top) and HST/ACS grism (bottom). A template spectrum is also shown fitted to both observations. (Figure kindly provided by Adam Riess.)

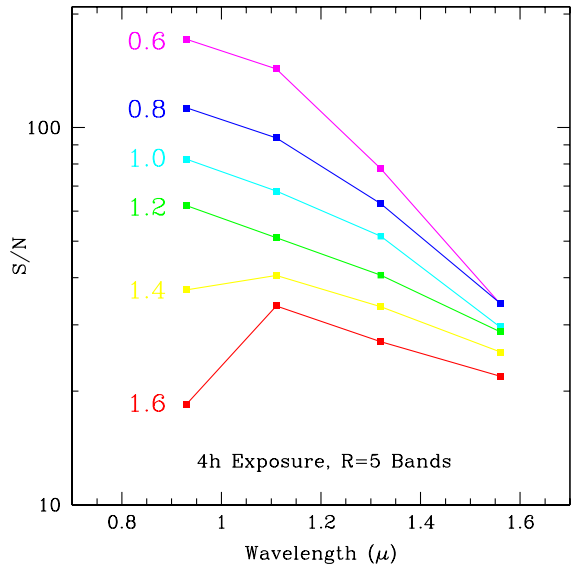

Fig. 3. S/N in 4 $R = 5$ continuous bandpasses. The grism spectra shown in Fig. 1 have been integrated to produce broad-band spectrophotometry. As before results are shown for redshifts 0.6, 0.8, 1.0, 1.2, 1.4, and 1.6 top-to-bottom.

cost, for a wide range of other interesting problems, many of which represent parallel investigations into the nature of dark energy. After 2 years, we will have NIR $R \sim 75$ time-sampled spectra for all objects in a 7.5 square-degree region of sky. Total exposure time will be 500+ hours, with implied 5σ depths in $R = 5$ broad bandpasses of 10 nJy. Of particular interest for investigating dark energy, we should be able to identify and characterize rich clusters of galaxies at $z > 1$. Forming galaxies at $z > 5$ as well as nearby brown dwarfs should also be readily detected.

References

Aldering, G. et al. 2004, astro-ph/0405232, PASP, submitted.
Blakeslee, J.P. et al., 2003. ApJ 589, 693.
Giavalisco, M., Sahu, K., Bohlin, R. 2002. STScI-ISR/WFC3-2002-12.
Hamuy, M., Pinto, P.A., 2002. ApJ 566, 63.
Linder, E.V., Huterer, D., 2003. PRD 67, 1303.
Nugent, P., Kim, A., Perlmutter, S., 2002. PASP 114, 803.
Percival, W.J. et al., 2002. MNRAS 337, 1068.
Perlmutter, S. et al., 1999. ApJ 517, 565.
Riess, A. et al., 1998. AJ 116, 1009.
Tonry, J.L. et al., 2003. ApJ 594, 1.

Available online at www.sciencedirect.com
SCIENCE DIRECT®
New Astronomy Reviews 49 (2005) 360–365
New Astronomy Reviews
www.elsevier.com/locate/newastrev

Dark energy and cosmic sound

D.J. Eisenstein

Steward Observatory, University of Arizona, Tucson, AZ 85721-0065, United States

Available online 19 October 2005

Abstract

I describe how acoustic oscillations imprinted into the late-time correlations of galaxies by baryonic physics at the epoch of recombination can be used as a cosmological standard ruler. Measurements of this length scale by large galaxy surveys would allow us to compute the angular diameter distance to and Hubble parameter at the redshifts of the survey. This in turn offers a robust way to measure the acceleration of the universe. I briefly present calculations of the statistical performance from baseline surveys; full details of the methods and results are available in Seo and Eisenstein [ApJ, 598 (2003) 720]. I discuss the advantages and disadvantages of the acoustic oscillation method relative to other dark energy probes.
© 2005 Published by Elsevier B.V.

Contents

1. General remarks . . . 360
2. Sound in space? . . . 363
3. Pros and cons . . . 364
Acknowledgments . . . 365
References . . . 365

1. General remarks

The unexpected late-time acceleration of the expansion of the universe (Riess et al., 1998; Perlmutter et al., 1999) ranks as one of the top problems in modern cosmology and physics. Sorting between the myriad proposed solutions will require observations of very high precision, as the differences under debate are typically at the percent level (see Fig. 1). The possibility of

E-mail address: deisenstein@as.arizona.edu.

1387-6473/$ - see front matter © 2005 Published by Elsevier B.V.
doi:10.1016/j.newar.2005.08.005

systematic error, due to the considerable level of precision required, the level of theoretical modeling for interpretation, and/or the need to compare observations at very different redshifts, leads us to seek multiple high precision probes of the cosmological expansion.

Baryonic acoustic oscillations imprinted into the galaxy power spectrum offer a new route to the measurement of dark energy (Eisenstein et al., 1998; Eisenstein, 2003; Blake and Glazebrook, 2003; Linder, 2003; Hu and Haiman, 2003; Seo and Eisenstein, 2003). Prior to the epoch of recombination, the enormous pressure of the cosmic microwave background (CMB) photons opposes cosmological collapse, leading to the establishment of acoustic modes (Peebles and Yu, 1970). When the baryons and electrons combine into atoms, the photons are released from the plasma, but both components are left in a perturbed state with a preferred length scale, namely the distance that a sound wave could travel in the age of the universe to that point. In the case of the photons, the acoustic mode history is manifested as the high-contrast Doppler peaks in today's temperature anisotropies (e.g., Bennett et al., 2003). However, the baryons are left in a similar state that, when mixed with the non-oscillating cold dark matter perturbations, leaves a small residual imprint in the clustering of matter at late times (see Eisenstein and Hu, 1998 for more discussion of this). Fig. 2 shows the resulting low-redshift power spectrum as a function of baryon fraction.

The preferred length scale of the acoustic oscillations, roughly 140 Mpc with overtones, depends only on the time scales of the early universe and the speed of sound in the baryon-photon plasma. Both of these can be measured to high precision from the details of the acoustic peaks in the CMB. With this, one can compute the length scale to better than 1% accuracy. The remaining problem is to measure it at low redshift.

In recent times, the oscillations appear as a faint set of wiggles in the power spectrum. The features are best measured at wavenumbers between $k = 0.05$ and $k = 0.30h$ Mpc^{-1} Fig. 2. On smaller scales, the amplitude is sharply reduced due to Silk damping. Hence, one requires surveys that can measure structure on 50 Mpc scales to very high accuracy. This pushes one to surveys with sizes of order 1 Gpc^3 and a million galaxies (Eisenstein, 2003).

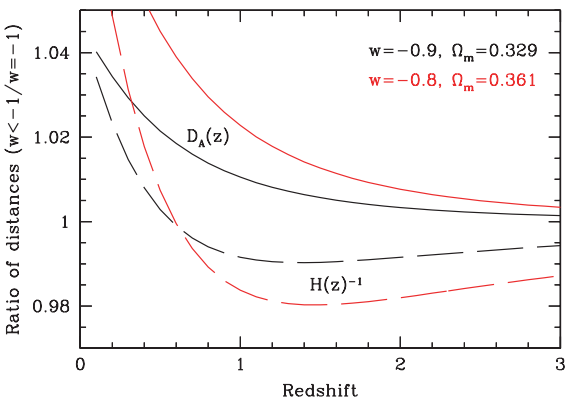

Fig. 1. The relative change in the angular diameter distance D_A and the Hubble parameter $H(z)$ for models with $w \neq -1$, as compared to one with $w = -1$. Here, we hold the quantities $\Omega_m h^2$ and the angular diameter distance to $z = 1000$ fixed, as these leave the CMB sky nearly unchanged. Distinguishing $w = -0.9$ from $w = -1$ requires percent-level precision. Note the considerable value that a very high precision measurement of H_0 would have!

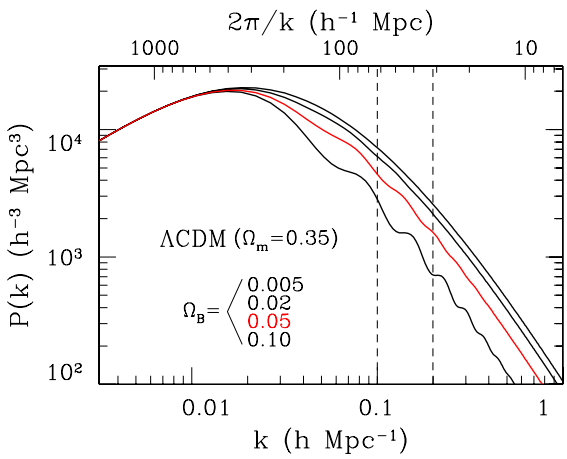

Fig. 2. The linear-regime matter power spectrum as a function of baryon fraction. Pure cold dark matter produce smooth power spectra, such as the top line. As baryons are added at fixed Ω_m, the strength of the acoustic oscillations increases and there is an overall suppression of power on small scales. From Eisenstein and Hu (1998).

One measures the oscillations along and across the line of sight as preferred scales in redshift and angular separations. Taking the ratio of these to the known physical scale allows one to measure the Hubble parameter $H(z)$ and the angular diameter distance $D_A(z)$, respectively, where z is the redshift of the survey (Eisenstein, 2003). Unlike the Alcock and Paczynski (1979) method, we know the length of the standard ruler, and so we can measure these two quantities directly rather than merely the product $H^{-1}D_A$.

In Seo and Eisenstein (2003), we presented calculations of the statistical precision available to a set of fiducial galaxy redshift surveys. We considered the Sloan Digital Sky Survey luminous red galaxy (Eisenstein et al., 2001) sample at $z \approx 0.3$ and two hypothetical higher redshift surveys: 1000 square degrees over the range $0.5 < z < 1.3$ with 900,000 galaxies and 150 square degrees over the range $2.5 < z < 3.5$ with 500,000 galaxies. An example of the type of power spectra that could be extracted from such a survey is shown in Fig. 3; one sees that the acoustic oscillations are easily detected and their scale could plausibly be measured. The resulting fractional precisions on $H(z)$ and $D_A(z)$ for these surveys are shown in Fig. 4. We then propagated these measurements to constraints on a dark energy model with equation of state $w = w_0 + w_1 z$. These constraints and those from a representative next generation supernova experiment are shown in Fig. 5.

Further details and results are described in Seo and Eisenstein (2003). In addition Blake and Glazebrook (2003), Hu and Haiman (2003), and Linder (2003) present similar analyses. While these works differ in certain aspects of methodology and scope, I think that they are all essentially in agreement.

Like any method, one must be wary of systematic errors that could affect the measurements. In the case of galaxy clustering, the major astrophysical issues are non-linear structure formation, redshift distortions, and galaxy clustering bias. All of these affect the clustering of galaxies on very large scales. However, none of them are show-stoppers because the acoustic oscillations manifest themselves as a preferred scale or equivalently as a harmonic sequence in power. Non-linear structure, redshift distortions, and bias do not treat $100h^{-1}$ Mpc differently from 90 or 110; their natural scales are much smaller, e.g., the size of the

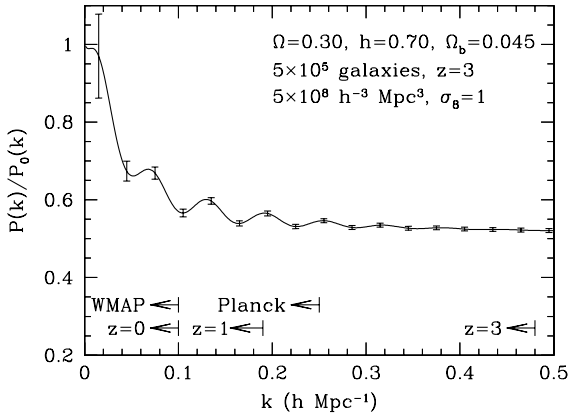

Fig. 3. The matter power spectrum for an $\Omega_m = 0.3$, $\Omega_b = 0.045$, $h = 0.7$ cosmology divided by the power spectrum for the same model but with $\Omega_b = 0$. The acoustic oscillations are clearly visible. Overplotted are the predicted statistical errors (Tegmark, 1997) for a redshift survey at $z = 3$ covering 150 square degrees and $5 \times 10^8 h^{-3}$ MPc^3 with 500,000 galaxies. The resulting number density of such galaxies is comparable to that of the Steidel et al. (1996) sample. At the bottom is the linear regime reach for galaxy surveys at different redshifts, along with the CMB satellites WMAP and Planck.

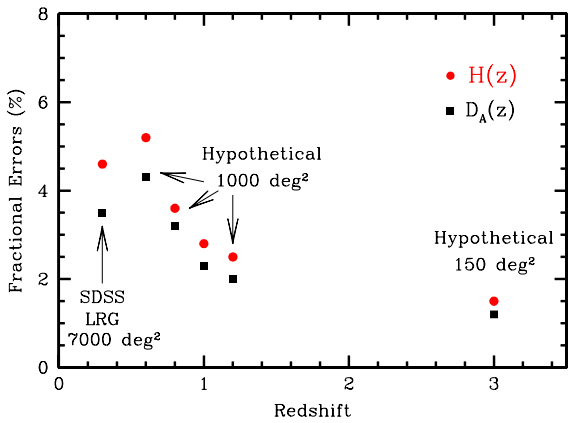

Fig. 4. The predicted 1–σ fractional errors on the Hubble parameter $H(z)$ and the angular diameter distance $D_A(z)$ from the fiducial surveys. The improvement as one goes to larger redshift is a combination of being able to use higher harmonics of the acoustic oscillations because of the receding non-linear structure scale and the variations in the assumed survey volumes. The key point is that high precision is possible, given large enough surveys. From Seo and Eisenstein (2003).

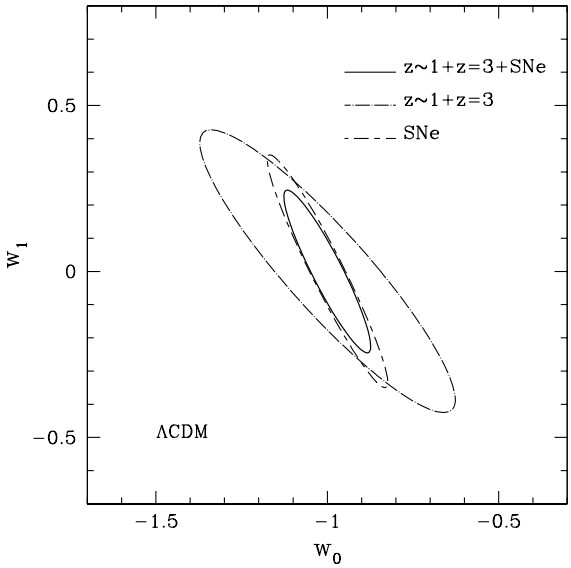

Fig. 5. The constraints on the dark energy equation of state model $w_0 + w_1 z$ when perturbing around a fiducial model of a cosmological constant. Shown are the results from the galaxy surveys (also including a Planck-style CMB experiment), from a supernova experiment, and from a combination of all. The supernova experiment was assumed to produce 1% errors in D_A for 16 independent redshift bins from $z = 0.05$ to 1.7, with a 5% overall uncertainty in the distance scale (i.e., H_0). Given that this reflects a relative calibration between low and high redshift of better than 0.01 mag, we feel that this is a good representation of a SNAP-level supernova experiment (Aldering et al., 2002). For the cosmological constant fiducial model, the supernova measurements are outperforming the galaxy surveys, although the combination is helpful. Fiducial models with $w > -1$ produce smaller errors for both experiments, with a more favorable outcome for the galaxy survey. From Seo and Eisenstein (2003).

largest halos and infall regions. Therefore they will affect the amplitude of the large-scale power spectrum, probably in a mildly scale-dependent way, but they do not create or shift the oscillations. This point was investigated numerically at $z = 0$ by Meiksin et al. (1999) and we are now studying higher redshifts (Seo and Eisenstein, 2004).

Imaging surveys using photometric redshift can recover a portion of the acoustic oscillation signature (Seo and Eisenstein, 2003). Redshift precision of only $\sigma_z = 0.04(1 + z)\,(1 - \sigma)$ is sufficient to keep the acoustic oscillations in phase from the front of a photo-z slice to the back. That means that one can measure the angular diameter distance. However, the errors per solid angle of sky are larger, so one must cover 10–20 times more sky than the spectroscopic equivalent. Of course, such surveys are within the reach and aspirations of facilities such as Pan-STARRS (http://pan-starrs.ifa.hawaii.edu) and LSST (http://www.lssto.org). Redshift precision of $\sigma_z = 0.003(1 + z)$ is required to resolve the acoustic peaks along the line of sight, so $H(z)$ cannot be measured directly with photometric redshift surveys, although a grism could reach this level of redshift precision. Cooray et al. (2001) discuss the use of photometric redshift surveys to constrain $D_A(z)$ by other signatures in the angular power spectrum.

2. Sound in space?

As this was a meeting on wide-field imaging from space, the question of whether the acoustic oscillation method requires space is apropos. Of course, at many redshifts, imaging (for the purpose of detection and colors, not morphology) and spectroscopy from the ground are straightforward.

However, there are some ways in which a space mission could be of great benefit. Most obviously, the redshift range between 1.4 and 2.0 is spectroscopically challenging from the ground due to the lack of strong features in the optical window. Recent ground-based work has had success at these redshift (e.g., Steidel et al., 2004; Abraham et al., 2004), but given that one needs of order a million redshifts, the integration times might be prohibitive.

Less obvious, the spectroscopic demands are large enough that preselection by photometric redshifts may be required to select the rare high-redshift luminous galaxies from the more numerous lower redshift galaxies. For the redshift range between 1.2 and 2.0, this may require near-infrared imaging data as the 4000 Å break shifts out beyond 1 μm. Getting the requisite deep IR imaging over 1000s of square degrees would certainly be easier in space.

One sees here that the advantage of space is particularly in the $1.4 < z < 2.0$ redshift range. The acoustic oscillation method, however, does not require continuous redshift coverage. Whether or not this redshift range is essential to the separation of plausible dark energy models is an open question. As the acoustic oscillation method is reaching

full form by $z \approx 1.5$, as the non-linear scale is finally small enough to allow us to recover several peaks, and dark energy is growing ever more subtle at higher redshifts, it is possible that a concerted effort at $z = 2$ is in fact the redshift of choice.

Slitless spectroscopy in space offers the possibility of huge multiplexing. Karl Glazebrook's talk at this conference described an ambitious plan in this regard. With ground-based programs discussing 1000 square degrees as a difficult goal for the next 10 years, the idea of going to 10,000 square degrees with a simple space mission may be compelling.

If one abandons spectroscopy in favor of photometric redshifts, near-infrared data is likely invaluable for the redshift range between 1.2 and 2.5 if one is to reach the required 4% goal. The panoramic option within the SNAP mission would be phenominal for acoustic oscillation science, as it would have complete photometric redshift coverage and sufficient depth to recover the oscillations out to $z \approx 4$. A ground-based survey such as LSST would have the depth, but it is not clear that photometric redshift accuracy would be sufficient over the full redshift range.

All of these comparisons of ground and space require detailed assessments of the ground-based prospects and the reach of particular surveys in the dark energy model spaces. This is on-going work.

3. Pros and cons

More generally, it is worth reviewing the advantages and disadvantages of the acoustic oscillation method relative to other methods. First, on the plus side, the acoustic oscillation method is a geometrical large-angle standard ruler test; it is not sensitive to dust or any form of small angle aberration. The ruler itself is based on clean linear-regime physics from the recombination epoch, which is very sensitively probed by the CMB. It is difficult to imagine astrophysical systematic effects on these scales that could confuse the measurement.

The acoustic oscillation method does not require highly precise measurements. Doing basic galaxy photometry and spectroscopy is a well-understood process, even at the required redshifts; we need only do it in a highly multiplexed, wide-field manner. It is not necessary to work with L^* galaxies; one need only reach densities 3–10% of this, and so one can choose to work with brighter or otherwise more convenient galaxies. Heroic levels of relative photometry, e.g., sub-percent, are not required for a spectroscopic sample, although a photometric redshift approach would stress the photometric accuracy more. Compared to the photometric precision required of supernovae and the image fidelity required of weak lensing, the acoustic oscillation method is straightforward.

However, one does need a large number of these "simple" observations over a large amount of sky. Existing instrumentation on 8-m class telescopes is not well-positioned to perform 1000 square degrees of spectroscopy. New instrumentation and a significant investment of telescope time would be required. An instrument such as KAOS (see http://www.noao.edu/kaos for an extensive description), with ~4000 fibers over a 1.5° field, would bring such surveys within reach. Of course, such surveys would have other science applications of their data, but in addition one should consider multiplexing multiple independent science programs on the same part of sky. It is likely that telescope pointings, not raw numbers of spectroscopic targets, are the limiting resource.

Because the method does depend upon calibration of the sound horizon standard ruler with the CMB anisotropies, there is some model dependence. However, these possibilities are more limited than one might think (Eisenstein and White, in press), partly because the CMB is so sensitive to anomalies at $z > 1000$ and partly because of the structure of the degeneracies.

The acoustic oscillation method works better at $z > 1$ and can carry distance measurements out to $z \sim 3$ or higher. It can directly measure $H(z)$, which is one derivative closer to $w(z)$ than D_A and the luminosity distance. These aspects mean that the acoustic oscillation method could be sensitive to unexpected properties of dark energy. On the other hand, the reduced performance at $z < 1$ is a disadvantage if the dark energy is close to the standard cosmological constant, because in these cases nearly all of the anomalous behavior is at low redshift. If the dark energy is close to a

cosmological constant, then methods involving weak lensing, cluster counting, and supernovae, all of which can or must place their attention at $z < 1$, are at a numerical advantage. As we have been surprised by the acceleration once and have no good theory for the dark energy, I regard the reach to $z = 3$ as an important advantage of the acoustic oscillation method, but of course the universe may turn out to be more boring.

In conclusion, the acoustic oscillation method is a robust method offering precision comparable to that of other methods. The simplicity of the physics and the individual measurements as well as the ability to measure the expansion of the universe at higher redshift are key advantages. The primary hurdle at present is the development of new wide-field, high multiplex spectroscopic facilities.

Acknowledgments

D.J.E. thanks Hee-Jong Seo for her collaborations on these topics. D.J.E. is supported by Grant AST-0098577 from the National Science Foundation and by an Alfred P. Sloan Research Fellowship.

References

Alcock, C., Paczynski, B., 1979. Nature 281, 358.
Abraham, R.G. et al., 2004. AJ 127, 2455.
Aldering, G., et al., 2002, SPIE, 4835, in press [astro-ph/0209550].
Bennett, C. et al., 2003. ApJS 148, 1.
Blake, C., Glazebrook, K., 2003. ApJ 594, 665.
Cooray, A., Hu, W., Huterer, D., Joffre, M., 2001. ApJ 557, L7.
Eisenstein, D.J., Hu, W., 1998. ApJ 496, 605.
Eisenstein, D.J., Hu, W., Tegmark, M., 1998. ApJ 504, L57.
Eisenstein, D.J. et al., 2001. AJ 122, 2267.
Eisenstein, D.J., 2003, in: Dey, A. (Ed.), Wide-field Multi-Object Spectroscopy, ASP Conference Series.
Eisenstein, D.J., White, M., in press.
Hu, W., Haiman, Z., 2003. PRD 68, 3004.
Linder, E.V., 2003. PRD 68, 3504.
Meiksin, A., White, M., Peacock, J.A., 1999. MNRAS 304, 851.
Peebles, P.J.E., Yu, J.T., 1970. ApJ 162, 815.
Perlmutter, S. et al., 1999. ApJ 517, 565.
Riess, A.G. et al., 1998. AJ 116, 1009.
Seo, H., Eisenstein, D.J., 2003. ApJ 598, 720.
Seo, H., Eisenstein, D.J. 2004, in: Sidney Wolff, (Ed.), Observing Dark Energy, ASP Conference Series.
Steidel, C.C., Giavalisco, M., Pettini, M., Dickinson, M., Adelberger, K.L., 1996. ApJ 462, L17.
Steidel, C.C., Shapley, A.E., Pettini, M., Adelberger, K.L., Erb, D.K., Reddy, N.A., Hunt, M.P., 2004. ApJ 604, 534.
Tegmark, M., 1997. PRL 79, 3806.

Available online at www.sciencedirect.com
SCIENCE DIRECT®
New Astronomy Reviews 49 (2005) 366–373
New Astronomy Reviews
www.elsevier.com/locate/newastrev

Why we need wide-field imaging from space to understand galaxy formation

R.S. Somerville

Space Telescope Science Institute, 3700 San Martin Dr., Baltimore, MD 21218, United States

Available online 23 September 2005

Abstract

Space-based imaging with the Hubble Space Telescope has demonstrated the many advantages of viewing galaxies from outside the Earth's atmosphere. Hubble has shown us the amazing complexity of galaxies in the nearby and high redshift universe in exquisite detail. However, because of the limited areas surveyed, the sample sizes remain relatively small. In order to go beyond "butterfly collecting" and unravel the underlying physical processes that shape galaxy formation, we need samples that span a broad range of environment as well as cosmic time, and that are large enough to sub-divide in many different ways. I discuss three broad science topics that would benefit from wide-field space-based surveys: (1) measuring the stellar mass assembly history as a function of morphological type and environment and directly constraining the galaxy merger rate; (2) understanding the connection between the processes that regulate star formation on sub-galactic scales and the overall global trends in star formation activity; (3) understanding the relationship between "normal" galaxies and AGN, and the processes that regulate black hole feeding and growth. I present quantitative predictions, based on a simple halo occupation model, for the field sizes needed to reduce the error due to field-to-field variance to less than 10%. For many of the populations of interest, this will require fields of ~10–100 square degrees.
© 2005 Elsevier B.V. All rights reserved.

Contents

1. Introduction . . . 367
2. When and how were galaxies assembled? . . . 368
3. The why of the cosmic star formation history . . . 369
4. The galaxy-black hole connection . . . 370
5. How wide is wide enough? . . . 370
6. Summary . . . 372

E-mail address: somerville@stsci.edu.

1387-6473/$ - see front matter © 2005 Elsevier B.V. All rights reserved.
doi:10.1016/j.newar.2005.08.006

Acknowledgments 372
References 372

1. Introduction

In every science, there is a progression from quantification, to drawing connections, to understanding an underlying pattern. In biology, we have moved from collecting butterflies to Darwin's Finches, and ultimately to the discovery of DNA. Galaxy formation is currently somewhere in between butterfly collecting and modern genetics. The steps that we astrophysicists need to undertake in this progression might be broadly summarized, thus:

1. Accurately quantify the galaxy population and its sub-populations (i.e., measure distribution functions like luminosity functions, mass functions, star formation rate functions, etc.).
2. Accurately characterize the scaling relationships obeyed by galaxies (Tully-Fisher, color-magnitude, size-luminosity, mass-metallicity, etc.).
3. Characterize the relationship between dark matter and galaxies.
4. Understand and isolate the physical processes responsible for the above observed relationships in the context of a comprehensive theory for structure formation.

In order to achieve the lofty goal of (4), we will need to obtain the characterizations 1–3 as a function of cosmic time and large scale environment, and sub-divided in many ways (e.g., luminosity functions as a function of galaxy type, color, size, etc.). The insights gleaned from recent large surveys of nearby galaxies such as the Sloan Digital Sky Survey have illustrated the power of large samples for uncovering patterns – indeed, the progress made in achieving goals 1–3 for the nearby galaxy population in the past few years is extremely impressive. Large numbers of objects are needed so that one can sub-divide the sample in many ways in order to disentangle the complex interplay of various properties, such as luminosity or mass, internal structure (morphological type), spectrophotometric properties (color or star formation history), and large scale environment. One needs to probe large volumes in order to overcome field-to-field variance and ensure that one samples a variety of environments, from superclusters to super-voids, and in order to discover rare objects.

The availability of moderately wide-field, deep optical imaging from the Advanced Camera for Surveys (ACS) on the Hubble Space Telescope (HST), along with complementary ground-based imaging and spectroscopy, has allowed us to begin to tackle these problems for the high redshift galaxy population. However, these studies are still profoundly hampered by small number statistics and uncertainties due to field-to-field variance, and this will almost certainly still be the case at the end of Hubble's lifetime.

For many applications in galaxy formation, there are several advantages of going to space. These include: the high spatial resolution and small, stable point-spread function over large areas; the low background especially in the Near Infra-red; and the high Strehl ratio. These advantages enable one to resolve objects that are physically small, study fine morphological details, detect distant objects (which are both small and faint), and study objects with large contrasts such as a faint host galaxy with a bright Active Nucleus. The lower background means that even in the optical, a 2-m telescope in space (e.g., Hubble) is competitive with 8–10 m class telescopes on the ground. Fig. 1 shows an image of the same field obtained with HST as part of the GOODS survey, and from the ground with the Suburu telescope. One can see the richness of detail in the galaxy population that would be missed in a ground-based image.

As others at this meeting have covered some of the most obvious galaxy-related "killer apps" for future space telescopes with wide-field imaging capabilities, such as gravitational lensing and the detailed reconstruction of star formation histories for nearby galaxies from resolved stellar popula-

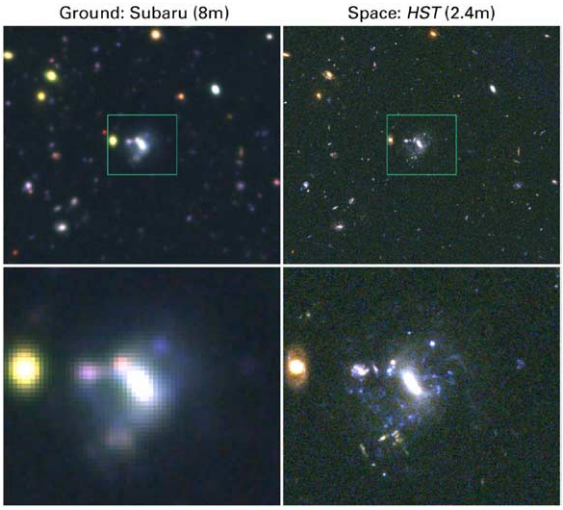

Fig. 1. Ground vs. space-based imaging of part of the GOODS field from Suburu (8 m; left) and HST (2 m; right). This figure illustrates the importance of very deep high-resolution imaging for probing the complex environments of galaxies at high redshift. Figure courtesy of L. Moustakas.

tion studies, I will mention here a few other topics related to galaxy formation that I believe will still be of interest at the end of Hubble's lifetime. Even if these particular topics are considered well-understood by then, I hope to illustrate a general principle of scientific inquiry that will let us move from butterfly collecting towards sequencing galactic DNA.

2. When and how were galaxies assembled?

A generic prediction of the hierarchical paradigm of structure formation is that massive objects should be less abundant in the past. While, within a given cosmological model, robust predictions can be made for the assembly history of the dark matter component, the assembly of *galaxies* depends on the complex and poorly understood baryonic physics of cooling, star formation, feedback, etc. A detailed census of galaxies as a function of mass over cosmic history therefore provides powerful constraints on the most uncertain aspects of galaxy formation theory. There has been a great deal of activity recently directed towards this goal, and various measurements of the stellar mass density out to $z \sim 3$–4 have been presented in the literature (see, e.g., Dickinson et al., 2003; numerous updated estimates have been published recently that I will not attempt to compile here). These measurements are typically based on galaxies detected in the rest-frame optical or at longer wavelength, with stellar mass estimates obtained by exploiting the correlation between mass-to-light ratio and color based on stellar population models. In some cases, a single color is used to estimate the stellar mass-to-light ratio (Bell and de Jong, 2001), while in others, simple star formation histories are fit to multi-band photometry (e.g., Papovich et al., 2001). There are well-known uncertainties in the masses due to the potential complexity of real star formation histories (especially recent bursts), and the degenerate effects of metallicity, dust, etc. The stellar Initial Mass Function introduces an additional systematic uncertainty in the mass-to-light ratio.

In order to obtain a complete census of galaxies at $z \sim 2$ (apparently the peak of star formation and quasar activity) and above, we require deep Near IR imaging over large areas (see Section 5 for estimates of the field sizes needed to overcome cosmic variance). Imaging with Spitzer's IRAC will greatly improve the present situation, but IRAC imaging of high redshift galaxies suffers from problems with deblending because of Spitzer's coarse resolution, and again it is unlikely that large enough fields will be imaged to the required depth to probe sub-L_* galaxies above $z \sim 2$. Some of this work can be done with new wide-field, high efficiency NIR cameras on ground based telescopes, but again, because of the high background in the NIR it will be a challenge to achieve the required combinations of area and depth, and one runs the risk of blending sources or missing small objects that are not resolved. Space-quality imaging is needed in order to measure the growth of stellar mass as a function of galaxy type, for example to measure the mass growth of stellar bulges, which may be directly connected with the growth of super-massive black holes. We also want to measure the build-up of stellar mass via mergers (another smoking gun of hierarchical structure formation). This will require detection of fine,

low contrast features such as tidal tails, which will be possible only with at least HST-like resolution.

The errors in the stellar mass budget at high redshift are currently dominated by: (a) uncertainties in the stellar mass estimates; (b) cosmic variance; (c) incompleteness. The stellar mass estimates could be put on a much more stable footing by combining total mass estimates from gravitational lensing (both statistically, from galaxy–galaxy lensing and for individual strong lens systems) with dynamical information (e.g., velocity dispersions) and cold gas measurements (e.g., from ALMA). A wide-field space telescope could simultaneously provide both the lensing data and the deep NIR imaging. Samples over fairly large contiguous fields will also allow us to measure the build-up of stellar mass as a function of large-scale density and to determine whether stellar mass assembly occurs earlier in overdense regions, as predicted by CDM. Coupled with reconstructions of the total (dark plus baryonic) mass density field from weak lensing, this will allow us to directly measure the "bias function", or the relationship of stellar mass to dark matter, over a large fraction of cosmic history.

3. The why of the cosmic star formation history

It is now well-established that the global star formation rate density (SFRD) peaked at a redshift of $z \sim 2$ or above, and has been dropping steadily ever since. The most recent results from GALEX indicate that the SFRD today is about a factor of five lower than it was at $z \sim 1$ (Schiminovich et al., 2005). These results beg the question of *why* this dramatic decline occurred, and why it began when it did. One can think of various possible explanations, such as:

1. The consumption rate of gas overtook the replenishment by new accretion. The decline is simply a result of a diminishing fuel supply.
2. Disks are smaller and denser at high redshift. Therefore, if the local Kennicutt relation between density and star formation rate still holds, star formation was more efficient at high redshift.
3. Galaxy–galaxy mergers were more common in the past, and these interactions triggered highly efficient bursts of star formation.

One can imagine other mechanisms, of course – such as galaxies falling into high temperature groups and filaments that strip or evaporate their gas. Factors such as metallicity and the changing UV background may play a role as well. With deep wide-field HST imaging, we can now begin to directly test these different scenarios. For example, Barden et al. (2005) found that the radii of disk galaxies at fixed stellar mass were nearly the same at $z \sim 1$ as they are today. This suggests that a drastic change in the *internal density* of galactic disks is unlikely to be responsible for the dropping star formation rate, although these measurements do not directly probe the size of the *gaseous* disks. On the other hand, Wolf et al. (2005) and Bell et al. (2005) found that only about 20–30% of the star formation at $z \sim 0.7$ is associated with galaxies that were obviously undergoing strong interactions, suggesting that the dropping merger rate is also a relatively minor factor (unless mergers of much smaller objects that did not produce obvious morphological distortions triggered significant amounts of star formation). Jogee et al. (2004) showed that the fraction of luminous spiral galaxies with large, strong bars was about the same at $z \sim 1$ as it is today. The results mentioned above are all based on the GEMS survey (Rix et al., 2004), a two-filter 0.25 square degrees survey with the ACS on HST. While GEMS is the largest space-based survey to have been analyzed so far, the number statistics are still barely adequate and field-to-field variance is a serious problem.

In order to better understand the forces that regulate or stimulate star formation in galaxies, it will be crucial to have high-resolution imaging (probing physical scales of hundreds of pc) in the rest optical and UV, as well as maps of the gas density, which ALMA will provide. In galaxies too distant to resolve individual stars, we can still obtain estimates of 'pixel-by-pixel' star formation histories, mapping the formation history as a function of spatial location within the object. Such studies with HST have revealed that even tiny dwarf galaxies have complex and varied star formation histories, in

many cases showing spatial variation across the galaxy, perhaps indicating the occurrence of a merger or some sort of local instability that triggered star formation.

4. The galaxy-black hole connection

The discovery of solid evidence for the presence of supermassive black holes in the centers of most or all galactic spheroids, as well as the realization that the mass of the black hole is tightly correlated with the mass of the spheroid, constitutes one of the most profound discoveries in astronomy. HST has played a critical role in these efforts, as well as in beginning to characterize the galaxies that host the black holes in the universe that are actively accreting, i.e., AGN and quasars. There is still no consensus on what physical process "activates" a black hole, and why some galaxies contain active holes while others are dormant. It has often been suggested that mergers and/or nuclear bars play a role, but the observational picture is far from clear. Recently, it was shown that in the nearby universe, weak AGN seem to reside in an unusual population of galaxies that are massive, bulge dominated, and contain *young* stellar populations (Kauffmann et al., 2003). Even more recent work by the GEMS team suggests that AGN at redshift $z \sim 0.7$ also seem to be located in massive, spheroid-dominated galaxies with unusually blue colors (Sánchez et al., 2004). The samples of high redshift AGN with Hubble imaging are still pathetically small, however (for example, the Sánchez et al. GEMS sample contains 15 objects).

AGN are rare, especially in the nearby universe, and studying a faint, diffuse host in the glare of the active nucleus is challenging even with the resolution and high Strehl ratio achievable from space. Adaptive optics may make some progress in this area (going to the NIR is helpful as the AGN are generally fainter there relative to the host), but there is no question that wide-field imaging from space would be the most efficient way to discover and characterize these objects. Characterizing the galaxies and environments that host active nuclei is not only of interest for understanding the physical processes that drive black hole growth – it is now widely believed that the influence of AGN on the ISM, IGM and ICM may be a crucial piece of missing physics in galaxy formation modelling. The energy injected by the AGN could very plausibly heat or drive out the gas from a forming galaxy, halting star formation and perhaps even shutting down cooling flows in groups and clusters. This process is now popularly invoked as a possible mechanism that could solve the so-called "over-cooling problem" and explain the observed bimodality of galaxy colors (Croton et al., in preparation, Somerville et al., in preparation).

5. How wide is wide enough?

By the end of Hubble's lifetime, it is very likely that the volume and number of independent sightlines probed by deep fields such as GOODS, GEMS, COSMOS, and the Extended Groth Strip (EGS) will still be insufficient to overcome the uncertainties due to field-to-field variance that have already been noted. It is even more unlikely that space-quality imaging of large enough contiguous areas will be available to allow one to effectively probe the effects of environment on high redshift galaxy properties. Here I give some estimates, based on a simple clustering model within the ΛCDM paradigm, that address the most basic question that we might want to ask with respect to field-to-field variance: how large an area do we need in order to reduce the uncertainty on *object counts* from field-to-field variance to less than 10%?

First a few words about the model. I use a combination of linear theory on very large scales and fits to numerical dissipationless simulations on smaller scales to compute the clustering properties of dark matter in a ΛCDM universe with the "concordance" values of the cosmological parameters ($\Omega_m = 0.3$, $\Omega_\Lambda = 0.7$, $H_0 = 70\ \mathrm{km\ s^{-1}\ Mpc^{-1}}$, $n_s = 1$, $\sigma_8 = 0.9$). I then use the now rather standard analytic formalism presented by Mo and White (1996) to compute the clustering of dark matter halos relative to the dark matter (in fact I use the more accurate model of Sheth and Tormen, 1999), and assume

that galaxies populate dark matter halos according to a "Halo Occupation Model". Details of the specific approach can be found in Moustakas and Somerville (2002, MS02). For simplicity, I consider two kinds of populations: galaxies that are *unbiased* with respect to the dark matter at each redshift ($b = 1$), and rare, clustered galaxies. Optically selected $L \sim L_*$ galaxies at $z = 0$ have $b \sim 1$ (e.g., Zehavi et al., 2002), as do star forming galaxies at $z \sim 1$ (e.g., Coil et al., 2004). In general, however, luminous galaxies at high redshift tend to be positively biased with respect to

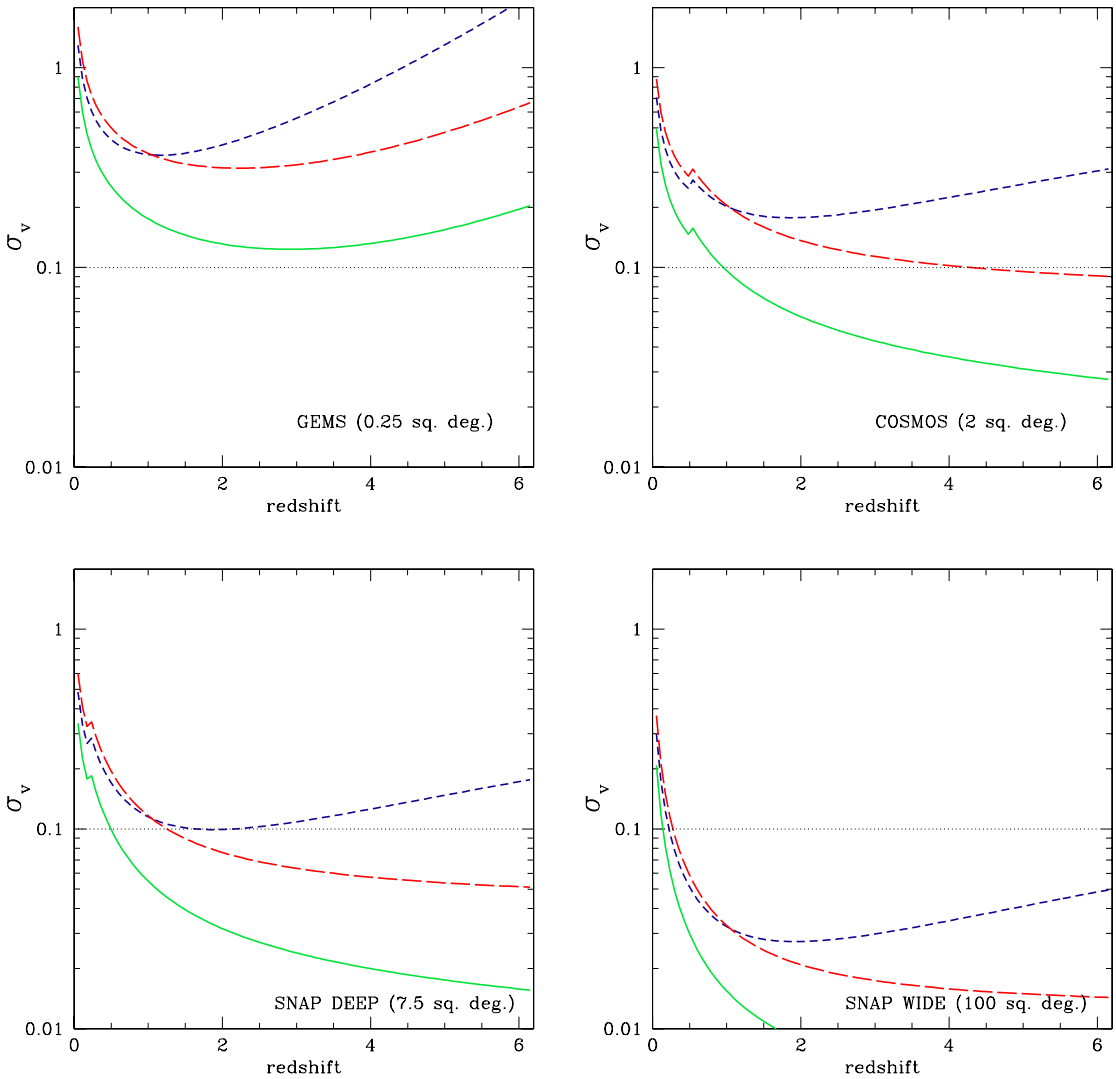

Fig. 2. Fractional error due to field-to-field variance as a function of redshift for galaxies that cluster like the dark matter ($b = 1$, solid line), and for strongly clustered galaxies (long and short dashed lines). The parameters of the halo occupation model for the "clustered" galaxies are fixed to match the number density and clustering of early type galaxies at $z = 0$ (see Moustakas and Somerville, 2002 for details). The short dashed line shows a model in which the parameters of the halo occupation function are assumed to remain constant with redshift. The long dashed line shows a model in which the minimum mass of halos that can host these galaxies is adjusted in order to keep their number density constant at all times. Results are shown for the GEMS survey (0.25 square degrees), the COSMOS survey (2 square degrees), and the planned SNAP DEEP (7 square degrees) and SNAP WIDE (100 square degrees) fields.

the dark matter (Lyman break galaxies at $z \sim 3$ have biases of about two to three; e.g., Adelberger et al., 2005) and red, massive, and early type galaxies tend to be more biased still (McCarthy et al., 2001; Daddi et al., 2003). I choose the parameters of the halo occupation function for the "rare" galaxy population to match the number density and correlation function for luminous ($L \sim L_*$) ellipticals in the nearby universe, and I then consider two possibilities for the evolution of these objects: (1) the halo occupation parameters do not change with time (i.e., a halo of a given mass always hosts the same number of these objects) and (2) constant number density (the minimum mass of a halo that can host such a galaxy is adjusted to keep the number density the same at all epochs). Again, see MS02 for more details.

Fig. 2 shows the *fractional* error ($\delta N/N$) in the number counts of objects due to field-to-field variance for redshift bins of $\Delta z = 0.1$ for the two largest existing HST fields, the GEMS survey (0.25 square degrees), and the COSMOS survey (2 square degrees). Even for COSMOS, cosmic variance is a significant source of uncertainty for strongly clustered objects (such as massive galaxies, proto-ellipticals, or AGN). Also shown are the same quantities for the proposed SNAP DEEP (7.5 square degrees) and SNAP WIDE (100 square degrees). With SNAP DEEP, cosmic variance is reduced to $\sim$10% at $z \sim 1$ for the clustered objects, and to a few percent for SNAP WIDE. Thus, these surveys will be well-suited to statistical studies of galaxy properties at high redshift.

6. Summary

I have presented several examples of questions in galaxy formation that will likely still be unsolved at the end of Hubble's lifetime, and that require space-based imaging in the optical and/or Near-IR:

- Space-based imaging is needed for more accurate and detailed characterization of the assembly history of stellar mass. Deep wide-field imaging will aid this cause by providing larger and more complete samples, and by providing lensing data that can be used as an important cross-check on the mass estimates. Space-quality images are crucial in order to measure the stellar mass as a function of galaxy type, in particular the mass assembly of stellar spheroids.
- Deep wide-field space-based imaging will help improve our understanding of what regulates star formation in galaxies at moderate and high redshift, including the role of bars, mergers, and spiral arms. This is crucial in order to understand the physical processes driving the evolution of the global star formation rate.
- The nature of galaxies hosting active black holes, including their type, large-scale environment, and merger history, is still poorly understood. It is now widely believed that the energy released by AGN could be a crucial missing piece in the puzzle of galaxy formation.
- Statistical studies of galaxy formation at high redshift require fields at least as large as the planned SNAP DEEP and SNAP WIDE surveys in order to control errors due to field-to-field variance for rare, clustered populations such as massive proto-ellipticals and AGN.

Acknowledgments

I like to thank the organizers for inviting me to participate in this meeting, and especially Dr. A. Fruchter for tirelessly encouraging me to finish this contribution. I also thank my collaborators on the GEMS team for allowing me to present pre-publication work at the meeting.

References

Adelberger, K.L., Steidel, C.C., Pettini, M., Shapley, A.E., Reddy, N.A., Erb, D.K., 2005. ApJ 619, 697.
Barden, M. et al., 2005. ApJ., in press. Available from: <astro-ph/0502416>.
Bell, E.F., de Jong, R.S., 2001. ApJ 550, 212.
Bell, E.F. et al., 2005. ApJ 625, 23. Available from: <astro-ph/0502246> .
Coil, A.L., Newman, J.A., Kaiser, N., Davis, M., Ma, C.-P., Kocevski, D.D., Koo, D.C., 2004. ApJ 617, 765.
Croton, D.J. et al., 2005. Preprint astro-ph/0508046.
Daddi, E. et al., 2003. ApJ 588, 50.
Dickinson, M., Papovich, C., Ferguson, H.C., Budavári, T., 2003. ApJ 587, 25.

Jogee et al., 2004. ApJ 615, 105.
Kauffmann et al., 2003. MNRAS 346, 1055.
McCarthy, P.J. et al., 2001. ApJ 560L, 131.
Mo, H.J., White, S.D.M., 1996. MNRAS 282, 347.
Moustakas, L.A., Somerville, R.S., 2002. ApJ 577, 1.
Papovich, C., Dickinson, M., Ferguson, H.C., 2001. ApJ 559, 620.
Rix, H.-W. et al., 2004. ApJS 152, 163.
Sánchez et al., 2004. ApJ 614, 586.
Schiminovich, D. et al., 2005. ApJ 619L, 47.
Sheth, R.K., Tormen, G., 1999. MNRAS 308, 119.
Somerville, R.S. et al., 2005. In preparation.
Wolf, C. et al., 2005. ApJ 630, 771. Available from: <astro-ph/0408289> .
Zehavi et al., 2002. ApJ 571, 172.

Available online at www.sciencedirect.com
SCIENCE DIRECT®
New Astronomy Reviews 49 (2005) 374–378
New Astronomy Reviews
www.elsevier.com/locate/newastrev

Monster redshift surveys through dispersive slitless imaging: The Baryon Oscillation Probe

Karl Glazebrook, Ivan Baldry *, Warren Moos, Jeff Kruk, Stephan McCandliss

Department of Physics and Astronomy, Johns Hopkins University, Baltimore, MD 21218, USA

Available online 12 September 2005

Abstract

Wide-field imaging from space should not forget the dispersive dimension. We consider the capability of space-based imaging with a slitless grism: because of the low near-infrared background in space and the high sky-density of high-redshift emission line galaxies this makes for a very powerful redshift machine with no moving parts. A small 1 m space telescope with a 0.5° field of view could measure redshifts for 10^7 galaxies at $0.5 < z < 2$ per year, this is a MIDEX class concept which we have dubbed 'The Baryon Oscillation Probe' as the primary science case would be constraining dark energy evolution via measurement of the baryonic oscillations in the galaxy power spectrum. These ideas are generalizable to other missions such as SNAP and DESTINY.
© 2005 Elsevier B.V. All rights reserved.

Contents

1. Dispersive space imaging . . . 375
2. The Baryon Oscillation Probe . . . 375
3. Baryon oscillations and dark energy constraints . . . 376
4. Conclusions . . . 378
Acknowledgments . . . 378
References . . . 378

* Corresponding author.
E-mail address: baldry@pha.jhu.edu (I. Baldry).

1387-6473/$ - see front matter © 2005 Elsevier B.V. All rights reserved.
doi:10.1016/j.newar.2005.08.007

1. Dispersive space imaging

Slitless dispersive imaging has a long history extending back to the early Schmidt plate objective prism surveys. The set up is an imaging system, a dispersing element (ideally located at a pupil of the imaging system to avoid aberrations, but this is not essential in slow beams) and a filter to delimit the bandpass. In essence the object forms its own slit due to its angular size, to first order the background over the field of view is uniform and is equal to the undispersed background through the same filter. From the ground this means the background remains bright when the object's light is dispersed and so one takes an enormous signal-to-noise (S/N) penalty. Because of this such surveys have generally been restricted to bright emission line galaxies in the local Universe (see the KISS survey (Wegner et al., 2003) for a recent example). For unresolved emission lines the S/N is independent of the spectral resolution of the disperser.

A low background environment greatly increases the sensitivity of slitless surveys. In space the background is dominated by solar scattered light from zodiacal dust and at 1.6 μm is ~1000× darker than on the ground (JWST, 2004) (there is some dependence on ecliptic latitude). On the Hubble Space Telescope both the ACS optical camera and the NICMOS near-infrared camera are equipped with grisms for slitless spectroscopy. This mode has been used on ACS for spectroscopy of Type 1a supernovae to $z = 2$ (Riess et al., 2004) and on NICMOS for detection of an abundant population of $z > 1$ Hα emission line galaxies (McCarthy et al., 1999). The strong evolution of the cosmological star-formation rate out to $z = 1$ means that their are many more bright emission line galaxies than would otherwise be the case (Hopkins et al., 2000). The space background peaks at 0.6 μm and so as one follows Hα to high-redshift both the strong evolution in the source population and the diminishing background act to counteract the cosmological dimming for the S/N. Going from $z = 0.2$–2 these effects work to give us a S/N boost of a factor of 30 and make the high-redshift regime accessible to small space telescopes.

2. The Baryon Oscillation Probe

During discussions at Johns Hopkins in 2003–2004 we developed a strawman concept for a MIDEX class space mission which could do large scale slitless redshift surveys. We called this the 'Baryon Oscillation Probe' as our primary science motivation was to probe the baryonic oscillations in the power spectrum of galaxy clustering (see below). Our strawman concept consisted of a 1 m telescope with a 0.5° FOV operating in the 1–2 μm near-infrared bandpass. This field would be sampled with 0.5″ pixels giving a 4096 × 4096 detector array requirement. A set of low-dispersion fixed grisms and filters would provide for dispersed slitless imaging. Our rough order-of-magnitude estimates of size, mass and cost put this spacecraft in the MIDEX class. Initial studies show that BOP could be done either in LEO (with active cooling) or at L2 (passive cooling). We use this strawman to demonstrate the power of the slitless concept.

The exposure times depend on redshift, the response of the system and the choice of blocking filters. Cosmological dimming makes the highest redshifts more difficult. Our baseline goal was to measure Hα over the redshift range $0.5 < z < 2$, this is the redshift range optimal for testing dark energy models (Linder and Huterer, 2003). To determine exposure times we use published luminosity functions for Hα in this redshift range (Hopkins et al., 2000):

$$[\log(L^*/W), \log(\phi^*/\mathrm{Mpc}^{-3}), \alpha] = [35.9, -3.1, -1.6]; \quad (1)$$

and set a luminosity limit as a function of redshift which gives critical number density sampling of the galaxy power spectrum for the purposes of the baryon oscillation science. We assumed the luminosity function L^* evolved as $(1+z)^3$ over $0 < z < 1$ and was constant for $z > 1$. This is a good match to the observed data of the cosmological star-formation rate evolution (Glazebrook et al., 2003). Following (Blake and Glazebrook, 2003) we adopt a density of galaxies n sufficient that the power spectrum $P(k)$ measurement is not shot-noise limited ($nP = 3$ in their criteria) and also a bias model for galaxies which evolves with redshift in order to match observations of low and high-redshift

galaxy clustering ($r_0 = 5\ h^{-1}$ Mpc $\simeq$ const.). This gives an Hα flux limit which is a function of redshift reaching 10^{-16} ergs cm^{-2} s^{-1} and a number density of 2000 deg^{-2} for the $1.75 < z < 2$ bin. As a cross-check on our luminosity function calculation we can count directly the number of sources in redshift bins vs. flux in the NICMOS grism fields (Hopkins et al., 2000) and find agreement with our numbers.

Given these flux limits the main design parameter affecting exposure times is the combined throughput vs. wavelength of the grism and blocking filter. A wider filter lets through Hα over a wider redshift range but also lets in more background which reduces S/N. Because the background spectrum is not flat it is advantageous to have a set of narrow filters rather than one large filter. Further the background is *higher at shorter wavelengths, i.e. low redshifts where the required flux limit is less deep.* This turns out to be critical – if we have the freedom to have an *abitrary* response function we find that an *optimized* filter would deliberately have a declining throughput at blue wavelengths. This reduces the background, benefiting long-wavelength high-redshift Hα. The sensitivity is reduced at low redshift but the lines are brighter so it does not matter. Fig. 1 shows a hypothetical two filter set designed in this manner which would give a *uniform* exposure time (1800 s) for the whole $0.5 < z < 2$ range. We have not explored the feasibility of such filters, but we note that to achieve the desired behavior one could change both the filter response or the grism response or a combination of both.

One issue for slitless surveys is ambiguous line identification. In principle multi-color photometry can be used to estimate redshifts and remove this ambiguity. However it is interesting to consider how well one can do with a single line. Using our evolving line luminosity function model we can estimate this by adopting reasonable values for fixed emission line ratios and assuming all the lines following the same cosmological evolution. We find that at our required flux limits Hα dominates, for example at $z = 1.9$ it contributes 72% of the sources. The principal contaminant turns out to be [SIII] 9532 Å which aliases Hα at $z = 1.1$ (27% of line sources). Even very crude broad-band data would suffice to eliminate such low-redshift galaxies. For [OIII] at $z = 2.8$ and [OII] at $z = 4.1$ we find contamination rates of 0.5% and 0.07%, respectively – their fluxes are heavily suppressed by cosmological dimming. These fractions were based on the assumption that $L^*/L^*_{\mathrm{H}\alpha} = (0.2, 0.3, 0.5)$ for [SIII], [OIII] and [OII], respectively.

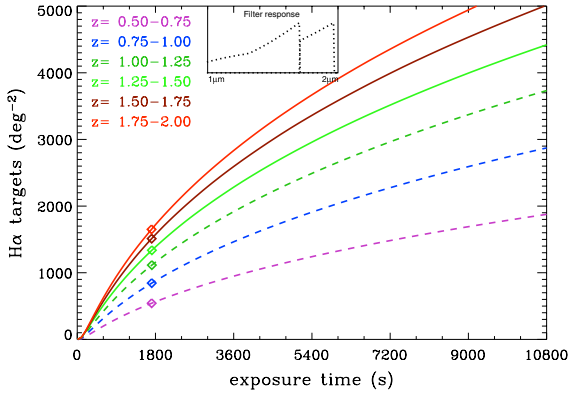

Fig. 1. Predicted number density of targets seen from BOP vs. exposure times for different redshift ranges using an optimized two filter set. The diamonds show the required number density for the baryon oscillation science at each redshift. The filters have been optimized to give equal exposure times for these points. The throughputs (+ grism response) of the optimized filter set vs. wavelength are shown in the inset. We assume a peak efficiency of 38% (effective area of 0.3 m^2) for first-order diffraction and that other orders do not contribute significantly to the background.

We also considered an alternate approach to BOP using the ultraviolet rather than the near-infrared and targeting Lyα emitters. We constructed an empirical model of their line luminosity function which matches the observed UV continuum luminosity function and Lyα equivalent width distribution of $z \sim 3$ Lyman break galaxies (Steidel et al., 1999; Shapley et al., 2003). We found the UV approach was not competitive – the exposure times were an order of magnitude larger. This is a combination of the much lower strength of the Lyα line and the fact that the background now *increases* towards higher redshifts (0–3).

3. Baryon oscillations and dark energy constraints

Of course there many possible science experiments BOP could address (see Section 4). We

choose to focus on one for illustration of the redshift survey power: detection of the baryon oscillations in the galaxy power spectrum and resulting constraints on dark energy.

Based on the field of view and exposure time we calculate BOP can redshift survey 2000 deg^2 and 10^7 objects per year. We assume our two filter optimized design and that each field is observed at two roll angles to improve deconvolution of spectral overlap. (This is also desirable to allow the zero point of the wavelength scale of each object to be determined, alternatively zeroth order could be used.)

The spectral resolution requirement remains to be determined precisely. Blake and Glazebrook (2003) determined for full $P(k)$ resolution: $\sigma_z/(1+z) \simeq 0.001$, which translates to $R = 125$ if the line can be centroided to a quarter of a resolution element at $S/N = 10$. However to resolve the nearby Hα and [NII] lines requires $R > 400$ so this might be preferable.

We assume a 5 year mission resulting in a survey of 10,000 deg^2 and apply the methodology of Glazebrook and Blake (2005; in press) to simulate the recovered power spectrum (Fig. 2) and resulting dark energy constraints (Fig. 3). The constraints are comparable to those delivered using the supernova technique by the Supernova Acceleration Probe SNAP (Aldering et al., 2005). As with the supernovae this requires independent accurate constraints on other cosmological parameters (e.g. Ω_m, H_0) from local surveys and the Cosmic Microwave Background measurements – we refer the reader to Glazebrook and Blake for a detailed discussion.

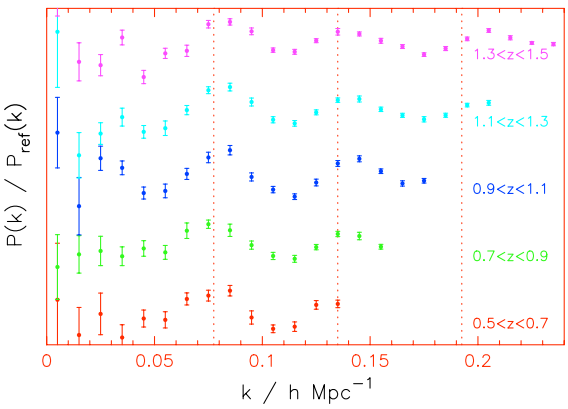

Fig. 2. Predicted galaxy power spectrum for a 10,000 deg^2 survey. The non-oscillatory component has been divided out and the power spectrum (linear regime only) is shown in redshift bins. The small error bars show the precise measurement possible on the baryonic oscillations (the 'standard ruler' for the dark energy test) possible with a survey of this size. In this case the model data is for a $w = -0.9$ simulated cosmology, the peaks visibly shift from their location in a $w = -1$ cosmology (vertical dotted lines).

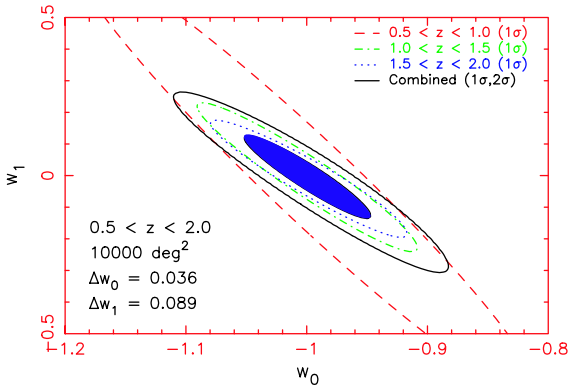

Fig. 3. Recovered constraints on a dark energy equation of state $w(z) = w_0 + w_1 z$ from a 10,000 deg^2 BOP survey. It can be seen that each redshift range is slightly non-degenerate with the others, the combined constraints are very tight and are comparable to the precision delivered using supernovae in the SNAP mission.

We note this proposed redshift survey improves by a factor of 10 on the most ambitious proposed future ground-based redshift survey. This is the KAOS concept (Dey et al., 2003) for the Gemini Telescope which could survey 1000 deg^2.

It is also interesting to consider that there is very little conceptual difference between BOP and *any* wide-field imaging space mission. Both require large detector arrays and wide-field optics, the only difference is provision of a grism. For example one could merge BOP with SNAP – this would add a completely independent method to the dark energy determination *and* with similar precision. It would also mean that the many millions of high-redshift galaxies imaged with SNAP could get spectroscopic follow-up in the same mission. Alternately BOP is very similar to the DESTINY concept (Lauer et al., 2004) which uses slitless spectroscopy to locate high-redshift supernovae (albeit at somewhat lower resolution).

4. Conclusions

We have outlined a concept (BOP) for a near-infrared space mission using slitless spectroscopy to do wide area redshift surveys an order of magnitude larger than existing ground based surveys such as SDSS and 2dFGRS in both number and volume and probing high-redshift ($0.5 < z < 2$). It represents a factor of 10 improvement on what could be done on the ground. Instrumentally, it represents a very simple hardware system which by taking advantage of the low background in space has no requirement for complex fiber or slit configuring machinery. Although lower backgrounds could be achieved with wide-field spectroscopic fiber or slit designs that have recently been proposed (McCandliss et al., 2004) these technologies are immature by spaceflight standards and as such must be considered risky at the present time.

BOP would serve diverse science goals: some other examples include studying the evolution of galaxy clustering, measuring the evolving luminosity function of star-forming galaxies as a function of metallicity and environment, providing redshift depth information for deep wide imaging surveys and searching for Lyα emission from young galaxies at $z > 7$. We have presented in detail BOP's ability to constrain dark energy using baryon oscillation measurements. It would deliver precision on the equation of state comparable to the SNAP mission but via a completely independent technique.

The BOP concept is generalizable to any wide-field space mission as long as a grism could be inserted in to the imaging system. We argue that in any such space mission the science-to-cost ratio of adding such a grism is enormous, and should be considered.

Acknowledgments

We would like to thank Chris Blake for assistance in producing Figs. 2 and 3 and Bob Woodruff from Lockheed Martin for useful design discussions. KG acknowledges generous funding from the David and Lucille Packard foundation.

References

Aldering, S.C.G., et al., 2005. PASP in press, astro-ph/0405232.
Blake, C., Glazebrook, K., 2003. ApJ 594, 665.
Dey, A., et al., 2003. The KAOS Purple Book.
Glazebrook, K., Blake, C., 2005. ApJ, in press.
Glazebrook, K. et al., 2003. ApJ 587, 55.
Hopkins, A.M., Connolly, A.J., Szalay, A.S., 2000. AJ 120, 2843.
The JWST, 2004. Background Simulator. Available from: http://www.stsci.edu/jwst/science/jms/jms_bgnd_form.html.
Lauer, T.R., et al., 2004. This proceedings.
Linder, E.V., Huterer, D., 2003. Phys. Rev. D 67, 081303.
McCarthy, P.J. et al., 1999. ApJ 520, 548.
McCandliss, S.R., France, K., Feldman, P.D., Glazebrook, K., Meurer, G., Bianchi, L., Moos, H.W., Kruk, J.W., Blair, W.P., Baldry, I., 2004. SPIE 5488, 709.
Riess, A.G. et al., 2004. ApJ 607, 665.
Steidel, C.C., Adelberger, K.L., Giavalisco, M., Dickinson, M., Pettini, M., 1999. ApJ 519, 1.
Shapley, A.E., Steidel, C.C., Pettini, M., Adelberger, K.L., 2003. ApJ 588, 65.
Wegner, G., Salzer, J.J., Jangren, A., Gronwall, C., Melbourne, J., 2003. AJ 125, 2373.

Available online at www.sciencedirect.com
SCIENCE DIRECT®
New Astronomy Reviews 49 (2005) 379–386
New Astronomy Reviews
www.elsevier.com/locate/newastrev

Galaxy evolution with future wide-field space missions

David W. Hogg

Center for Cosmology and Particle Physics, Department of Physics, New York University, 4 Washington Place, New York, NY 10003, United States

Available online 28 September 2005

Abstract

Future studies of: (1) galaxy property relationships, (2) environmental dependencies, and (3) the merger rate and accretion histories will require: (a) large solid angle (with large area/boundary ratio), (b) multi-band imaging, (c) high signal-to-noise and high resolution imaging, and (d) spectroscopy. All of these things will be provided by the next generation of wide-field surveys.
© 2005 Published by Elsevier B.V.

Keywords: Galaxies: formation; Galaxies: evolution; Galaxies: structure

Contents

1. Introduction . . . 380
2. How to design galaxy evolution experiments . . . 380
   2.1. Think of data as a source of information . . . 380
   2.2. Try to measure things that are at least plausibly amenable to timely prediction . . . 381
3. Multi-variate galaxy properties . . . 381
4. Galaxy environments . . . 382
5. Galaxy merger and accretion event rates . . . 384
6. Conclusion . . . 386
   Acknowledgments . . . 386
   References . . . 386

E-mail address: david.hogg@nyu.edu.

1387-6473/$ - see front matter © 2005 Published by Elsevier B.V.
doi:10.1016/j.newar.2005.08.008

1. Introduction

I am extremely pleased by what I have heard at this meeting: All the proposed future wide-field space imaging missions will be wonderful for studying galaxy evolution. A great deal of what we know about galaxies and galaxy evolution has come from large surveys, and sometimes those surveys were not really intended to study galaxies in the first place; or, if they were, what we learned about galaxies was not what we expected to learn. This means that if awesome space hardware is being used to execute a great observing plan, the data will have a big impact on the study of galaxy evolution.

Before I begin, let me point out Fig. 1, which shows my favorite galaxy in the nearby Universe, M51, as observed by the Sloan Digital Sky Survey (SDSS) (York et al., 2000; Abazajian et al., 2004). This image shows an incredibly detailed interaction between an early-type galaxy and a late-type galaxy, where the spiral structure seems to have been raised or influenced by the interaction. Within the spiral arms, you can see star formation regions and dusty regions, and you can see a coherent differentiation of material that persists along the spiral arms. You can see dust accreting out of the spiral arms onto the early-type galaxy and in fact fueling a small line-emitting point source at the center of that early-type galaxy. You can see low surface-brightness tidal tails and loops of old stars that swirl around the pair. This image is astonishing in its information content, but I need to emphasize here *we don't know how to use any of that information to understand galaxy evolution!*

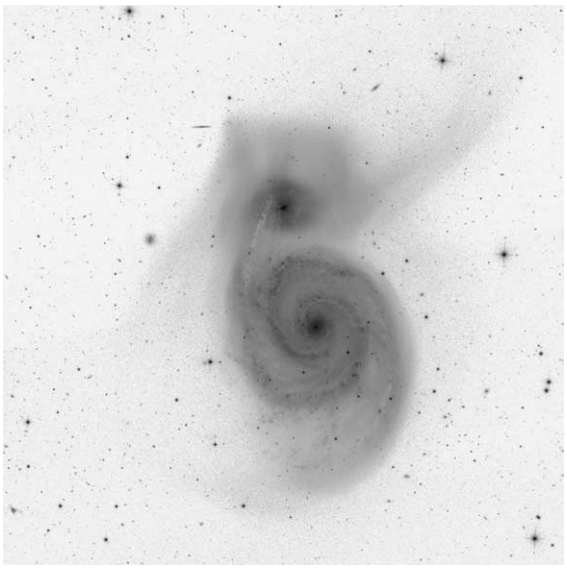

Fig. 1. SDSS *r*-band mosaic (home-made at NYU from raw SDSS data) of a 20×20 arcmin^2 patch of the sky including M51. North is up. The color version (not shown) of this picture shows tremendous detail, including systematic segregation of dust and young stars in the spiral arms, and nuclear activity in the early-type (northern) member of the pair.

Okay, that's an exaggeration. There is a literature on using some aspects of tidal and spiral features to understand some aspects of galaxy evolution. But it is not an exaggeration to say that in the vast majority of galaxy modeling, we are lucky to have predictions for galaxy colors, stellar masses, or disk rotation velocities. Even then, most of the (non-fine-tuned) predictions are in stark contradiction to basic observational facts. It is also not an exaggeration to say that (because of all the difficult gastrophysics) we have *never* seen the output of a calculation or a simulation look anything even remotely like Fig. 1!

Perhaps this should be taken as a call to theory. Indeed, it is a great time to be working on galaxy evolution theoretically and numerically, and great progress is being made. But at this meeting we are talking about new *data.*

2. How to design galaxy evolution experiments

When you are designing an astronomical experiment to study physical phenomena and you have very little a priori understanding of what measurements are going to be most interesting or constraining, there are a few heuristics I and my collaborators have established. Here are the two following reactions:

2.1. Think of data as a source of information

By "information" here I mean the quantity (described by Shannon, 1949) that is measured in bits and that looks like an "entropy." I mean, when

faced with decisions about experimental design, or data analysis, when possible, make a quantitative comparison of the amount of information you can obtain by different methods, and choose the most informative path (provided you can afford to do so!).

I will give one example of this later, in the area of data analysis, where the application of this principle is quite obvious. There are many others, relating to experimental design, for instance regarding *sampling* of the point spread function, and *wavelength overlap* of filter bandpasses in multi-band surveys, both of which are beyond the scope of this contribution, but on which the question of information has some non-intuitive things to say.

2.2. Try to measure things that are at least plausibly amenable to timely prediction

Recall our picture of M51 (Fig. 1). It teems with information. This information is good, and I expect that my grandchildren *will* understand galaxies in a way that *does* use all the bits of information in that glorious picture, but in the short term if we want to be productive, we have to measure quantities that are amenable to prediction. So I am deprecating detailed morphology. I am promoting colors, luminosities, sizes, kinematic temperatures, angular momenta, masses and mass ratios of gas, stars, and dark matter, clustering, infall, recent and large accretion events, star formation rates, etc. Right now we have to hit galaxies with blunt tools.

For the remainder of this talk, I am going to walk you through three areas in which I am investigating galaxy evolution, in order to shamelessly and unfairly plug my own work. It is also the case that everything I am doing now at low redshift will be possible at much higher redshift and smaller angular scales and more diverse wavelengths with next-generation imaging. That plus a bit of theoretical development, and the study of galaxy evolution will be transformed.

3. Multi-variate galaxy properties

Galaxy properties show many precise, nonlinear inter-relationships. Given the physical processes involved in gravitational collapse and star formation, this is not surprising. What *is* surprising is the rich detail that we are finding and quantifying, which could not have been adequately revealed without huge data sets. Every one of the Baroque relationships we find will have to appear in any successful model of galaxy formation and evolution!

Fig. 2 (taken from Blanton et al. (2003a)) shows bivariate distributions of pairs of seven galaxy properties: four optical colors, surface brightness, radial profile shape as measured by the concentration (Sérsic index) n, and absolute magnitude for 183,487 galaxies taken from early days of the SDSS. Several classic, well-known relations among galaxy properties are evident at extremely high signal-to-noise ratio: the color–color relations of galaxies, the color–magnitude relations, the magnitude–surface brightness relation, and the dependence of density on color and absolute magnitude. Because the galaxies contributing to Fig. 2 have been weighted by i-band luminosity per sampling volume $V_{\max}$, it also shows that most of the luminosity density in the Universe is likely in the absolute magnitude and surface brightness ranges shown.

It is also possible to see, especially in the concentration n plots, the two populations of bulge-dominated and disk-dominated galaxies show up as a bimodality (this is also clearly visible in the top left panel of Fig. 5). By slicing the space, we can show that most of the relationships between parameters, in particular the color–magnitude relations, show stronger correlations for these two types of galaxies taken separately than for all galaxies taken together.

One warning: Two-dimensional projections of very high dimensionality spaces can be complicated and misleading.

One polemic: None of the observed relationships among galaxy properties are linear, so why would anyone ever measure any of them with a linear tool, like principal components analysis? Let us stop using linear tools on nonlinear data!

The future holds this kind of exploration at much higher redshift, where we ought to see the differential evolution of the different types of galaxies – the different parts of the multi-dimensional

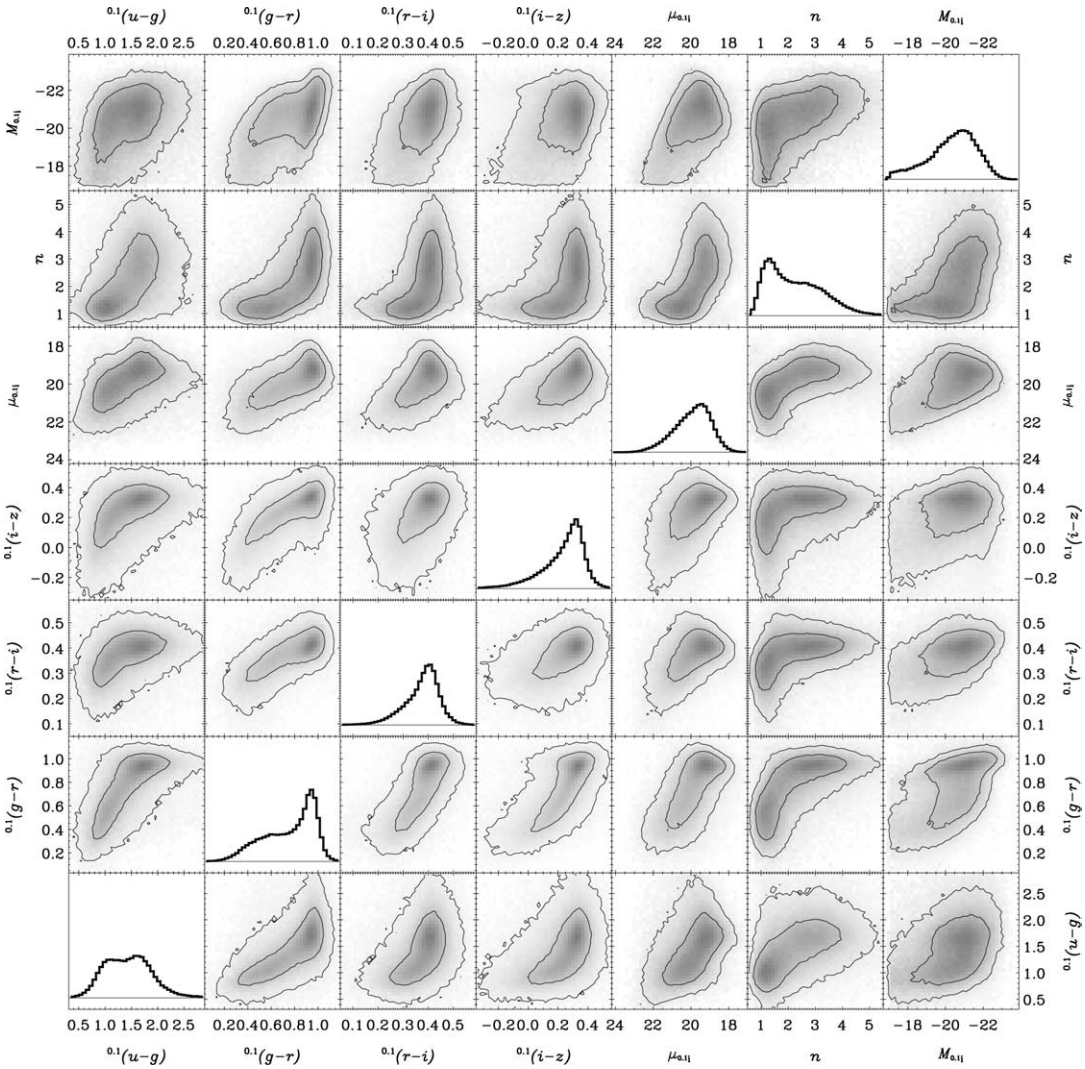

Fig. 2. From Blanton et al. (2003a): The projection of the luminosity density distribution for 183,487 SDSS galaxies (all contributing galaxies are weighted by luminosity divided by $V_{\max}$) of galaxies in our seven-dimensional space of colors, surface brightness, concentration n, and luminosity, onto each pair of dimensions. All images have a square-root stretch applied to increase the dynamic range of the plot. Contours indicate the regions containing 68% and 95% of the total luminosity density of galaxies in the SDSS sample used. The upper and lower triangles are mirror images. The histograms along the diagonal show the distribution of galaxies in each single dimension. The luminosity density contribution from galaxies below the absolute magnitude and surface brightness limits of this sample is likely to be very small.

space – and to a more diverse set of measurements at a wider range of wavelengths. For this we need: (a) large numbers of galaxies surveyed (10^5 or, better, 10^6), (b) high resolution and high signal-to-noise imaging, and (c) redshifts (spectroscopic or photometric, I do not care, so long as they are accurate).

4. Galaxy environments

Any gravitationally driven cosmogony has more dense regions of the Universe collapsing first, and creating structure more rapidly. Thus, regions of different overdensity have galaxies created under different relationships of gravitational, gas

cooling, and star-formation timescales. Indeed, we find that the distribution of galaxy properties is a strong function of environment.

The dirty laundry is that *all measures of galaxy environmental density are low in signal-to-noise*. This is because they all depend on just a small number of nearby objects and the inverse square root of a small number is a (relatively) large number! So our principle of information comes in: we should not ask, say, how mean galaxy properties depend on environment, we should ask how mean galaxy environments depend on galaxy properties! We want to do the experiment that *maximizes the information content* of our results.

After all, when theory has advanced far enough to reproduce what we see, theory can explain either result (properties vs. environment or environment vs. properties), but the result with the much higher signal-to-noise will be much more constraining (usually).

Fig. 3 (taken from Hogg et al. (2003)) shows the mean environmental density as a function of color and magnitude for some 115,000 galaxies taken from the SDSS spectroscopic sample. We find that, at constant color, overdensity is independent of luminosity for galaxies with the blue colors of spirals. This suggests that, at fixed star-formation history, spiral-galaxy mass is a very weak function of

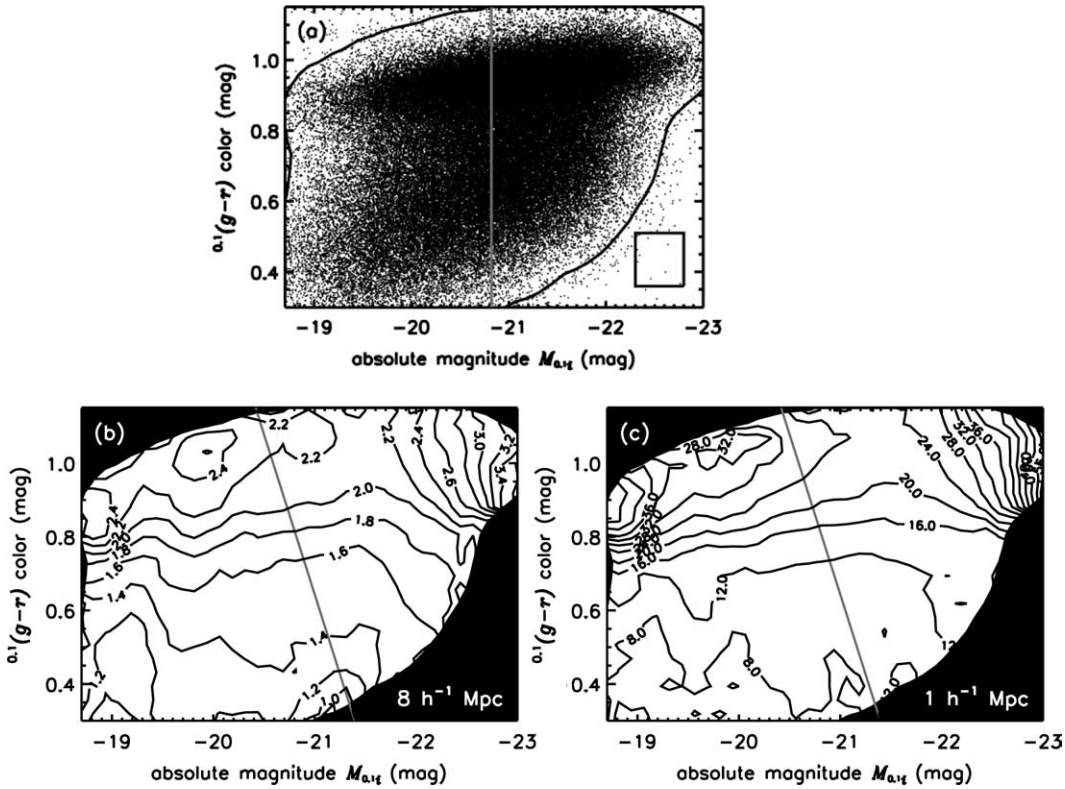

Fig. 3. From Hogg et al., 2003: Panel (a) shows the luminosity and color of each galaxy in a sample of 115,000 SDSS galaxies. A vertical gray line shows the characteristic luminosity L^* Blanton et al. (2003b). Panel (b) shows the $1/V_{\max}$-weighted mean galaxy environment overdensity $\langle\delta_8\rangle$ in 8 h^{-1} Mpc comoving-space spheres computed in a sliding, rectangular box of luminosity width $\Delta M_{0.1_i} = 0.5$ mag and color height $\Delta^{0.1}(g-r) = 0.15$ mag. The box size and shape is shown on the lower right corner of panel (a). The gray line indicates, roughly, a locus of constant total stellar mass Bell and de Jong (2001). Panel (c) shows the weighted mean overdensity $\langle\delta_1\rangle$ in 1 h^{-1} Mpc spheres (deprojected from imaging catalogs in the extremely clever manner of Eisenstein (2003)). Note that different *kinds* of overdensity estimators are used for the two different length scales. The mean environment overdensity is not shown at colors and luminosities at which there are <200 galaxies inside the box; this region is indicated with a border on panel (a).

environment. Overdensity does depend on luminosity for galaxies with the red colors of early types.

Fig. 4 (taken from Blanton et al. (in press)) is similar, but shows more properties, and for subsamples of the full population, cut by absolute magnitude. This figure shows that color is, indeed, very strongly related to environment, in the sense that at fixed color and magnitude, there is very little additional dependence on the structural parameters of surface brightness and concentration.

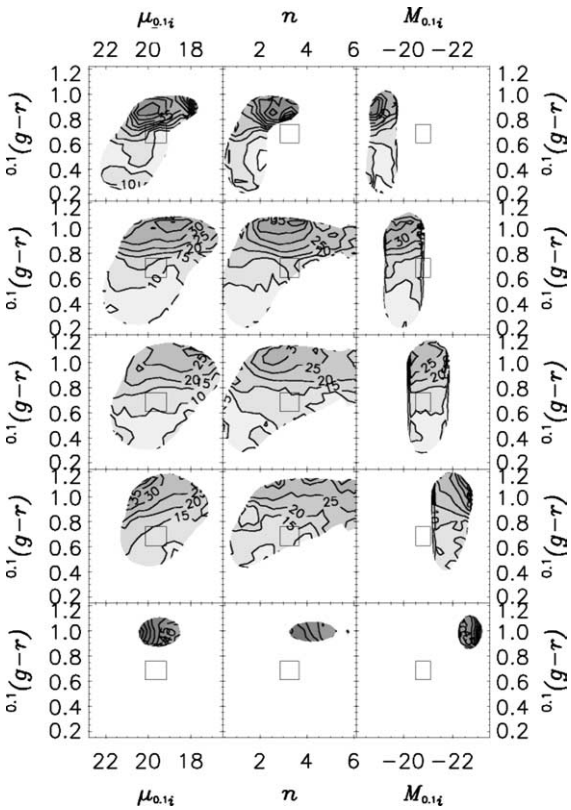

Fig. 4. From Blanton et al. (in press): Similar to Fig. 3, but showing the dependence of the 1 h^{-1} Mpc environment on color, surface brightness, concentration, and luminosity for several small ranges of absolute magnitude. Each panel shows strong dependence of environment on color, but very little *residual dependence* on surface brightness or concentration, the more "morphological" or structural parameters. This figure suggests that the morphology–density relation in SDSS appears to be a by-product of the color–density relation and the morphology–color relation.

Is the morphology–density relationship "simply" a by-product of the color–density relationship and the color-morphology relationship? SDSS says "yes".

There is the catch, though: This is a statement purely about the *information* contained about galaxy environments and galaxy properties *in the SDSS dataset.* That information is a product of what is really out there *times* what the SDSS measures well. And the SDSS measures colors extremely well and morphological properties less well.

This is the flip side of thinking about data as information: The result of every experiment contains not all the information that exists in the system being observed, but is degraded by the finite dynamic range of its measurements.

Again, the future is to increase the redshift and wavelength range of these studies, and start to make the environment as a function of redshift work that will start to see the different timescales of collapse and galaxy formation. For this, we need: (a) large solid angle to boundary ratio (e.g., 100×100 Mpc^2 field size at the redshift of interest) to get good environment coverage, (b) multi-band imaging, (c) high resolution and high signal-to-noise imaging, and (d) redshifts.

5. Galaxy merger and accretion event rates

In the CDM paradigm, the fundamental process of evolution is merging. Small things form early and merge into larger and larger things as time goes on. Of course, CDM is a description of the dark matter and we observe "only" the galaxies, but nonetheless, we expect merging to provide a key connection between observations and theory.

In the local Universe, clear evidence of galaxy mergers is rare (one's need is to only note that every single talk ever given on galaxy–galaxy merging shows the same example: the Antennae). This rarity could be due to a low merger rate, or a short timescale on which the evidence of merging fades or becomes ambiguous.

In the Antennae, and indeed in most obvious mergers in the nearby Universe, it is apparent that starbursts are triggered. Indeed, they must be if the end products of major mergers are

bulge-dominated galaxies, since bulge-dominated galaxies show alpha enhancement in their chemical abundances, unavoidably implicating large, short, brief star formation events.

Fortunately, we know quite a bit about the stars created in starbursts; in particular A stars are easy to find in galaxy spectra (because of strong Balmer absorption) and they are known to have lifetimes of 10^9 yr; A stars are the perfect tracers of merger-induced starbursts: they are easy to find and live for a known time.

Fig. 5 (taken from Quintero et al. (2004)) compares post-starburst "K + A" galaxies with the bulk of the SDSS sample. The post-starburst galaxies were identified on the basis of having excess A stars relative to the amount of ionizing O and B stars – they are galaxies that are being observed more than 10^7 but less than 10^9 yr after a starburst. What the Figure shows is that these galaxies are bluer than bulge-dominated galaxies, but similar in radial profile, just as if they will "fade" into normal bulge-dominated galaxies. We also find that the luminosity distribution of K + A galaxies is similar to that of the total galaxy population, and that they are found in the field; the K + A galaxies do not primarily lie in the high-density environments or clusters typical of bulge-dominated populations.

In the work Quintero et al. (2004), the inferred rate density for K + A galaxy formation is $\sim 10^{-4}$

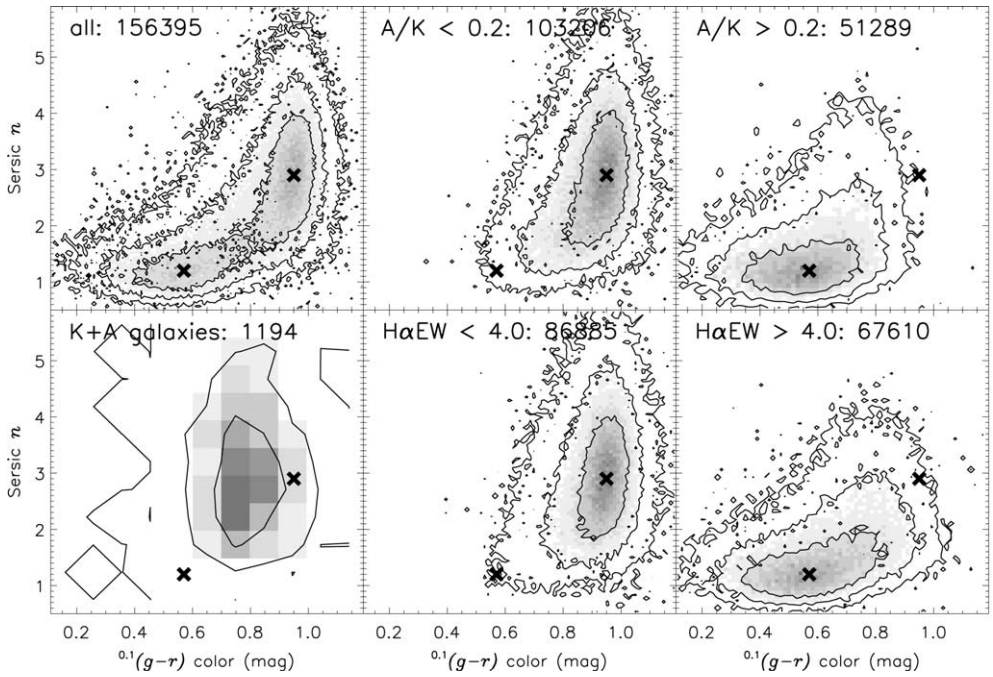

Fig. 5. From Quintero et al. (2004): The top left panel shows the distribution of luminosity density from 156,395 galaxies from the SDSS in the color–concentration plane. The color is measured in blueshifted SDSS bandpasses $^{0.1}g$ and $^{0.1}r$, and the concentration n is found by fitting the radial profile in the band. Each galaxy data point has been weighted by the ratio of its luminosity $L_{0.1_i}$ in the $^{0.1}i$ band to its comoving selection volume $V_{\max}$, so the distribution of weight in the plot is proportional to comoving luminosity density. The contours enclose 52.0%, 84.3%, and 96.6% of the total luminosity density. In this panel, galaxies separate into disk-dominated (blue, low n) and bulge-dominated (red, high n) populations, marked by crosses. The other panels show similar plots, but for different sub-samples, cut on A/K (see Quintero et al. (2004) for a definition) and HαEW. The "K + A" panel shows those galaxies making the high A/K cut and the low HαEW cut; these are the post-starburst galaxies. Galaxies selected to have low A/K or low HαEW appear to be concentrated (bulge-dominated); galaxies selected to have high A/K or high HαEW appear to be exponential (disk-dominated). The K + A galaxies – the post-starburst galaxies – have the colors of disk-dominated galaxies but many have the radial profiles of bulge-dominated galaxies.

h^3 Mpc^{-3} Gyr^{-1} at redshift $z \sim 0.1$, or about 1% of the galaxy population per Gyr. This rate is low relative to naive applications of CDM. Is it *really* too low? It depends on what kinds of events trigger starbursts. The rate is way too low if there are processes other than merging that can provide triggers. It is just right if the majority of mergers out there do not cause any star formation at all.

For the future, everything I have spoken about comes together here, because we expect that the environments in which these kinds of "events" occur will be a strong function of redshift. We also expect very strong evolution in the rate as the structure in the Universe slows its growth and the expansion starts to accelerate. Finally, correlating spectral (in this case, stellar populations) results with imaging (in this case, tidal features) will be highly productive. So the future for this kind of work is very bright. What we need is: (a) large survey volume (e.g., 10^{-2} Gpc^3) to measure rare events, (b) high signal-to-noise spectroscopy or multi-band imaging, and (c) deep, flat imaging for tidal features.

6. Conclusion

Is the galaxy–galaxy merger rate as high as it ought to be given the standard dark-matter paradigm? Has it been so in the past, and do the interactions trace different environments at different times?

Is star-formation history the only galaxy property affected by environment? If so, how do galaxy morphologies "know" about their star-formation histories?

Can the detailed regularities of galaxies be reproduced with simple theoretical ideas, or are galaxies hopelessly complex?

The punchline of this talk is that the next generation of wide-field imaging from space will do everything we need for this next generation of galaxy science, which will span a much bigger redshift range, a wider and more diversified wavelength bandpass range, and – we must hope – more focused, more theoretically motivated, and more informative measures of galaxy properties.

Acknowledgments

It is my pleasure to thank Mike Blanton for a rewarding and fruitful collaboration on all these issues. This research made use of the NASA Astrophysics Data System, and was partially supported by NASA (grant NAG5-11669) and NSF (grant PHY-0101738).

References

Abazajian, K. et al., 2004. AJ 128, 502.
Bell, E.F., de Jong, R.S., 2001. ApJ 550, 212.
Blanton, M.R., Eisenstein, D.J., Hogg, D.W., Schlegel, D.J., Brinkmann, J., 2005. ApJ 629, 143.
Blanton, M.R. et al., 2003a. ApJ 594, 186.
Blanton, M.R. et al., 2003b. ApJ 592, 819.
Eisenstein, D.J., 2003. ApJ 586, 718.
Hogg, D.W. et al., 2003. ApJ 585, L5.
Quintero, A.D. et al., 2004. ApJ 602, 190.
Shannon, C.E., 1949. The Mathematical Theory of Communication. University of Illinois Press, Urbana, IL.
York, D. et al., 2000. AJ 120, 1579.

Available online at www.sciencedirect.com
SCIENCE DIRECT®
New Astronomy Reviews 49 (2005) 387–391
New Astronomy Reviews
www.elsevier.com/locate/newastrev

The SNAP strong lens survey

Phil Marshall *, Roger Blandford, Masao Sako

Kavli Institute for Particle Astrophysics and Cosmology, P.O. Box 20450, MS29, Stanford, CA 94309, USA

Available online 3 October 2005

Abstract

Basic considerations of lens detection and identification indicate that a wide field survey of the types planned for weak lensing and Type Ia SNe with SNAP are close to optimal for the optical detection of strong lenses. Such a "piggy-back" survey might be expected even pessimistically to provide a catalogue of a few thousand new strong lenses, with the numbers dominated by systems of faint blue galaxies lensed by foreground ellipticals. After sketching out our strategy for detecting and measuring these galaxy lenses using the SNAP images, we discuss some of the scientific applications of such a large sample of gravitational lenses: in particular we comment on the partition of information between lens structure, the source population properties and cosmology. Understanding this partitioning is key to assessing strong lens cosmography's value as a cosmological probe.
Published by Elsevier B.V.

Contents

1. Introduction . . . 387
2. Predicting elliptical lens numbers . . . 388
3. Science from the elliptical lens sample . . . 389
4. Conclusions . . . 391
Acknowledgements . . . 391
References . . . 391

1. Introduction

The proposed SNAP satellite, whilst designed for measuring the luminosity distance of Type Ia Supernovae as a function of their redshift

* Corresponding author.
E-mail address: pjm@slac.stanford.edu (P. Marshall).

1387-6473/$ - see front matter. Published by Elsevier B.V.
doi:10.1016/j.newar.2005.08.009

(Perlmutter et al., 1999; Riess et al., 2004) and probing the large-scale structure in the Universe through weak gravitational lensing (Rhodes et al., 2001), will be an observatory offering high angular resolution optical imaging (PSF FWHM $\sim 0.12''$) over a wide survey field ($1000\,\mathrm{deg}^2$) in many (9) filters (Aldering and The SNAP Collaboration, 2004). This potent combination satisfies the basic requirements of an optical strong gravitational lensing survey. Experience with radio surveys such as CLASS (Myers et al., 2003) suggests that around one in 1000 high redshift objects may be strongly lensed, whilst the lensing rate for the less visible but far more numerous faint optical galaxies in the optical appears to be significantly lower. These numbers prompt for the examination of very large areas of sky. However, the majority of the multiple-imaging events occur on arcsecond angular scales, requiring sub-arcsecond resolution for their discovery. Finally, the identification of a strong lens system hinges on the achromatic nature of lensing: multi-colour imaging is of enormous value in the initial identification of a lens.

The lensing cross-section in the Universe is dominated by the many massive elliptical galaxies lying at redshifts of 1 or less (Turner et al., 1984); galaxy clusters provide more cross-section per object but are rarer. The following strategy suggests itself: search in the vicinity of (easily classified) elliptical galaxies, with (well-understood) photometric redshifts, for characteristic patterns of similarly coloured images. Similar algorithms have been applied to spectroscopic data (Bolton et al., 2004) and, principally visually, to HST image data (Ratnatunga et al., 1999; Fassnacht et al., 2004). Many lens systems may be expected from simply filtering the 9 filter photometric catalogue from the weak lensing analysis; others will be found by digging deeper into the wings of the lens galaxy light. We begin to quantify the success of SNAP in this regard below. Cluster gravitational lenses are perhaps best discovered by a similarly targeted search for elongated images around congregations of red sequence galaxies (Lenzen et al., 2004; Gladders et al., 2003), followed by an iterative search for more multiple images. Whilst forming part of the ongoing SNAP strong lensing survey project, these lens systems are not discussed here. Instead, we focus on the elliptical galaxy lenses and some of the science they enable.

2. Predicting elliptical lens numbers

The leftmost columns of Table 1 give the vital statistics of the two baseline surveys planned for SNAP's initial 4-year observing period. In this work we investigate the capabilities of a "piggyback" survey, just using the images taken for the two primary experiments and placing no extra demands on the mission.

The expected numbers of lenses are given by the following equations:

$$N_{\mathrm{lens}} = \int X \cdot \frac{\mathrm{d}^2 N_{\mathrm{d}}}{\mathrm{d}z_{\mathrm{d}}\,\mathrm{d}\sigma_{\mathrm{d}}} \cdot \frac{\mathrm{d}^2 N_{\mathrm{s}}}{\mathrm{d}z_{\mathrm{s}}\,\mathrm{d}m_{\mathrm{s}}}\,\mathrm{d}z_{\mathrm{d}}\,\mathrm{d}\sigma_{\mathrm{d}}\,\mathrm{d}z_{\mathrm{s}}\,\mathrm{d}m_{\mathrm{s}}, \quad (1)$$

$$X(z_{\mathrm{d}}, \sigma_{\mathrm{d}}, z_{\mathrm{s}}, m_{\mathrm{s}}) = \int^{\beta_{\mathrm{crit}}} 2\pi S(\beta, \ldots)\, d^2\beta. \quad (2)$$

We follow Mitchell et al. Mitchell et al. (2004) and use the SDSS elliptical galaxy velocity function for the deflector population $\mathrm{d}^2N_{\mathrm{d}}/\mathrm{d}z_{\mathrm{d}}\,\mathrm{d}\sigma_{\mathrm{d}}$; for the faint galaxy sources ($\mathrm{d}^2N_{\mathrm{s}}/\mathrm{d}z_{\mathrm{s}}\,\mathrm{d}m_{\mathrm{s}}$) we extrapolate somewhat conservatively the HDF galaxy counts from Casertano et al. (2000) and apply the model redshift distribution of Massey et al. (2004). For the quasar sources we use the 2dF luminosity functions from Boyle et al. (2000) and Croom et al. (2004), noting that these analyses give different faint end slopes. The final piece of Eq. (1) is the

Table 1
Proposed primary SNAP surveys, and projected elliptical strong gravitational lens numbers

Survey	Ω (deg^2)	AB magnitude limit	$N_{\mathrm{lens,\ galaxies}}$	$N_{\mathrm{lens,\ quasars}}$
Deep (SNIa)	15	30.6	5000	Few–few tens
Wide (WL)	1000	28.3	50,000	100–1000

The magnitude limits are for point sources in the B band (filter 1).

cross-section for producing an observable multiple image system. This quantity is an integral over the source plane, and is dependent on the lens properties (assumed for simplicity to be singular isothermal spheres (Koopmans et al., 2003)), but also the details of the detection process. A multiple image system was taken as having been detected if three pixels of the surface brightness peaks were three times higher than the noise level in the filter 1 image, provided the images were separated by twice the PSF FWHM.

The results of this simple calculation are shown in the righthand columns of Table 1: they suggest that around 1–2% of elliptical galaxies have a multiple image system associated with them. The lensed quasar numbers are most sensitive to the (as yet somewhat poorly measured) faint-end slope of the luminosity function. The galaxy–galaxy lens count prediction is quite sensitive to our ability to separate the lens galaxy light from the source image: the above selection function made no allowance for the lens galaxy. An approximate actual success rate was obtained by visual inspection of a small sample of lenses drawn from the probability distribution defined by the integrand in Eq. (1). Fig. 1 gives an example of a lens system measurable with SNAP, and a system that may well have escaped detection by eye; in these images, the 9 filters have been crudely grouped in threes for the colourisation, and a square root stretch applied. Our preliminary estimate is that as many as 1 in 5 galaxy–galaxy strong lens systems expected from the "invisible lens" selection function will actually be detectable and measurable in the SNAP images; the quasar lenses will be much easier to detect, but their numbers are still uncertain by an order of magnitude or so. We may hope to improve the galaxy–galaxy lens detection rate with sophisticated 9-filter lens finding algorithms, but for now we anticipate a catalogue of some 10,000 strong lenses, dominated by galaxy–galaxy lenses detected in the weak lensing survey.

3. Science from the elliptical lens sample

The expected SNAP lens sample would contain much information on the elliptical galaxy mass

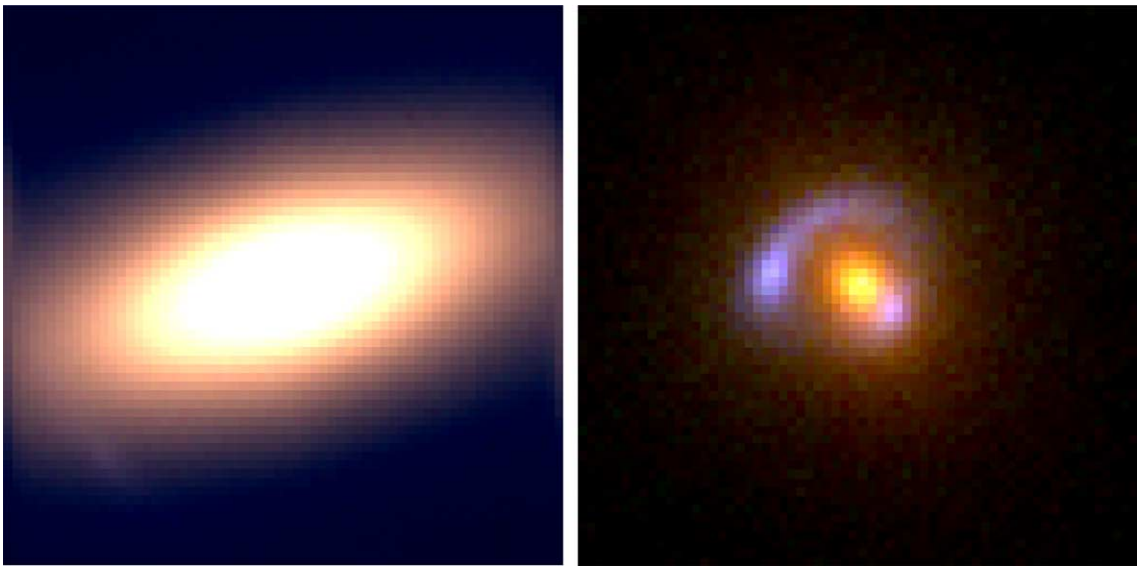

Fig. 1. Simulated typical strong lens systems, as they would be observed with SNAP (these images are 9 filter composites). The fields are centred on the (yellow) elliptical lens galaxy; the lensed background source galaxies appear as (blue) arcs with $\sim 1''$ curvature radii. The left hand panel highlights the observational challenge of detecting lensed images in the presence of obscuration by the lens light (the arc is to the lower left): the 9 filters will be invaluable here. (For interpretation of the references to colour in this figure legend, the reader is referred to the web version of this article.)

distributions, the source redshifts and cosmology. How is the information partitioned? An approximate answer to this can be found by qualitatively identifying the subsets of the lens catalogue with discriminating power in each field. In the lefthand panel of Fig. 2 we show how the redshift distribution of galaxies too faint for spectroscopy can begin to be investigated using a snapshot spectroscopic follow-up campaign on the candidate lens galaxies (providing knowledge of the lens mass and lens redshift). Those systems where the lens and source planes are closely separated give the tightest constraint on the source redshift. Conversely, a subsample of the SNAP strong lens catalogue possessing well-understood source redshifts would open up the possibility of a cosmographic study (Paczynski and Gorski, 1981, 1997). The image separation is dependent on cosmology, being proportional to the ratio of angular diameter distances $D_{ds}(z_d,z_s)/D_s(z_s)$.

The righthand panel of Fig. 2 shows the constraints available in the $\Omega_m - w$ plane (assuming a flat Universe) from various cosmographic experiments. A conservative estimate of 5000 suitable lenses (with image separations detected and measured to 1/3 of a pixel precision), with photometric redshift uncertainties of 0.02 (lens) and 0.2 (source) and the lens mass just estimated from the SDSS Faber Jackson relation (Bernardi et al., 2003) yields interesting, but not competitive, precision. Tighter constraints are gained by focussing on sub-samples of the catalogue and targeting them for spectroscopic follow-up observation. Constraining the mass with spectral velocity dispersion measurements has the biggest effect, suggesting that the SNAP data alone are best used to investigate the mass distribution of elliptical galaxies within an assumed cosmological model. The next step is the assessment of the effect of the lens modelling on the dark energy parameter accuracy.

As seen above, SNAP will detect a significant number of lensed quasars and provide HST-quality optical imaging data for these objects, promising to greatly improve the strong lensing measurement of H_0. What will be needed are complementary time delay measurements: the deep SN survey (with its 4-day observing cadence) could provide time delays for some tens of lensed quasar systems, but the much larger weak lensing survey will only provide single epoch images. There will be a number of survey telescopes operational at the same time as SNAP that could provide time delays for these latter ob-

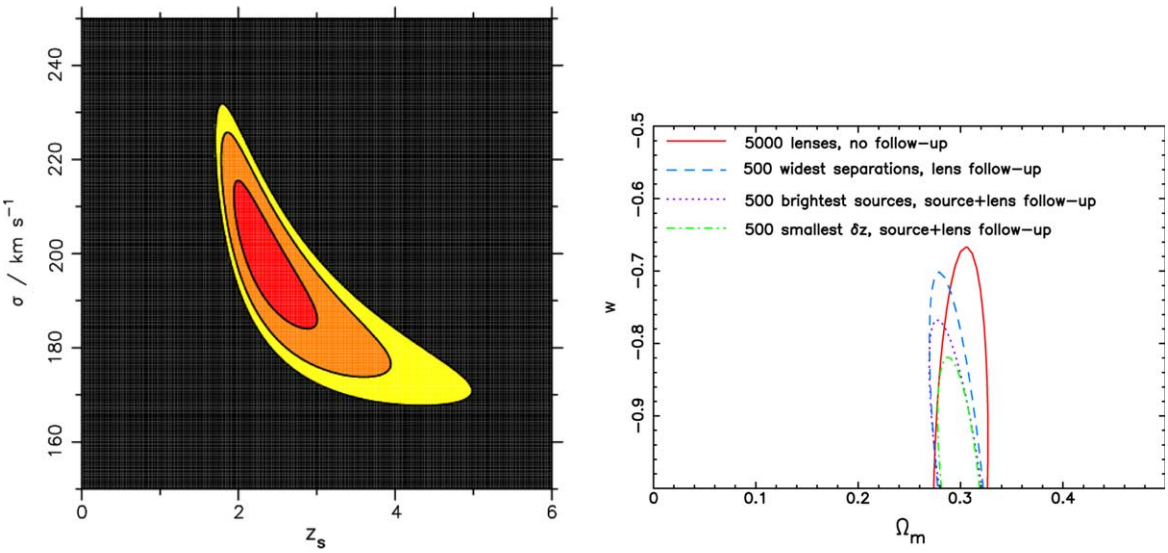

Fig. 2. Left: Source redshift measurement ($z_s = 2.3$) from a $z_d = 1.1$ lens. Right: Strong lens cosmography from various, and relatively unambitious, subsamples of a SNAP catalogue.

jects; these, together with the SNAP imaging data, should provide excellent constraints on the Hubble constant and allow its scatter (which is sensitive to small-scale mass fluctuations along the line-of-sight) to be investigated.

4. Conclusions

The width and depth of the proposed SNAP observing programmes, their multi-colour nature, and the excellent image quality are all well-suited to a strong lens search. Targeting the elliptical galaxies, we believe that the achromatic excesses in the images can be extracted; the resulting catalogue, containing an unprecedented number of multiple image systems, may then be used for many astrophysical and cosmological experiments, with just a few touched upon here. We anticipate that complementary observations in the spectral and temporal domains will be very important for getting the most out of the SNAP data.

Acknowledgements

We thank Dragan Huterer and Charlie Baltay for useful discussions. This work was supported by the Department of Energy contract DE-AC3-76SF00515 to SLAC.

References

Aldering, G., The SNAP Collaboration, 2004. PASP submitted for publication. Available from: astro-ph/0405232.
Bernardi, M. et al., 2003. AJ 125, 1849.
Bolton, A.S., Burles, S., Schlegel, D.J., Eisenstein, D.J., Brinkmann, J., 2004. AJ 127, 1860.
Boyle, B. et al., 2000. MNRAS 317, 1014.
Casertano, S. et al., 2000. AJ 120, 2747.
Croom, S.M. et al., 2004. MNRAS 349, 1397.
Fassnacht, C.D., Moustakas, L.A., Casertano, S., Ferguson, H.C., Lucas, R.A., Park, Y., 2004. ApJL 600, 155.
Gladders, M.D., Hoekstra, H., Yee, H.K.C., Hall, P.B., Barrientos, L.F., 2003. ApJ 593, 48.
Im, M., Griffiths, R.E., Ratnatunga, K.U., 1997. ApJ 475, 457.
Koopmans, L.V.E. et al., 2003. ApJ 599, 70–85.
Lenzen, F., Schindler, S., Scherzer, O., 2004. A&A 416, 391.
Massey, R. et al., 2004. AJ 127, 3089.
Mitchell, J.L., Keeton, C.R., Frieman, J.A., Sheth, R.K., 2004. Available from: astro-ph/0401138.
Myers, S.T. et al., 2003. MNRAS 341, 1.
Paczynski, B., Gorski, K., 1981. ApJL 248, L101.
Perlmutter, S. et al., 1999. ApJ 517, 565.
Ratnatunga, K.U., Griffiths, R.E., Ostrander, E.J., 1999. AJ 117, 2010.
Rhodes, J., Refregier, A., Groth, E.J., 2001. ApJL 552, 85.
Riess, A.G. et al., 2004. ApJ 607, 665.
Turner, E.L., Ostriker, J.P., Gott, J.R., 1984. ApJ 284, 1.

Available online at www.sciencedirect.com
SCIENCE DIRECT®
New Astronomy Reviews 49 (2005) 392–395
New Astronomy Reviews
www.elsevier.com/locate/newastrev

Weak lensing studies from space with GEMS

C. Heymans [a,*], M.L. Brown [b], M. Barden [a], J. Caldwell [c], B. Häußler [a], K. Jahnke [d], H.-W. Rix [a], S. Beckwith [c], E.F. Bell [a], A. Borch [a], S. Jogee [c], D.H. McIntosh [e], K. Meisenheimer [a], C. Peng [f], S. Sánchez [d], R. Somerville [c], A.N. Taylor [b], L. Wisotzki [d], C. Wolf [g]

[a] *Max-Planck-Institut für Astronomie, D-69117, Heidelberg, Germany*
[b] *University of Edinburgh, Edinburgh, EH9 3HJ, UK*
[c] *Space Telescope Science Institute, Baltimore MD, 21218, USA*
[d] *Astrophysikalisches Insitut Potsdam, D-14482 Potsdam, Germany*
[e] *University of Massachusetts, Amherst, MA 01003, USA*
[f] *University of Arizona, Tuscon AZ, 85721, USA*
[g] *University of Oxford, Oxford, OX1 3RH, UK*

Available online 26 September 2005

Abstract

The Galaxy Evolution from Morphology and SEDs (GEMS) survey is the largest contiguous field ever imaged in colour by HST with the Advanced Camera for Surveys (ACS), spanning some 900 square arcmins in the Chandra deep field south (CDFS). We discuss the power of the ACS for weak lensing studies and present preliminary results from our cosmic shear analysis of GEMS. Selecting a subset of GEMS galaxies which are resolved in deep ground-based R-band imaging of the CDFS from the COMBO-17 survey, we compare the cosmic shear signal determined from the ground and from space.
© 2005 Published by Elsevier B.V.

Contents

1. Introduction 393
2. The ACS PSF 393
3. Analysis: the shear correlation function 393

* Corresponding author.
E-mail address: heymans@mpia.de (C. Heymans).

1387-6473/$ - see front matter © 2005 Published by Elsevier B.V.
doi:10.1016/j.newar.2005.08.010

4. Comparison with COMBO-17 ground based data . . . 394
5. Conclusion . . . 395
References . . . 395

1. Introduction

Weak gravitational lensing by large scale structure shears images of background galaxies, inducing weak correlations in the observed ellipticities of galaxies, where the amplitude and angular dependence of these correlations are directly related to the nonlinear matter power spectrum $P_\delta(k)$ and the geometry of the Universe (see Bartelmann and Schneider, 2001 and references within). Following the success of the first generation of cosmic shear surveys several ground based surveys are currently underway that will image of the order of a hundred square degrees, providing exquisite data sets for future weak lensing analysis. These surveys will however be subject to atmospheric seeing which erases the weak lensing shear information from all galaxies smaller than the size of the seeing disk. This, in effect, limits the maximum depth of ground based weak lensing surveys and hence the sensitivity, leading to proposals for future deep wide-field space-based observations such as JDEM and DUNE.

With the installation of the ACS on HST, relatively wide-field space-based weak lensing studies are now feasible and in this conference proceeding we present the detection of weak gravitational lensing by large scale structure in F606W Galaxy Evolution from Morphology and SEDs (GEMS) data which has a resolved galaxy number density of $\sim$100 galaxies per square arcmin (see Rix, 2004 for an overview of the GEMS survey).

2. The ACS PSF

The accuracy of any weak lensing analysis depends critically on the correction for the distorting point spread function (PSF) of the telescope and camera, characterised through images of stellar objects. As a result of the wide field of view of the ACS, the relative stability of the ACS PSF over time, and the observing strategy of GEMS, whereby all but three out of the 63 ACS images were taken in the space of 20 days, the PSF of the ACS in the time period of the GEMS observations is very well characterised.

We use the method of KSB+ (Kaiser et al., 1995; Luppino and Kaiser, 1997; Hoekstra et al., 1998) to invert the effects of the PSF smearing and shearing in order to recover an unbiased estimate of galaxy shear γ. Fig. 1 shows the variation in the measured KSB+ PSF correction vector p across the ACS field of view clearly revealing the anisotropy of the PSF distortion which is at the level of $\sim$5%. We model p with a two-dimensional second order polynomial which we then use to correct all galaxy ellipticities in the GEMS mosaic. Owing to the non-Gaussian nature of the PSF, p changes as a function of galaxy size r_g and we therefore create models $p(r_g)$. Note that for the GOODS images (Giavalisco, 2004), which comprise the central 15 ACS tiles of the GEMS mosaic, we characterise a second set of PSF models using all stars imaged by GOODS, as the different dithering patterns of GOODS and GEMS impacts somewhat on the PSF. The right panel of Fig. 1 shows that the correlation between galaxy ellipticity and stellar ellipticity (upper panel) is successfully removed by the PSF correction (lower panel).

3. Analysis: the shear correlation function

We measure the mean shear correlation function $\langle \gamma_r^t \gamma_r^t \rangle_\theta$ and full statistical covariance matrix from the GEMS data using a modified jackknife method. With knowledge of the survey redshift distribution, the shear correlation function can be directly related to the nonlinear mass power spectrum P_δ, where the exact relationship can be found in Bartelmann and Schneider (2001). We estimate the median redshift z_m of the GEMS survey based on redshifts from the COMBO-17

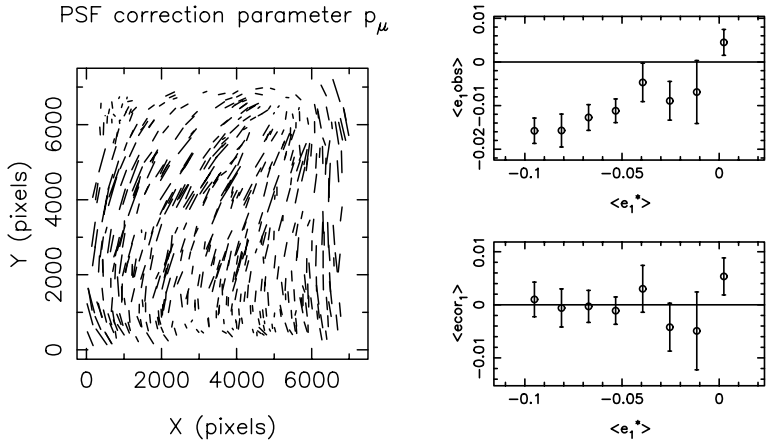

Fig. 1. The variation in the measured PSF correction vector p across the ACS field of view (left). Galaxy ellipticities are corrected for the PSF distortion such that the correlation between galaxy ellipticity and stellar ellipticity seen before PSF correction (upper right) is removed (lower right).

survey (Wolf, 2004) and VVDS survey (Le Fevre, 2004), finding $z_m = 0.95 \pm 0.1$. Fig. 2 shows our preliminary measurement of the GEMS tangential and radial shear correlation functions with the theoretical model for a survey with $z_m = 0.95$, calculated for a ΛCDM cosmology with the amplitude of the matter power spectrum $\sigma_8 = 0.85$ as found by WMAP (Spergel, 2003), over-plotted. Our results are consistent with this concordant model, although we do note that our error bars are statistical and do not include the uncertainty arising from cosmic variance. The CDFS is a factor of two under-dense in massive galaxies (Wolf, 2003) and we would therefore expect the measurement of σ_8 from this field to be lower than the Universal σ_8.

4. Comparison with COMBO-17 ground based data

COMBO-17 is a deep multi-colour survey spanning 1.25 square degrees in five separate regions, carried out with the WFI/ESO 2.2 m (Brown et al., 2003). The deep R-band COMBO-17 data in the CDFS allows us to compare the CDFS cosmic shear signal measured from space-based data and from ground-based data. We select a subsample of GEMS galaxies that are resolved in the

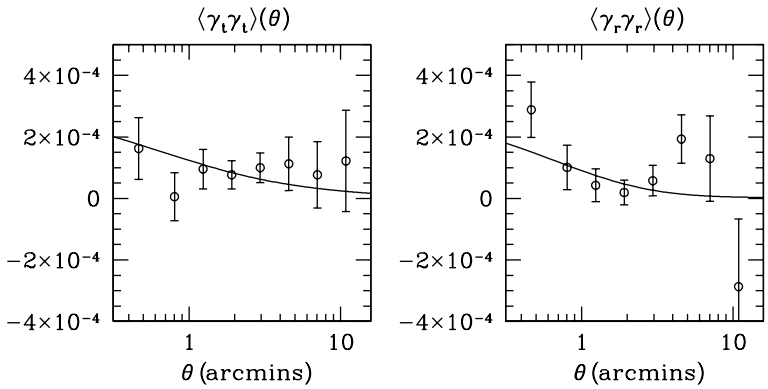

Fig. 2. The GEMS shear correlation function; $\langle\gamma_t\gamma_t\rangle_\theta$ (left) and $\langle\gamma_r\gamma_r\rangle_\theta$ (right). The correlation function prediction for a flat ΛCDM cosmology ($\Omega_m = 0.3$, $\Omega_\Lambda = 0.7$) with $\sigma_8 = 0.85$ is over-plotted.

COMBO-17 data, finding good agreement between galaxy shear estimated from GEMS data and from COMBO-17 data. We calculate the shear correlation function for this galaxy subsample which although producing a very noisy result, reveals that the noise in the GEMS galaxy catalogue is less than that from the COMBO-17 catalogue, showing that the measurement of galaxy shear is improved with space-based imaging.

5. Conclusion

We have detected weak lensing by large scale structure in the GEMS survey, demonstrating the power of the ACS on HST for this type of study. The comparison of space-based GEMS data and ground-based COMBO-17 data has shown that galaxy shear is measured to a higher accuracy from space-based data and this evidence, combined with the threefold increase in resolved galaxy number density that comes with HST data, shows that space-based imaging is truly superior to ground-based imaging for weak lensing studies, supporting the drive towards large wide-field imaging surveys from space. A more detailed description of our GEMS weak lensing analysis can be found in Heymans et al. (2005), and our comparison with ground-based data can be found in Brown et al. (in preparation).

References

Bartelmann, M., Schneider, P., 2001. PhR 340, 291.
Brown, M., Taylor, A., Bacon, D., Gray, M., Dye, S., Meisenheimer, K., Wolf, C., 2003. MNRAS 341, 100.
Giavalisco, M.GOODS Collaboration, 2004. ApJ (Lett.) 600, L93–L98.
Heymans et al., 2005. MNRAS 361, 160.
Hoekstra, H., Franx, M., Kuijken, K., Squires, G., 1998. ApJ 504, 636.
Kaiser, N., Squires, G., Broadhurst, T., 1995. ApJ 449, 460–475.
Le Fevre, O., VVDS Team, 2004. A&A 428, 1043.
Luppino, G.A., Kaiser, N., 1997. ApJ 475, 20.
Rix, H.GEMS Collaboration, 2004. ApJ Suppl. 152, 163–173.
Spergel, D.WMAP Collaboration, 2003. ApJ Suppl. 148, 175–194.
Wolf, C.COMBO-17 Collaboration, 2004. A& A 421, 913.
Wolf, C.COMBO-17 Collaboration, 2003. A&A 401, 73.

Available online at www.sciencedirect.com
SCIENCE DIRECT®
New Astronomy Reviews 49 (2005) 396–399
New Astronomy Reviews
www.elsevier.com/locate/newastrev

General astrophysics with the optical terrestrial planet finder mission

Karl Stapelfeldt [a], Chas Beichman [b,*], Marc Kuchner [c]

[a] *MS 183-900, Jet Propulsion Laboratory, California Institute of Technology, Pasadena, CA 91109, United States*
[b] *Michelson Science Center, Mail Stop 100-22, California Institute of Technology, Pasadena, CA 91125, United States*
[c] *Astrophysics Department, Peyton Hall, Princeton University, Princeton, NJ 08544, United States*

Available online 19 October 2005

Abstract

The Terrestrial Planet Finder (TPF) mission is being designed to directly detect terrestrial planets in the habitable zones around nearby FGK stars, and to spectrally characterize them for the presence of biomarkers. TPF is now planned as two missions: $a \sim \times 3.5$ m optical coronagraphic telescope (TPF-C) to fly circa 2014; and a formation-flying infrared nulling interferometer (TPF-I) to follow several years later. While high contrast performance and planet-finding will remain the primary science drivers for both missions, the project has begun to consider possible extensions to their capabilities that would enable progress in other important areas of astrophysics. For example, deep extragalactic surveys could be enabled by adding a camera with a several arcminute field of view to TPF-C. Here, we give an overview of the TPF-C project, and offer initial suggestions for its application to general astrophysics.
© 2005 Published by Elsevier B.V.

Contents

1. Introduction . . . 397
2. Current description of TPF-C . . . 397
3. A "wider field" camera for TPF-C . . . 397
4. Concluding remarks . . . 399
Acknowledgements . . . 399

* Corresponding author.
E-mail address: chas@ipac.caltech.edu (C. Beichman).

1387-6473/$ - see front matter © 2005 Published by Elsevier B.V.
doi:10.1016/j.newar.2005.08.011

1. Introduction

Direct detection and spectral characterization of extrasolar planets is a key goal for future NASA space observatories. Current space imaging systems (and ground adaptive optics systems in development) fall 3–4 orders of magnitude short of the needed dynamic range. To develop the needed new capabilities, a NASA/university/industry team has been studying potential architectures for a Terrestrial Planet Finder (TPF) space observatory mission under the leadership of the Jet Propulsion Laboratory (JPL). The contrast challenge is easiest in the thermal infrared: 10^{-7} for a planet of Earth's size and temperature, when observing at a wavelength of 10 μm. A thermal infrared nulling interferometer, consisting of multiple ~3 m cryogenic telescopes on separate formation-flying spacecraft ~100 m apart, would be required at these wavelengths. At visible wavelengths, planets are seen by reflected light instead of thermal emission, and an Earth-like planet in the habitable zone presents a contrast of 10^{-10} to its parent star. Here a single, highly stable 6–8 m telescope operating at room temperature could achieve the mission goals, provided that a high-performance coronagraph instrument was available.

Major progress toward demonstrating the needed coronagraph performance has recently taken place in system-level tests at JPL. A prototype Lyot coronagraph, equipped with a precision deformable mirror (3200 actuators), has demonstrated vacuum contrast performance of 1–2×10^{-9} at an angular separation of four Airy rings. This progress, in combination with the strong scientific desire for multiwavelength spectral characterization of exoplanets, has led NASA to re-define the TPF project as two successive missions: an optical coronagraph (TPF-C) to fly first, circa 2014; and an infrared interferometer (TPF-I) to follow a few years later. International collaboration is being sought for both missions, with details still under discussion with ESA.

2. Current description of TPF-C

The relatively unusual configuration of the TPF-C observatory (Fig. 1) is motivated by the requirements of its high contrast imaging mission. The primary mirror is a 6–8 m × 3.5 m ellipse: this enables V-band terrestrial planet searches in a minimum of ~50 suitable target stars, while retaining a monolithic configuration that can be launched in existing rocket shrouds. The telescope has an off-axis design, to minimize diffraction effects and maximize coronagraph throughput. To provide very high thermal stability, the telescope is enclosed in a multi-layer V-groove sunshade, and will be operated in either Earth-trailing or L2 orbits. The large sunshade dictates a solar sail to counterbalance radiation pressure torques on the spacecraft. Milliarcsec-level pointing will be required to maintain alignment of the bright target star on the coronagraph occulting spot.

TPF-C's main instrument will be a coronagraphic camera operating over the wavelength range $0.35 < \lambda < 1.05$ μm. It will have a very modest field of view, perhaps 30″ in diameter, with a corrected high contrast dark field extending to a radius of ~1″ from the bright central star. The science camera will also serve as a wavefront sensor to derive the adaptive correction settings for the deformable mirror (DM), which must be set and maintained to sub-angstrom accuracy to achieve the required contrast. The camera will ideally provide multispectral imaging, at resolutions from 5 to 70, in order to separate planets from residual stellar speckles, and to characterize their atmospheres.

Terrestrial exoplanets are very faint targets, with typical $V = 28$–31. Exposure times of a day or two will be needed to detect them. Repeat observations at multiple epochs will be needed to mitigate against unfavorable planetary elongations or illumination phases. Thus each of the ~50 target stars will be searched for a week of cumulative integration time. In systems where candidate planets are detected, follow-up observations to establish common proper motion, constrain orbital elements, and spectroscopically characterize the planet will add weeks of additional integration time per target.

3. A "wider field" camera for TPF-C

The TPF-C telescope will have ~5× the collecting area of HST, and up to 3× the spatial resolution.

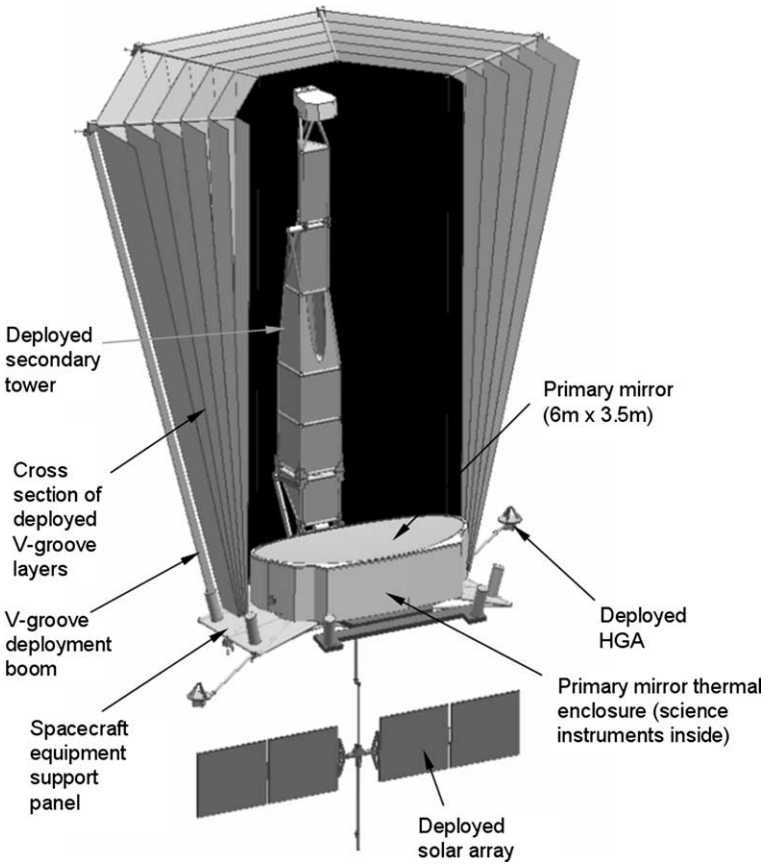

Fig. 1. TPF-C conceptual design as of summer 2004. The foreground half of the V-groove sunshade has been cut away for clarity. A solar sail counterbalancing the solar pressure torques on the sunshade, and located on the boom beyond the solar arrays, is not shown.

It is clear that such a telescope could be a tremendous resource for general astrophysical investigations, particularly if additional instrumentation can be provided. The TPF project has begun to consider how additional instruments might be accommodated in the science payload, subject to two key constraints: (1) The primary planet-finding mission must not be compromised; and (2) any additional instrument must be relatively simple and affordable. It is anticipated that an upper limit of 25% of the observing time could be dedicated to other astrophysics programs, as planet-finding investigations already fill the bulk of TPF-C's 5 year design life.

The specific design of an additional TPF-C instrument will emerge from an open proposal process. Nevertheless, it is clear that a wider field optical camera ($5' \times 5'$, for example) would be a very capable instrument on TPF-C. In particular, the week-long cumulative integration times required for planet searches would provide an excellent opportunity for parallel deep field observations near the TPF target stars. Each of these 50+ deep fields would be observed 1.7 mag deeper than the HST Ultra Deep Field, while the multiple observation epochs needed for planet finding would enable supernova searches. In the (say) 10 stars where follow-up planetary spectroscopy is carried out, the ultimate depth of these parallel deep fields could reach 3 mag beyond the UDF. Careful control of stray light will be required to realize these gains, but this is already a high design priority for the primary planet search mission.

In addition to parallel deep field science, a broad range of dedicated observations can be contemplated with "wider field" camera: stellar population studies in crowded fields, allowing the star formation histories to be derived for a wide range of galaxy types; the study of Cepheid variables in the Coma cluster; resolving the substructure of strong lensing arcs to constrain the dark matter distribution in clusters of galaxies; morphological classification of high z galaxies, tracking galaxy evolution and complementing JWST deep fields; and counts of faint Kuiper Belt Objects. The main coronagraphic camera should also find applications outside of planet-finding: studies of quasar host galaxies, the structure of dust shells around post-main-sequence stars, and dynamical masses for rare stellar types.

4. Concluding remarks

Extrasolar planet discoveries during the past decade have pointed the way to exciting new research opportunities for space astronomy. By pushing back the frontiers of high contrast, high resolution optical imaging toward the goal of direct detection of Earth-like planets, a broad range of new fundamental astrophysics also is enabled. This is the promise and goal of the TPF-C mission.

Acknowledgements

The authors thank TPF's Science Working Group and Design Team for their inputs to this paper. This work was supported by the TPF pre-project at JPL, under NASA Contract 1407.

Available online at www.sciencedirect.com
SCIENCE DIRECT®
New Astronomy Reviews 49 (2005) 400–406
New Astronomy Reviews
www.elsevier.com/locate/newastrev

Observing cluster galaxies and their progenitors with JDEM

Pieter G. van Dokkum

Department of Astronomy, Yale University, New Haven, CT 06520-8101, United States

Available online 13 September 2005

Abstract

The Joint Dark Energy Mission (JDEM) is expected to have a field-of-view that is several orders of magnitude larger than that of current instruments on the Hubble Space Telescope, with only slightly reduced sensitivity and resolution. This contribution gives a brief discussion of the impact that JDEM would have on studies of galaxies in clusters at $0.5 < z < 2$ and of the most massive galaxies at higher redshift. Of particular importance is JDEMs unique wide-field near-IR capability, enabling the selection and morphological study of high redshift galaxies in the rest-frame optical rather than the rest-frame ultra-violet.
© 2005 Published by Elsevier B.V.

Contents

1. Introduction . . . 401
2. What are we learning from HST? . . . 401
   2.1. Evolution of early-type galaxies . . . 401
   2.2. Morphological evolution: interaction with the environment . . . 402
3. The role of JDEM . . . 403
   3.1. The infall regions of clusters . . . 403
   3.2. Progenitors at $z > 2$ . . . 404
   3.3. JDEM design considerations . . . 406
   References . . . 406

E-mail address: pieter.vandokkum@yale.edu.

1387-6473/$ - see front matter © 2005 Published by Elsevier B.V.
doi:10.1016/j.newar.2005.08.012

1. Introduction

The primary goal of the Joint Dark Energy Mission (JDEM) is to improve our understanding of the nature of dark energy through accurate brightness measurements of Type Ia supernovae (SNe) out to $z \approx 1.7$. However, JDEM could have a profound impact on many other fields of astronomy: if it is designed as a wide-field optical/near-IR survey telescope, whose full-resolution data are saved and sent to Earth, it will be a tremendous improvement over current facilities and an ideal complement to the "pencil-beam" JWST. Compared to the current capabilities of HST, JDEM would have a field-of-view 100× greater in the optical and 1500× greater in the near-infrared, with only slightly lower sensitivity and resolution. The Deep Survey envisioned by the SNAP collaboration (Aldering et al., submitted) would image an area of 15 degrees^2 in 9 optical/near-IR filters to greater depth than the Hubble Ultra Deep Field.

Many applications of JDEM were highlighted at the meeting, including the impact it will have on the studies of large scale structure (see contribution by Daniel Eisenstein), galaxy formation (Rachel Somerville), and galaxy evolution (David Hogg). This contribution focuses on the importance of JDEM for the study of galaxy clusters at $0.5 < z < 2$ and of the likely progenitors of cluster galaxies at higher redshift. A SNAP-like design is assumed, i.e., a wide field optical/near-IR imager.

Studies of the formation and evolution of cluster galaxies give insight in the assembly and star formation history of the most massive disk- and spheroidal galaxies in the Universe. Because of their high masses and old stellar populations they provide important tests of the hierarchical paradigm for galaxy formation: in these models galaxies are built up slowly through a combination of mergers and star formation, and more massive galaxies are predicted to have assembled more recently (e.g., Meza et al., 2003). The evolution of cluster galaxies is also important for understanding galaxies at very high redshifts. In hierarchical models the first objects form preferentially in overdense regions, which evolve into groups and clusters at the present day. Specifically, Baugh et al. (1998) predict that the descendants of $z \approx 3$ Lyman break galaxies (LBGs) typically live in halos of circular velocity >400 km s^{-1} today, compared to ~250 km s^{-1} for galaxies that did not have a LBG progenitor. These arguments also apply to the descendants of the brightest galaxies at $z \sim 7$ and beyond, and to the highest redshift quasars.

2. What are we learning from HST?

As so many other fields, the study of cluster galaxies has benefited greatly from the combination of HST imaging and spectroscopy with 8–10 m ground-based telescopes in the past decade. At the time of the meeting, about 60 distant clusters had been observed with WFPC2 and about 30 with ACS (excluding snapshot programs). The clusters were selected in X-rays or in the optical/near-IR, and span a redshift range $0.2 \lesssim z \lesssim 1.4$. The vast majority of the HST observations cover just a single central pointing of <10 arcmin^2, and only a handful studies have observed areas larger than the equivalent of ≈4 independent pointings (e.g. van Dokkum et al., 1998a; Treu et al., 2003).

2.1. Evolution of early-type galaxies

Early-types (elliptical and S0 galaxies) constitute ~80% of the galaxy population in the cores of nearby clusters (Dressler, 1980). They form a very homogeneous population: at a given mass, they show a very small scatter in their colors, luminosities, and line indices. This high degree of regularity is expressed in tight scaling relations between color and magnitude (Bower et al., 1992), velocity dispersion and Mg line strength (e.g. Bender et al., 1993), and velocity dispersion, radius, and surface brightness (the Fundamental Plane; Djorgovski and Davis, 1987).

Studies of the redshift evolution of these relations are in remarkable agreement. The evolution of their colors (e.g. Ellis et al., 1997; Stanford et al., 1998; Blakeslee et al., 2003), M/L ratios and Fundamental Plane (e.g. van Dokkum et al.,

1998b; Kelson et al., 2000; van Dokkum and Stanford, 2003; Wuyts et al., 2004), and line indices (Bender et al., 1998; Kelson et al., 2001) show that massive early-type galaxies remain a very homogeneous population over the entire redshift range $0 < z < 1.3$.

The strongest constraints on the mean age of the stars in early-type galaxies have come from studies of the Fundamental Plane (FP). Fig. 1(a) shows the evolution of the mean M/L_B ratio of early-type galaxies with masses $>10^{11}$ $M_\odot$, as determined from the FP (van Dokkum et al. in prep.). The evolution is well described by the passive fading of a stellar population formed at $z \approx 2.8$ (indicated by the line), with very small cluster-to-cluster scatter. The best constraints on the galaxy–galaxy scatter in the ages have come from HST studies of the color–magnitude relation. By combining data from the literature with new ACS images of a cluster at $z = 1.24$ Blakeslee et al. (2003) find that the scatter in rest-frame $U - B$ colors is only a few percent independent of redshift (Fig. 1(b)).

2.2. Morphological evolution: interaction with the environment

It has been known for a long time that this simple picture of early formation and passive evolution cannot be complete. The earliest evidence for significant recent evolution in cluster environments was the discovery of the Butcher–Oemler effect: the increase with redshift of the fraction of blue galaxies in clusters (e.g. Butcher and Oemler, 1978; Ellingson et al., 2001; de Propris et al., 2003). Furthermore, HST studies of the central regions of clusters have demonstrated a decreasing fraction of early-type galaxies with redshift (Dressler et al., 1997; van Dokkum and Franx, 2001; Smith et al., 2005): the early-type fraction in clusters at $z \sim 1$ is ≈50%, compared to ≈80% in the local universe. This trend is qualitatively consistent with the larger fraction of blue galaxies at higher redshift, although there is no one-to-one relation between morphology and color, in particular at bright magnitudes (e.g. Poggianti et al., 1999; de Propris et al., 2003). Also, galaxies have been

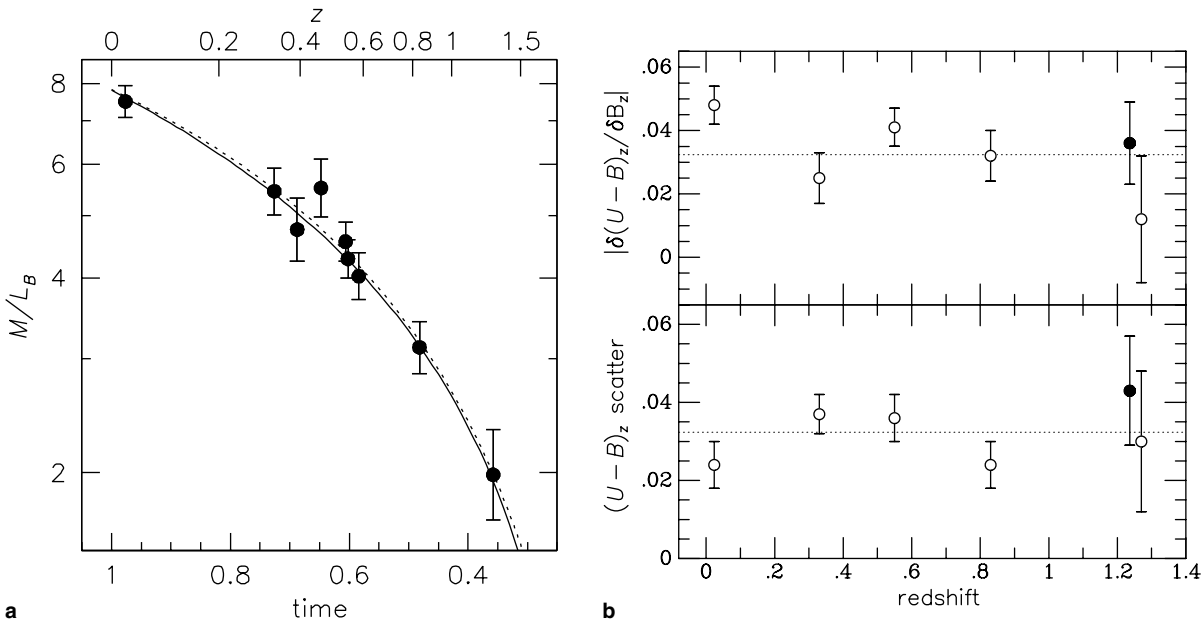

Fig. 1. Early-type galaxies in the cores of rich clusters appear to evolve slowly and regularly. The evolution of their M/L_B ratios is consistent with passive fading of stellar populations formed at $z \approx 3$ (panel a; van Dokkum et al., 1998b and in prep.), and there is no evidence for evolution in the slope or scatter of their color–magnitude relation (panel b; Blakeslee et al., 2003).

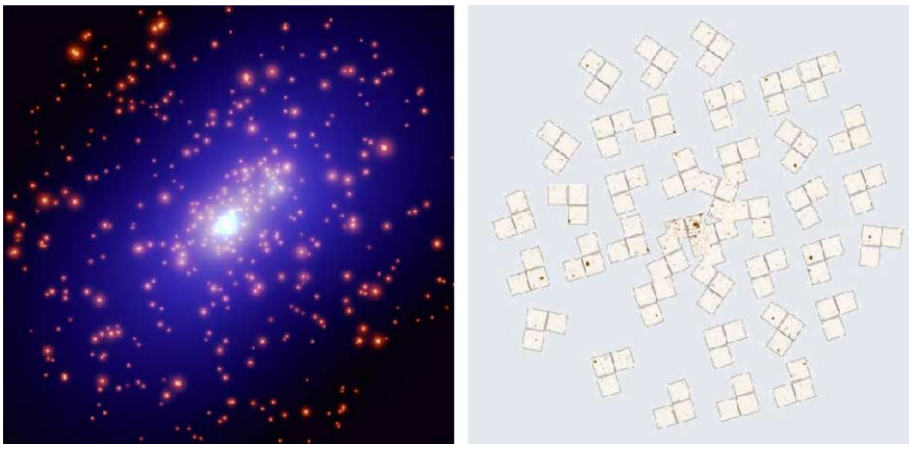

Fig. 2. Wide angle views of the cluster CL 0024 + 16 at $z = 0.39$. Left: mass map, with dark matter shown in blue and luminous matter in red (Kneib et al., 2003). Right: 39 HST WFPC2 pointings sparsely sample a $\sim 27'$ diameter field (Treu et al., 2003). Imaging such large areas with HST is inefficient in the optical, and virtually impossible in the near-infrared.

"caught in the act" of transforming their morphology and/or spectral type. Examples are "E + A" galaxies, which have early-type spectra with strong Balmer lines indicating a recent star burst; red merger systems found in several clusters at $z \sim 1$ (e.g. van Dokkum et al., 1999); and galaxies being stripped of their cold gas in the Virgo cluster (e.g. Kenney et al., 2004).

These effects are probably at least in part driven by infall of galaxies from the field. Clusters are expected to accrete a significant fraction of their final mass after their initial collapse (e.g. Diaferio et al., 2001). Simulations and observations suggest that the infalling galaxies are likely to radically change their star formation rate and morphology as a result of interactions with other galaxies and the hot X-ray gas (e.g. Abraham et al., 1996; Moore et al., 1996; Abadi et al., 1999; Poggianti et al., 1999; Ellingson et al., 2001; Kodama et al., 2001). The details of these processes are not well understood, largely because of the difficulty of studying clusters out to the virial radius and beyond (i.e., to $R \sim 10$ Mpc). Treu et al. (2003) showed that with a large investment of HST time radial trends in morphology can be established out to the virial radius. However, as demonstrated in Fig. 2 HST is very inefficient in covering such large areas, in particular in the near-infrared.

Whatever the cause, morphological transformations severely complicate the interpretation of studies of galaxy evolution in clusters. First of all, it means that we cannot equate the mean age of the stars in a galaxy to its "assembly age", the time since the galaxy took on its current appearance. Furthermore, if many present-day early-types were recently transformed from (field) spiral galaxies their progenitors are not included in samples of $z \sim 1$ cluster early-type galaxies. This "progenitor bias" may cause us to underestimate the evolution of early-type galaxies in clusters (van Dokkum and Franx, 2001). The effects of this bias can be quantified by determining the mechanism and rate of morphological transformations in clusters, or by interpreting the observed evolution of cluster galaxies in the context of a full cosmological simulation (e.g. Diaferio et al., 2001). Both approaches are ambitious, and require a much better understanding of physical processes in the infall regions.

3. The role of JDEM

3.1. The infall regions of clusters

The large field-of-view of JDEM will enable simultaneous study of clusters and the large scale structure in which they are embedded. The

build-up of clusters through infall of galaxies and groups along filaments can be studied in detail, and the morphological changes that are thought to occur in the infall regions can be quantified. A SNAP-like JDEM design will observe the entire field shown in Fig. 2 in a single exposure, and owing to its unique near-IR capability can extend wide-field studies of clusters to $z \sim 2$. Among specific questions that JDEM would address are the morphological composition of galaxies in filaments and infalling groups; the merger rate as a function of local density and dynamical state; and the prevalence of "passive spirals" (e.g. Goto et al., 2003). The broader aims are to determine the rate and mechanisms of morphological transformations as a function of redshift.

A cluster survey could target specific clusters (selected in X-rays, or by their Sunyaev–Zel'dovich effect), but could also piggyback on planned SNe searches. Extrapolating from lower redshifts one may expect >10 rich clusters in SNAP's Deep Survey and >500 in its Wide-field Survey, depending on the imposed mass and redshift cutoff. The clusters can be selected from the weak lensing maps produced as part of the survey (Wittman et al., 2001; Aldering et al., submitted); from X-ray surveys that will likely be planned in the Deep Survey area (see the contribution by Neil Brandt); and with the Gladders and Yee (2000) red sequence technique, which is probably the most efficient method beyond $z \sim 1$. The detailed weak lensing maps are not only useful for selecting clusters, but also characterize the dark matter substructure of clusters and their surroundings at $0.5 \lesssim z \lesssim 1.2$ (Hoekstra et al., 2000).

The extreme depth of the Deep Survey also opens up the interesting possibility of seeing the "tidal tracks" left by infalling galaxies. Simulations suggest that clusters should be riddled with ultra-low surface brightness tidal debris (e.g. Dubinski, 1999), providing a fossil record of the orbits of galaxies similar to that provided by stars in the Galactic halo. It may also be possible to see faint tidal features around a large fraction of elliptical galaxies, if they were assembled at relatively low redshift through "dry mergers"[1] involving little gas (van Dokkum et al., 1999; Bell et al., 2004).

3.2. Progenitors at $z > 2$

Galaxy overdensities have been identified out to $z \sim 4$ and beyond, by selecting galaxies in narrow-band filters centered on the redshifted Lyα line (e.g. Venemans et al., 2002) or by the Lyman break technique (Steidel et al., 1998). However, normal galaxies in the nearby universe and known cluster galaxies out to $z \sim 1.5$ would not be selected in this way, as they are too faint in the rest-frame ultraviolet. The top panels of Fig. 4 illustrate the effect of selecting galaxies in the UV: the GALEX view of M31 only shows the OB associations, missing most of the stellar mass.

The bias toward unobscured star forming galaxies inherent in the Lyman break technique can be avoided by selecting galaxies in the rest-frame optical rather than the rest-frame UV, using their redshifted Balmer- or 4000 Å-break. This selection is difficult due to the relative weakness of the Balmer break and the high sky brightness in the near-IR, and has only recently become feasible with the advent of high quality, large format near-IR detectors on large telescopes. Using very deep VLT images with a total area of $\approx$30 arcmin^2 we recently found a large population of galaxies at $2 < z < 3$ whose rest-frame optical colors are much redder than those of LBGs (Franx et al., 2003; van Dokkum et al., 2003; Förster Schreiber et al., 2004). The galaxies are efficiently selected by the simple observed color criterion $J - K_s > 2.3$. They are very massive (up to $\sim 5 \times 10^{11}$ $M_\odot$; van Dokkum et al., 2004) and appear to be highly clustered (Daddi et al., 2003). Their colors, Hα equivalent widths, line widths, stellar masses, and metallicities are similar to massive star forming galaxies in the nearby universe (van Dokkum et al., 2004; Förster Schreiber et al., 2004; Fig. 3). Most are bright in the near-IR but too faint in the observer's optical to be selected by the Lyman break technique. Their masses, clustering, and colors strongly suggest that they are progenitors of today's early-type galaxies.

The strong field-to-field variations induced by their clustering (see, e.g. Labbé et al., 2003) imply

[1] Rachel Somerville's term.

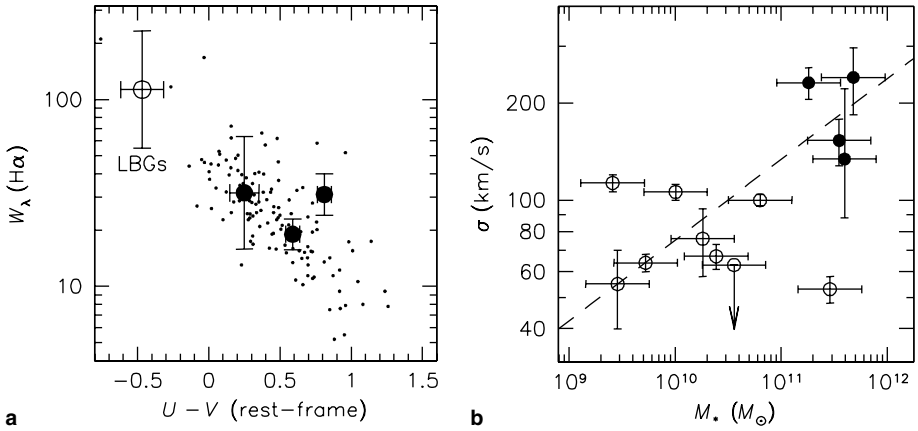

Fig. 3. Properties of $z \sim 3$ galaxies selected in the rest-frame UV (LBGs/open circles; from Pettini et al., 2001 and Shapley et al., 2001) and $z \sim 2.5$ galaxies selected by their red rest-frame optical colors (solid circles). The small sample of red $z \sim 2.5$ galaxies has lower Hα equivalent widths, higher stellar masses, and higher line widths than typical UV-selected $z \sim 3$ galaxies (from van Dokkum et al., 2004).

that large areas need to be imaged to determine accurate surface densities and correlation functions. However, deep, large area near-IR surveys are notoriously difficult. Using ~200 h of VLT observing time FIRES surveyed an area of only 30 arcmin^2 for red $z > 2$ galaxies (Franx et al., 2003; Förster Schreiber et al., 2004). Although we are currently extending this area in the MUSYC project[2], there is no telescope/instrument configuration on the horizon that can compete with JDEM in the near-IR. In addition to exquisite photometry JDEM will provide morphologies in the rest-frame UV and optical of all detected $z > 2$ galaxies. The bottom panels of Fig. 4 illustrate the importance of having multi-wavelength morphological information for any $z > 2$ galaxy which has a mix of young and old stars. This near-IR selected galaxy in the UDF has an irregular morphology in the optical ACS image, but is regular and concentrated in the near-IR NICMOS image (Toft et al., 2005). SNAP's Deep Survey would cover a ~5000× larger area and go ~3 mag deeper in the near-IR than the UDF NICMOS campaign (Thompson et al., 2005), at comparable resolution. If stellar mass correlates with line width at $z > 2$ (as indicated by current data; see Fig. 3(b)), it may be possible to determine the distribution function of halo circular velocities of galaxies at $z \sim 2.5$ from JDEM photometry alone.

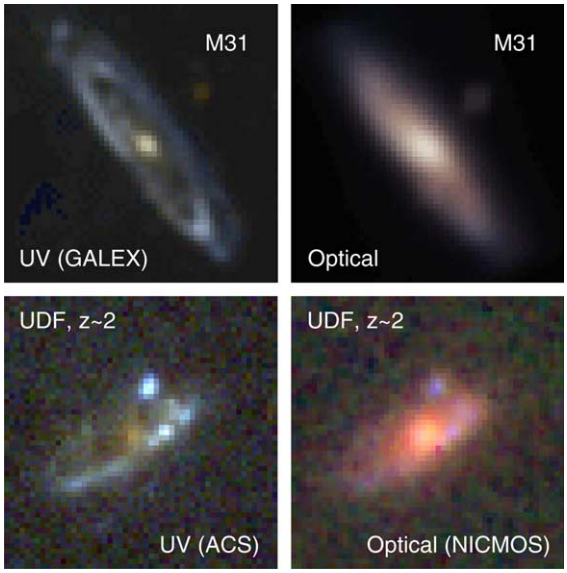

Fig. 4. Comparison of morphology in the rest-frame UV and the rest-frame optical, for M31 (top panels) and a red galaxy at $z \approx 2$ in the HST Ultra Deep Field (bottom panels; Toft et al., 2005). The images have the same resolution and physical scale (40×40 kpc), but arbitrary relative intensity scaling. Galaxies whose stars have a range of ages can look very different in the rest-frame UV and the rest-frame optical. For such objects the rest-frame UV will miss most of the stellar mass.

[2] Multi-wavelength Survey by Yale-Chile; www.astro.yale.edu/MUSYC/.

3.3. JDEM design considerations

JDEM will obviously be optimized for the identification and follow-up of high redshift SNe. Nevertheless, it is interesting to consider how well the current design specifications are suited for the study of high redshift galaxies. In terms of resolution the current SNAP design is similar to the Wide Field camera of WFPC2 in the optical and the NIC3 camera in the near-IR. As demonstrated in Fig. 4, NIC3's resolution is sufficient to determine the morphologies of normal spiral and elliptical galaxies at arbitrary redshift. However, for resolving bulges, dwarf galaxies, and individual star forming complexes at $z \gtrsim 0.5$ one would have to sacrifice area for smaller ($\sim 0.10''$) pixels in the near-IR.

The reddest JDEM filters determine the highest redshifts at which the Lyman- and Balmer-breaks can be isolated. In the current design SNAPs reddest filters are at 1.24 and 1.44 μm, implying a maximum redshift for measuring the Balmer break of ~ 2.4, and a maximum Lyman "dropout" redshift of $9-10$. Given the potential of JDEM as a survey companion to JWST the addition of a redder filter at ~ 1.6 μm or beyond would be highly valuable.

Taking spectra of JDEM sources will be a formidable challenge, in particular in the near-infrared. As even the spectroscopic limit of a 30 m ground-based telescope will be 5–6 mag brighter in the near-IR than the limit of SNAPs Deep Survey, the best follow-up capability will be offered by the multi-object NIRSpec on JWST.

References

Abadi, M.G., Moore, B., Bower, R.G., 1999. MNRAS 308, 947.
Abraham, R.G. et al., 1996. ApJ 471, 694.
Aldering, G. et al., submitted. PASP (astro-ph/0405232).
Baugh, C.M., Cole, S., Frenk, C.S., Lacey, C.G., 1998. ApJ 498, 504.
Bell, E. et al., 2004. ApJ 608, 752.
Bender, R., Burstein, D., Faber, S.M., 1993. ApJ 411, 153.
Bender, R. et al., 1998. ApJ 493, 529.
Blakeslee, J.P. et al., 2003. ApJ 596, L143.
Bower, R.G., Lucey, J.R., Ellis, R.S., 1992. MNRAS 254, 601.
Butcher, H., Oemler Jr., A., 1978. ApJ 219, 18.
Daddi, E. et al., 2003. ApJ 588, 50.
de Propris, R., Stanford, S.A., Eisenhardt, P.R., Dickinson, M., 2003. ApJ 598, 20.
Diaferio, A. et al., 2001. MNRAS 323, 999.
Djorgovski, S., Davis, M., 1987. ApJ 313, 59.
Dressler, A., 1980. ApJ 236, 351.
Dressler, A. et al., 1997. ApJ 490, 577.
Dubinski, J. 1999. In: Merritt, D., Valluri, M., Sellwood, J.A. (Eds.), Galaxy Dynamics. ASP 182, p. 491.
Ellingson, E., Lin, H., Yee, H.K.C., Carlberg, R.G., 2001. ApJ 547, 609.
Ellis, R.S. et al., 1997. ApJ 483, 582.
Franx, M. et al., 2003. ApJ 587, L79.
Förster Schreiber, N.M. et al., 2004. ApJ 616, 40.
Gladders, M.D., Yee, H.K.C., 2000. AJ 120, 2148.
Goto, T. et al., 2003. PASJ 55, 757.
Hoekstra, H., Franx, M., Kuijken, K., 2000. ApJ 532, 88.
Kelson, D., Illingworth, G., van Dokkum, P., Franx, M., 2000. ApJ 531, 184.
Kelson, D., Illingworth, G., Franx, M., van Dokkum, P., 2001. ApJ 552, L17.
Kenney, J.D.P., van Gorkom, J.H., Vollmer, B., 2004. AJ 127, 3361.
Kneib, J.-P. et al., 2003. ApJ 598, 804.
Kodama, T., Smail, I., Nakata, F., Okamura, S., Bower, R.G., 2001. ApJ 562, L9.
Labbé, I. et al., 2003. AJ 125, 1107.
Meza, A., Navarro, J.F., Steinmetz, M., Eke, V.R., 2003. ApJ 590, 619.
Moore, B. et al., 1996. Nature 379, 613.
Pettini, M. et al., 2001. ApJ 554, 981.
Poggianti, B. et al., 1999. ApJ 518, 576.
Shapley, A. et al., 2001. ApJ 562, 95.
Smith, G.P., Kneib, J.-P., Smail, I., Mazzotta, P., Ebeling, H., Czoske, O., 2005. MNRAS 359, 417.
Stanford, S.A., Eisenhardt, P.R., Dickinson, M., 1998. ApJ 492, 461.
Steidel, C.C. et al., 1998. ApJ 492, 428.
Thompson, R.I. et al., 2005. AJ 130, 1.
Toft, S., van Dokkum, P., Franx, M., Thompson, R.I., Illingworth, G.D., Bouwens, R.J., Kriek, M., 2005. ApJ 625, L9.
Treu, T. et al., 2003. ApJ 591, 53.
van Dokkum, P.G. et al., 1998a. ApJ 500, 714.
van Dokkum, P.G., Franx, M., Kelson, D.D., Illingworth, G.D., 1998b. ApJ 504, L17.
van Dokkum, P.G., Franx, M., Fabricant, D., Kelson, D.D., Illingworth, G.D., 1999. ApJ 520, L95.
van Dokkum, P.G., Franx, M., 2001. ApJ 553, 90.
van Dokkum, P.G., Stanford, S.A., 2003. ApJ 585, 78.
van Dokkum, P.G. et al., 2003. ApJ 587, L83.
van Dokkum, P.G. et al., 2004. ApJ 611, 703.
van Dokkum, P.G., van der Marel, R. 2005 (in preparation).
Venemans, B.P. et al., 2002. ApJ 569, L11.
Wittman, D., Tyson, J.A., Margoniner, V.E., Cohen, J.G., Dell'Antonio, I.P., 2001. ApJ 557, L89.
Wuyts, S., van Dokkum, P.G., Kelson, D.D., Franx, M., Illingworth, G.D., 2004. ApJ 605, 677.

Available online at www.sciencedirect.com
SCIENCE DIRECT®
New Astronomy Reviews 49 (2005) 407–412
New Astronomy Reviews
www.elsevier.com/locate/newastrev

The infrared sky

E.L. Wright

Physics and Astronomy Department, UCLA Astronomy, P.O. Box 951547, Los Angeles, CA 90095-1547, USA

Available online 12 September 2005

Abstract

The infrared sky from space is the sum of a cosmic signal from galaxies, quasars, and perhaps more exotic sources; and foregrounds from the Milky Way and from the Solar System. At a distance of 1 AU from the Sun, the foreground from interplanetary dust is very bright between 5 and 100 μm, but "very bright" is still several million times fainter than the background produced by ground-based telescopes. In the near infrared 1–2.2 μm range the space infrared sky is a thousand times fainter than the OH nightglow from the Earth's atmosphere. As a result of these advantages, wide-field imaging from space in the infrared can be an incredibly sensitive method to study the Universe.
© 2005 Elsevier B.V. All rights reserved.

Contents

1. Introduction . . . 407
2. The total infrared sky . . . 408
3. Telescope cooling requirements . . . 408
4. Detector performance requirements . . . 409
5. JDEM requirements . . . 409
6. Conclusion . . . 411
References . . . 411

1. Introduction

The infrared sky on Earth is very bright, leading George Rieke to compare infrared astronomy to

E-mail address: wright@astro.ucla.edu

1387-6473/$ - see front matter © 2005 Elsevier B.V. All rights reserved.
doi:10.1016/j.newar.2005.08.013

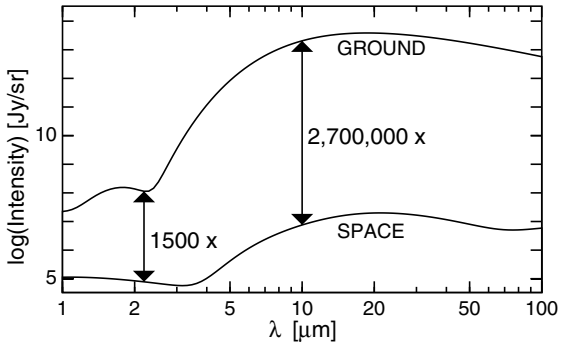

Fig. 1. The infrared sky brightness from the Earth, dominated by the OH nightglow and thermal emission from ambient temperature telescopes at 0 °C, compared to the sky brightness from space at 1 AU from the Sun, dominated by scattered Sunlight and thermal radiation from interplanetary dust.

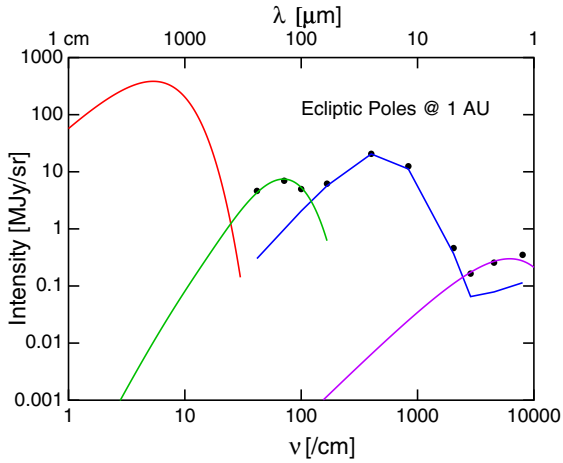

Fig. 2. The intensity averaged over the DIRBE mission of the ecliptic poles. The dots are the DIRBE data, while the red curve is the FIRAS data and a Planck function at 2.725 K, the green curve is a scaled version of the FIRAS spectrum of the interstellar dust in the Milky Way, the blue line is a model of the zodiacal dust fit to the DIRBE data, and the magenta curve is an approximation to galactic starlight. (For interpretation of the references to color in this figure legend, the reader is referred to the web version of this article.)

observing stars in the daytime with a telescope made out of fluorescent lights. From space the situation is much improved, with the total sky brightness down by three orders of magnitude in the near infrared and more than six orders of magnitude in the thermal infrared. Fig. 1 shows the sky brightness on the Earth compared to the sky brightness from space 1 AU from the Sun.

2. The total infrared sky

The diffuse infrared background experiment (DIRBE) on the cosmic background explorer made observations of the total intensity of the sky in ten bands from 1.25 to 240 μm (Hauser et al., 1998). The total intensity at the ecliptic poles from DIRBE and FIRAS data is shown in Fig. 2. One can clearly see two windows in this foreground emission: one at 200–500 μm and another at 3 μm. These windows provide an opportunity for extremely sensitive imaging from space. The curves plotted on this graph are the CMB, a 2.725 K blackbody, a scaled version of the FIRAS spectrum of the Milky Way (Wright et al., 1991),

$$I_\nu = 1.54 \times 10^{-4} \left(\frac{100\,\mu\text{m}}{\lambda}\right)^2 (B_\nu(20.4) + 6.7 B_\nu(4.77)) \tag{1}$$

a model for the interplanetary dust (Wright, 1996), and an estimate for the stellar light in the Milky Way: $5 \times 10^{-13} B_\nu(10^{3.5}\ \text{K})$.

3. Telescope cooling requirements

The brightness of the infrared sky defines the maximum temperature a telescope can have without degrading the mission sensitivity. Since optical surfaces normally have rather low emissivities, cooling the optics to the Planck brightness temperature of the infrared sky will lead to minimal degradation of performance. Fig. 4 shows this temperature as function of wavelength. Also shown on this plot is the temperature of the outer shell of the Spitzer Space Telescope, which is passively cooled in an environment 1 AU from the Sun but far enough away from the Earth that it is not a significant thermal source. Clearly, it is rather easy to use a passively cooled telescope in the 3 μm window in the zodiacal foreground.

4. Detector performance requirements

When designing space-based wide-field imaging missions one naturally wants to achieve background-limited sensitivity. Fig. 3 show the same data as Fig. 2 but in a different representation. Here, the y-axis shows the photon rate on a diffraction-limited pixel with 100% transmission and 100% bandwidth. Furthermore, one usually oversamples the diffraction-limited point spread function so a pixel in a real experiment will receive only about a few percent of this photon rate. Clearly, the dark current requirements for background-limited imaging are well below 1 e/s in the 3 μm window in the zodiacal light, but 10,000 e/s would be acceptable at 300 μm.

A simple order of magnitude estimate shows that the detectors must be much colder than the optics temperature requirement. The photon arrival rate on a unit area in a blackbody is $O(\nu^2 e^{-x}/c^2)$ where $x = h\nu/kT_B$ is $\gg 1$. In fact x is usually 25–40 for the space-based backgrounds in Fig. 4. On the other side of the detector surface one has phonons that can also be detected, and the phonon arrival rate is $O(\nu^2 e^{-x'}/c_s^2)$ where c_s is the sound speed and $x' = h\nu_{min}/kT_D$. Here, $h\nu_{min}$ is the minimum energy that can produce a charge carrier in the detector, so clearly ν_{min} has to be less than the observing frequency ν. Usually ν_{min} corresponds to the cutoff wavelength of the detector but in some cases it can be smaller. Because $c^2/c_s^2 \approx 10^{10}$, one needs to have $x' > x + 23$, and thus the detectors usually need to be two to three times colder than the optics. Even so, there is no problem running passively cooled optics and HgCdTe detectors at full natural background-limited sensitivity in the 3 μm window through the zodiacal light.

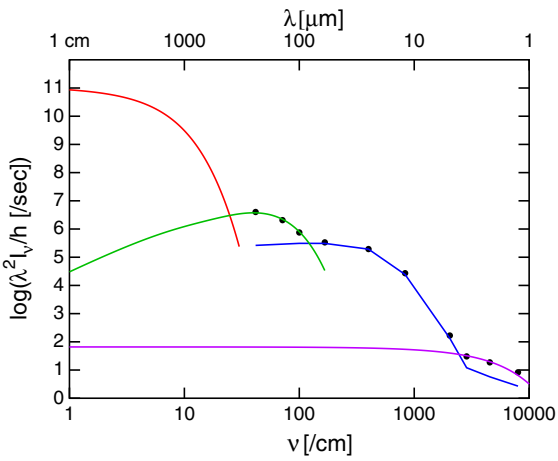

Fig. 3. The photon rate on a diffraction-limited pixel ($A\Omega = \lambda^2$) in a band with $\Delta\lambda = \lambda$. To achieve background-limited performance, the dark current should be less than 1% of these values.

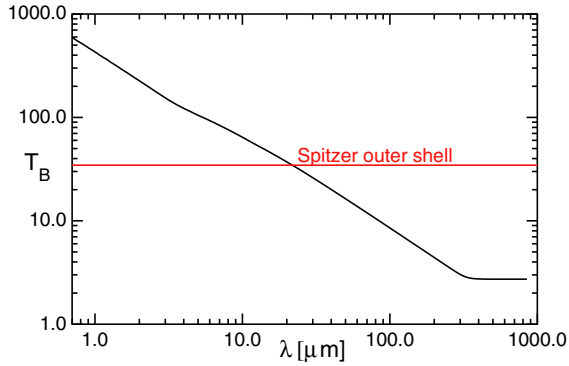

Fig. 4. The Planck brightness temperature of the infrared sky in space 1 AU from the Sun. The temperature achieved by passively cooling the Spitzer Space Telescope outer shell is indicated.

5. JDEM requirements

The Joint Dark Energy Mission (JDEM) is supposed to provide data about the dark energy. One convenient but not physically motivated parametrization of the dark energy is in terms of a time varying ratio between the pressure and the density, with $w \equiv P/\rho c^2 = w_0 + 2w'(1-a)$ where $a(t) \equiv 1/(1+z)$ is the scale factor of the Universe (Aldering et al., 2004). When $w \neq -1$ there should be a dynamical coupling between the dark energy and matter, leading to an inhomogeneous dark energy density, and this is neglected in the simple w, w' model. But the luminosity distance can easily be computed in the w, w' model allowing for quick parameter sensitivity studies. It turns out that the luminosity distance vs. redshift data for supernovae only constrain two directions in the four parameter space spanned by Ω_M, Ω_X, w and w'.

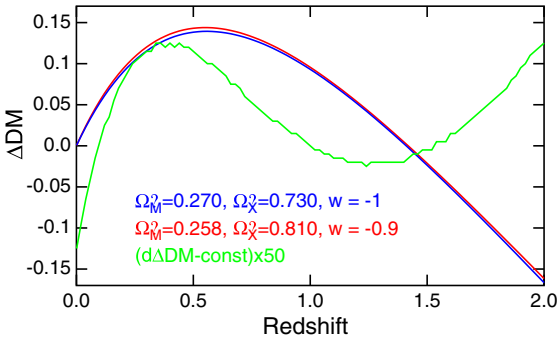

Fig. 5. Degeneracy between the WMAP concordance model with $w = -1$ and a model with $w = -0.9$. The difference is only ± 2 millimag. Supernovae alone cannot determine w.

Figs. 5 and 6 show that the other two directions are essentially unconstrained by observations of supernova brightness in the redshift range $0 < z < 2$.

All of the calculations that claim that supernova data can determine w and w' have made some poorly justified assumptions. For example, the assumption that the Universe is flat ($\Omega_M + \Omega_X = 1$) is often made. But the flatness of the Universe is clearly something that needs to be determined from the data. Often the assumption of a flat Universe is justified on the basis of simplicity, but simplicity also implies that $\Omega_X = 0$. Or the CMB is cited in justifying the assumption of a flat Universe. But the CMB data does not say the Universe is flat! The CMB data are perfectly happy with a closed $\Omega_M = 1.3$, $\Omega_X = 0$ model. Only when combined with the supernova data, and the assumption that $w = -1$, do the CMB data imply a flat Universe. To then turn this around and try to find w is clearly circular reasoning.

Where then can the additional constraints on Ω_M, Ω_X, w and w' be found? The CMB data, in particular the location of the acoustic peaks, provide one independent constraint. And weak lensing surveys offer another constraint by measuring the growth of perturbations as a function of redshift. But weak lensing observations require a very high density of background sources, and thus a high sensitivity to typical galaxies. Typical stars in typical galaxies are much redder than supernovae, and galaxies are redshifted as well, leading to a requirement for longer wavelength observations. Fig. 7 shows how the sensitivity of a proposed panoramic survey by SNAP to $z = 3$ background galaxies could be increased by a factor of 20 by extending the wavelength coverage out to 3.5 μm. Note that I recalculated the plotted sensitivities

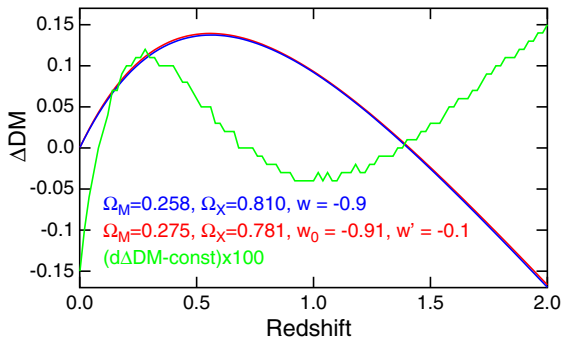

Fig. 6. Degeneracy between the model in Fig. 5 with $w' = 0$ and the a model with $w' = 0.1$. The difference is only ± 1 millimag. Supernovae alone cannot determine w'.

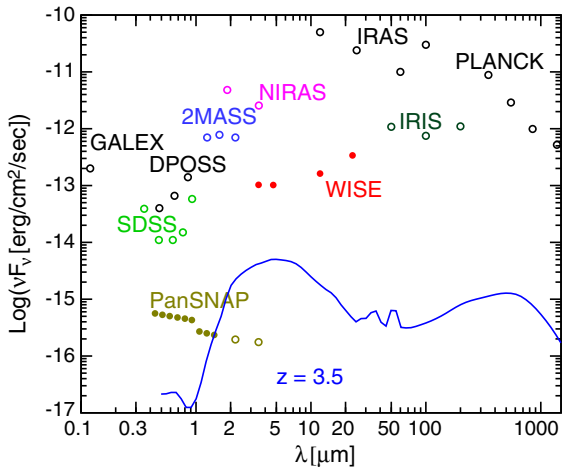

Fig. 7. 5σ point source sensitivities of various existing or planned wide-field surveys. NIRAS is the 1988 SMEX proposal by Giovanni Fazio, E.L. Wright and others that led indirectly to the 2MASS survey. The Wide-field Infrared Survey Explorer is a MidEx under study that has a planned launch in 2008. The panoramic survey that might be performed by SNAP is labeled PanSNAP. The open circles at 2.2 and 3.5 μm are not currently planned for SNAP, but would be 20 times more sensitive to old stellar populations in $z = 3$ galaxies than longest currently planned band in SNAP.

for all the SNAP bands and generally agree with published estimates (Aldering et al., 2004).

This sensitivity at 3.5 μm is two magnitudes fainter than the faintest reported number counts from Spitzer (Fazio et al., 2004). Since the Spitzer counts exceed 10^5 per square degree, the counts from a panoramic SNAP survey would be about $10^{5.4}$ per square degree if the wavelength coverage of SNAP is extended to 3.5 μm.

But this sensitivity at 3.5 μm will require rethinking the implementation of JDEM. The Hubble Space Telescope was designed in the 1980s, without planning for sensitive infrared instruments, and as a result has heated mirrors made out of ULE glass. ULE is not ultra-low expansion except in a narrow range of temperature near room temperature. The recently released Hubble Ultra-Deep Field shows the unfortunate consequences of this decades old decision: even though the NICMOS exposure time per position is only a few percent of the ACS exposure, the NICMOS image clearly goes to higher redshift. And NICMOS cannot even use its 2.2 μm capability because of the heated mirrors.

The James Webb Space Telescope (Gardner, 2003) will use passively cooled optics and actively cooled detectors to operate in the $0.6 < \lambda < 25$ μm range with high sensitivity. The Wide-field Infrared Survey Explorer (WISE) will survey the entire sky with sensitivities better than the requirements shown in Fig. 7, and thus provide a sky survey suitable for planning JWST observations.

WISE (Duval et al., 2004) will have four bands at 3.5, 4.7, 12 and 23 μm and will be able to detect old, cold brown dwarfs in the Solar neighborhood as well as Ultraluminous Infrared Galaxies at redshifts up to $z = 3$. WISE will be in a nearly polar Sun-synchronous low Earth orbit like IRAS and COBE and will scan a circle perpendicular to the Earth–Sun line once per orbit while looking away from the Earth. After 6 months the precession of the orbit will have swept this scan circle across the entire sky.

WISE will take exposures every 11 s with 1024×1024 pixel arrays in each of its four bands. The 40 cm diameter WISE telescope will scan at a constant rate while an internal scan mirror freezes an image of the sky on the arrays. This scan method is very similar to the method employed by the 2MASS survey.

The current catalogs of stars close to the Sun are surprisingly incomplete. In fact, the third closest star to the Sun was discovered in 2003 with a proper motion of 5″ per year (Teegarden et al., 2003)! When brown dwarfs are included, it is likely that only one-third of the stars within 5 pc have been identified. Most of the missing objects will be old low mass brown dwarfs with luminosities considerably smaller than the $2.6 \times 10^{-6} L_\odot$ of 2MASS 1415-09 (Vrba et al., 2004). WISE will be able to detect brown dwarfs down to $10^{-8} L_\odot$ at the distance of Proxima Cen, and there could be two such objects within the 10 pc[3] closer to the Sun than Proxima Cen.

At much greater distances our knowledge of active galactic nuclei, QSOs and ultra-luminous starburst galaxies is also incomplete because these objects are often obscured by tremendous amounts of dust. WISE should be able to detect about 10^7 galaxies at 23 μm and 5–6% of these will have redshifts $z > 2$.

All of these objects that can be found by WISE will be of great interest for followup observations using the JWST. A 2 m diameter, passively cooled, wide field telescope working in the near infrared would fill a valuable niche between the wide but shallow survey of WISE and the ultra-sensitive but narrow field capability of JWST.

6. Conclusion

The Joint Dark Energy Mission goals require many different kinds of data, not just supernova brightness vs. redshift. A high sensitivity to faint redshifted galaxies will be essential, and in the space environment 1 AU from the Sun the highest sensitivity is obtained at 3 μm (Wright, 1985). Thus JDEM should cover the wavelength range $\lambda < 4$ μm, and this can easily be achieved using passively cooled optics and detectors.

References

Aldering, G., et al., 2004. Supernova Acceleration Probe: A Satellite Experiment to Study the Nature of the Dark Energy, PASP, TBD, TBD (astro-ph/0405232).

Duval, V., Irace, W., Mainzer, A., Wright, E., 2004. The Wide-Field Infrared Survey Explorer (WISE), SPIE, TBD, TBD. E. Wright, P. Eisenhardt and the WISE Science Team, Paper 11.03 at the 204th Meeting of the AAS, vol. 5487, p. 101.

Gardner, J., et al., 2003. Science with the James Webb Space Telescope, BAAS, 203rd Meeting, Paper 124.01.

Fazio, G., et al., 2004. Number Counts at $3 < \lambda < 10$ μm from the Spitzer Space Telescope, ApJS, TBD, TBD (astro-ph/0405595), vol. 154, p. 39.

Hauser, M. et al., 1998. The COBE diffuse infrared background experiment search for the cosmic infrared background. I. limits and detections. ApJ 508, 25.

Teegarden, B., Pravdo, S., Hicks, M., Lawrence, K., Shaklan, S., Covey, K., Fraser, O., Hawley, S., McGlynn, T., Reid, I., 2003. Discovery of a new nearby star. ApJL 589, L51.

Vrba, F. et al., 2004. Preliminary parallaxes of 40 L and T dwarfs from the US naval observatory infrared astrometry program. AJ 127, 2948.

Wright, E.L., 1985. On using a space telescope to detect faint galaxies. PASP 91, 451.

Wright, E.L., 1996. Angular power spectra of the COBE DIRBE maps. ApJ 496, 1.

Wright, E.L. et al., 1991. Preliminary spectral observations of the galaxy with a 7° beam by the cosmic background explorer (COBE). ApJ 381, 200.

Available online at www.sciencedirect.com
SCIENCE DIRECT®
New Astronomy Reviews 49 (2005) 413–416
New Astronomy Reviews
www.elsevier.com/locate/newastrev

Wide-field imaging from space of early-type galaxies and their globular clusters

Stephen E. Zepf

Department of Physics and Astronomy, Michigan State University, East Lansing, MI 48824, USA

Available online 21 September 2005

Abstract

Wide-field imaging from space will reveal a wealth of information about the globular cluster systems of any galaxies in the local universe that are observed by such a mission. Individual globular clusters around galaxies in the local universe have compact sizes that are ideal for the excellent spatial resolution afforded by space-based imaging, while systems of these globular clusters have large spatial extent that can only be fully explored by wide-field imaging. One example of the science return from such a study is the determination of the major formation epoch(s) of galaxies from the ages of their globular clusters determined via their optical to near-infrared colors. A second example is determining the sites of metal-poor globular cluster formation from their cosmological bias, which constrains the formation of structures early in the universe.
© 2005 Elsevier B.V. All rights reserved.

Contents

1. Why JDEM imaging of globular cluster systems . . . 413
2. Constraints on the formation epoch(s) of elliptical galaxies . . . 414
3. Cosmological bias of metal-poor globular cluster populations . . . 415
Acknowledgments . . . 415
References . . . 415

1. Why JDEM imaging of globular cluster systems

Globular clusters are invaluable fossil records of the early formation history of the galaxy in

E-mail address: zepf@msu.edu.

1387-6473/$ - see front matter © 2005 Elsevier B.V. All rights reserved.
doi:10.1016/j.newar.2005.08.014

which they are located. Composed of roughly one million stars that formed at the same time with similar composition and that have remained bound for up to a Hubble time, each globular cluster provides an observable record of the age, metallicity, and kinematics at the time it was formed. Because these quantities are determined for individual globulars, studies of globular cluster systems can constrain the *distribution* of the ages and metallicities rather than the global average of these key galaxy quantities revealed by most studies of the integrated light of galaxies. Globular clusters are also observed to form in major starbursting episodes in the local universe, so their properties provide a way to trace the major formation episodes in their host galaxies. Moreover, because typical globular clusters contain roughly one million stars, they are bright and can be readily observed as individual objects out to sufficient distances ($\sim$15 Mpc) to obtain a significant sample of elliptical galaxies. This allows the investigation of the formation history of massive early-type galaxies that are absent in the Local Group, but make up the majority of stellar mass in the local universe (e.g., Hogg et al., 2002). Consequently, studies of globular cluster systems have long played an important role in constraining how and when the major formation episodes in galaxies occurred (e.g., Ashman and Zepf, 1998; Harris, 2001).

The study of extragalactic globular cluster systems has been revolutionized by space-based imaging with the Hubble Space Telescope. This is in large part because the size of extragalactic globular clusters is very well matched to diffraction limited optical imaging with a 2-m class telescope. Specifically, a typical globular cluster half-light radius of several pc at a distance of 10 Mpc corresponds to $\sim$0.05″ on the sky. However, in one critical aspect, the study of extragalactic globular cluster systems is not well suited to HST imaging. The systems of globular cluster systems around massive early-type galaxies extend into the halos of the galaxies, covering tens of arcminutes on the sky (e.g., Rhode and Zepf, 2004 and references therein). Therefore, wide fields of view are required in order to accurately determine total properties of globular cluster systems around galaxies. Moreover, the outer halos of galaxies may hold unique clues to the assembly history of galaxies, and globular clusters are one of the few probes available in these regions. In this contribution, we highlight two key science questions that would be addressed by wide-field, space-based imaging of galaxies in the local universe and their globular cluster systems.

2. Constraints on the formation epoch(s) of elliptical galaxies

Globular cluster systems are key tools for determining the formation history of elliptical galaxies because the ages and metallicites of their globular clusters can potentially be determined, thereby yielding the major formation epoch(s) of the host galaxies. Studies in optical colors have revealed that globular cluster systems of elliptical galaxies often have color distributions with two or more peaks (e.g., Kundu and Whitmore, 2001; Larsen et al., 2001). This is one of the clearest signs that elliptical galaxies form eposidically, and is consistent with earlier predictions for elliptical galaxies formed by the mergers of disk galaxies (Ashman and Zepf, 1992). While the optical colors of globular cluster systems indicate an episodic formation history, they do not significantly constrain *when* these events occur. This is because optical colors alone cannot generally distinguish between different age and metallicity combinations (the age-metallicity degeneracy). In some specific cases with strongly bimodal color distributions, the cluster systems must be mostly old and have a bimodal metallicity distribution to account for the red and blue populations (e.g., Zepf and Ashman, 1993). However, a general understanding of the age and metallicity distribution of globular cluster systems requires the breaking of the age-metallicity degeneracy. The addition of near-infrared photometry to optical data provides a way to break the age-metallicity degeneracy (e.g., Puzia, 2002). The basis for this technique is that the flux of a simple stellar population in the near-infrared is primarily sensitive to metallicity, while optical fluxes have a greater sensitivity to age. This approach has resulted in the first identification of a substantial population of intermediate-age globular clusters in an ordinary elliptical galaxy (Puzia,

2002), and studies are now being carried out of larger samples of galaxies (e.g., Hempel et al., 2003). However, these studies are limited to the inner regions of galaxies because of the modest size of current near-infrared arrays and also, more fundamentally, because of the low surface density of globular clusters in the outer regions of galaxies. Specifically, even with careful image classification and multicolor selection, contamination of globular cluster samples in wide-field ground-based imaging is a concern (e.g., Rhode and Zepf, 2001). As demonstrated by HST, imaging at 0.1″ resolution effectively eliminates most of this concern by separating background galaxies, foreground stars, and globular clusters (e.g., Kundu et al., 1999).

Any JDEM observations of early-type galaxies in the local universe would provide optical and near-infrared luminosities of their globular clusters over a wide field with little contamination. This would then allow the use of the optical to near-infrared technique to determine the ages and metallicities of the major formation epoch(s) of these galaxies from the inner regions out into their halos. This would place important constraints on the formation history of elliptical galaxies, particularly in their outer regions for which there are few other constraints.

3. Cosmological bias of metal-poor globular cluster populations

The low metallicity and the "halo"-like extended spatial distribution of metal-poor globular cluster systems suggests that they generally formed at high redshift. These objects may therefore be the best available fossil records of structure formation at early epochs. One way to address the question of the formation sites of metal-poor globular clusters is to determine their "cosmological bias". Specifically, galactic halos that are more massive and in denser environments will tend to have more of their mass collapsed by a given redshift than halos of lower mass and in poorer environments. Thus, a given formation redshift for metal-poor globular clusters translates directly into a specific prediction for the 'biasing" of metal-poor clusters towards higher mass halos, with the adoption of a constant formation efficiency of globular clusters per collapsed halo mass. This can be further tested by comparison with the spatial distribution of the metal poor clusters, which is also dependent on formation epoch and halo mass (see Rhode and Zepf, 2004; Santos, 2003).

To determine the cosmological bias of the metal-poor globular clusters, their total number and spatial distribution around galaxies of different masses and environments are required. Current work along these lines has primarily utilized the ground-based CCD Mosaic cameras covering fields of roughly $30' \times 30'$ (e.g., Rhode and Zepf, 2004). These data are a significant improvement over those available earlier, and the field size covers most or all of the metal-poor globular cluster systems of a broad range of galaxies in the local universe. However, as discussed in the previous section, space-based imaging is invaluable for identifying globular clusters over these large fields. Therefore, JDEM imaging of galaxies in the local universe would provide high quality total numbers and spatial profiles of the metal-poor component of globular cluster systems for the determination of the biasing of this population. This would then constrain when and where these structures formed early in the universe.

Acknowledgments

I thank my many collaborators on projects related to those described above, and acknowledge support from NASA Long-Term Space Astrophysics Grant NAG 5-11319.

References

Ashman, K.M., Zepf, S.E., 1992. ApJ 384, 50.
Ashman, K.M., Zepf, S.E., 1998. Globular Cluster Systems. Cambridge University Press, Cambridge.
Harris, W.E., 2001. In: Labhardt, L., Binggeli, B. (Eds.), Star Clusters. Springer, Berlin, p. 223.
Hempel, M. et al., 2003. A&A 405, 487.
Hogg, D.W. et al., 2002. AJ 124, 646.
Kundu, A. et al., 1999. ApJ 513, 733.

Kundu, A., Whitmore, B.C., 2001. AJ 121, 2950.
Larsen, S.S. et al., 2001. AJ 121, 2974.
Puzia, T.H., 2002. A&A 391, 453.
Rhode, K.L., Zepf, S.E., 2001. AJ 121, 210.
Rhode, K.L., Zepf, S.E., 2004. AJ 127, 302.
Santos, M.R., 2003. In: Kissler-Patig, M. (Ed.), Extragalactic Globular Cluster Systems. Springer, Berlin, p. 348.
Zepf, S.E., Ashman, K.M., 1993. MNRAS 264, 611.

Available online at www.sciencedirect.com
SCIENCE DIRECT®
New Astronomy Reviews 49 (2005) 417–419
New Astronomy Reviews
www.elsevier.com/locate/newastrev

Probing the universe at redshift 10 and beyond

Wei Zheng

Department of Physics and Astronomy, Johns Hopkins University, Baltimore, MD 21218, United States

The *PRIME* Team
Available online 12 September 2005

Abstract

The signature of objects in the very early universe lies deep in the near infrared bands. The Primordial Explorer (*PRIME*) is a proposed NASA Explorer-class mission aimed at the $z > 10$ universe. *PRIME* will find the youngest and the most luminous galaxies and quasars, thereby enabling the determination of the epoch of galaxy formation and that of reionization of the intergalactic medium.
© 2005 Published by Elsevier B.V.

Contents

1. The "dark ages" . . . 417
2. *PRIME*: the primordial explorer . . . 418
3. Number of objects at $z > 10$ . . . 418
References . . . 419

1. The "dark ages"

Remarkable progress has been made recently in our understanding of the very early universe: The discovery of galaxies at redshift of $z \sim 7$ (Kodaira et al., 2003; Kneib et al., 2004) leads us over ~93% of the look-back time since the Big Bang. The spectra of luminous quasars at $z > 6$ suggest (Fan et al., 2003) that we may have already witnessed the beginning of reionization of the intergalactic medium (IGM), an important milestone for cosmology.

Simulations with cosmological models suggest that the small-scale fluctuations in the IGM grew under the influence of gravity and eventually formed the first generation of baryonic objects

E-mail address: zheng@pha.jhu.edu.

1387-6473/$ - see front matter © 2005 Published by Elsevier B.V.
doi:10.1016/j.newar.2005.08.015

such as stars, galaxies, and quasars. Recent results of the Wilkinson Microwave Anisotropy Probe (*WMAP*, Spergel et al., 2003) confirm with unprecedented precision that the seeds for baryonic matter started to form at $z \sim 1000$ and suggest that the first generation of stars appeared ~200 million years after the Big Bang, i.e., at $z \sim 20$. The energetic emission from young galaxies and quasars eventually reionize the IGM, ending the so-called "dark ages".

One of the major frontiers in cosmology is the universe beyond redshift 10. The backbone of our exploration is the James Webb Space Telescope (*JWST*). To fully realize *JWST*'s power, a deep infrared survey is highly desirable. The recent images of the Hubble Ultra Deep Field (HUDF) represent our deepest view of the early universe to date, but significantly larger fields of view are needed to study the luminosity function and other properties of $z > 6$ objects.

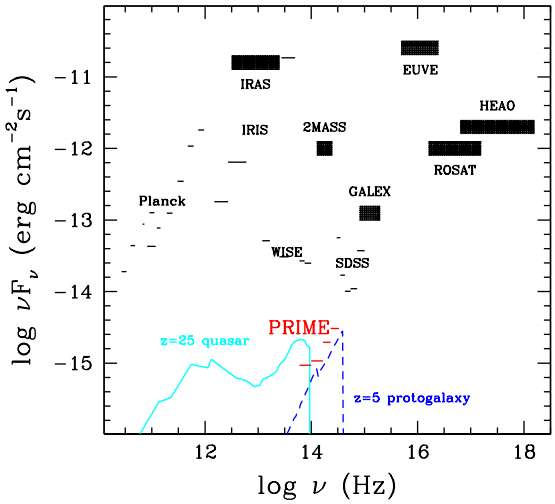

Fig. 1. Sensitivity of large-scale surveys. Only those that cover at least 1/4 of the sky are included. Overplotted are simulated spectra of a quasar and a galaxy. *PRIME* can reach 20–100 times deeper in its deep mode.

2. *PRIME*: the primordial explorer

To bridge the gap between the *WMAP* results at $z \sim 20$ and our current knowledge of the universe at $z \sim 6$–10, significant wide-field capability is needed in the near-infrared band. We have developed a mission concept *PRIME*, the Primordial Explorer. It is a NASA Explorer-class mission to carry out a deep survey in the near infrared by obtaining images in four bands between 0.9 and 3.5 μm. As shown in Fig. 1, *PRIME* is in the right band and right sensitivity to catch the signature of some most interesting objects. This third generation will be approximately 1000 times more sensitive than 2MASS in its wide survey mode. *PRIME* is also capable of deep survey at various scales. At the level of one square degree, for example, it may reach AB magnitudes comparable to that of the HUDF. *PRIME* will therefore profoundly enhance the capability of *JWST* and the largest ground-based telescopes.

The current participating institutions in the *PRIME* project are Johns Hopkins University, Space Telescope Science Institute, Max-Planck-Institut für Astronomie, and Goddard Space Flight Center.

3. Number of objects at $z > 10$

The latest SDSS discoveries suggest that quasars may be found in much earlier epoches, i.e., $z > 10$. The quasar phenomenon is believed to originate from a supermassive black hole at the center of large halos. The current estimates (Fan, in this proceedings) suggest that there are approximately 100 quasars of $z \sim 6$ in the entire sky, to a limiting magnitude of AB ~ 20. If the massive black holes in these quasars took long time to build, they are likely to exit at redshift 10 and beyond. Their high-redshift counterparts will be fainter (Haiman and Loeb, 2001), as the result of: (1) the Doppler effect and (2) a smaller center mass and accretion rate. Our estimates suggest that, at limiting magnitude of 24, *PRIME* will be able to find approximately 50 such luminous quasars at $z \sim 10$. The spectra of these quasars are powerful probe of the IGM reionization at $z > 10$.

Hierarchical models predict that large galaxies like the Milky Way formed earlier than quasars.

While *JWST* will find many high-z galaxies via deep imaging, most of them will be foreground galaxies at $z < 10$. It is estimated (Loeb and Barkana, 2001) that the number of $z \sim 15$ galaxies at a given limiting magnitude is 2 decades smaller than at $z \sim 10$ and that of $z \sim$ 20 galaxies by 4 decades. It is therefore necessary to search beyond "deep fields" in order to find the youngest galaxies. The large number of galaxies at $z > 10$ found in the *PRIME* survey will enable us to study the correlation of galaxy distribution and that of the microwave background discovered by *WMAP*. For the brightest, *JWST* will be able to obtain their spectra, which will provide invaluable clues to the physical conditions in these "infant" galaxies.

References

Fan, X. et al., 2003. A survey of $z > 5.7$ quasars in the sloan digital sky survey. II. Discovery of three additional quasars at $z > 6$. AJ 125, 1649–1659.

Haiman, Z., Loeb, A., 2001. What is the highest plausible redshift of luminous quasars? ApJ 552, 459–463.

Kodaira, K. et al., 2003. The discovery of two lyman α emitters beyond redshift 6 in the subaru deep field. PASJ 55, L17–L21.

Kneib, J.-P., Ellis, R.S., Santos, M.R., Richard, J., 2004. A probable $z \sim 7$ galaxy strongly lensed by the rich cluster A2218: exploring the dark ages. ApJ 607, 697–703.

Loeb, A., Barkana, R., 2001. The reionization of the universe by the first stars and quasars. ARAA 39, 19–66.

Spergel, D.N. et al., 2003. First-year wilkinson microwave anisotropy probe (*WMAP*) observations: determination of cosmological parameters. ApJS 148, 175–194.

Available online at www.sciencedirect.com
SCIENCE DIRECT®
New Astronomy Reviews 49 (2005) 420–423
New Astronomy Reviews
www.elsevier.com/locate/newastrev

Spitzer 24 μm observations of optical/near-IR selected extremely red galaxies: Evidence for assembly of massive galaxies at $z \sim 1$–2?

Lin Yan

Spitzer Science Center, MS220-6, Caltech, Pasadena, CA 91108, United States

Available online 3 October 2005

Abstract

Optical/near-IR colors have been widely used to select $z > 1$ galaxies with old stellar populations. However, because a single color can not separate dust reddening from old stars, the relative fractions of dusty starbursts and old early type galaxies in an optical/near-IR selected sample are unknown. In this talk, I present the first, direct measurement of the fraction of dusty sources in a sample of extremely red galaxies with $(R - K_s) \geqslant 5.3$ mag and $K_s < 20.2$ mag, using 24 μm mid-infrared data from the *Spitzer Space Telescope*. Combining deep 24 μm, K_s- and R-band data over an area of ~64 sq.arcmin in the ELAIS N1 field of the Spitzer First Look Survey (FLS), we find that $50 \pm 6\%$ of our ERO sample have measureable 24 μm flux above the 3σ flux limit of 40 μJy. This flux limit corresponds to a SFR of 12 $M_{\odot}$/yr at $z \sim 1$, much more sensitive than any previous long wavelength measurement. The significant implication is that our deep 24 μm observations have revealed for the first time galaxies being assembled together at $z \sim 1$. Some of the starburst EROs are in the midst of violent transformation to become massive early type galaxies at the epoch of $z \sim 1$–2.
© 2005 Published by Elsevier B.V.

Contents

1. Background and data reduction . . . 421
2. Results and Implications. . . . 421
   2.1. The 24 μm detected EROs . . . 421
   2.2. The nature of the EROs with 24 μm emission . . . 421
   2.3. Summary and implications. . . . 422
   References. . . . 422

E-mail address: lyan@ipac.caltech.edu.

1387-6473/$ - see front matter © 2005 Published by Elsevier B.V.
doi:10.1016/j.newar.2005.08.016

1. Background and data reduction

Optical/near-IR colors, such as $(R - K_s)$ or $(I - K_s)$ have been commonly used in wide-area surveys to select old stellar populations at $z \sim 1$–2 (see Cimatti et al., 2002; McCarthy, submitted, for the review of this subject). However, these color selections are also sensitive to dust-reddened, star-forming systems, and examples of both passively evolving ellipticals and dusty starburst EROs have been found (see McCarthy, submitted, for references). The relative contribution of these two galaxy types is unknown. MIPS 24 μm data from the *Spitzer Space Telescope* offer the first opportunity to directly address this critical issue. Dusty, star-forming galaxies are clearly distinguished from early-type galaxies at mid-IR wavelengths. The results presented here have been published in the ApJS Spitzer special issue (Yan et al., in press). The primary dataset used in this work include deep optical R, near-IR K and Spitzer 24 μm data in the ELAIS N1 field. R and K_s were taken at the KPNO and Palomar, and reach 3σ of 25.2 and 21 mag, respectively. The 24 μm images were taken with roughly 4000 s exposure time and have the final 3σ flux limit of 40 μJy.

2. Results and Implications

2.1. The 24 μm detected EROs

We produced a catalog of 129 galaxies with $(R - K_s > 5.3)$ mag over 64 sq.arcmin. Of the 129 EROs, 65 ($50 \pm 6\%$) have 24 μm emission with flux greater than 40 μJy. The fraction of 24 μm detected EROs becomes slightly higher for redder sources, with $56 \pm 15\%$ and $67 \pm 30\%$ for $(R - K_s) \geqslant 6.0$ and $(R - K_s) \geqslant 6.5$ mag, respectively. However, the errors of these fractions are large due to the shallow R band limit. Deeper data would be needed to reduce the uncertainties. We find that 70% of the 24 μm EROs have $f_{24\ \mu m} > 90$ μJy and that the mean 24 μm flux of the ERO sample is 167 μJy.

2.2. The nature of the EROs with 24 μm emission

What types of galaxies are the 24 μm detected EROs? In Fig. 1(a), we present a 24–0.7 and 24–2.2 μm color–color diagram showing that 24 μm-detected EROs (*red squares*) are clearly separated from EROs without 24 μm emission (*green points*), as well as the general non-ERO population (*black and blue*). This suggests that the MIR/Optical and MIR/NIR colors of 24 μm-detected EROs are unique, distinguishing them from other populations. Fig. 1(b) presents the expected colors as a function of redshift for various SED templates, assuming no evolution. The SEDs for M51, M82 and Mrk231 are taken from Silva et al. (1998), D. Fadda et al., and Chary and Elbaz (2001), and M31 bulge SED is from Soifer et al. (1986) combined with a 10 Gyr theoretical SED from Bruzual and Charlot.

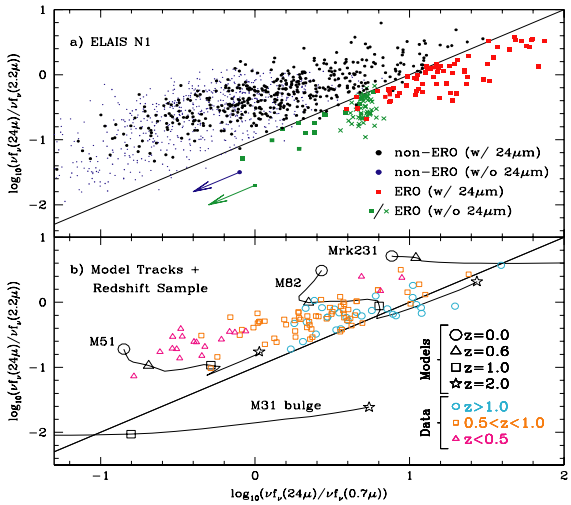

Fig. 1. The two panels show $\log_{10}(\nu f_\nu(24\ \mu m)/\nu f_\nu(0.7\ \mu m))$ versus $\log_{10}(\nu f_\nu(24\ \mu m)/\nu f_\nu(8\ \mu m))$. Panel (a) presents the data from ELAIS N1. In this panel, *red/green squares* represent EROs with/without 24 μm detections. For the non-24 μm EROs, the green crosses have only upper limits in the R-band. The *black/blue points* represent the full K_s-selected sample with/without 24 μm detections. The plotted colors of sources not detected at 24 μm are upper limits and could move down to lower-right corner of the diagram, as illustrated by the *green and blue arrows*. The *black solid line* in both panels represents constant $(R - K_s) = 5.3$ mag color. Panel (b) shows the computed color–color tracks as a function of redshift for a set of SED templates of local, well-known galaxies. The subset of the FLSV sample with measured spectroscopic redshifts are overplotted for three different redshift bins: $z < 0.5$ (*magenta open triangles*); $0.5 < z < 1.0$ (*orange open squares*); and $z > 1.0$ (*cyan open circles*). (For interpretation of the references to color in this figure legend, the reader is referred to the web version of this article.)

For comparison, a sample of 112, 24 μm sources with known spectroscopic redshifts are marked to show the actual redshift range of the 24 μm EROs in ELAIS N1. Of these 112 redshifts, 10 are 24 μm-detected EROs with $0.8 < z_{\rm spec} < 1.3$, and the optical spectra of these 10 sources all have [OII]3727 Å emission line.

Comparing Figs. 1(a) and (b), we reach the following conclusions: (1) 24 μm-detected EROs in the ELAIS N1 field with $(R - K_{\rm s}) \geqslant 5.3$ mag, $K_{\rm s} < 20.2$ mag, and $f_\nu(24\ \mu{\rm m}) > 40$ μJy are infrared bright sources at $z \geqslant 1$. They have colors similar to starbursts like M82 at $z \geqslant 1$, or dust reddened AGN like Mrk231 at $z \geqslant 0.7$. Their colors are too red to be explained by any normal spiral or old stellar populations at any redshifts. (2) The likely redshift range of these 24 μm EROs is $z \geqslant 1$, as predicted from the model SEDs of M82 and Mrk231. This is further confirmed by comparison to the Keck spectroscopic sample from the FLSV. (3). The remaining half of the ERO population are probably galaxies with old stellar populations at $z \sim 1$, as suggested by the tracks in Fig. 1(b). In a forthcoming analysis, we should be able to set better constraints on the ages and masses of these systems by combining with the Spitzer IRAC photometry.

Half of the ELAIS N1 ERO sample have 24 μm dust emission. The key question is what their infrared luminosities are. In the previous section, we conclude that the 24 μm-detected EROs have colors similar to M82, however, Fig. 1(a) does not set any constraints on either their luminosities or masses. At $z \sim 1$ the observed 24 μm luminosity roughly corresponds to the rest-frame IRAS 12 μm luminosity, within a factor of 2. The Spitzer 24 μm filter is narrower than the IRAS 12 μm filter, but ignoring this difference, a crude conversion of the observed Spitzer 24 μm flux can be made to place a lower limit on the rest-frame IRAS 12 μm luminosity. We can infer the total infrared luminosity of 24 μm sources at $z \sim 1$ by using the correlation between the 12 μm luminosity (νL_ν(12 μm)) and the infrared luminosity $L_{\rm IR}$(8–1000 μm), $L_{\rm IR} = 0.89 \times (\nu L_\nu(12\ \mu{\rm m}))^{1.094}\ {\rm L}_\odot$ (Soifer et al., 1989). The mean flux (167 μJy) of the 24 μm-detected EROs in ELAIS N1 implies the $L_{\rm IR} \sim 3 \times 10^{11}\ {\rm L}_\odot$ at $z = 1.0$ and $L_{\rm IR} \sim 10^{12}\ {\rm L}_\odot$ at $z = 1.5$, similar to that of local LIRGs and ULIGs. The corresponding SFR is 50–170 $M_\odot$/yr, using $\mathrm{SFR} = 1.71 \times 10^{-10} L_{\rm IR}$ ($M_\odot$/yr). We emphasize that the ELAIS N1 24 μm data is very deep so that 3σ flux limit of 40 μJy corresponds to a SFR of 12 $M_\odot$/yr, which is more sensitive than the deepest 1.4 GHz observation (Smail et al., 2002).

2.3. Summary and implications

Our result suggests that a significant fraction of EROs are extremely active starbursts (LIRGs or ULIGs). If the time scale of this starbursting phase is on the order of 10^8/yr, as inferred from local LIRGs and ULIGs, we can set a lower limit to the mass of these 24 μm-detected EROs as $\mathrm{SFR} \times \tau = 50{-}170 \times 10^8 = 5 \times 10^9{-}2 \times 10^{10}\ \ {\rm M}_\odot$. If the EROs *without* detectable 24 μm are indeed massive systems with old stellar populations at $z \sim 1$ as measured by several recent surveys (Glazebrook et al., in print), one plausible connection between the starburst and early-type ERO populations is that the former may be in the process of transforming into the latter, as initially postulated by Kormendy and Sanders (1992). In the hierarchical clustering paradigm, it could be interpreted that our deep 24 μm observations are capturing a massive galaxy population in the midst of violent transformation – possibly in the process of assembly via mergers/starbursts at the epoch of $z \sim 1$–2. The accurate determination of the stellar and dynamical masses of these starburst EROs at $z \sim 1$–2 will be critical for the resolution of this question. Finally, the measurement of volume averaged mass density at $z \sim 1$–2 would require a better understanding of the physical source of the integrated K-band light – whether from dusty systems or from old stars.

References

Chary, R., Elbaz, D., 2001. ApJ 556, 562.
Cimatti, A. et al., 2002. A&A 381, 68.
Glazebrook, K. et al., 2004. Nature 430, 181. astroph/0401037.
Kormendy, J., Sanders, D., 1992. ApJL 390, 53.

McCarthy, P.J., submitted. AR&AA.
Silva, L., Granato, G.L., Bressan, A., Danese, L., 1998. ApJ 509, 103.
Smail, I. et al., 2002. ApJ 581, 844.
Soifer, B.T., Boehmer, L., Neugebauer, G., Sanders, D.B., 1989. AJ 98, 766.
Soifer, B.T. et al., 1986. ApJ 304, 651.
Yan, L. et al., 2004. ApJS 154, 75.

Available online at www.sciencedirect.com
SCIENCE DIRECT®
New Astronomy Reviews 49 (2005) 424–429
New Astronomy Reviews
www.elsevier.com/locate/newastrev

Microlensing search for planets ☆

Andrew Gould

Department of Astronomy, Ohio State University, Columbus, OH 43210, USA

Available online 13 September 2005

Abstract

Using gravitational microlensing, a space-based wide-field imager could carry out a search for planets with greater sensitivity than any other technique. Because the amplitude of the microlensing signature is independent of planet mass, the survey would extend down to Mars-mass planets, at least a decade below other techniques. While most sensitive to planets in the so-called "lensing zone" (roughly 1–5 AU from star), the microlensing technique probes planets over a broad range of separations, and is the only method that is sensitive to free-floating planets. It is also the only technique capable of conducting a planetary census at a wide range of Galactocentric distances.
© 2005 Published by Elsevier B.V.

Contents

1. Introduction . . . 425
2. Microlensing basics . . . 425
3. Microlensing by planets . . . 426
4. Planet searches from the ground . . . 426
5. Why wide field imaging from space? . . . 427
6. What would a microlensing survey do? . . . 427
   6.1. Low-mass planets . . . 427
   6.2. High signal-to-noise ratio . . . 427
   6.3. Free-floating planets . . . 428
   6.4. Galactic census . . . 428
   6.5. Planet masses . . . 428

☆ Expanded version of a talk presented at Wide Field Imaging from Space (Berkeley, CA, May 2004).

E-mail address: gould.34@osu.edu.

1387-6473/$ - see front matter © 2005 Published by Elsevier B.V.
doi:10.1016/j.newar.2005.08.017

7. Conclusion . . . 429
Acknowledgments . . . 429
References . . . 429

1. Introduction

A wide field imager in space would enable a massive survey for planets extending down to one Earth mass, or even a factor 10 smaller, using the technique of gravitational microlensing.

The reason that microlensing is potentially so much more sensitive to low-mass planets, and the reason that a wide field space imager is needed to realize this potential are closely related. For all other planet-search techniques, the strength of the signal declines with the planet mass, either linearly (radial velocities, astrometry, pulsar timing) or as the 2/3 power (transits). By contrast, for microlensing, the strength of the signal remains constant as the planet mass drops (until it reaches its threshold at about the mass of Mars). However, the probability that the planet will give rise to a signal and the duration of that signal both decline as the square root of the planet mass. Hence, to achieve sensitivity to Earth mass planets requires a survey that monitors literally 100 million stars, with nearly continuous 10-min sampling over many months. These characteristics can only be fully realized using a wide field imager in space.

Microlensing planet-finder satellites have been discussed for several years (Bennett and Rhie, 2002). While the specific designs have varied, all require 1–2 m class telescopes with several square degree fields that are sampled at slightly worse resolution than the diffraction limit. This allows for maximum areal coverage (which as we will see is critical), while still effectively achieving the diffraction limit through drizzling. Thus, the characteristics of these satellites are essentially the same as those required for supernova (SN) searches. Indeed, one incarnation of this satellite, called JDEEM, would spend three 8-month campaigns searching for planets, and two intervening 16-month campaigns searching for SNe. In this contribution, I will not distinguish between various possible configurations for the satellite, as these change its capabilities by only of order a factor 2.

2. Microlensing basics

When two stars become closely aligned, the one in front (the "lens") bends the light from the one in back (the "source"), The source is then broken up into two images, each of which is distorted and magnified. The separation of these images is of order the angular Einstein radius, $\theta_{\rm E}$

$$\theta_{\rm E} = \sqrt{\kappa M \pi_{\rm rel}} = 2.9{\rm mas}\sqrt{\frac{M}{M_\odot}\frac{\pi_{\rm rel}}{\rm mas}}, \tag{1}$$

where M is the mass of the lens, $\pi_{\rm rel}$ is the lens-source relative parallax, and $\kappa \equiv 4G/(c^2{\rm AU})$. For Galactic microlensing, the two images are typically separated by less than 1 mas, and hence are not resolved. However, since the combined area of the images is larger than that of the source by a factor

$$A = \frac{u^2+2}{u\sqrt{u^2+4}}, \quad u \equiv \frac{\theta_{\rm rel}}{\theta_{\rm E}}. \tag{2}$$

(Paczyński, 1986), and since by Liouville's theorem surface brightness is conserved, the source brightens by the same magnification factor A. Here, $\theta_{\rm rel}$ is the source-lens projected separation. By the Pythagorean theorem, the source-lens separation u as a function of time t is given by

$$u^2 = \frac{(t-t_0)^2}{t_{\rm E}^2} + u_0^2, \tag{3}$$

where t_0 is the time of closest approach, $u_0 = u(t_0)$ is the impact parameter, and $t_{\rm E}$ is the Einstein-radius crossing time. Hence, microlensing events are simple lightcurves characterized by three parameters $(t_0, u_0, t_{\rm E})$, which is fortunate because

otherwise they could not be distinguished from the much more numerous variable stars.

The probability that any given source is microlensed at any given time [i.e., $u(t) < 1$] is called the optical depth τ. For microlensing toward the Galactic bulge, $\tau \sim 2 \times 10^{-6}$. Hence, 10s of millions of stars must be monitored to find a significant number of microlensing events. Nevertheless, more than 2000 have been found, the majority by the OGLE and MACHO microlensing collaborations. These groups employ wide field ($\sim$0.5 deg^2) cameras on 1.5 m telescopes, which are entirely dedicated to microlensing searches.

3. Microlensing by planets

The previous description strictly applies only to point lenses. Naively one might think that binaries would generate lightcurves that were the sum of two single-star lenses. In fact, the additional lens creates an "astigmatism" in the magnification field of the first lens, which can give rise to much more complicated lightcurves, including "caustics", regions of formally infinite magnification. This applies to double lenses of any sort, whether binary stars or planetary systems (Mao and Paczyński, 1991). However, while binary-lens lightcurves can be dominated by the riotous behavior of caustics, planetary lightcurves are typically much simpler. For the majority of the event they look like simple single-star lightcurves, except for a brief interval when the lightcurve is perturbed by the presence of the planet. The reason for this is simple, the planetary Einstein radius, $\theta_{\mathrm{E,p}}$ is smaller than θ_{E} of the star by the square root of their mass ratio

$$\theta_{\mathrm{E,p}} = q^{1/2}\theta_{\mathrm{E}}, \quad q \equiv \frac{m_{\mathrm{p}}}{M}. \tag{4}$$

Only if one of the two images of the primary lens comes "close" to the planet, will it significantly perturb the lightcurve. "Close" is defined by the size of the planetary Einstein radius $\theta_{\mathrm{E,p}}$ and by the size (or degree of magnification) of the image. This simple picture permits one to grasp all the main characteristics of planetary microlensing.

First, since $\theta_{\mathrm{E,p}} \propto m_{\mathrm{p}}^{1/2}$, the probability that a given planetary companion will actually affect a microlensing lightcurve is also proportional to $m_{\mathrm{p}}^{1/2}$. Second, microlensing is much more sensitive to planets that happen to lie close to the "Einstein ring", the circle of angular radius θ_{E} about the star. For Galactic microlensing, this radius typically corresponds to about 2.5 AU. Professional microlensers speak of a "lensing zone" between 0.6 and 1.6 Einstein radii. Microlensing can still detect planets at other radii, but it is most sensitive here. Third, the duration of the perturbation is proportional to $\theta_{\mathrm{E,p}}$ and so to $m_{\mathrm{p}}^{1/2}$. *However, the form and amplitude of the perturbation do not depend on the planet mass* (Gould and Loeb, 1992).

The bottom line is that if one hopes to detect low-mass planets, one must survey a huge number of stars and one must monitor them every few minutes. First, the chance that any given star is microlensed is only $\tau \sim 2 \times 10^{-6}$. Even if all these stars have Earth-mass planets, the chance they will perturb the lightcurve is only $\mathcal{O}(q^{1/2})$, or 0.2% for Earth-mass planets of solar-type stars. This probability is enhanced if the planet is in the lensing zone, but it is still small. And the fraction of stars with Earth-mass planets may itself be small. Finally, the duration of the planetary event is only $\sim$1.5 h $(m_{\mathrm{p}}/M_{\oplus})^{1/2}$.

4. Planet searches from the ground

Ground-based microlensing searches for planets have been carried out for almost a decade. Because even Jupiter-mass planets generate deviations that last only about 1 day, while the surveys that find microlensing events typically monitor their fields only once per day, it is impossible to reliably detect planets from the surveys themselves. Planet-search groups therefore rely on the survey groups to provide them with alerts of ongoing events, and then monitor the most promising of these much more intensively. Gaudi et al. (2002) analyzed 44 such monitored events in 5 years of data from the PLANET collaboration (Albrow et al., 1998). They failed to find any planets, but were able to put significant upper limits on the planets of bulge stars. Recently, however,

Bond et al. (2004) reported the first secure microlensing detection of a planet. As predicted from theory, the lightcurve looks like a normal single-star microlensing event, except that it suddenly and dramatically deviates from this course as it undergoes two caustic crossings within a few days. Microlensing surveys are becoming more efficient, both discovering more events (700 this year alone) and finding the high-magnification events before peak when they are most sensitive to planets. It may be that many planets will be discovered over the next few years.

5. Why wide field imaging from space?

However, to achieve the full potential of microlensing will require a new survey using wide-field space-based imaging. The reason is simple. The probability of detecting an Earth mass planets toward a given source is of the order $\sim q^{1/2}\tau \sim 4\times10^{-9}$, even if every star has one such planet. Hence, the rate of detection is

$$\Gamma \sim \frac{\alpha f q^{1/2}\tau}{t_{\rm E}} \sim 5\times10^{-8}\ {\rm yr}^{-1}\alpha f, \qquad (5)$$

where f is the fraction of stars with Earth-mass planets and α is a numerical factor that might be as large as 5 or so for planets in the lensing zone. Thus, clearly one must survey of order 10^8 stars with a frequency of several observations per hour to detect a respectable number of Earths. Still this is far more robust than any other method that has been proposed for detecting Earth-mass planets.

The sheer number of stars that must be monitored implies that the source population has to include the upper main sequence: there are simply not enough brighter stars within a few square degrees and it is impossible to cover larger areas while still maintaining the cadence needed to detect the short deviations induced by Earth-mass planets. These faint stars cannot generally be resolved from the ground, but are easily resolved from space. While microlensing by unresolved stars can be successfully tracked using difference imaging, the increased background light in the unresolved images significantly degrades the photometric precision.

6. What would a microlensing survey do?

Microlensing probes planet parameter space in several directions that are orthogonal to other techniques.

6.1. Low-mass planets

As mentioned above, the size of planetary signature in microlensing events remains the same as the planet mass decreases. It is true that the both the probability and duration of the planetary deviations decline as the square root of the mass, and both effects imply that sensitivity falls with mass. However, given a large enough survey, there will be robust detections of planets down to very small masses. This is in sharp contrast to all other methods, in which the planetary signatures always fall sharply with mass.

Now, it should be noted that the microlensing signature does eventually diminish when the planetary Einstein radius $\theta_{\rm E,p}$ falls below the size of the source star, θ_*. Below this point, the planet perturbs only a small fraction of the star's light. However, for main-sequence stars, $\theta_* \sim 0.6$ μas, this occurs at masses $m_{\rm p} \sim 5\times10^{-7}\ M_\odot$, which is to say the mass of Mars.

A survey lasting 4 years using a 1.5 m telescope and a 2 deg^2 camera, would detect 10 Mars-mass planets or 100 Earth-mass planets, assuming that every star had one such planet in the lensing zone. Higher mass planets would have correspondingly higher rates.

6.2. High signal-to-noise ratio

Because of the intrinsic difficulty of detecting Earth-mass planets, most experiments benchmark their capabilities to very low signal-to-noise ratio (S/N), e.g., $\mathrm{S/N} \equiv \sqrt{\Delta\chi^2} = 8$. This threshold is adopted because it eliminates false positives from Gaussian statistics. However, the experience of cutting-edge difficult-to-repeat experiments shows that much higher thresholds are required in practice to avoid false-positives from unanticipated backgrounds. Typically, experimenters are driven to $\mathrm{S/N} > 25$ (Gould et al., 2003). For other techniques (such as transits, radial velocities, and

astrometry) the number of detections fall as a high power $N \propto (\mathrm{S/N})^{-\gamma}$, with $\gamma \sim 2.4$. Hence, setting a higher (and more realistic) threshold would dramatically reduce the number of reliable detections. By contrast, for microlensing $\gamma \sim 1$, implying that the ensemble of microlensing detections is far more robust in the face of unanticipated systematics.

6.3. Free-floating planets

Most theories of planet formation predict that a large number of planets will be ejected from their planetary systems during or after the epoch of their assembly. For example, it is possible that 10 or even 100 Earth-mass planets might have been ejected during the formation of the ice giants Uranus and Neptune. It would be difficult to test these theories without a capacity to detect the free-floating planets that arise from such ejections. Only microlensing can detect this population: all other techniques rely on the effect of the planet on its parent star (either jostling the star's position or blocking its light). Hence, they can only detect planets that are bound to their parent star. Microlensing, by contrast, relies on the fact that the planet's gravity can bend the light from a *background* star, and this effect does not require the proximity of a "host star". It is true that the microlensing effect is *enhanced* if the planet lies in the "lensing zone" of its host star, but the effect remains at larger distances from the host, including infinite distances.

6.4. Galactic census

By its very nature, microlensing detects planets at a range of distances from within a kpc or so of the Sun to the Galactic bulge. Other techniques generally probe stars at much closer distances. It is true that some transit searches also probe stars at several kpc, but these experiments are only sensitive to Jupiter-mass planets at very close star-planet separations.

6.5. Planet masses

A key parameter in characterizing a planet is its mass. The only technique that routinely yields a planet mass is astrometry. Radial velocities yields $M \sin i$, which is a very good (but not perfect) proxy for the mass because for random inclinations, the $\sin i$ distribution is strongly peaked toward unity. Transits do not yield masses at all, although if the mass is large enough, it is possible to derive the mass from follow-up radial-velocity observations. Unfortunately, Earth-mass planets do not generate measurable radial-velocity variations.

How does microlensing fit into this picture? Microlensing routinely yields planet/star *mass ratios*, rather than planet masses per se (Gould and Loeb, 1992). While this parameter is also important in characterizing the planet, one would also like to know under what circumstances it is possible to go farther and extract a mass.

To measure the mass m_{p}, given the knowledge of $q = m_{\mathrm{p}}/M$, one must somehow determine the star mass M. For about 1/3 of the events, the lens star will be visible. From its color and magnitude, one can make a good estimate of its mass.

When the lens star is not visible, it will still often be possible to constrain or measure its mass. Microlens masses can be found by measuring two higher-order parameters, the angular Einstein radius θ_{E} and the projected Einstein radius $\tilde{r}_{\mathrm{E}}$. Specifically, $M = (c^2/4G)\theta_{\mathrm{E}}\tilde{r}_{\mathrm{E}}$. There are two primary methods to measure θ_{E}. First, if the source transits a caustic, the timing of the caustic crossing yields $\rho = \theta_*/\theta_{\mathrm{E}}$. Then, from the color and magnitude of the source, one can determine θ_* (e.g., Yoo et al., 2004), and so $\theta_{\mathrm{E}} = \theta_*/\rho$. While caustic crossings are rare for microlensing events as a whole, they are fairly common for planetary events simply because the planet cannot be detected unless the source passes pretty close to the planetary caustic. The second method is to directly measure the lens-source relative proper motion $\vec{\mu}_{\mathrm{rel}}$ by resolving the source and lens (e.g., Alcock et al., 2001). Then one obtains $\theta_{\mathrm{E}} = \mu_{\mathrm{rel}} t_{\mathrm{E}}$ and the direction as well. Of course, this method yields no additional masses over and above the 1/3 direct detections mentioned above, but it does provide a useful check.

There are also two principal ways to measure $\tilde{r}_{\mathrm{E}}$. The first is from the distortion of the lightcurve induced by the Earth's accelerated motion. One then finds the ration $\pi_{\mathrm{E}} = \mathrm{AU}/\tilde{r}_{\mathrm{E}}$, and so $\tilde{r}_{\mathrm{E}}$ itself

(Gould, 1992). The second is to compare the event as seen from the Earth and a satellite. One then finds the ratio of $\tilde{r}_E$ to the (known) Earth-satellite distance (Refsdal, 1966). For typical events, the first method does not really work because the event is over before the Earth has significantly changed its direction. However, even in these cases, the high-precision photometry of the wide field space camera would be adequate to measure a single component of the *vector* microlens parallax $\vec{\pi}_E$, whose magnitude is π_E and whose direction is that of $\vec{\mu}_{rel}$ (Gould et al., 2003). Hence, if the direction of motion were already known (as it would be if the lens were resolved), then the full $\vec{\pi}_E$ could be recovered, and so the mass. Again, however, this does not add to the tally of planet masses. Nevertheless, even if one measured θ_E and only one component of the $\vec{\pi}_E$, the mass would be significantly constrained.

It is possible to obtain fully accurate masses, even when the lens is not visible, provided the satellite is in L2 orbit, as it would be under some proposed designs for a Dark Energy (SNe) satellite. In this case, one could determine the direction of motion by combining the Earth-motion parallax effect with the difference in the event as seen from the Earth and satellite. As above, one would recover both the full $\vec{\pi}_E$ and θ_E and so the mass (Gould et al., 2003). The satellite must be at least of order the distance to L2 because otherwise the projected planetary Einstein radius $\tilde{r}_{E,p} = \sqrt{q}\tilde{r}_E$, would be too small to cause a noticeable difference in the two light curves.

In brief, planet/star mass ratios will be obtained routinely. Planet masses will be easily obtained for about 1/3 of the events, and it is possible, with some significant additional effort, to obtain masses for many of the rest.

7. Conclusion

Microlensing is a remarkably powerful technique for searching for planets. It is much more sensitive to low-mass planets than any other technique, and also much more robust in the face of unanticipated backgrounds. Among planetary search techniques, it is the only method capable of finding free-floating planets or taking a census of planets throughout the Galaxy. The full potential of the microlensing technique can only be achieved in a space-based wide field survey.

Acknowledgments

Supported by the National Science Foundation Grant AST 02-01266.

References

Albrow, M.D. et al., 1998. The 1995 pilot campaign of PLANET: searching for microlensing anomalies through precise, rapid, round-the-clock monitoring. ApJ 509, 687–702.

Alcock, C. et al., 2001. Detection of a microlens in the Milky Way. Nature 414, 617–619.

Bennett, D.P., Rhie, S.H., 2002. Simulation of a space-based microlensing survey for terrestrial extrasolar planets. ApJ 574, 985–1003.

Bond, I.A. et al., 2004. OGLE 2003-BLG-235/MOA 2003-BLG-53: a planetary microlensing event. ApJ 606, L155–L158.

Gaudi, B.S. et al., 2002. Microlensing constraints on the frequency of Jupiter-mass companions: analysis of five years of PLANET photometry. ApJ 566, 463–499.

Gould, A., 1992. Extending the MACHO search to $\sim 10^6\ M_\odot$. ApJ 392, 442–451.

Gould, A., Loeb, A., 1992. Discovering planetary systems through gravitational microlenses. ApJ 396, 104–114.

Gould, A., Gaudi, B.S., Han, C., 2003. Resolving the microlens mass degeneracy for Earth-mass planets. ApJ 591, L53–L56.

Mao, S., Paczyński, B., 1991. Gravitational microlensing by double stars and planetary systems. ApJ 374, L37–L40.

Paczyński, B., 1986. Gravitational microlensing by the galactic halo. ApJ 304, 1–5.

Refsdal, S., 1966. On the possibility of determining the distances and masses of stars from the gravitational lens effect. MNRAS 134, 315–319.

Yoo, J. et al., 2004. OGLE-2003-BLG-262: finite-source effects from a point-mass lens. ApJ 603, 139–151.

Available online at www.sciencedirect.com
SCIENCE DIRECT®
New Astronomy Reviews 49 (2005) 430–435
New Astronomy Reviews
www.elsevier.com/locate/newastrev

X-ray surveys and wide-field optical/near-infrared imaging with JDEM

W.N. Brandt

Department of Astronomy and Astrophysics, The Pennsylvania State University, 525 Davey Laboratory, University Park, PA 16802, United States

Available online 12 September 2005

Abstract

I briefly describe a few important scientific issues that could be addressed effectively via the combination of data from *JDEM* and X-ray missions. The topics covered are largely focused on active galactic nuclei (AGN) and include (1) the selection of AGN via X-ray emission and optical variability, (2) nuclear outbursts in galaxies due to transient fueling of their supermassive black holes, (3) moderate-luminosity AGN at high redshift ($z > 4$) found via application of "dropout" techniques to X-ray sources, and (4) the host-galaxy morphologies of X-ray selected AGN. I also describe the substantial challenges to obtaining wide-field X-ray data with sufficient sensitivity to complement *JDEM* properly.
© 2005 Elsevier B.V. All rights reserved.

Contents

1. Introduction . . . 431
2. The selection of AGN via X-ray emission and optical variability . . . 431
3. Nuclear outbursts in galaxies . . . 432
4. Moderate-luminosity AGN at high redshift . . . 433
5. The host-galaxy morphologies of X-ray selected AGN . . . 434
6. Some general prospects for X-ray support of JDEM . . . 434
Acknowledgments . . . 435
References . . . 435

E-mail address: niel@astro.psu.edu.

1387-6473/$ - see front matter © 2005 Elsevier B.V. All rights reserved.
doi:10.1016/j.newar.2005.08.018

1. Introduction

Extragalactic X-ray surveys have dramatically advanced over the past five years, largely due to the flood of data from the *Chandra X-ray Observatory* (hereafter *Chandra*) and the *X-ray Multi-Mirror Mission-Newton* (hereafter *XMM-Newton*). The superb X-ray mirrors and charge-coupled device (CCD) detectors on these observatories provide large source samples detected to ≈0.5–10 keV flux levels that are up to 50–250 times lower than those of previous X-ray missions. They furthermore provide high-quality X-ray source positions with accuracies of ≈0.3–3″, allowing reliable matching to multiwavelength counterparts. About 40 extragalactic surveys are presently underway utilizing data from *Chandra* and *XMM-Newton*.

While a broad diversity of sources are found in *Chandra* and *XMM-Newton* surveys, it is clear that the majority of the detected sources are active galactic nuclei (AGN). In fact, deep *Chandra* and *XMM-Newton* surveys have found the highest AGN sky densities to date, reaching ≈7200 deg^{-2} (e.g., Bauer et al., 2004). X-ray surveys appear to have excellent, although not perfect, completeness when compared to other multiwavelength methods for finding AGN.

Many of the AGN found in *Chandra* and *XMM-Newton* surveys are faint at optical and other wavelengths, often having *I* magnitudes of 23–27 (see Fig. 1). They also often have modest optical luminosities so that, without superb imaging from space, there is substantial blending of the light from the AGN and its host galaxy. Thus, sensitive and high-resolution imaging at multiple wavelengths and over relatively large fields is required for optimal follow-up studies.[1] Such imaging has typically lagged behind the X-ray data due to observational expense, but the *Joint Dark Energy Mission* (*JDEM*) would dramatically reverse this situation, likely leaving X-ray astronomers scrambling to "catch up."

Below I will briefly describe a few exciting science projects that would be enabled by combining data from *JDEM* and X-ray missions such as *Chandra*, *Constellation-X*, *DUO*, *EXIST*, *Generation-X*, *NuSTAR*, *XEUS*, and *XMM-Newton*. I will focus on AGN-driven science as AGN are the numerically dominant source population in extragalactic X-ray surveys. However, wonderful *JDEM*/X-ray science should also be possible for clusters and groups of galaxies, large-scale structures, starburst galaxies, normal galaxies, and other classes of objects.

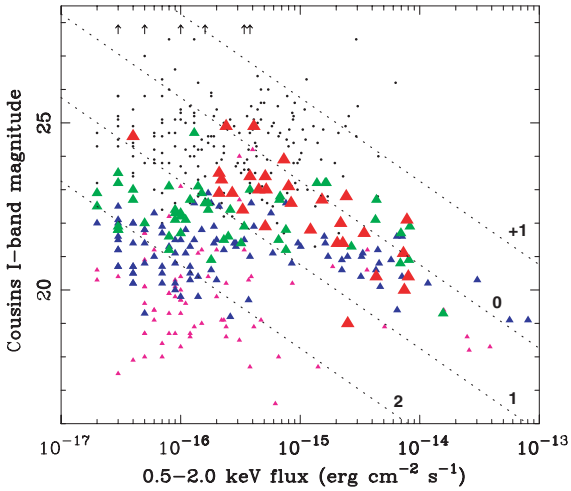

Fig. 1. *I*-band magnitude versus 0.5–2 keV flux for extragalactic X-ray sources in the 2 Ms Chandra Deep Field-North (CDF-N) observation. Sources with redshifts of 0–0.5, 0.5–1, 1–2, and 2–6 are shown as violet, blue, green, and red filled triangles, respectively (symbol sizes also increase with redshift). Small black dots indicate sources without measured redshifts. The slanted, dotted lines indicate constant values of $\log(f_X/f_I)$; the respective $\log(f_X/f_I)$ values are labeled. (For interpretation of the references to color in this figure legend, the reader is referred to the web version of this article.)

2. The selection of AGN via X-ray emission and optical variability

Deep optical variability surveys are one of the only methods competitive with X-ray surveys at efficiently finding high sky densities of AGN. For example, Sarajedini et al. (2003) report the discovery of 16 variable galactic nuclei in the Hubble Deep Field-North (HDF-N) based on analyses of two *HST V*-band images taken five years apart

[1] The effective field of view for *Chandra* (*XMM-Newton*) is ~1/12 deg^2 (~1/5 deg^2), and most of the surveys mentioned above use 1–20 such fields.

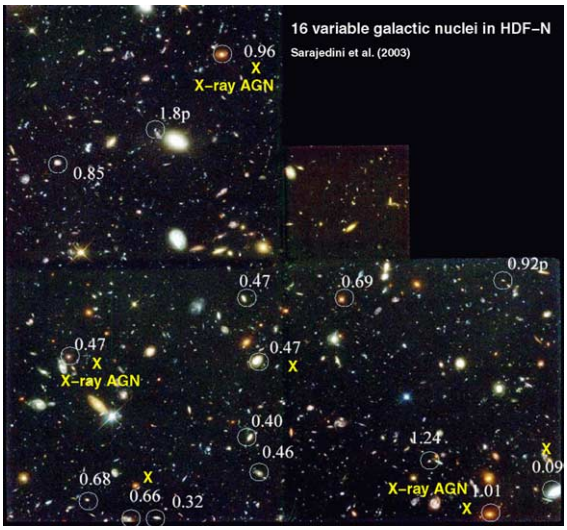

Fig. 2. *HST* image of the HDF-N showing the 16 galaxies with optically variable nuclei (circled and labeled with redshifts). The galaxies with both variable nuclei and X-ray detections are marked with "X" symbols; those that are clear X-ray AGN are labeled as such (there are additional X-ray AGN in the HDF-N that have not shown variable nuclei). Adapted from Alexander et al. (2003) and Sarajedini et al. (2003).

(see Fig. 2). The derived AGN sky density is in the range ≈2000–11,000 deg^{-2}. The precise sky density depends upon the amount of contamination by nuclear supernovae and statistical outliers, but it is clearly higher than that from most optical spectroscopic surveys and is plausibly comparable to that from the deepest X-ray surveys (see Section 1).

While X-ray selection and optical variability selection have respectable overlap in the AGN found (see Fig. 2), each method also finds AGN missed by the other. For example, there are at least 2–3 X-ray AGN in the HDF-N not identified by Sarajedini et al. (2003). Conversely, at least some of the variable galactic nuclei of Sarajedini et al. (2003) may be X-ray weak AGN lying below the detection threshold of even the 2 Ms CDF-N exposure. These AGN might be X-ray weak due to a low bolometric power, or they might have emaciated accretion-disk coronae that cannot produce X-rays effectively.

As currently planned, *JDEM* should find at least 30,000–90,000 variability selected AGN in its 15 deg^2 deep survey. An even larger number of AGN should be found in its wider surveys. If appropriately matched X-ray data were obtained (see Section 6), joint *JDEM* and X-ray techniques could be applied to generate the largest and most complete census of moderate-luminosity, typical AGN out to high redshift. X-ray sources could be scrutinized especially carefully for optically variable nuclei in the *JDEM* data, and X-ray stacking techniques could be used to study the average X-ray properties of AGN not detected individually. The large solid-angle coverage would allow the AGN population to be probed consistently over a wide range of luminosity; the present data have poor coverage of luminous, rare AGN.

3. Nuclear outbursts in galaxies

X-ray surveys, mainly with *ROSAT*, have discovered about seven large-amplitude X-ray outbursts from galactic nuclei (e.g., Donley et al., 2002; Komossa, 2002; Vaughan et al., 2004). These events have variability amplitudes of 50–400 or more, peak X-ray luminosities comparable to those of local Seyfert galaxies, soft X-ray spectra, and decay timescales of months to years (see Fig. 3(a)). They are observed in both inactive and active galaxies. In inactive galaxies the event rate is ≈10^{-5} yr^{-1}, while in active galaxies the event rate appears to be ≈100 times higher. These outbursts are probably associated with transient fueling events of supermassive black holes (SMBHs). Fueling may occur when a star or planet is tidally disrupted, or in some cases it may be due to accretion-disk instabilities.

JDEM observations should allow the discovery of additional outbursts from galactic nuclei. The X-ray outbursts above are plausibly expected to induce accompanying optical variability, and there is direct evidence for such optical variability in at least the case of IC 3599 (Brandt et al., 1995; Grupe et al., 1995). Furthermore, optical outbursts have been detected from a few galaxies without near-simultaneous X-ray coverage, including NGC 4552 (Cappellari et al., 1999) and perhaps NGC 1068 (de Vaucouleurs, 1991). These outbursts should be distinguishable from nuclear

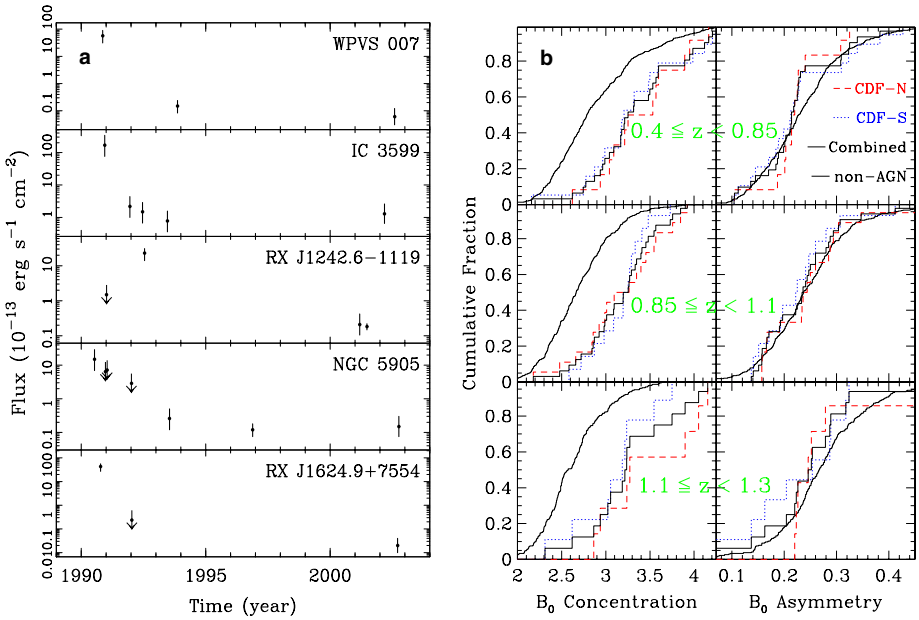

Fig. 3. (a) Historical X-ray light curves (from 0.3 to 2 keV) of five large-amplitude X-ray outbursts from galactic nuclei. WPVS 007, IC 3599, and NGC 5905 appear to be active galaxies, while the other two appear inactive. From Vaughan et al. (2004). (b) Cumulative distribution functions of rest-frame *B*-band concentration index and asymmetry index for GOODS AGN hosts from the CDF-N and CDF-S. Cumulative distribution functions for normal field galaxies are also shown for comparison. Note that AGN hosts have more concentrated light profiles than normal field galaxies, but that there is no significant difference in asymmetry (from Grogin et al. (2005)).

supernovae based upon their spectral properties and light curves.

The current data suggest that *JDEM* should detect 2–20 optical outbursts from galactic nuclei in its deep, wide-field, and panoramic surveys. However, this estimate suffers from significant statistical and systematic uncertainties, and *JDEM* observations will allow by far the best determination of the frequency of optical outbursts throughout the Universe. Optical outbursts discovered by *JDEM* should be rapidly followed-up with X-ray and multiwavelength observatories to determine the nature of these events. Presently, the lack of rapid multiwavelength follow-up studies is a major hindrance to understanding.

4. Moderate-luminosity AGN at high redshift

Combined *JDEM* and X-ray studies should allow the discovery of hundreds of moderate-luminosity AGN at $z \approx 4$–6; only ≈6 such AGN are known presently. These AGN have luminosities comparable to those of local Seyfert galaxies and low-power quasars, and at $z \approx 4$–6 their space density is much higher than for the rare, highly luminous quasars found by, e.g., the Sloan Digital Sky Survey (e.g., Cristiani et al., 2004). Moderate-luminosity AGN at $z \approx 4$–6 can be selected effectively via the application of optical/near-infrared "dropout" techniques to X-ray sources. Without complementary X-ray data, many such AGN in the *JDEM* data will be difficult and observationally expensive to identify as they often have only modest AGN signatures in the optical/near-infrared. X-ray stacking techniques could also be applied to the tens of thousands of $z \approx 4$–6 *JDEM*-discovered galaxies that are not detected individually in X-rays. Such stacking would tightly constrain the frequency of low-luminosity AGN as well as X-ray emission associated with star formation.

Near-infrared *JDEM* observations of X-ray sources should also break the current AGN redshift

"barrier" at $z \approx 6.5$, allowing the discovery of AGN out to $z \sim 10$. A small number of $z > 6.5$ candidates have already been identified in current deep X-ray surveys as extreme X-ray-to-optical ratio sources, but most and perhaps all probably lie at lower redshifts (Koekemoer et al., 2004). Wide fields with sensitive *JDEM* and X-ray coverage would hopefully generate enough $z \approx 6.5$–10 AGN to elucidate how the black holes formed by the deaths of the first stars grew to make luminous quasars at $z \approx 4$–6.

5. The host-galaxy morphologies of X-ray selected AGN

High-resolution optical and near-infrared imaging, such as that to be provided by *JDEM*, is required to mitigate light blending between many moderate-luminosity AGN and their host galaxies, thereby allowing the hosts to be studied reliably (see Section 1). Grogin et al. (2005) have recently studied the host galaxies of samples of 100–200 moderate-luminosity, X-ray selected AGN at $z = 0.4$–1.3 using *HST* imaging from the Great Observatories Origins Deep Survey (GOODS). They find that these AGN are preferentially hosted by galaxies with concentrated light profiles, generally corresponding to more bulge-dominated morphologies (see Fig. 3(b)). Similar results have been derived from Sersic-model fitting by B.D. Simmons et al., in preparation. Grogin et al. (2005) suggest that the locally observed relations between SMBH mass and host-galaxy properties are already in place at $z \approx 1$ (see, e.g., Graham et al., 2001 for the local relation between SMBH mass and concentration). *JDEM* imaging would allow these results to be refined using much larger samples, so that AGN of closely matched luminosity and other properties could be studied in fine redshift bins. Furthermore, the near-infrared capabilities of *JDEM* would allow investigation of SMBH/host-galaxy relations at $z \gtrsim 1.3$, provided sufficient near-infrared sensitivity is achieved to overcome surface-brightness dimming. The discovery of an epoch beyond which SMBHs and their host galaxies lose their tight relations would help to constrain models of SMBH/galaxy co-evolution.

Grogin et al. (2005) also investigated if their moderate-luminosity AGN samples showed enhanced merging or interaction activity relative to normal field galaxies, using an asymmetry index and near-neighbor counts (see Fig. 3(b)). They found no evidence for enhanced merging or interactions, results that are broadly consistent with those found for small samples of more luminous quasars (see, e.g., Section 7 of Dunlop et al., 2003). Wide fields surveyed by both *JDEM* and X-ray missions would provide much larger AGN samples with good source statistics spanning a range of at least 10,000 in nuclear luminosity. More subtle differences in merging and interaction activity might then become statistically detectable, and differences could be searched for sensitively in subsets of the AGN population.

6. Some general prospects for X-ray support of JDEM

There are substantial challenges to obtaining wide-field X-ray data with sufficient sensitivity to complement *JDEM* properly. The exquisitely sensitive imaging of *JDEM* will routinely reach $I = 27$–30. To obtain reliable X-ray counterparts to optical sources at these faint flux levels, sub-arcsecond X-ray positions are required. Given the X-ray-to-optical flux ratios observed for X-ray selected sources (see Fig. 1), X-ray sensitivities of $\approx 10^{-17}$–10^{-16} erg cm^{-2} s^{-1} (from 0.5–2 keV) are required to complement *JDEM* naturally.[2] Such sensitivities correspond to *Chandra* exposures of 0.2–2 Ms. Thus, the total *Chandra* exposure required to cover the 15 deg^2 *JDEM* deep survey area appropriately would be $\approx$1–10 yr; the wide-field ($\approx$500 deg^2) and panoramic ($\approx$8000 deg^2) *JDEM* surveys would require much more *Chandra*

[2] Note that some superb high-energy survey missions currently being planned, such as *DUO* and *EXIST*, target comparatively bright X-ray flux levels that will not naturally match the sensitive optical/near-infrared imaging of *JDEM*. Most of the sources found by these high-energy survey missions are expected to have counterparts with $I = 18$–23. *JDEM* will typically reach flux levels $\sim$1500 times fainter than these counterparts.

exposure. Even if *Chandra* survives until the launch of *JDEM* in ≈2014, *Chandra* time-allocation committees may be hesitant to allocate the requisite enormous exposure!

Future X-ray missions with larger photon collecting areas coupled with excellent angular resolution, such as ESA's *XEUS* and NASA's *Generation-X*, offer better prospects for complementing *JDEM* effectively. The nominal launch date for *XEUS* of ≈2015 is fairly well synchronized with that of *JDEM*, and *XEUS* could obtain appropriate coverage of the *JDEM* deep survey area in ≈0.1–1 yr. *Generation-X*, currently under study as a NASA Space Science Vision Mission, would probably not begin operation until after ≈2020. It could appropriately survey the *JDEM* deep survey area in about a week and could also complement the *JDEM* wide-field and panoramic surveys.

Acknowledgments

I thank D.M. Alexander, F.E. Bauer, N.A. Grogin, A.M. Koekemoer, B.D. Lehmer, V.L. Sarajedini, B.D. Simmons, A.T. Steffen, C.M. Urry, and C. Vignali for helpful discussions. Funding from NSF CAREER award AST-9983783 and CXC Grant GO2-3187A is gratefully acknowledged.

References

Alexander, D.M., Bauer, F.E., Brandt, W.N., et al., 2003. The Chandra Deep Field-North Survey. XIII. 2 Ms Point-Source Catalogs. AJ 126, 539–574.

Bauer, F.E., Alexander, D.M., Brandt, W.N., et al., 2004. The Fall of AGN and the Rise of Star-Forming Galaxies: A Close Look at the Chandra Deep Field X-ray Number Counts. AJ 128, 2048–2065.

Brandt, W.N., Pounds, K.A., Fink, H., 1995. The unusual X-ray and optical properties of the ultrasoft active galactic nucleus Zwicky 159.034 (RE J1237 + 264). MNRAS 273, 47–52.

Cappellari, M., Renzini, A., Greggio, L., et al., 1999. The mini-active galactic nucleus at the center of the Elliptical Galaxy NGC 4552 with Hubble Space Telescope. ApJ 519, 117–133.

Cristiani, S., Alexander, D.M., Bauer, F.E., et al., 2004. The space density of high-redshift QSOs in the Great Observatories Origins Deep Survey. ApJ 600, L119–L122.

de Vaucouleurs, G., 1991. Flare-up in the nucleus of NGC 1068 in 1980? The Observatory 111, 122–123.

Donley, J.L., Brandt, W.N., Eracleous, M., Boller, Th., 2002. Large-amplitude X-ray outbursts from galactic nuclei: A systematic survey using ROSAT Archival Data. AJ 124, 1308–1321.

Dunlop, J.S., McLure, R.J., Kukula, M.J., et al., 2003. Quasars, their host galaxies and their central black holes. MNRAS 340, 1095–1135.

Graham, A.W., Erwin, P., Caon, N., Trujillo, I., 2001. A correlation between galaxy light concentration and supermassive black hole mass. ApJ 563, L11–L14.

Grogin, N.A., Conselice, C.J., Chatzichristou, E., et al., 2005. GOODS AGN host structural parameters and environment: evidence for black hole-bulge correlation and against Merger-AGN connection at $z \sim 0.4$–1.3. ApJ 627, L97–L100.

Grupe, D., Beuermann, K., Mannheim, K., et al., 1995. X-ray outburst of the peculiar Seyfert Galaxy IC 3599. A&A 299, L5–L8.

Koekemoer, A., Alexander, D.M., Bauer, F.E., et al., 2004. A possible new population of sources with extreme X-ray/optical ratios. ApJ 600, L123–L126.

Komossa, S., 2002. X-ray evidence for supermassive black holes at the centers of nearby, non-active galaxies. Rev. Mod. Ast. 15, 27–56.

Sarajedini, V.L., Gilliland, R.L., Kasm, C., 2003. A V-Band Survey for variable galactic nuclei in the Hubble Deep Field. ApJ 599, 173–184.

Vaughan, S., Edelson, R., Warwick, R.S., 2004. Chandra observations of five X-ray transient galactic nuclei. MNRAS 349, L1–L5.

Available online at www.sciencedirect.com
SCIENCE DIRECT®
New Astronomy Reviews 49 (2005) 436–439
New Astronomy Reviews
www.elsevier.com/locate/newastrev

EXIST: All-sky hard X-ray imaging and spectral–temporal survey for black holes ☆

Jonathan E. Grindlay *

Harvard-Smithsonian CfA, 60 Garden St., Cambridge, MA 02138, United States

The EXIST Team

Available online 30 September 2005

Abstract

The energetic X-ray imaging survey telescope (EXIST) is under study for the proposed Black Hole Finder Probe, one of the three *Einstein Probe* missions in NASA's proposed Beyond Einstein Program. EXIST would have unique capabilities: it would survey the full sky at 5–600 keV each 95 min orbit with 0.9–5′, 10 μs–45 min and ∼0.5–5 keV resolution to locate sources to 10″ and enable black holes to be surveyed and studied on all scales. With a 1y/5σ survey sensitivity F_x (40–80 keV) $\sim 5 \times 10^{-13}$ erg cm^{-2} s^{-1}, comparable to the ROSAT soft X-ray (0.3–2.5 keV) sky survey, a large sample ($\gtrsim$ 2–4 $\times 10^4$) of obscured AGN will be identified and a complete sample of accreting stellar mass BHs in the Galaxy will be found. The all-sky/all-time coverage will allow rare events to be measured, such as possible stellar disruption flares from dormant AGN out to ∼100 Mpc. A large sample (∼2–3/day) of GRBs will be located ($\lesssim$10″) at sensitivities and bandwidths much greater than previously and likely yield the highest redshift events and constraints on Pop III BHs. An outline of the mission design from the ongoing concept study is presented.
© 2005 Elsevier B.V. All rights reserved.

Contents

1. Introduction . . . 437
2. Black hole finder probe science to EXIST . . . 437
   2.1. Revealing obscured or dormant super massive BHs . . . 437
   2.2. Measuring the birth of the first BHs . . . 437
   2.3. Studying BHs in the Galaxy and AGN as probes . . . 438

☆ Paper presented at Wide Field Surveys meeting.

* Tel.: +1 617 495 7204; fax: +1 617 495 7356.
E-mail address: josh@cfa.harvard.edu.

1387-6473/$ - see front matter © 2005 Elsevier B.V. All rights reserved.
doi:10.1016/j.newar.2005.08.019

3. Telescope and detector concept 438
Acknowledgments 439
References. 439

1. Introduction

Of the wide-field surveys considered at this meeting, one is likely widest of all: temporally resolved imaging in hard X-rays (~5–600 keV) of the full sky every 95 min. This is possible with a satellite-borne coded aperture imaging telescope array with very wide "fully coded" field of view that scans with a photon-counting detector array over the full sky each orbit. Such is the concept for the energetic X-ray imaging survey telescope (EXIST), originally recommended by the Decadal Survey as a possible ISS mission and then considered as a Free Flyer (Grindlay et al., 2003), and now under study to be the Black Hole Finder Probe in NASA's *Beyond Einstein* Program. The unique all-sky/all-time imaging capability of EXIST opens the temporal survey window and is highly complementary to LSST (or any Wide-Field OIR surveys) and LISA. The hard X-ray band is particularly well matched for detection and study of accreting black holes, from stellar mass ($\sim 10 M_{\odot}$) in X-ray binaries to supermassive ($\sim 10^{7-9} M_{\odot}$) in galactic nuclei, which characteristically emit their peak luminosity in a broad band around ~100 keV. At energies above ~7 keV, photoelectric absorption by column densities $N_{\rm H} \gtrsim 10^{23-24}\,{\rm cm}^{-2}$ in galactic nuclei or X-ray binaries in the Galaxy becomes negligible and black holes can be seen until $N_{\rm H} \gtrsim 10^{25}\,{\rm cm}^{-2}$ and they are obscured by Compton scattering.

2. Black hole finder probe science to EXIST

The Black Hole Finder Probe (BHFP) should enable the most comprehensive survey for black holes, from super massive to stellar, yet undertaken. The EXIST concept for BHFP would emphasize three primary science objectives, described below along with related science goals.

2.1. Revealing obscured or dormant super massive BHs

'The all-sky hard X-ray imaging survey would reveal Type 2 (obscured) AGN and nearby ($\lesssim$300 Mpc) stellar tidal disruption events in normal galaxies. The Type 2 survey will probe the bulk of the cosmic X-ray background (CXB), which is only ~50–70% resolved by Chandra and XMM at energies 6–8 keV according to Worsley et al. (submitted), who conclude the missing CXB requires a large population of AGN with $N_{\rm H} \sim 10^{23-24}\,{\rm cm}^{-2}$ and unabsorbed $L_x \sim 10^{43-44}\,{\rm erg\,s}^{-1}$ primarily at $z \sim 0.5$–1.5. EXIST would provide a full sky sample of these objects out to $z \sim 0.3$, and more luminous Type 2 Seyferts and QSOs with $L_x \sim 10^{45}$ and $\sim 10^{46}\,{\rm erg\,s}^{-1}$ out to $z \sim 1$ and 3, respectively, to constrain the growth and evolution of super massive BHs in the universe. EXIST would provide the first full-sky survey for dormant BHs in galactic nuclei from the expected disruption of stars. If just 1% of this accretion luminosity is released in a hard X-ray component (as found for virtually all Eddington-rate events), some 10–30 events/y should be seen out to ~100 Mpc (Grindlay, 2004). The significantly increased sensitivity of EXIST vs. the BAT on Swift, both at $\lesssim$15 and $\gtrsim$ 150 keV, should enable detection of the prompt ~5 keV burst predicted by Kobayashi et al. (2004), providing a LISA trigger for nearby (~10 Mpc) disruption events.

2.2. Measuring the birth of the first BHs

EXIST would conduct the highest sensitivity and bandwidth survey for GRBs out to limiting $z \sim 15$ for most burst fluences detected at $z \lesssim 5$ by BATSE (Band, 2003). The broad spectral coverage and very large FoV of EXIST would maximize the detection of the extremes of GRBs: those at the highest z or low luminosity events and X-ray flashes at lower z. EXIST will allow

the determination of GRB spectra and the peak energy flux, E_{peak}, in a νF_ν broad band spectrum, which may allow GRBs to be calibrated as standard candles (Ghirlanda et al., 2004) and thus allow cosmological redshifts directly from GRB spectra. The active anti-coincidence side-shields (over 8 m^2 of CsI) also would allow the upper energy range for GRBs detected with EXIST to be extended to ~10 MeV, or significantly beyond the ~600 keV limit of the primary imaging detectors (see below), thus enabling GRBs from Pop III BHs to be compared directly with those at lower redshifts detected at ~10–1000 MeV by GLAST.

2.3. Studying BHs in the Galaxy and AGN as probes

By continually measuring spectra and time variability of accreting BHs in brighter AGN and galactic X-ray binaries, EXIST will constrain their physics and evolution. The population of galactic BHs accreting from both high and low mass companion stars will be measured from both persistent and transient sources. EXIST would study the full population of obscured accreting BHs suggested by the INTEGRAL survey of the galactic bulge (Revnivtsev et al., 2004). BH populations would be probed in high mass binaries such as the intrinsically absorbed possible sgBe system IGR J16318-4848 discovered with INTEGRAL and identified (Filliatre and Chaty, 2004) with an IR counterpart that resembles the peculiar transient CI Cam. BHs in low mass binaries would be seen as X-ray "novae", with characteristic hard spectra and L_x (20–100 keV) $\sim 10^{38}$ erg s^{-1} and $\tau \sim 10$ d decay time (cf. McClintock and Remillard, 2005, MR05), could be studied in detail in the Galaxy and LMC/SMC and detected as "new" sources out to the Andromeda Galaxy (super-flares from soft gamma-ray repeaters, magnetars, are detected out to Virgo). For brighter stellar mass BHs and transients and AGN, the continuous and long-duration monitoring will allow measures of QPOs that appear to correlate with BH mass (MR05) and (for AGN vs. Cyg X-1) accretion luminosity (Leighly, 2004). For non-thermal and jet-dominated BHs such as microquasars and Blazars, EXIST spectra and variability coordinated with IR-TeV observations will constrain the BH-jet interface. Notably, for Blazars, simultaneous EXIST spectra and GeV–TeV spectra from GLAST and VERITAS will anchor the underlying SSC model (e.g., Katarzynski et al., 2004) to enable measurement of the cosmic diffuse IR background flux from the observed vs. predicted cutoff in the GeV–TeV spectrum.

3. Telescope and detector concept

The EXIST Concept Study mission design (Fig. 1) would include two large area and FoV coded aperture telescope arrays: a high energy telescope (HET; 10–600 keV) and a low energy telescope (LET; 5–30 keV). The HET is an array of 6×3 coded aperture telescopes covering a $131° \times 65°$ fully coded/flat-response FoV (and $153° \times 87°$ FWHM FoV) with total detector area of 5.6 m^2 of imaging (1.25 mm pixels) CZT. The LET is 4 arrays of 7×1 coded aperture telescopes covering a similar FoV with total detector area of 1.3 m^2 of imaging (0.158 mm strips or pixels) Si. The angular resolution of the HET and LET are 5′ and 0.9′, respectively, or well below source confusion limits for the AGN surface density at F_x (20–40 keV) $\gtrsim 5 \times 10^{-13}$ cgs as well as faint hard X-ray sources in the Galaxy, and sufficient to allow $\gtrsim 5\sigma$ threshold detections to be centroided to $\lesssim 10''$ to enable correct optical/IR identifications.

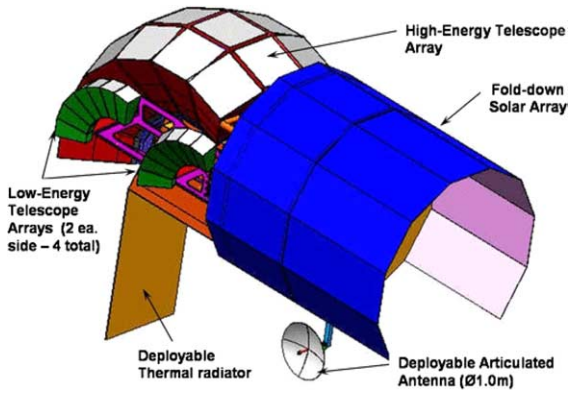

Fig. 1. EXIST on orbit. The $131° \times 65°$ FoV of the HET array is zenith-oriented with the long direction perpendicular to the orbit velocity vector and "nodded" by ±20° every ~20 min so that the full sky is scanned each orbit.

Acknowledgments

I thank the EXIST team for their role in defining the mission science and concept (see http://exist.gsfc.nasa.gov/). This work was partly supported by NASA Grant NNG04GK33G for the EXIST concept study.

References

Band, D., 2003. ApJ 588, 945.
Filliatre, P., Chaty, S., 2004. ApJ 616, 469.
Ghirlanda, G., Ghisellini, G., Lazzati, D., Firmani, C., 2004. ApJ 613, L13.
Grindlay, J.E. et al., 2003. Proc. SPIE 4851, 331.
Grindlay, J.E., 2004. AIPC 714, 413.
Katarzynski, K. et al., 2004. astro-ph/0412405.
Kobayashi, S. et al., 2004. ApJ 615, 855.
Leighly, K., 2004. astro-ph/0412636.
McClintock, J., Remillard, R., 2005. In: Lewin, W.H.G., van der Klis, M. (Eds.), Compact Stellar X-ray Sources. Cambridge University Press (MR05).
Revnivtsev, M., Sunyaev, R., Varshalovich, D., et al., 2004. Astr. Lett. 30, 382.
Worsley, M.A., et al., 2004. MNRAS astro-ph/0412266 (submitted).

Available online at www.sciencedirect.com
SCIENCE DIRECT®
New Astronomy Reviews 49 (2005) 440–446
New Astronomy Reviews
www.elsevier.com/locate/newastrev

Lessons from the GOODS

Mauro Giavalisco

Space Telescope Science Institute, 3700 San Martin Dr., Baltimore, MD 21218, United States

Available online 19 October 2005

Abstract

The Great Observatories Origins Deep Survey (GOODS) is a multi-facility project that combines data from NASA's Hubble, Chandra and Spitzer space telescopes with spectroscopy and ancillary optical and near-IR imaging from the ground (VLT, Keck, Gemini, Subaru, NOAO) to provide a database for studying galaxy and AGN evolution up to redshifts $z \sim 6.5$ and higher. The survey covers $\sim$0.1 deg^2 in two fields, one in each celestial hemisphere, centered around the historical Hubble Deep Field (HDF) and Chandra Deep Field (CDF). The Spitzer and the Hubble images, which nears the depth of the HDF, are matched in sensitivity to sample the spectral energy distribution of even very blue sources with comparable signal-to-noise ratios. The GOODS combination of depth, angular resolution, wavelength and area coverage is currently unparalleled by other extragalactic surveys, and here we review some areas in the field of galaxy evolution where GOODS had brought (or will soon bring) significant progress and where it will need further work.
© 2005 Elsevier B.V. All rights reserved.

Keywords: Cosmology: observations; Galaxies: formation; Galaxies: evolution; Galaxies: distances and redshifts

Contents

1. Introduction . . . 441
2. The great observatories origins deep survey . . . 441
3. The evolution of the rest-frame UV luminosity function . . . 442
4. Testing the galaxy-dark matter physical association. . . . 443
5. Galaxies at very high redshift . . . 444
6. Conclusions. . . . 446
Acknowledgments . . . 446
References. . . . 446

E-mail address: mauro@stsci.edu.

1387-6473/$ - see front matter © 2005 Elsevier B.V. All rights reserved.
doi:10.1016/j.newar.2005.08.021

1. Introduction

Great advances in telescopes and instrumentations, both ground-based and space-borne, have vastly pushed the boundaries of our exploration of distant galaxies backward in time. With galaxies now identified all the way to $z \sim 7$ or even more (Bouwens et al., 2004; Bouwens et al., 2005; Mobasher et al., submitted), we are now capable of observing galaxies at nearly any epoch when galaxies exist. And while the remaining few hundred millions years of unexplored cosmic time hold the key to understand how the galactogenesis started (but this is another story, for a new survey and a future meeting), even more important is the fact that we can now identify galaxies with a variety of spectral types at such early times. These range from relatively unobscured, blue star-forming galaxies that are identified with great efficiency by means of multi-band optical CCD imaging (Steidel et al., 2003; Giavalisco et al., 2004b) to highly obscured starburst or passively evolving very red galaxies that can be detected only at near-IR wavelengths (Dickinson et al., 2000; Labbe' et al., 2005; van Dokkum et al., 2004; Moustakas et al., 2004; Mobasher et al., submitted), including pretty much everything in between (Adelberger et al., 2004; Steidel et al., 2004; Daddi et al., 2004).

2. The great observatories origins deep survey

While the existence of the galaxies has been empirically proved, measuring and understanding their physical properties, such as mass, luminosity function, stellar mass, star-formation rate, metallicity, dust content, age, clustering, morphology, is still in its infancy for most of these galaxy "types". Not only there is a wide unbalance in our relative knowledge of the properties of the various types at high redshift (e.g., $z > 1.5$), with unobscured starburst galaxies being the best studied case (see Giavalisco, 2002 for a review), but at $z \gtrsim 2$ only a dozen of red galaxies at most have been spectroscopically confirmed or otherwise identified (see van Dokkum et al., 2004 and Mobasher et al., submitted). At redshift $z \gtrsim 5$ empirical information is very sketchy for any galaxy types.

To take into account dust obscuration, be sensitive to galaxies with no ongoing star formation, account for the fact that only the optical rest-frame near-IR emission is useful to probe the stellar mass, as well as to satisfy the requirements of color selection and push to higher and higher redshifts require deep multi-band observations over a very extended wavelength range. Because the target galaxies appear, by necessity, very faint, an effective survey also needs to reach very faint fluxes, with sensitivities at each band across the wavelength range matched. For example $z_{\rm AB} \sim 26$ is required to reach $L^*_{\rm UV}$ at $z \sim 7$ (assuming the same rest-frame UV luminosity function of Lyman-break galaxies at $z \sim 3$ and $\sim$4, Giavalisco et al., 2004b), but at least a mag fainter is necessary to measure the luminosity function (all magnitude here are in the AB scale). Matched near-IR limits would be around $\sim$26 mag or so to ensure sensitivity to blue sources, while at mid-infrared, e.g., the Spitzer Space Telescope (SST) IRAC bands at 3.6, 5.28 and 12 μm bands, the same requirements implies limits from a fraction to a few μJy. In addition to an extended wavelength coverage, if one is to fit the observed broad-band photometry to spectral energy distribution templates to derived either accurate photometric redshifts or (if the redshift is known) physical parameters of the galaxies such as mass, age, metallicity, and obscuration, one also needs to sample the spectral range reasonably well. This means that in addition to the *HST* ACS and *SST* IRAC AND MIPS bands one also needs to provide the near-IR JHK bands. These need to be observed from ground-based facilities, since the small field size of NICMOS on *HST* would make the observations prohibitely expensive. Finally, one also needs to cover a reasonably large area to provide some safety against the effects of cosmic variance.

To satisfy in sufficient measure all these requirements necessarily implies large surveys. The Great Observatories Origins Deep Survey (GOODS) unites very deep observations from space and from ground-based facilities to provide the first (and currently only) truly panchromatic faint survey over a relatively large sky area. The two GOODS fields, centered around the HDF-North and CDF-South, cover a total of 0.1 deg^2 include imaging observations taken with Chandra, *HST*, *SST*, the ESO

VLT, Subaru and NOAO. It also includes spectroscopic coverage with the Keck, the VLT and Gemini. The *HST* ACS data consist of B_{435}, V_{606}, i_{775} and z_{850} images, reaching a sensitivity of 27.5, 27.9, 27.0 and 26.7 mag (10-σ, sources contained within 0.5″ diameter circular aperture); the *SST* data consist of IRAC images at 3.6, 4.5, 5.8 and 8.0 μm reaching 0.11, 0.24, 1.35, 1.66 μJy (5-σ), and of MIPS images at 24 μm reaching 20.0 μm (5-σ). An overview of GOODS is presented in Giavalisco et al. (2004a). Here, we simply remind that all GOODS data, raw and reduced, and the source catalogs are publicly available and can be obtained from the team's Web sites (e.g., www.stsci.edu/science/goods/).

3. The evolution of the rest-frame UV luminosity function

The wavelength coverage, sensitivity to compact sources, and area coverage of the GOODS ACS images make them very well suited to measure the rest-frame UV luminosity function of LBGs at redshift $4 \lesssim z \lesssim 6$. This complements ground-based surveys at $z \sim 3$ (Steidel et al., 1999) and makes it possible to study, among other things, the evolution of the star formation and the contribution to the cosmic UV emissivity from LBGs. The basic methodology of the measures is discussed in Giavalisco et al. (2004b), including the selection criteria of the samples and the measure of the redshift distribution, and we refer the reader to that publication for details. Here, we present the results from improved measures at $z \sim 4$ and $\sim$5 obtained from the full stack of the ACS data (in the above paper only 3/5 of the data were used) and refer to an upcoming paper (Giavalisco et al., in preparation) for a full discussion. Figs. 1 and 2 show the basic result of this work, namely that the rest-frame UV luminosity function of LBGs undergoes only a modest amount of evolution from $z \sim 3$ to $\sim$5.

In Fig. 1, the Schechter fit to the GOODS data is compared to similar data by Steidel et al. (1999), who found that the UV luminosity function of their

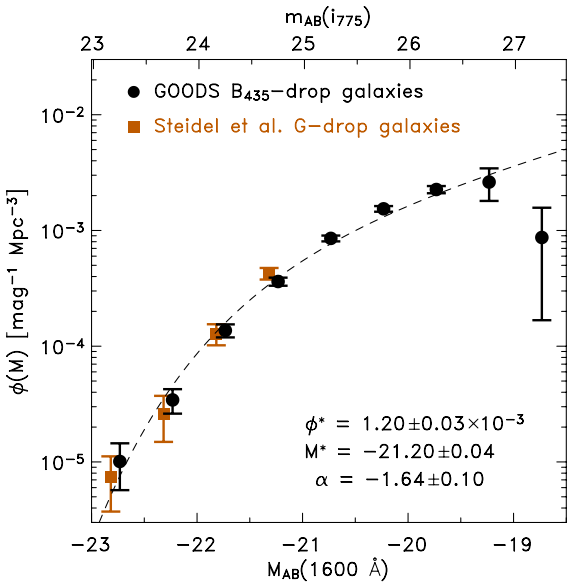

Fig. 1. The Schechter function fit to the luminosity function of B_{435}-band dropouts at $z \sim 4$ selected from the GOODS ACS images (black line and data points). The red points are from a similar sample of *G*-band dropouts by Steidel et al. (1999), who found that the $z \sim 4$ luminosity function is, within the errors, the same as at $z \sim 3$. See (Giavalisco et al., 2004b) for details on the selections and the measure.

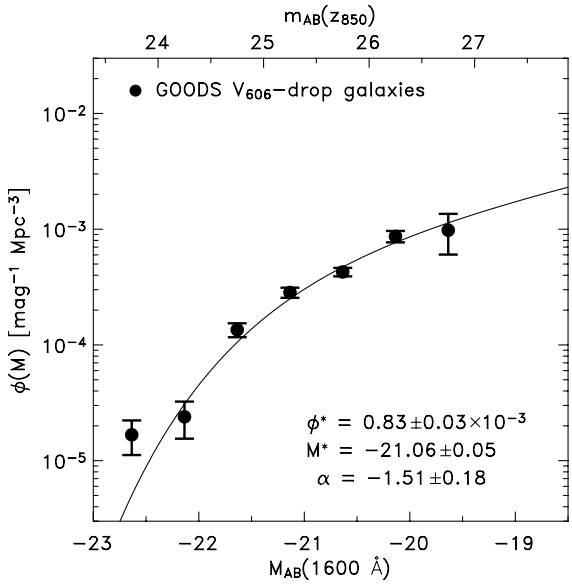

Fig. 2. The Schechter function fit to the luminosity function of $V_{6\text{–}6}$-band dropouts at $z \sim 5$ selected from the GOODS ACS images. Note the very mild evolution from $z \sim 4$ and, in turn, from $z \sim 3$.

G-band dropouts at $z \sim 4$, shown in Fig. 1 as red points, is, within the uncertainty, the same as that of LBG at $z \sim 3$ (U-band dropouts). A comparison with the parameters of the luminosity function of U-band dropouts at $z \sim 3$ (Steidel et al., 1999) shows that they are, essentially, the same as at $z \sim 4$. Thus, the figure shows not only an excellent agreement between the GOODS study and the previous $z \sim 4$ investigation, but also a lack of evolution in the UV luminosity function of LBGs between $z \sim 2.5$ and $z \sim 4.5$ (the near and far ends of the redshift distribution function of the U and B-band dropouts). Note the increased depth of GOODS, by about 1.5 mag, which allows a much better characterization of the shape of the luminosity function. Fig. 2 shows that the fit for the V_{606}-band dropouts at $z \sim 5$, also showing a very mild evolution. An apparent ~50% decrease in the volume density is accompanied by slightly fainter value of L^*, while the two slopes are, within the errors, the same.

As discussed by Dickinson et al. (2004) and Giavalisco et al. (2004b), the GOODS ACS data also allow the selection of LBGs at $z \sim 6$ (i_{775}-band dropouts), and in the latter paper we even report a measure of the UV luminosity density of these galaxies. Even with the new (slightly) deeper data, however, the luminosity function of the i_{775}-band dropouts remains significantly more uncertain than the lower redshift cases. Because the GOODS Team will soon release a new deeper version of the reduced data (version v2.0), which includes a z_{850}-band with 3× the exposure time compared to the current version, we will postpone the discussion of the $z \sim 6$ luminosity function to a later time. This, however, does not prevent to estimate the luminosity density, thanks to the pronounced covariance between the parameters of the luminosity function. Fig. 3 shows the plot of the UV luminosity density at 1500 Å and also of the associated star-formation density of the GOODS dropouts as a function of redshifts.

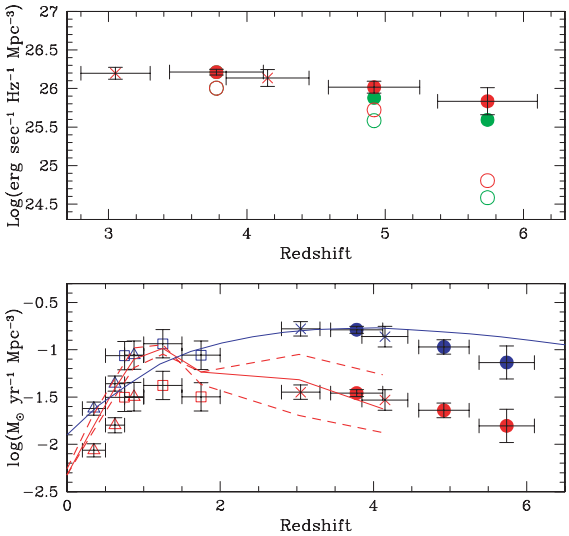

Fig. 3. (Top) The rest-frame 1500 Å luminosity density of B_{450}, V_{606} and i_{775}-band dropouts as a function of redshifts (filled symbols). The red symbols correspond to integrating along the fitted luminosity function down to the luminosity of the $z \sim 4$ sample; the green symbols show the integral down to the luminosity of the sample. The crosses are from Steidel et al. (1999). (Bottom) The star-formation rate density as a function of redshifts estimated from the above luminosity density (red points only), with (blue) and without (red) the correction for dust obscuration proposed by Steidel et al. (1999). The blue curve is from semi-analytical models and the red-curves are derived from the evolution of damped Lymna-alpha absorbers (see Giavalisco et al., 2004b for an explanation of all symbols). Note the mildly decrease in the cosmic activity of star formation traced by LBGs toward high redshift, a factor ~3 down from $z \sim 3$ and 4. (For interpretation of the references to colour in this figure legend, the reader is referred to the web version of this article.)

4. Testing the galaxy-dark matter physical association

Even if its areal coverage is not large in absolute value, the depth of GOODS ACS images is such that it yields large samples of LBGs. There are about 2500 B_{4353}-band dropouts and ≈1000 V_{606}-band dropouts in the GOODS fields, which are well suited for clustering analysis (Lee et al., in preparation). The study of the clustering properties of LBGs at faint levels complements very nicely analogous studies done with ground-based survey because they test the dependence of clustering with the UV luminosity, which in turns test the dependence of the star-formation activity on the total mass (gravity) of the galaxies and the presence of halo substructure. These tests provide empirical constants to the prime paradigm of our theoretical framework of galaxy formation,

namely that galaxies form when the baryonic gas cools and condenses in the potential wells of dark matter halos.

Fig. 4 plots the two-point angular correlation function of the faint sample of GOODS B_{435}-band dropouts and shows that this is not well described by a power law. Rather, it is explained by the sum of two contributions, a large-scale terms due to the halo–halo clustering, and a small-scale one, due to substructure within the individual halos. The angular clustering of brighter LBGs does not show this deviation from the power law behaviour, even when the measures are characterized by very high S/N (Adelberger et al., 2004).

Fig. 5 clarifies the physical origin of the deviation. The plot shows the mean number of faint neighbors, i.e., LBGs with $z_{850} \geqslant 26$, around very bright LBGs, namely those with $z_{850} \leqslant 24.5$ (filled symbols), and around less bright ones, those with $24.7 \leqslant z_{850} \leqslant 25.2$ (hollow symbols). The top panels show the cumulative number of neighbors, with the dashed line representing the number expected if the galaxies were correlated only according to the large-scale component of $w(\theta)$. The bottom panels show the differential mean number of neighbors around the brighter galaxies divided by that round the fainter ones. There is a clear tendency of bright galaxies to surround themselves with faint ones at scales of $\approx 20''$, or about 140 kpc (proper distance) at $z \sim 4$. This is a clear detection of halo substructure in bright LBGs, which presumably mark the site of massive halos.

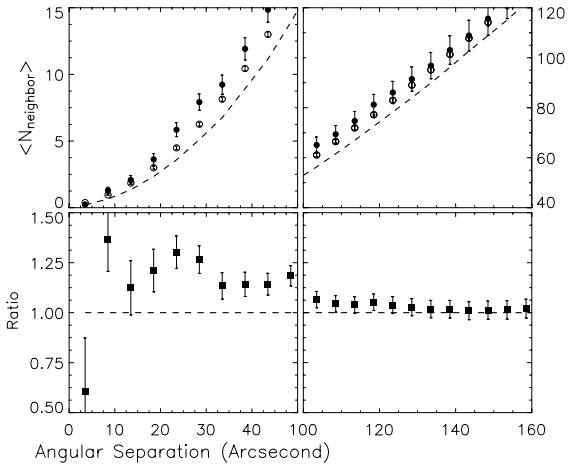

Fig. 5. The mean number of faint neighbors ($z_{850} \geqslant 26$) around very bright ($z_{850} \leqslant 24.5$, filled symbols) and less bright ($24.7 \leqslant z_{850} \leqslant 25.2$, hollow symbols) galaxies. The top panels show the cumulative number of neighbors, with the dashed line representing the number expected if the galaxies were correlated like the large-scale component. The bottom panels show the differential mean number of neighbors around the brighter galaxies divided by that round the fainter ones. Note the clear tendency of bright galaxies to be surrounded by faint ones at scales of $\approx 20''$, or about 140 kpc (proper distance) at $z \sim 4$. This is a clear detection of halo substructure.

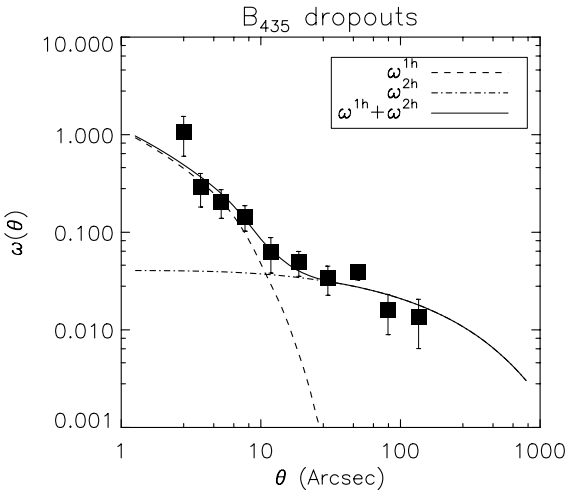

Fig. 4. The two-point angular correlation function of B_{435}-band dropouts down to $z_{850} \leqslant 27$. The angular clustering is well explained as the sum of two components, a large-scale contribution due to the halo–halo clustering, and a small-scale one due to the substructure within the halos. It is possible to observe the latter contribution with good S/N thanks to the faint sample.

Lee et al. (in preparation) also discuss the measure of clustering segregation, namely the tendency of bright LBGs to cluster more strongly than fainter ones. The implication is that brighter galaxies are hosted in more massive halos, showing a direct link between a physical parameter of the dark matter structure, the mass, and the star-formation activity (which powers the UV luminosity) of the hosted galaxies.

5. Galaxies at very high redshift

Very high sensitivity at near and mid-IR wavelengths is another strength of GOODS, which al-

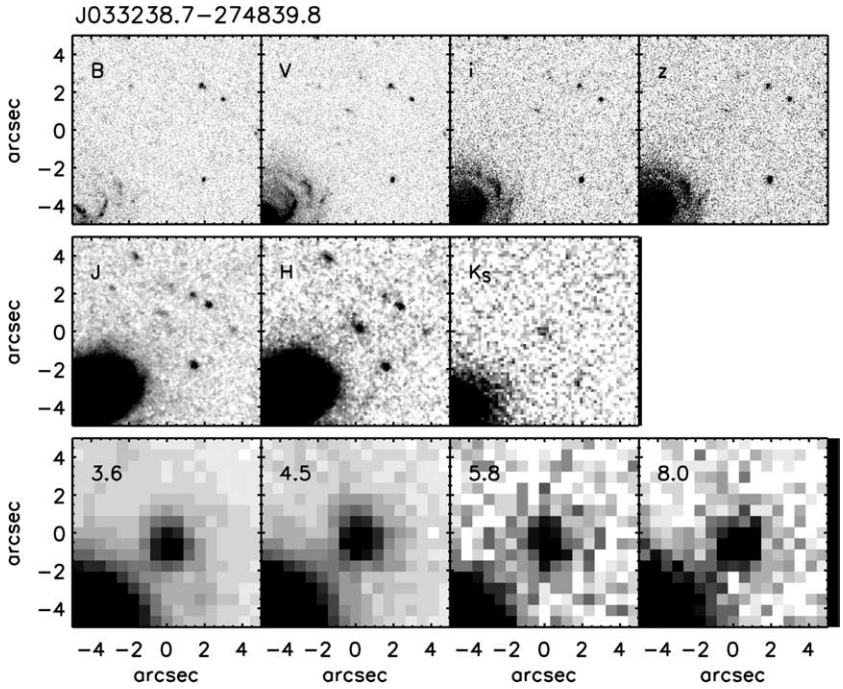

Fig. 6. ACS B_{435}, V_{606}, i_{775}, and z_{850}, NICMOS J and H, VLT ISAAC K_s and Spitzer 3.6, 4.5, 5.8 and 8.0 μm images of a candidate post-starburst galaxy at $z \sim 7$ discovered by Mobasher et al. (submitted) in the GOODS Southern field.

lows us to search for general galaxies (not just LBGs) at very high redshifts, such as the object identified from its J–H colors by Mobasher et al. (submitted). This galaxies, discovered in the GOODS CDF-S field, is also located in the HUDF, which provided even deeper ACS and J and H (NICMOS) photometry than that available from the native GOODS data. This helps better characterizing this extremely interesting objects. Fig. 6 shows the ACS, NICMOS and IRAC images of the galaxy, while the large panel of Fig. 7 shows the spectral energy distribution (SED) that best fits the observed photometry (red curve). This is one of a post-starburst galaxy several hundred million years old, with a stellar mass of about 6×10^{11} $M_{\odot}$ observed at a redshift $z = 7$.

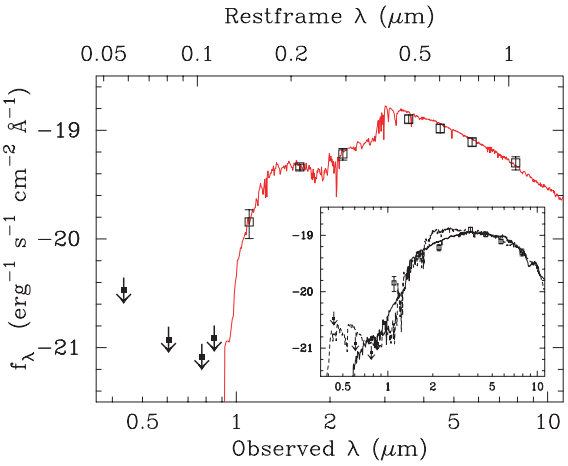

Fig. 7. The best-fit SED to the observed photometry of the $z \sim 7$ post-starburst candidate galaxy. The small inset shows the SED of a heavily dust obscured starburst galaxy at $z \sim 3$, a much less likely solutions because of the much higher value of the χ^2.

In other words, at a time when the universe was about 5.5% of this current age this galaxy had already put together a stellar mass 8 times bigger than that of the Milky Way. The small inset of Fig. 7 shows the SED associated to a local minimum of the χ^2, which is that of a very dusty starburst galaxy at $z \sim 3$. This solution, however, is strongly disfavourite by the much large value of χ^2. Because objects like this one are very rare, it

is very difficult to say anything with some degree of confidence about their volume density and thus about their cosmic significance. The galaxy has so much stellar mass that if it has a M/L value that resembles that of local galaxy it very likely sits in a very massive and thus rare peak of the density field. Inferring anything about the volume density in this circumstances is very dangerous, because of the very strong effect of cosmic variance. This illustrates one of the area where GOODS can be improved, namely enlarging the area coverage.

6. Conclusions

The great value of GOODS rests in its unique combination of depth, surveyed area and wavelength coverage. For this, the survey is still unsurpassed, and it is yielding a deep insight into many aspects of galaxy evolution that range from the association of visible matter and dark matter, to the assembly history of stellar mass in galaxies, to the dust obscuration properties of starburst galaxies and the measure of their star formation rates, to the evolution of galaxies morphology, and to the quest for the most distant galaxies. Its main weakness is its small area coverage in absolute terms, which sometimes implies significant uncertainties in the significance of certain discovery, such as the existence of very massive, dead (i.e., non-star forming) galaxies at $z \sim 7$.

Acknowledgments

Work supported by NASA through grants HST-GO09425.01-A and HST-GO09583.01 from the Space Telescope Science Institute, which is operated by the Association of Universities for Research in Astronomy, under NASA contract NAS5-26555.

References

Adelberger, K.L., Steidel, C.C., Shapley, A.E., Hunt, M.P., Erb, D.K., Reddy, N.A., Pettini, M., 2004. ApJ 607, 226.

Bouwens, R.J., Thompson, R.I., Illingworth, G.D, Franx, M., 2004. ApJ 616, 79.

Bouwens, R.J., Illingworth, G.D, Thompson, R.I., Franx, M., van Dokkum, P.G., Fan, X., Dickinson, M.E., Eisenstein, D.J., Rieke, M.J., 2005. ApJ 624, 5.

Daddi, E., Cimatti, A., Renzini, A., Fontana, A., Mignoli, M., Pozzetti, L., Tozzi, P., Zamorani, G., 2004. ApJ 617, 746.

Dickinson, M., Hanley, C., Elston, R., Eisenhardt, P.R., Stanford, S.A., Adelberger, K.L., Shapley, A., Steidel, C.C., Papovich, C., Szalay, A.S., et al., 2000. ApJ 531, 624.

Dickinson, M., Stern, D., Giavalisco, M., Ferguson, H.C., Tsvetanov, Z., Chornock, R., Cristiani, S., Dawson, S., Dey, A., Filippenko, A.V., et al., 2004. ApJ 600, 99.

Giavalisco, M., 2002. ARA&A 40, 579.

Giavalisco, M., Dickinson, M., Ferguson, H.C., Ravindranath, S., Kretchmer, C., Moustakas, L.A., Madau, P., Fall, S.M., Gardner, J.P., Livio, M., et al., 2004b. ApJ 600, 103.

Giavalisco, M. et al., 2004a. ApJ 600, 93.

Labbe', I., Huang, J., Franx, M., Rudnick, G., Barmby, P., Daddi, E., van Dokkum, P.G., Fazio, G.G., Schreiber-Forster, N.M., Moorwood, A.F.M., et al., 2005. ApJ 624, 81.

Mobasher, B., Dickinson, M., Ferguson, H.C., Giavalisco, M., Wiklind, T., Srak, D., Ellis, R.S., Fall, M., Grogin, N.A., Moustakas, L., Panagia, N., Sosey, M., Stiavelli, M., Bergeron, E., Casertano, S., Ingram, P., Koekemoer, A., Labbe', I., Livio, M., Rogers, B., Scarlatta, C., Venet, J., Renzini, A., Rosati, P., Kuntschner, H., Kümmel, M., Walsh, J.R., submitted for publication. ApJ.

Moustakas, L.A., Casertano, S., Conselice, C.J., Dickinson, M.E., Eisenhardt, P., Ferguson, H.C., Giavalisco, M., Grogin, N.A., Koekemoer, A.M., Lucas, R.A., et al., 2004. ApJ 600, 131.

Steidel, C.C., Adelberger, K.L., Giavalisco, M., Dickinson, M., Pettini, M., Kellogg, B., 1999. ApJ 519, 1.

Steidel, C.C., Adelberger, K.L., Shapley, A.E., Pettini, M., Dickinson, M., Giavalisco, M., 2003. ApJ 592, 728.

Steidel, C.C., Shapley, A.E., Pettini, M., Adelberger, K.L., Erb, D.K., Reddy, N.A., Hunt, M.P., 2004. ApJ 604, 534.

van Dokkum, P.G., Franx, M., Forster-Schreiber, N.M., Illingworth, G.D., Daddi, E., Knudsen, Kirsten K., Labbe', I., Moorwood, A., Rix, H.-W., Rottgering, H., et al., 2004. ApJ 611, 703.

Available online at www.sciencedirect.com
SCIENCE DIRECT®
New Astronomy Reviews 49 (2005) 447–452
New Astronomy Reviews
www.elsevier.com/locate/newastrev

Galactic structure from wide-field surveys

Heidi Jo Newberg

Rensselaer Polytechnic Institute, Troy, NY 12180, United States

Available online 22 September 2005

Abstract

The possible contributions of a wide-field space imager, such as might be designed for a JDEM mission (such as SNAP or DESTINY), to Galactic structure are explored. The Sloan Digital Sky Survey serves as an example of an extragalactic survey that has made important contributions to our understanding of the distribution of Galactic stars, showing in particular how imaging alone can make major contributions. Since we expect the imaged sources in JDEM to be faint ($20 < V < 30$), the images will sample Galactic stars fainter than G dwarfs, including white dwarfs and brown dwarfs. Many of these stars have evolved little, and are good tracers of stellar formation histories. A faint imager will discover large numbers of faint main sequence stars and brown dwarfs. Brighter stars will be sampled in other galaxies. There is also great promise for the astrometric capability of a wide-field imager in space.
© 2005 Elsevier B.V. All rights reserved.

Contents

1. Introduction . . . 448
2. Galactic structure from the Sloan Digital Sky Survey . . . 448
3. Galactic structure from JDEM photometry . . . 449
4. Galactic structure from JDEM spectroscopy . . . 450
5. Galactic structure from JDEM astrometry . . . 451
6. Conclusion . . . 451
Acknowledgment . . . 452
References . . . 452

E-mail address: newbeh@rpi.edu.

1387-6473/$ - see front matter © 2005 Elsevier B.V. All rights reserved.
doi:10.1016/j.newar.2005.08.020

1. Introduction

The Milky Way galaxy extends over 40,000 sq. deg. on the sky, making it ideally suited to wide-field observations. It is composed of stars, gas and dust, and (presumably) dark matter; the dark matter has not yet been directly detected. The gas can be studied through its position in the sky, radial velocity, column density, and composition. Stars are characterized by their location in the sky, position, three-dimensional space velocities (radial velocities and proper motions). The mass, age, and chemical composition of an individual star can be estimated from optical spectra.

The Milky Way is the only galaxy for which we expect to collect comprehensive stellar information in the next two decades (from wide-field surveys such as RAVE, QUEST, SDSS II/SEGUE, Pan-STARRS, GAIA, etc.). Many other speakers have remarked on the detail and complexity of external galaxies that we are now able to discern. Studies of our own Milky Way will allow us to understand similar details, including their spatial, kinematic, and stellar properties. Additionally, the dark matter in our galaxy is revealed by the motions of stars. The better we understand the detailed motions of stars in the Galaxy, the better resolution we will have on the spatial distribution of dark matter.

Two famous, competing papers have shaped our understanding of the formation of the Milky Way Galaxy: Eggen et al. (1962), who presented a "rapid collapse" model of the Galaxy, and Searle and Zinn (1978), who presented a Galaxy formation model with hierarchical merging. Paradoxically, the first author of the monolithic collapse paper, Eggen, is also known for "Eggen's Spaghetti Sky," because his impression from visually observing the distribution of Galactic stars was that it was clumpy and not uniform. Wide-field surveys of the sky, including the Sloan Digital Sky Survey (SDSS) are showing that his impression was correct. Modern N-body simulations and discoveries of tidal streams are validating the claim that galaxies form by hierarchical merging, but have not ruled out the possibility that the collapse was rapid, in the sense that most of the merging happened very early in galaxy formation. However, there is no longer a clear idea that the spheroid population of stars was "left behind" during the collapse; rather, a substantial fraction, or maybe all, of the spheroid was formed through accretion of stellar systems.

2. Galactic structure from the Sloan Digital Sky Survey

The SDSS was designed to trace the 3D spatial structures of external galaxies, and to avoid as many Galactic stars as possible. However, Galactic stars cannot be avoided entirely, and the millions that have slipped through the cracks have allowed us to make many discoveries and prove the usefulness of wide-field imaging for discovering Galactic substructure, especially when combined with even limited spectroscopy. Table 1 lists some of the major discoveries from SDSS imaging data.

The primary technique used in these discoveries was to eyeball a two-dimensional plot (color-magnitude, magnitude vs. angle, angle vs. angle). In many cases, the data that were plotted were selected using some of the many possible dimensions (including magnitude, four colors, and two angles on the sky). The only case in which nearly the full dimensionality of the data was used was in the discovery and analysis of the tidal tails of Pal 5, in which a color-magnitude convolution kernel in multidimensional space was used to trace the tail. What is apparent in these papers is that it is no longer essential to understand the individual properties of each star to determine the global properties of the stellar populations from which they were drawn. The discoveries are made statistically. For example, the tidal stream in the Galactic plane was discovered from the distribution of apparent magnitudes of stars selected in $g - r$ color. We did not determine the absolute magnitudes, distances, or physical properties of any given star, but rather argued that most of the stars of the color we selected would be F turnoff stars.

Ultimately, we would like to build a global model of the Galaxy that statistically describes all of the stars in all of the dimensions, including velocities if available. To achieve this, we will need to develop techniques that will optimize this fit

Table 1
SDSS contributions to galactic structure

Traced the Sagittarius dwarf tidal stream in RR Lyrae stars	Ivezic (2000)
Discovery of the Sagittarius tidal stream in A-type stars	Yanny (2000)
Measurement of the scale height of the thick disk	Chen (2001)
Ruled out tidal tails for the Draco dwarf galaxy system	Odenkirchen (2001)
Discovery of a tidal stream in the Galactic plane	Newberg (2002), Yanny (2003)
Discovery and analysis of tidal tails in Pal 5	Odenkirchen (2003)
Discovery of Sagittarius tidal debris 90 kpc from the Galactic center	Newberg (2003)
Extrapolation of the density of the Sgr stream in the solar neighborhood	Freese (2004)
Discovery of Andromeda IX and other M31 halo debris	Zucker (2004a,b)

using millions of stars, a dozen attributes, and incomplete information. Such a description can be matched to formation scenarios that include the evolution of mass density and the formation of stars. These aims will be addressed as part of a proposed extension to the SDSS, called SDSS II.

SDSS II includes three new projects, which would use the existing SDSS hardware, software, and operational infrastructure after the SDSS survey ends in June 2005. The three projects are: (1) LEGACY – completing spectroscopy of $V < 19$ galaxies in a contiguous area of the North Galactic Cap, (2) SEGUE – a new survey of 4000 sq. deg. of low Galactic latitude imaging and spectroscopy of 250,000 Galactic stars to extend SDSS Galactic structure studies, and (3) Supernovae – obtaining light curves for ~200 Type Ia Supernovas on the southern Celestial Equator. The three year SDSS II project will cost $15 million, of which about half has already been raised. The SEGUE project will extend the database of photometry of $14 < g < 23$ stars to low Galactic latitudes and sparsely sample the kinematics and stellar properties of Galactic stars with $14 < g < 20.3$, using medium resolution spectroscopy.

3. Galactic structure from JDEM photometry

Wide-field imaging from very high redshift supernova searches might also prove to be a gold mine for Galactic structure, as it will probe the stellar populations to extremely faint magnitudes. The SDSS data have shown that photometric surveys can be used to: (1) discover spatial density through statistical photometric parallax, (2) separate stellar populations by turnoff color (which is related to the population's age and metallicity), and (3) discover tidal streams from globular clusters and dwarf galaxies in the Galactic halo. When repeated, or used in conjunction with previous surveys, they can (4) contribute to proper motion and parallax measurements, and (5) locate variable objects. Since the stars of the Milky Way cover the entire sky, more sky coverage will always be better for Galactic structure measurements. Ultraviolet and optical colors are necessary for studying turnoff stars, and wavelength coverage longwards of about 1 μm are required to discover brown dwarfs.

The SNAP program has circulated a possible set of sky surveys, which include two deep surveys ($20 < V < 30$; ~7.5 sq. deg. each), a wide-field survey ($20 < V < 27.7$; ~500 sq. deg.), and a panoramic survey ($20 < V < 26.7$; ~8000 sq. deg.). The deep surveys will include 120 co-added scans taken with a 4-day cadence. All of the surveys will produce images in six optical passbands (0.44–0.92 μm) that are designed to reduce complication in calculating K-corrections, but may not include standard filters.

The current design of the DESTINY satellite will not allow imaging, but will produce spectrophotometry from a grism survey that will allow NIR photometric measurements to be computed. The field of view and depth of the survey(s) has not been specified, but presumably will be similar to the deep SNAP survey.

An important measure of a survey's ability to study Galactic structure is the distances to which stars of a given type will be observable. Table 2

Table 2
Distance at which we can see individual stars

	$M(V)$	$D(V=20)$	$D(V=27)$	$D(V=30)$
O5 V	−5.7	1.4 Mpc	35 Mpc	140 Mpc
B5 V	−1.2	170 kpc	4 Mpc	17 Mpc
M5 III	−0.3	115 kpc	2.9 Mpc	11 Mpc
K5 III	−0.2	110 kpc	2.8 Mpc	11 Mpc
G5 III	0.9	66 kpc	1.7 Mpc	6.6 Mpc
A5 V	1.95	41 kpc	1.0 Mpc	4.1 Mpc
F5 V	3.5	20 kpc	500 kpc	2.0 Mpc
G5 V	5.1	10 kpc	240 kpc	950 kpc
K5 V	7.35	3.4 kpc	85 kpc	340 kpc
M5 V	12.3	0.35 kpc	8.7 kpc	35 kpc

lists common stellar spectral types, followed by an estimate of the absolute V magnitude (Cox, 2000). The third column lists the minimum distance at which stars of a given stellar type would be visible, assuming that stars brighter than $V = 20$ would be saturated. The fourth column lists the maximum distance that the stellar type would be visible in the "wide-field" program, assuming the limiting magnitude is $V = 27$. The fifth column lists the maximum distance that the stellar type would be visible in the co-added images of a "deep north" and "deep south" surveys.

We then compare the distance ranges over which we can see these stars to astronomical distance scales. O5 main sequence stars, for example, are visible at distances somewhat further than the Andromeda galaxy to well past the "Great Wall." K and M giant stars in the local group are saturated, but can be discovered more than half way to the Virgo cluster of galaxies.

Intrinsically brighter stars, which have traditionally been used to trace more distant parts of the Milky Way, will be discovered instead in other galaxies or in the space between them.

Since the known extent of the Milky Way halo is about 100 kpc, the Galactic stars in this survey that would most impact Galactic structure models are main sequence stars of spectral type G and later. These stars are very numerous in the Galaxy, and have the advantage that they have not evolved much in the lifetime of the Universe, so they will give us an unbiased history of star formation. White dwarfs have absolute magnitudes similar to K and M dwarfs and fainter, and will also be swept up by the survey.

Table 2 does not include absolute magnitudes for the recently discovered L and T dwarf stars, since these stars are virtually unobservable in the visual band. The absolute magnitude of these brown dwarf stars is $M_J \sim 14$ (Vrba (2004)). SNAPs near-infrared observations will be able to sample these stars at distances out to 3 kpc from the Sun, and four times further in a co-added deep region. The survey would identify an unprecedented number of brown dwarf stars, representing all stellar components of the Galaxy.

Since there has not been a survey this large and this deep, one might expect to find additional classes of even fainter objects – lower mass brown dwarfs or cooler white dwarfs for example – very close to the Sun.

4. Galactic structure from JDEM spectroscopy

Modern Galactic structure surveys typically target the kinematics of Galactic stars to discriminate structures. Examples of large, wide-area surveys targeting Galactic structure through kinematics are SDSS II ($R \sim 1800$; 250,000 stars), RAVE ($R \sim 10{,}000$; 50,000,000 stars; $V < 16$; starting 2006), and RVS on GAIA (Perryman, 2002) ($R = 11{,}500$; all-sky; $V \sim <18$). The pilot project for RAVE uses spectral resolution $R \sim 4000$ and will obtain 100,000 Galactic stars to $V = 12$. Classification spectra for stars typically have one Angstrom resolution (or better) at optical wavelengths, though the SDSS has had reasonable success with high signal-to-noise optical spectra with about two Angstroms resolution. Lower resolutions will not allow determinations of stellar properties. SDSS II will produce radial velocity accuracy of ~15 km/s, which is capable of distinguishing large tidal streams and broad components of the Galaxy. Larger surveys such as RAVE and GAIA take advantage of much higher resolution that will allow them to find and characterize dynamically colder substructures, and to better separate stellar properties.

Since the DESTINY satellite will measure spectra for Galactic stars in the field of view, these spectra could be used to compute photometric measurements matched to standard NIR filters,

which could be an advantage over the SNAP photometry. The proposed spectral resolutions of the SNAP and DESTINY ($R \sim 75$) satellites are much too low to allow spectral classifications and useful radial velocities for Galactic stars.

5. Galactic structure from JDEM astrometry

The proposed SNAP imager has a plate scale of 0.10 arcsec/pixel, which is designed to cover as much sky as possible at the expense of undersampling the stellar PSF. Anderson and King (2000) have shown that even undersampled space images can produce high quality astrometry as long as the PSF can be well determined – typically requiring dithering techniques, fields that are not too crowded, and an instrumental stellar profile that is reasonably stable. Using HST images, they show that 0.02 pixel astrometric accuracy can be obtained in a single image. Since the systematics are better than 0.002 pixels, multiple observations can reliably be combined to improve the accuracy by $\sqrt{N}$. The actual astrometric capability of the SNAP imager should be calculated in light of both its hardware and observational strategy, but for brainstorming purposes we will assume that the astrometric accuracy is within a factor of two of 1 mas; the astrometry for the deep fields should be several times better than this. The currently proposed wider surveys would provide precision astrometry for millions of faint Galactic stars.

While the astrometric accuracy of the SNAP satellite is comparable to the Hipparcos mission, the difference in magnitude limits probed is striking. The Hipparcos satellite targeted stars with $V < 12.4$, while the SNAP satellite will image stars with $V > 20$. In the deeper, multiply-imaged regions of the sky, the SNAP satellite is capable of producing distances good to 10% for stars within 300 pc of the Sun; the stars that will not saturate the detector at these distances will be primarily the L and T brown dwarfs. The accuracy of the derived proper motions depends on the time between observations. A baseline of one year will produce proper motion measurements somewhat longer than the astrometric accuracy, say a couple of mas/yr. The astrometric information will complement the astrometry that will be produced with GAIA, which images only to $V = 20$.

The space density of L/T dwarfs is expected to be about twice that of stars (Hawley, 2003), so SNAP could serendipitously find distances to hundreds of these low mass stars and brown dwarfs in 15 sq. deg. of deep imaging, and measure proper motions for thousands of faint stars.

6. Conclusion

The purpose of this presentation was to explore the possibilities for learning about Galactic structure from a SNAP or DESTINY satellite. From an examination of Table 2, one finds that most of the stars that have traditionally been used to explore Galactic structure are so bright that we see them more easily in other galaxies than in our own. This highlights the capability of this satellite to make substantial contributions to our knowledge of the stellar content of nearby galaxies.

The opportunity for a supernova space imaging satellite to contribute to knowledge of our own galaxy is by using intermediate and low mass stars to trace structure. These stars have been little-used in studies of Galactic structure because their faint luminosities make them difficult to study. However, they are potentially very interesting because they have higher space densities and have evolved little since formation. These stars will give us a better sense of the formation histories of Milky Way stellar populations.

The SNAP surveys will discover large numbers of faint main sequence stars and brown dwarfs, which will allow exploration of the faint end of the initial mass function (IMF) as a function of population. These low mass stars will also be traced through the thick disk and spheroid populations, so population comparisons can be obtained. Since these faint stars have very large absorption bands in their spectra, it is possible that some physical properties of these stars could be determined from the photometry alone.

There is also great promise for the astrometric capability of a wide-field imager in space. A satellite could produce positions for millions of faint Galactic stars with the accuracy of the Hipparcos

satellite. Because only a small (15 sq. deg.) region of the sky will be imaged in multiple epochs, the number of stars with measured parallaxes and proper motions will be much smaller than the all-sky Hipparcos survey. However, an important high-accuracy image of the faint sky can be compared with images from smaller deep images that are already available and with future wide-field imaging that will reach similar limiting magnitudes.

Acknowledgment

Funding for this research was provided by Research Corporation and the National Science Foundation (AST 03-07571).

References

Anderson, J., King, I.R., 2000. Toward high-precision astrometry with WFPC2. I. Deriving an accurate point-spread function. PASP 112, 1360–1382.

Chen, B. et al., 2001. Stellar population studies with the SDSS I. The vertical distribution of stars in the Milky Way. ApJ 553, 184–197.

Cox, A.N., 2000. Allen's Astrophysical Quantities. Springer, New York.

Eggen, O.J., Lynden-Bell, D., Sandage, A.R., 1962. Evidence from the motions of old stars that the Galaxy collapsed. ApJ 136, 748–766.

Freese, K. et al., 2004. Effects of the Sagittarius Dwarf tidal stream on dark matter detectors. PhRvL 92, 111301.

Hawley, S.L., 2003. An insider's view of brown dwarfs, in: A. Brown, G.M. Harper, T.R. Ayres (Eds.), The Future of Cool-Star Astrophysics: 12th Cambridge Workshop on Cool Stars, Stellar Systems, and the Sun, University of Colorado, pp. 97–109.

Ivezic, Z., 2000. Candidate RR Lyrae stars found in the sloan digital sky survey commissioning data. AJ 120, 963–977.

Newberg, H.J. et al., 2002. The ghost of Sagittarius and lumps in the Halo of the Milky Way. ApL 569, 245–274.

Newberg, H.J. et al., 2003. Sagittarius tidal debris 90 kiloparsecs from the galactic center. ApL 596, L191–L194.

Odenkirchen, M. et al., 2001. New insights on the draco dwarf spheroidal galaxy from the sloan digital sky survey: a larger radius and no tidal tails. AJ 122, 2538–2553.

Odenkirchen, M. et al., 2003. The extended tails of palomar 5: a 10° arc of globular cluster tidal debris. AJ 126, 2385–2407.

Perryman, M.A.C., 2002. GAIA: an introduction to the project. In: Bienaymé, O., Turon, C. (Eds.), Proceeding of the Les Houches School, EAS Publication Series, vol. 2. EDP Sciences, pp. 3–26.

Searle, L., Zinn, R., 1978. Compositions of halo clusters and the formation of the galactic halo. ApJ 225, 357–379.

Vrba, F.J. et al., 2004. Preliminary parallaxes of 40 L and T dwarfs from the US naval observatory infrared astrometry program. AJ 127, 2948–2968.

Yanny, B. et al., 2000. Identification of A-colored stars and structure in the halo of the Milky Way from sloan digital sky survey commissioning data. ApJ 540, 825–841.

Yanny, B. et al., 2003. A low-latitude halo stream around the Milky Way. ApJ 588, 824–841.

Zucker, D.B. et al., 2004a. Andromeda IX: a new dwarf spheroidal satellite of M31. ApL 612, L121–L124.

Zucker, D.B. et al., 2004b. A new giant stellar structure in the outer halo of M31. ApL 612, L117–L120.

Available online at www.sciencedirect.com
SCIENCE DIRECT®
New Astronomy Reviews 49 (2005) 453–460
New Astronomy Reviews
www.elsevier.com/locate/newastrev

Star formation histories in local group dwarf galaxies

Evan D. Skillman

Astronomy Department, University of Minnesota, 116 Church Street, SE, Minneapolis, MN 55455, USA

Available online 19 September 2005

Abstract

I review observations made with the Hubble Space Telescope which have improved our view of both *recent* (ages $\leqslant$1 Gyr) and *ancient* (ages $\geqslant$1 Gyr) star formation histories in dwarf galaxies. The method of reconstructing recent star formation histories has been well tested, and now the major challenge is to build a large database of suitable observations of nearby dwarf irregular galaxies. With the exception of the dSph companions of our Galaxy, questions concerning the ancient star formation histories of nearby galaxies are stymied by a lack of suitably deep imaging observations. The few observations which do exist provide tantalizing evidence of strong evolution in star formation rates. This evolution is likely due to environmental effects, and we may be seeing evidence of the effects of reionization on the star formation histories of dwarf galaxies. Due to its wide field of view and its excellent imaging resolution, the proposed model for SNAP could solve these problems.
© 2005 Elsevier B.V. All rights reserved.

Contents

1. Mapping recent star formation in nearby dwarf galaxies: testing our knowledge of the star formation process . . . 454
   1.1. Results from the HST with WFPC2 and ACS . . . 454
   1.2. The possibilities of wide-field imaging from space . . . 457
2. Ancient star formation histories . . . 457
   2.1. Results from the HST . . . 457
   2.2. The future: wide field imaging from space with SNAP? . . . 459
   Acknowledgments . . . 459
   References . . . 459

E-mail address: skill001@umn.edu.

1387-6473/$ - see front matter © 2005 Elsevier B.V. All rights reserved.
doi:10.1016/j.newar.2005.08.022

1. Mapping recent star formation in nearby dwarf galaxies: testing our knowledge of the star formation process

1.1. Results from the HST with WFPC2 and ACS

The first HST color magnitude diagram (CMD) of the stars in the nearby dwarf irregular (dI) galaxy Sextans A (Dohm-Palmer et al., 1997) revealed for the first time a clear separation between the brightest main sequence stars and the "blue loop" (or blue helium burning – BHeB) stars. The separation of the main sequence stars and the BHeB stars was made possible by the high angular resolution of the HST (reducing photometric errors due to blends) and the low metallicity of Sextans A which leads to low differential reddening (Fig. 1).

These BHeB stars afford a special opportunity to study the recent star formation histories (SFHs) of nearby galaxies. Because the position of a BHeB star in the CMD represents a unique age (as opposed to, for example, the main sequence or the red giant branch where a single position can correspond to a large range of ages), one can convert the BHeB luminosity function directly into a SFH (with the assumption of a universal initial mass function). The main limiting factor of this technique is that the position of the BHeB stars blends into the red clump at an age between 0.5 and 1 Gyr.

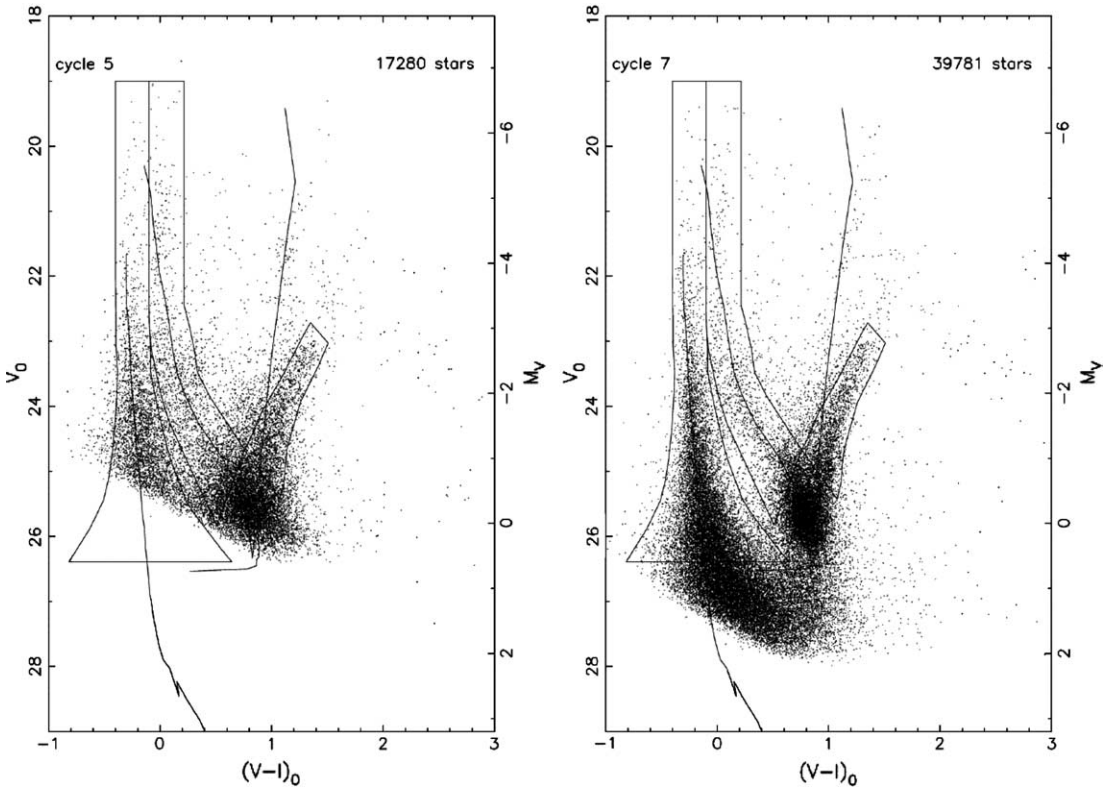

Fig. 1. Color-magnitude diagrams for Sextans A (Dohm-Palmer et al., 2002). The left panel shows Cycle 5 WFPC2 data (1 orbit each in V and I), and the right panel shows Cycle 7 data (8 orbits in V and 16 orbits in I). The increased photometric sensitivity of the Cycle 7 data reveals the entire sequence of BHeB stars merging into the red clump. The curves come from the stellar evolution models of Bertelli et al. (1994) and indicate the main sequence, the blue edge of the He-burning loop, and the red edge of the He-burning loop. The polygonal regions indicate the selection regions for the MS, BHeB, and RGB. The agreement between the model curves and the data is excellent.

Translating the BHeB luminosity function into a SFH depends on the accuracy of the stellar evolution models. We have different lines of evidence that the stellar evolution models provide an excellent guide to this stage of evolution. The first evidence came from the early HST observations themselves. Although the position of the blueward extension of the stellar evolution tracks is a strong function of both metallicity and stellar mass, excellent agreement between observations and models was found by choosing the stellar evolution tracks for the metallicity determined from the HII region abundances for Sextans A. This is a very important point. There are no low metallicity, young stellar clusters in the Milky Way galaxy or the Magellanic Clouds which allow the stellar evolution modelers to calibrate their codes in this regime (the oxygen abundance in Sextans A is a factor 3 lower than in the Small Magellanic Cloud). When these stars are first observed in the extragalactic context, the agreement with models can be taken as confirmation of a prediction.

In recent studies Dohm-Palmer et al. (2002), and Dolphin et al. (2003) used deep HST photometry of Sextans A to compare recent SFHs recovered from both the main-sequence stars and the BHeB stars independently and collectively. The excellent agreement between these independent star formation rate (SFR) calculations is a confirmation for the legitimacy of using the BHeB stars to calculate the recent SFH. Additionally Dohm-Palmer and Skillman (2002) used the HST observations of Sextans A to compare the ratio of blue to red supergiants as a function of age, or, equivalently, mass. This ratio provides an observational constraint on the relative lifetimes of these two phases that is a sensitive test for convection, mass-loss, and rotation parameters. The functional form of the observed ratio matches the model extremely well.

Given these tests of reliability of the stellar models, we feel confident that using the BHeB stars to construct recent SFHs is well justified. Dohm-Palmer et al. (1998) employed HST photometry of four nearby dIs (Sextans A, Leo A, Pegasus, and GR 8) and derived recent SFHs for these galaxies (Fig. 2). At the time, the surprising result was the lack of bursts or episodes of

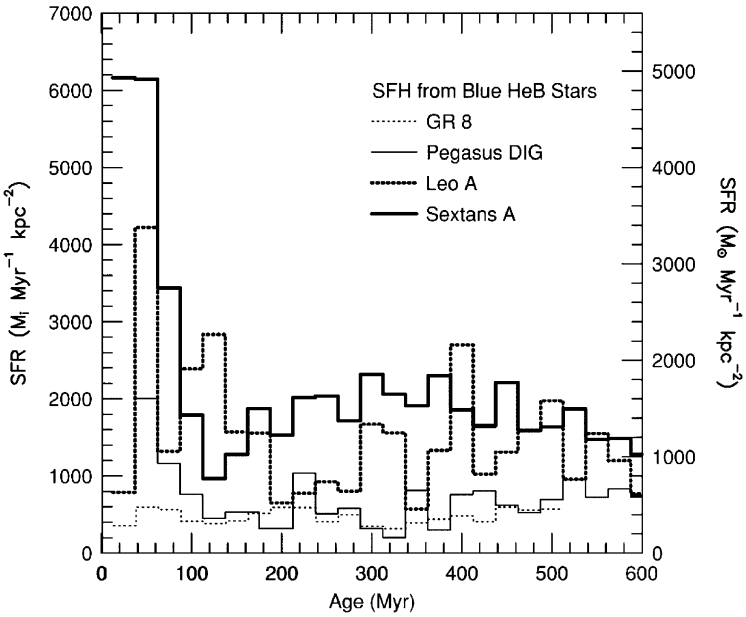

Fig. 2. The recent SFHs of four nearby dI galaxies derived from the BHeB luminosity function (Dohm-Palmer et al., 1998). Despite the relatively high time resolution which increases the sensitivity to variations, none of the galaxies show evidence for strong bursts of star formation, and there is little evidence for periods of no star formation.

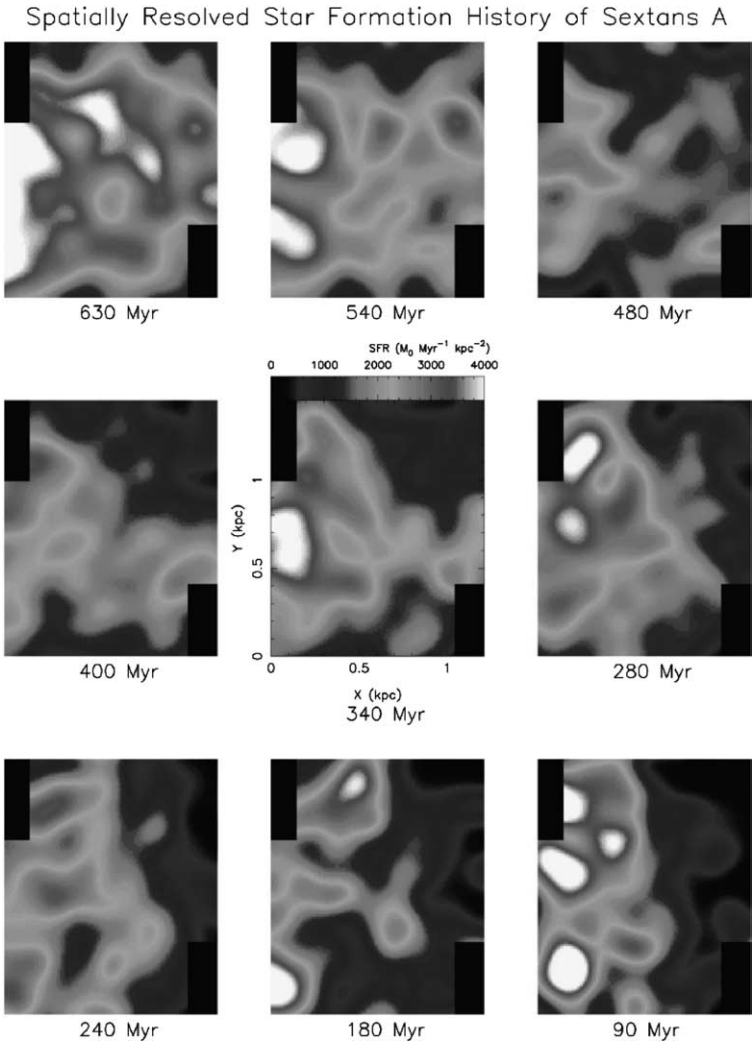

Fig. 3. The spatially resolved SFH of Sextans A. The nine panels show selected still frames from the full movie. The movie was convolved with a Gaussian kernel (80 pc and 30 Myr). The intensity transfer function and spatial reference is labeled on the central frame. You can see this is color by going to the reference publication. The frames are not uniformly distributed in time; rather they were chosen to highlight peaks and valleys in the SFR. Most of the activity is found on the left side of the maps, and it is found in two primary zones: upper left and lower right. The lower right zone is associated with the highest column density neutral gas (From Dohm-Palmer et al. (2002)).

enhanced star formation. With time bins of only 25 Myr for the last 500 Myr, with the possible exception of mildly enhanced SFRs in the last 50 Myr for Sextans A and Leo A, all four galaxies are best described as nearly constant SFRs. In retrospect, perhaps the lack of truly zero SFRs is as surprising as the lack of periods of enhanced star formation. These nearly constant, low level SFRs confirm the (Hunter and Gallagher, 1985) picture for low surface brightness dIs as "down but not out," and the conclusion of Tosi and Greggio and their collaborators that the duration of truly quiescent phases must be very short compared to the active phase (e.g., Tosi et al., 1991).

Because the BHeB star can be assigned a unique age, studying their spatial distribution allows the

reconstruction of spatially resolved SFHs. Fig. 3 demonstrates this for Sextans A. Note that three regions experience repeated episodes of star formation (Dohm-Palmer et al., 2002). When compared to the present day HI distribution, two of these zones are associated with high column density neutral gas, while the third, and oldest, is not. Our interpretation of this pattern is that star formation begins on the edge of a gas cloud and progressively eats away at the cloud, breaking it up and inducing later star formation. Putting all of this together gives a picture of quasi-continuous star formation in present day dwarf galaxies, where bursts are the exception and not the rule.

1.2. The possibilities of wide-field imaging from space

I think that the studies that I have reviewed are giving us a glimpse of the real picture, but a more ambitious observational project is necessary to quantify the results. Ultimately, the questions of importance of bursts and spatial patterns in star formation are statistical in nature and require large statistically significant studies. A large sample of galaxies with spatially resolved SFHs will allow correlation studies with the physical properties of the galaxy. Note that two WFPC2 fields only covered the central regions in Sextans A.

Because of the increased areal coverage, sensitivity, and resolution of the Advanced Camera for Surveys (compared to WFPC2) one gets a sense of what is possible. Fig. 4 shows a CMD from ACS observations of a dI at a distance of 3.6 Mpc (roughly 2.5 times the distance of Sextans A). Once again we see the main sequence and BHeB star well resolved so a spatially resolved SFH will be possible. There are roughly 100 dwarf irregular galaxies within 5 Mpc which allow us to sample recent SFHs over a range mass and environment.

Finally, it is important to note that studying recent star formation in the large spiral galaxies is also desirable (perhaps even more so since they dominate the dwarfs in terms of total mass). There are two technical reasons why it is easier to reconstruct recent SFHs in dIs than in spirals. First, because of their higher metallicities, differential extinction is a much larger problem in spiral galaxies, and separating the BHeB stars from the MS is problematic. Second, because dwarf irregular galaxies show nearly solid-body rotation across their optical extents, spatial relationships are preserved over long times (as opposed to the shear observed in spiral galaxies). The second problem is not a show-stopper (one would expect star formation regions to diffuse more quickly, but that is of interest itself). The first problem is best approached with shorter wavelength observations that would allow line of sight reddening corrections for each star. The shorter wavelength observations necessary may be beyond the specifications of the current SNAP model.

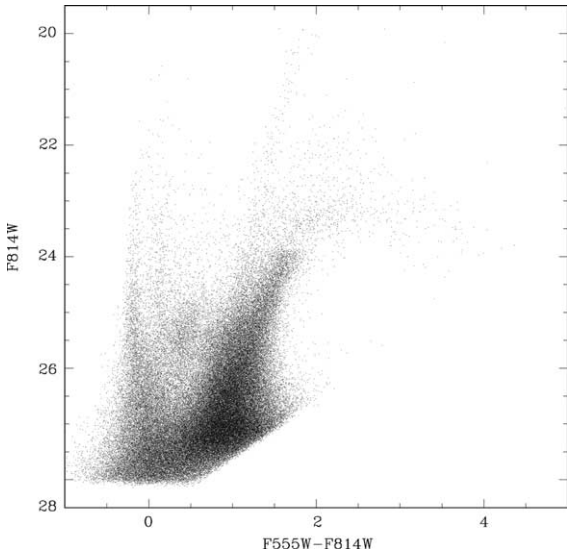

Fig. 4. A CMD for the M81 group dI IC2574 from ACS observations (6400 s integration time in both V and I from our GO-program 9755, PI = Walter). Using Dolphot, over 200,000 stars were identified in the ACS field which is roughly 3.5×3.5 kpc. At a nominal distance of 3.6 Mpc and a metallicity of 1/6th of solar, the sequence of blue supergiants is clearly resolved from the main sequence. Thus, we can derive a spatially resolved SFH from these observations.

2. Ancient star formation histories

2.1. Results from the HST

Recently Skillman et al. (2003) published a SFH for a halo field in IC 1613, a Local Group dI, based on relatively deep HST WFPC2

observations (Fig. 5). This is the deepest CMD of an isolated dI. Although detailed SFH studies exist for other dIs, no dIs at distances beyond the Magellanic Clouds have been observed to the depth of the present study of IC 1613 ($M_V \simeq +3.4$). Given the density–morphology relationship in the Local Group, the dI galaxies are at much greater distances than the dSphs, and, thus, have correspondingly shallower CMDs. As a result, it has been difficult to make direct comparisons between the CMDs of dI and dSph galaxies.

The complete SFH for the halo field in IC 1613 is shown in Fig. 6. The main feature seen in the SFH is an extended event from ~2 Gyr ago until 5–10 Gyr ago. While there has been star formation since that event (a significant amount coming 0.5 Gyr ago), the bulk of the stars in this region of IC 1613 come from the earlier age. Although Dolphin et al. (2001) found RR Lyraes in this field, the ancient ($\geqslant$10 Gyr) SFR was well below the lifetime average. Thus, to first order, star formation in IC 1613 appears to have occurred predominantly at intermediate ages. This is also characteristic of several of the outer MW dSph satellites (specifically Carina, Fornax, Leo II and Leo I). A particularly interesting (and to me surprising) comparison is between IC 1613 and Leo I; both appear to be dominated by star formation at the same intermediate ages (Gallart et al., 1999; Dolphin, 2002). In Fig. 6, we compare the SFH and age metallicity relationship for IC 1613 and Leo I (both using the method of Dolphin (2002)). Fig. 6 shows that the SFHs and AMRs for IC 1613 and Leo I, when derived via identical methodology, are nearly identical.

One possible interpretation of Fig. 6 is that, absent the youngest stars, is it possible that there are no differences between the stellar populations of

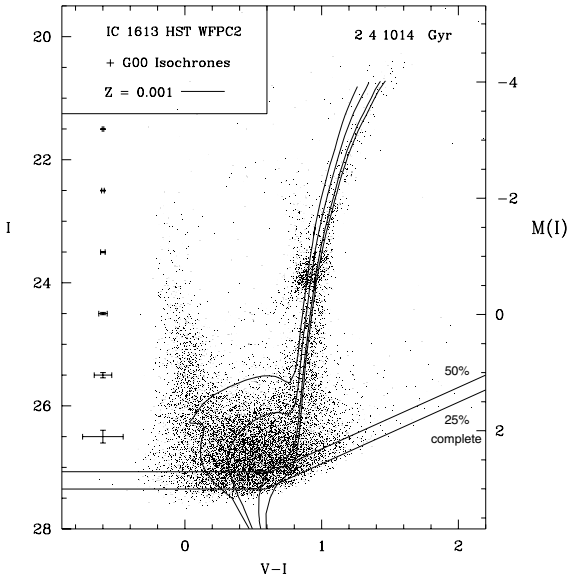

Fig. 5. CMD of IC 1613 derived from HST WFPC2 observations. Isochrones for a metallicity of $Z = 0.001$ and ages of 2, 4, 10, and 14 Gyr from Girardi et al. (2000) have been added in order to show the limitations of the observations in terms of MS ages. MS turnoffs back to intermediate ages (~5 Gyr) are well represented in the observations, but the oldest MS turnoffs (~10 Gyr) fall below the 50% completeness limit and are not represented. Thus, constraints on the oldest populations will need to come from the evolved stars.

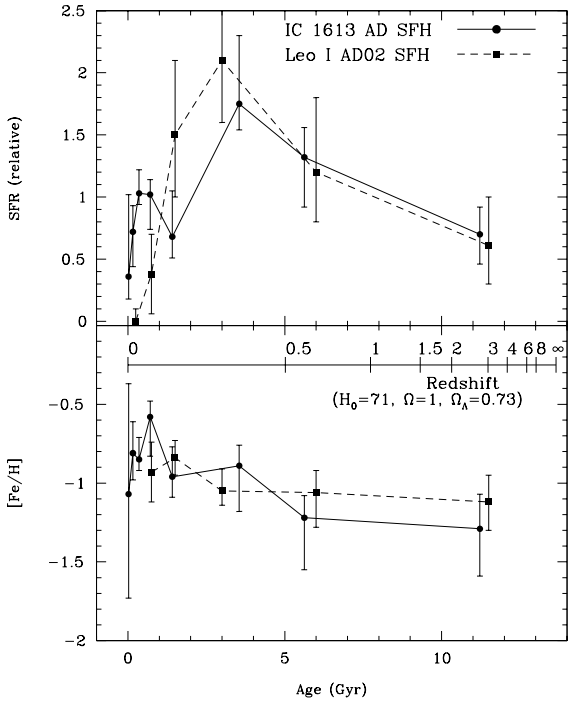

Fig. 6. Comparison of SFHs and metal enrichment histories for IC 1613 and the dSph Leo I (both derived via the Dolphin method (Dolphin, 2002; Skillman et al., 2003)). The star formation and metal enrichment histories appear nearly identical. A timeline comparing redshift to real time has been added for the noted cosmology. Note that the bulk of the star formation and chemical enrichment has occurred at $z < 1.0$.

isolated dI and dSphs which are more distant from their parent galaxies. The implication is that some dI and dSph galaxies have similar progenitors; the differences which we see today are due to environmental influences during the lifetimes of the galaxies which allow one type of galaxy to retain its gas and form stars up the present and another not. Certainly the morphological census of the Local Group has evolved with time. One possible environmental factor is the radiation background. The ionizing background can heat the ISM in low mass halos and reduce the rate of radiative cooling by reducing the number of neutral atoms. The photoionizing background will reduce the fraction of gas which collapses, suppressing star formation until later times ($z \leqslant 1$) when then background decreases and the gas can cool (see discussion in Skillman et al., 2003).

There are other dI galaxies for which it has been suggested that most of the stars have been formed relatively recently. Our earlier study of Leo A (Tolstoy et al., 1998) suggested that the majority of the star formation had occurred in the last 2 Gyr. Dolphin et al. (2002) discovered RR Lyraes in Leo A, and thus the presence of very early star formation, but converting the number of RR Lyrae stars to an early SFR is very uncertain. A similar SFH is found for Sextans A. From a relatively deep ($M_V \simeq +2.0$) CMD, (Dolphin et al., 2003) find that while there is evidence for very old stars in Sextans A, the SFR at intermediate ages (3–10 Gyr) was quite low, and the SFR has been the highest in the last 2 Gyr.

2.2. The future: wide field imaging from space with SNAP?

One of the fundamental conclusions of the IC 1613 study, that star formation was relatively low at ages older than 7 Gyr compared to intermediate ages, is only possible with the present depth of photometry. In order to be able to determine whether this is a general feature of low mass dIs or particular to IC 1613, CMDs of similar depth are needed for a large sample of dIs. At present, this is only possible with the HST for Local Group galaxies.

Some of the requirements for this type of work (wide field of view) are easily met by the current model for SNAP – (10′ is already great). However, a small pixel size (0.05″) which optimally samples the PSF may chafe a bit against the current design. Nonetheless, a wide field of view with imaging capability comparable to that of the HST will revolutionize the field of observing stellar populations in nearby galaxies.

Acknowledgments

I thank the conference organizers for inviting me to give this talk and for organizing a very lively conference. This review covers much of the work of a very fruitful collaboration which I am grateful to have been part of. I gratefully acknowledge partial support of my research from a NASA LTSARP Grant No. NAG5-9221 and the University of Minnesota.

References

Bertelli, G., Bressan, A., Chiosi, C., Fagotto, F., Nasi, E., 1994. A&AS 106, 275.

Dohm-Palmer, R.C., Skillman, E.D., 2002. The ratio of blue to red supergiants in sextans a from hubble space telescope imaging. AJ 123, 1433–1437.

Dohm-Palmer, R.C., Skillman, E.D., Saha, A., Tolstoy, E., Mateo, M., Gallagher, J., Hoessel, J., Chiosi, C., Dufour, R.J., 1997. The dwarf irregular galaxy sextans A. I. HST photometry of the resolved stars. AJ 114, 2514–2526.

Dohm-Palmer, R.C., Skillman, E.D., Gallagher, J., Tolstoy, E., Mateo, M., Dufour, R.J., Saha, A., Hoessel, J., Chiosi, C., 1998. The recent star formation history of GR 8 from HST photometry of the resolved stars. AJ 116, 1227–1243.

Dohm-Palmer, R.C., Skillman, E.D., Mateo, M., Saha, A., Dolphin, A., Tolstoy, E., Gallagher, J.S., Cole, A.A., 2002. Deep HST imaging of sextans A. I. The spatially resolved recent star formation history. AJ 123, 813–831.

Dolphin, A.E., 2002. Numerical methods of star formation history measurement and applications to seven Dwarf spheroidals. MNRAS 332, 91–108.

Dolphin, A.E., Saha, A., Skillman, E.D., Tolstoy, E., Cole, A.A., Dohm-Palmer, R.C., Gallagher, J.S., Mateo, M., Hoessel, J.G., 2001. Deep HST imaging of IC 1613. I. Variable stars and distance. ApJ 550, 554–569.

Dolphin, A.E., Saha, A., Claver, J., Skillman, E.D., Cole, A.A., Gallagher, J.S., Tolstoy, E., Dohm-Palmer, R.C., Mateo, M., 2002. Variable stars in Leo A: RR Lyrae Stars, short-period cepheids, and implications. AJ 123, 3154–3198.

Dolphin, A.E., Saha, A., Skillman, E.D., Dohm-Palmer, R.C., Tolstoy, E., Cole, A.A., Gallagher, J.S., Hoessel, J.C., Mateo, M., 2003. Deep hubble space telescope imaging of sextans A. III. The star formation history. AJ 126, 187–196.

Gallart, C., Freedman, W., Aparicio, A., Bertelli, G., Chiosi, C., 1999. The star formation history of the local group galaxy Leo I. AJ 118, 2245–2261.

Girardi, L., Bressan, A., Bertelli, G., Chiosi, C., 2000. A&AS 141, 371.

Hunter, D.A., Gallagher, J.S., 1985. Star-forming properties and histories of dwarf irregular galaxies – down but not out. ApJS 58, 533–560.

Skillman, E.D., Tolstoy, E., Cole, A.A., Dolphin, A.E., Saha, A., Gallagher, J.S., Dohm-Palmer, R.C., Mateo, M., 2003. Deep hubble space telescope imaging of IC 1613. II. The star formation history. ApJ 596, 253–272.

Tolstoy, E., Gallagher, J., Cole, A., Saha, A., Dohm-Palmer, R., Skillman, E., Mateo, M., Hurley-Keller, D., 1998. WFPC2 observations of Leo A: A predominantly young galaxy within the local group. AJ 116, 244–1262.

Tosi, M., Greggio, L., Marconi, G., Focardi, P., 1991. Star formation in Dwarf irregular galaxies – Sextans B. AJ 102, 951–974.

Available online at www.sciencedirect.com
SCIENCE DIRECT®
New Astronomy Reviews 49 (2005) 461–464
New Astronomy Reviews
www.elsevier.com/locate/newastrev

The COSMOS 2-degree HST/ACS survey ☆

Anton M. Koekemoer [a,*], Nick Z. Scoville [b]

[a] *Space Telescope Science Institute, 3700 San Martin Drive, Baltimore, MD 21218, United States*
[b] *Department of Astronomy, California Institute of Technology, Mail Code 105-24, Pasadena, CA 91125, United States*

Available online 22 September 2005

Abstract

The COSMOS survey is the largest contiguous imaging project ever undertaken with the Hubble Space Telescope, using ACS/WFC to image a 2 square degree low-background equatorial field in 600 orbits with the F814W (I) filter. The survey is providing over 2 million objects with a 10σ detection limit AB(I) < 27, with a sky coverage of 10 billion ACS pixels at a scale of 50 milliarcseconds/pixel. The principal goal of the project is to probe the formation and evolution of structures with size scales from galaxies to Coma-size clusters during the peak period of galaxy, AGN and star formation activity (redshifts ~0.5–3). The first half of the Cycle 12 data are now in hand, and some of the main preliminary science results from these data will be discussed. Two of the main scientific drivers for the project are to map the distribution of large scale structure in dark matter through weak lensing, and to measure the evolution of galaxies in the context of large scale structure. In addition, the large area of the survey is serving a wealth of other science topics, including comparatively rare high-luminosity AGN, starbursts and extremely red galaxies at high redshift. Combined with a wide range of ancillary datasets from X-ray through radio, this survey is becoming a truly unique Hubble legacy for understanding the evolution of the visible and dark universe.
© 2005 Elsevier B.V. All rights reserved.

Keywords: Cosmology: observations; Cosmology: dark matter; Cosmology: large-scale structure of universe; Galaxies: evolution; Surveys

Contents

1. Introduction 462
2. Scientific design 462

☆ Based on observations with the NASA/ESA Hubble Space Telescope obtained at the Space Telescope Science Institute, which is operated by the Association of Universities for Research in Astronomy (AURA), Inc., under NASA Contract NAS5-26555.

* Corresponding author.
E-mail addresses: koekemoe@stsci.edu (A.M. Koekemoer), nzs@astro.caltech.edu (N.Z. Scoville).

1387-6473/$ - see front matter © 2005 Elsevier B.V. All rights reserved.
doi:10.1016/j.newar.2005.08.023

3. Implications for future wide field missions 463
Reference 464

1. Introduction

A principal goal of observational cosmology is to trace the history of star formation and active galactic nuclei (AGN), along with the mass assembly history of galaxies, as a function of redshift and environment over the age of the universe. While the rate of galaxy evolution and the morphological mix of galaxies are thought to be strongly dependent upon the local density in the large scale structure (LSS), this is well established only in the nearby universe, through surveys such as the 2dF and SDSS. Since galaxy interactions drive much of the activity in the early universe, it is therefore crucial to sample the full range of overdensities in the LSS environment at all redshifts, up to and including $z \sim 1$–3 where the apparent peak in star formation activity occurs.

In addition to covering a sufficiently large area to sample the full range of LSS, it is also important to obtain sufficient angular resolution to resolve galaxies at the redshifts of interest on sub-kiloparsec scales, to allow sufficiently detailed study of their morphology. This also enables measurements of weak lensing to be carried out with great accuracy, thereby providing direct mass maps of the underlying overdensities. The COSMOS survey is specifically designed to address these questions by obtaining nearly 600 orbits of imaging with the Hubble Space Telescope (HST) Advanced Camera for Surveys (ACS) over an area of about 2 square degrees.

2. Scientific design

The fundamental design of the COSMOS survey aims to be able to cover a comoving volume similar to that sampled by the SDSS, corresponding to about 150 Mpc on a side, at redshifts of 2–3 when starformation activity was at its peak. This is sufficient to sample all scales currently envisaged for LSS, up to masses $\geqslant 2 \times 10^{14} M_{\odot}$. In addition, the sensitivity of the observations reaches to 10σ detection limits of AB(I) ~ 27, sufficient to fully characterize the morphology, multiplicity and interactions of L^* galaxies out to $z \sim 2$–3.

The area of 2 square degrees is covered using the ACS/WFC detectors, spending a total of one orbit on each pointing (2400s), divided into four sub-exposures that are dithered to improve PSF sampling and eliminate cosmic rays and bad pixels. The ACS/WFC camera consists of two detectors, each of which is 2048×4096 pixels at $0.05''$/pixel, thus covering a field of view of $\sim 3'$. Imaging the full 2 square degrees therefore requires a grid of about 24×24 pointings, corresponding to a total extent of $\sim 1.4^\circ \times 1.4^\circ$, and sampling the sky with $\sim 10^{10}$ pixels, each 50 milliarcseconds in size (see Fig. 1).

The COSMOS observations form the largest contiguous area ever observed with HST, and in fact are so extensive that they had to be divided between Cycles 12 and 13, in addition to having forced a pointing change because of irreconcilable scheduling problems arising from the initial pointing. As of May 2004, all the Cycle 12 data have been obtained, covering the central $\sim 1^\circ \times 1^\circ$, thereby already making this project the largest contiguous area ever observed by HST.

In addition to the HST data, the project also includes significant investments of time from other facilities including Subaru, VLT, VLA, XMM, and other related proposals submitted to Chandra and Spitzer. The final survey will provide a wealth of data on over 2 million galaxies, including several thousand X-ray emitting AGN, at least 100 X-ray clusters, and samples of several tens of thousands of Lyman break galaxies, EROS, and other red galaxies at high redshift, in addition to the detailed maps of dark matter and LSS.

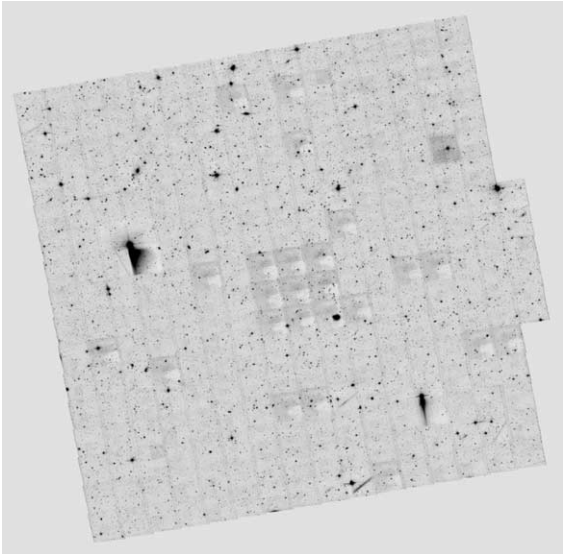

Fig. 1. The full HST/ACS dataset from the first half of the COSMOS project, obtained from October 2003 to May 2004 during Cycle 12. This field covers a total of 270 pointings, each pointing being a single-orbit, four-exposure dithered observation with the ACS/WFC camera which is 4096×4096 pixels on a side with a pixel scale of 0.05″/pixel. Therefore, this initial dataset delivers about 5×10^9 pixels covering about 1 million galaxies.

The incoming HST data are processed on a cluster of linux computers at the Space Telescope Science Institute, using the MultiDrizzle program (Koekemoer et al., 2002). This involves initial registration of the dithered exposures for each pointing, subsequent drizzling and cosmic ray rejection, followed by final drizzle combination to form a cleaned, rectified image for each of the pointings. Catalogs are then run using SExtractor on the cleaned images and morphological parameters extracted to quantify the galaxy sizes, shapes and types.

The initial catalogs on the field contain $\sim$4–5×10^5 sources, and have enabled the construction of preliminary mass maps derived from weak lensing shear measurements around several concentrations in the field. These are being examined as a function of redshift using a combination of photometric and spectroscopic redshifts (see Fig. 2).

3. Implications for future wide field missions

The COSMOS survey is demonstrating the practicality of large-area, high resolution space-based surveys providing detailed morphological information on large samples ($\sim 10^6$) of galaxies on sub-kpc scales up to redshifts $\sim$2–3. This is crucial for directly constraining the morphological properties of the galaxies themselves, quantifying

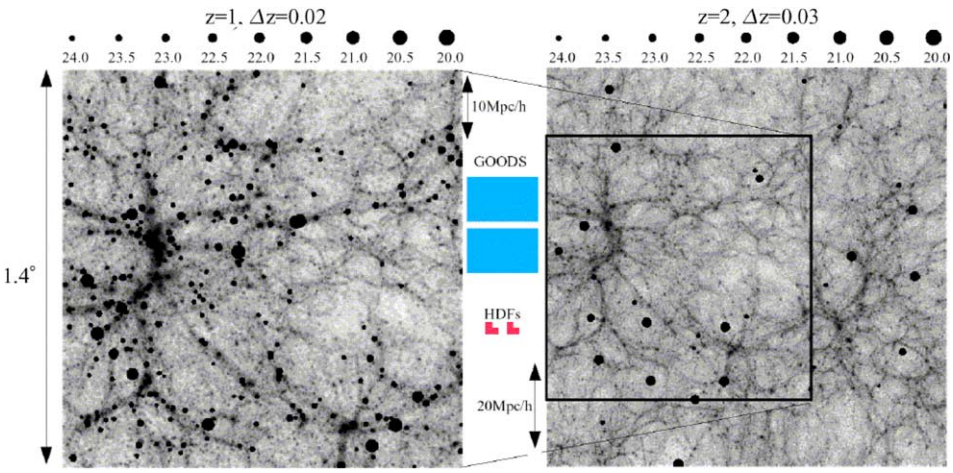

Fig. 2. Two slices from an LSS simulation (Frenk et al., priv. comm) at redshifts 1 and 2, showing the comoving volume sampled by COSMOS in each case. The figure shows a comparison to previous HST surveys and demonstrates the importance of going to an area at least 1° across, corresponding to over 100 Mpc at these redshifts which is necessary to help mitigate cosmic variance.

the morphological mix of their environments, and obtaining detailed mass maps based on their weak lensing shear. While it is unlikely that HST will provide any further surveys with significantly large contiguous area than COSMOS, the techniques learned from COSMOS will readily serve as a useful precursor to future wide-field space-based missions, particularly in terms of laying the technical groundwork, as well as indicating the most promising directions of scientific parameter space to investigate.

Reference

Koekemoer, A.M., Fruchter, A.S., Hook, R.N., Hack, W., 2002. HST Calibration workshop. In: Arribas, S., Koekemoer, A.M., Whitmore, B. (Eds.), (STScI: Baltimore), 337.

Available online at www.sciencedirect.com
SCIENCE DIRECT®
New Astronomy Reviews 49 (2005) 465–473
New Astronomy Reviews
www.elsevier.com/locate/newastrev

Wide field imaging from space: Galaxy formation from nearby stellar populations ☆

R. Michael Rich

Department of Physics and Astronomy, Physics and Astronomy Building, 430 Portola Plaza, Box 951547, Los Angeles, CA 90095-1547, United States

Available online 28 September 2005

Abstract

A wide field, high resolution imaging facility in space would enable breakthrough science in the study of stellar populations. Optical high resolution imaging at the diffraction limit of a 2 m telescope is a minimum requirement.

In the Galaxy and Local Group, proper motion studies could settle the contribution of cool white dwarfs to the halo dark matter mass and define the dynamics of the Galactic bulge. The white dwarf cooling age method could be applied to a larger number of globular clusters and could include measurements covering the whole of a given cluster. This powerful method can constrain the age of the Universe as well as the early star formation history of globular clusters. A wide field imager could derive main sequence turnoff ages for the interaction streams and multiple globular clusters in the M31 halo, as well as in other Local Group galaxies. Imaging in the halos of nearby galaxies to 10 Mpc, including the Virgo cluster, could map out tidal streams and debris tail and would help to define the stellar populations (and therefore the assembly history and nature of) Galactic halos.
© 2005 Published by Elsevier B.V.

Contents

1. Introduction 466
2. The science case 466
   2.1. Can other facilities do this science? 467
3. Technical needs 468
4. Science programs 469
   4.1. Age of the oldest stars from the white dwarf cooling sequence in globular clusters 469

☆ Support is acknowledged from NASA, through the Galaxy Evolution Explorer and the from the Space Telescope Science Institute.
E-mail address: rmr@astro.ucla.edu.

1387-6473/$ - see front matter © 2005 Published by Elsevier B.V.
doi:10.1016/j.newar.2005.08.024

4.2. Galactic bulge . . . 470
4.3. Local Group halos . . . 470
5. Beyond the Local Group . . . 471
Acknowledgment . . . 473
References . . . 473

1. Introduction

The Hubble Space Telescope has in its 10 year lifetime changed the face of astronomy. In few subject areas has this been more true than in stellar populations. For Galactic populations, HST imaging gave us the clear detection of white dwarf cooling sequences, and even the white dwarf luminosity function with an age constraint of 12.7 Gyr for the age of the Universe (Hansen et al., 2002, 2004). The color-magnitude diagrams of globular clusters in the Magellanic Clouds (e.g., Rich et al., 2001) and dwarf spheroidal galaxies are now exquisitely defined down to the main sequence turnoff point. One of the last frontiers has been the study of distant exotic stellar populations such as those in the tidal tails of interacting galaxies, but this barrier has also fallen (Saviane et al., 2004). HST imaging is fundamentally limited by the small field of view. This is also the case for every other high resolution space based imaging system that is planned, other than a SNAP type mission. Interesting observations in this subject area require the longest practical exposure times. Either one hopes for a mission such as TPF-C (a next generation HST) or for an acceptable point spread function delivered by JWST. Even if these missions take place, the coverage of large contiguous areas will still be difficult and time consuming, requiring many pointings. Such programs may be undertaken, but rarely if ever for stellar populations problems. JWST may gain a factor of 10 in speed over HST, but will have an imager of roughly the same area as ACS. The relatively modest speed gain pales versus the thousands of pointings required to cover an area of a few square degrees.

The slope of the initial mass function and radial gradients in white dwarf properties, remain as major sources of uncertainty in constraining the age of globular clusters from the white dwarf cooling curve method. One would dearly wish to explore the variations in main sequence turnoff luminosity and horizontal branch morphology across the complex structure of the M31 halo. Tidal streams covering tens of square arcminutes might be detected in the halos of nearby galaxies, mapped by the distribution of their red giants. All of these programs demand wide field imaging.

In the following we consider a SNAP reference mission: a 2.0 m telescope, detector area of $35' \times 35'$, $0.10''\,\mathrm{pix}^{-1}$ and most importantly, 0.35–1.0 μm range; we also consider an IR channel with similar properties.

2. The science case

The following represent just some of the problems that could profitably be addressed by wide field imaging in space:

1. Survey low luminosity stars and the mass function in the halo and bulge; settle the problem of whether white dwarfs contribute to halo dark matter.
2. From the WD luminosity functions, derive more precise relative ages of, and possibly reconstruction of star formation histories of, the nearest Galactic globular clusters, using the white dwarf cooling method.
3. Are the ages of the oldest stars (e.g., M92) the same over the whole of the Local Group? Did the character of star formation change post reionization and is there a record of it?
4. A large scale survey for microlensing in the bulge and halo of M31.

5. Resolve the stellar populations in low surface brightness galaxies and tidal tails out to 15 Mpc.
6. Stellar populations in tidal streams, satellites, and halos, with age constraints, to 10 Mpc.
7. Star formation histories for the outer disks and satellites of Local Group galaxies.
8. Very long integrations to study the ages of halos and satellites in the Virgo cluster.

Will these topics be interesting in 2012? Much depends of course on how long HST continues to operate. It is unlikely that any other high resolution facility will come online earlier, other than improved adaptive optics (very much a small field proposition). Even with HST operating until 2008 or 2010, it is unlikely that great progress will be made in these areas, simply because of the difficulty and expense of covering large areas of the sky. Approximately 300 orbits will be invested in the study of 1–2 more globular clusters for the WD luminosity function, but there will not be integrations of 100 orbits at each of three positions in a cluster, the requirement for addressing radial gradients. One can imagine 300 orbits (about a Deep Field size campaign) to study several field positions in M31, but not the 500 orbits needed to reach the main sequence turnoff point for 5 globular clusters (although certainly such a program will be proposed). Only when one contemplates a 10 m optical/UV space telescope does the efficiency of single small area pointings begin to look attractive compared with a wide field imager on a 2 m space telescope.

The more difficult question is whether the science itself will remain current. Galaxy evolution appears to be a healthy subject with many challenging problems, and it is unlikely that it will be "solved" to the extent that study of the local Universe is not interesting. The relative importance of processes such as gas accretion, interactions, and ingestion of companions will be well addressed in nearby galaxy studies.

The relative ages of the oldest populations and their formation order is also a subject best addressed by direct measurements on nearby galaxies. Even if JWST is actually able to image the "first light" it will probably be very difficult to "see" the formation of the first globular clusters. The formation events giving rise to low surface brightness features such as disks and halos will likely be lost due to the $(1+z)^4$ surface brightness dimming. Such questions as whether there is a simultaneous era of ignition in the Local Group are best settled by direct measurement of the turnoff luminosity of the oldest stars, rather than by guessing at the order, origin, and significance of very low luminosity starbursts at the edge of JWST detection.

Will galaxy formation still be an interesting problem? It is possible to complain that the history of galaxies is not a sufficiently fundamental problem in comparison to say the search for planets of life in the Universe. However, it is a danger to leave the decision of what an important problem is to popular culture. The formation and evolution of galaxies remains a fundamentally interesting problem and wide field imaging of the nearby Universe will offer a major contribution to that subject area.

2.1. Can other facilities do this science?

HST has the same aperture as a SNAP-type mission, but lacks wide field imaging. Given the factor of 50 gain in survey speed possible, HST is not competitive. JWST had the potential to compete in the IR, but its downsized focal plane is a problem. The attained spatial resolution in the infrared will be little better than that of HST. Ground-based AO even with laser guide stars faces a multitude of hurdles. Point spread function variation and difficulty in calibration are some of the issues. Fifteen ($V \sim 17$) mag guide stars are still required for tip/tilt correction. Corrected fields are small. And even with the best ground-based AO systems there remains an uncorrected halo around all images, with the fraction of light in the halo varying as a function of field position and time. For complex and crowded fields, no techniques compete with space based imaging.

Deep ground-based imaging with 6–10 m telescopes might be competitive with a space based system. However, the best optical imaging attained

from the ground is 0.25″ for a few minutes at a time. Future technologies such as that employed by PAN STARRS are intriguing but far from proven. Following a decade of HST imaging no ground-based imaging improvement scheme has proven competitive, especially when precise photometry is required.

3. Technical needs

In an ideal world, this science works best if the wide field covers a large contiguous area and it is possible to tile that area. Fig. 1 shows the complex morphology of the M31 halo. Ferguson et al. (2002) map the giant branch tip and suggest regions containing intermediate age stars. From the color of the red giant branch, subtle metallicity variations are inferred. A deep wide field image would likely read the main sequence turnoff, turning suggested age variations into secure measurements. Whole dwarf galaxies are also tens of arcminutes in extent; the wide field is critical.

The second requirement is for optical imaging. Because metal line blanketing is more important at visible wavelengths, it is possible to infer metallicity from the red giant branch using optical colors, whereas the factor of two smaller dependence of color on metallicity in the infrared makes this a much harder measurement (Fig. 2). Finally, the aim should be to obtain the highest possible spatial resolution. Why make the effort to attain the wide field if image quality is sacrificed?

The science aim is to make precise measurements of age and metallicity for resolved stellar populations. The best precision is from ages mea-

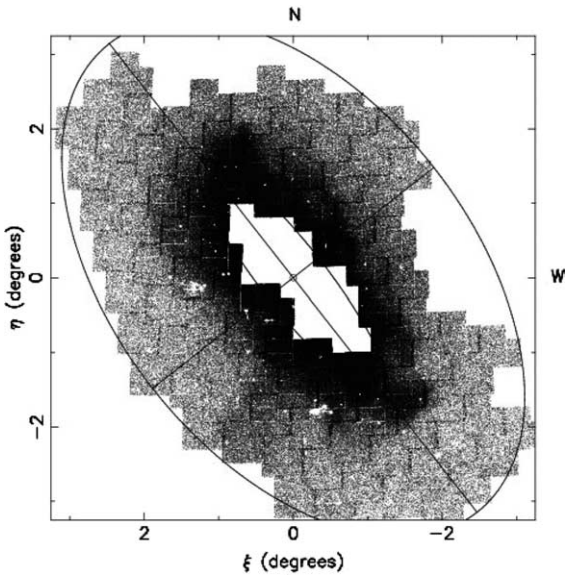

Fig. 1. This map of the M31 halo was derived by mapping the number density of red giant stars using a ground-based wide field CCD imager (Ferguson et al., 2002). We would like to know whether the different regions correspond to stellar populations of different ages. There is tantalizing evidence that the major axis fields lying 30 kpc or more distant from the nucleus may yet be dominated by disk stars; AGB star counts suggest that some of the plumes in the NE are younger. A wide field imager in space would have a 0.5° or greater field while ACS on board HST covers only 1/100 the area. In a similar vain it would be of great interest to undertake deep imaging of Galactic dwarf spheroidal galaxies, where young stellar populations are suspected.

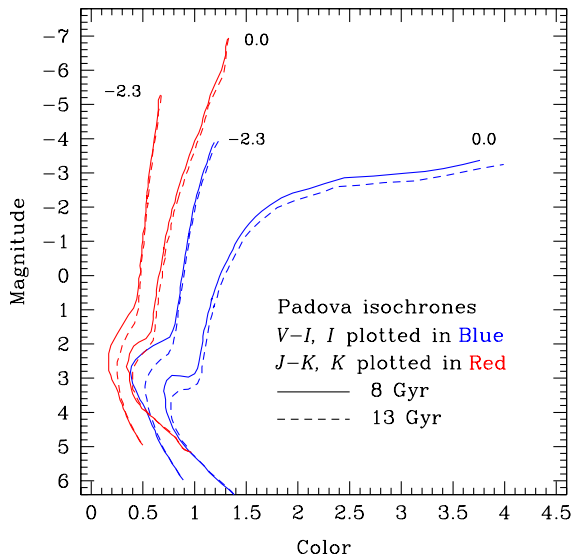

Fig. 2. This figure shows simple stellar populations of age 8 and 13 Gyr and [Fe/H] = − 2.3 and Solar, respectively, with the full locus from the main sequence turnoff to the red giant branch. Notice that the full range in color is far greater for the optical (V,I) isochrones than for the infrared. Optical measurements give more accurate age and metallicity measurements for a given S/N. (For interpretation of the references to colour in this figure legend, the reader is referred to the web version of this article.)

sured from the old main sequence turnoff point at $M_V = +4.5$. A wide field imaging telescope employing the best technology could get photometric measurements to $V \sim 32$. The limit of an accurate turnoff age measurement for a complex population is shown the color-magnitude diagram of the M31 halo from Brown et al. (2003). Wide field measurements of the old main sequence turnoff is unlikely to be feasible for distance modulus exceeding 25, One may contemplate a heroic integration that conceivably reaches the main sequence turnoff at modulus 26.5, just reaching M81.

Image crowding is the most severe problem. The deepest photometry will be reserved for low surface brightness regions – outer disks, and halos. In general $\mathrm{sur}f(m) > (m - M)_0 - 2.5\log(L_\mathrm{T}/L_\odot) + M_\odot$, where L_T is the total luminosity in a given passband, in Solar units per sq. arcsec (see Rich, 1998). In the practical sense, pushing 2 mag more in distance forces a corresponding push to 2 mag fainter in surface brightness.

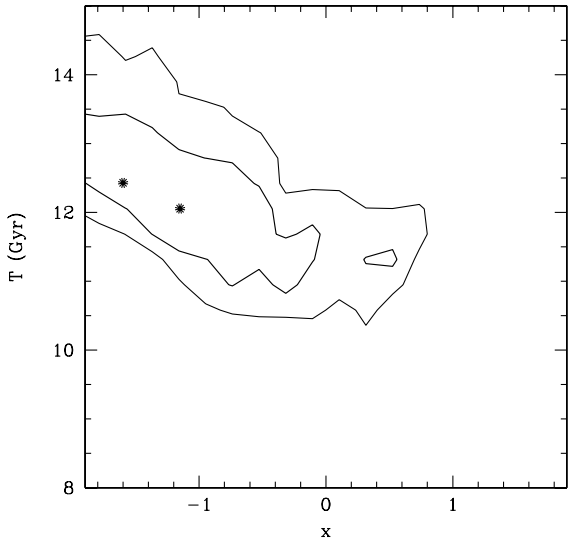

Fig. 3. White dwarf cooling age of the globular cluster M4 plotted against the slope of the stellar initial mass function x (Hansen et al., 2004). The relatively large uncertainty in the WD cooling age would be <0.1 Gyr if the analysis were performed using data for all white dwarfs in M4, which could be easily accomplished with a wide field imaging mission.

4. Science programs

4.1. Age of the oldest stars from the white dwarf cooling sequence in globular clusters

A 2.5 m telescope in space is capable of reaching very faint stellar magnitudes ($V \sim 30$). An integration of 120 HST orbits was sufficient to reach near the end of the white dwarf cooling sequence in the globular cluster M4. In principle, one may fit the shape of the white dwarf luminosity function to constrain the age of the oldest stars (Fig. 3). Hansen et al. (2004) derive an age of 12.1 Gyr (95% lower limit of 10.5 Gyr) for the globular cluster M4 using this approach. There is significant covariance between the derived age and the slope of the mass function x. Unfortunately, much also depends on the dynamical state of the globular cluster. The white dwarf cooling method itself would be compromised if binary mass transfer resets the cooling "clock" for some fraction of WD (Hurley and Shara, 2003); a wide field survey would help to assess better the binary issue. A deep wide field imaging campaign would improve the precision of the age constraint by increasing the numbers of measured white dwarfs. If multicolor imaging were obtained, it would be possible to exclude the non-DA white dwarfs on the basis of their colors, reducing another uncertainty. During the lifetime of HST, it reasonable to assume that at most 3 clusters will be studied in depth, and then only in one small ACS field. A SNAP-type mission would revisit these clusters, but with a wide field study, and might well add several more. A space based mission is crucial for this problem as high spatial resolution is required to deal with crowding and scattered light from bright stars.

Hansen has performed a simulation in which the white dwarf luminosity function is measured for an entire cluster, an increase of a factor of 10 in the numbers of WD compared to Fig. 3 and with the analysis of Hansen et al. (2004). The age estimate now becomes an amazing 12.61 ± 0.02 Gyr. The troublesome x is constrained to dx better than 0.1 as well. If the 5 clusters cited in Hansen's (2004) review were observed, one could get a tight constraint on the formation timescale of the Galactic

halo and the age of the Universe. While not solving the dark matter problem, this would have to be considered a significant contribution.

There is a dark matter problem connected to white dwarfs, however by the time of this proposed mission, it i s likely to be solved. This is the question of whether ancient white dwarfs may account for some fraction of the baryonic dark matter. A proper motion survey by Oppenheimer et al. (2001) suggested that an old white dwarf population, perhaps accounting for a few per cent of the dark matter, might be present. This population would be distinct in nature from that related to the stellar halo. Subsequent studies (e.g., Reid et al., 2001; Salim et al., 2004) fail to confirm the dark matter interpretation. However, a decisive result awaits a deep wide area survey. A SNAP type mission would be powerful in its capability to reach faint magnitudes and to cover wide areas. However, ground-based wide field imagers and survey telescopes will be attacking this problem, which is not affected by crowded fields.

4.2. Galactic bulge

Wide field imaging of the Galactic bulge is being contemplated as a MIDEX class mission (Microlensing Planet Finder; Bennett et al., 2004). The aim is to stare at the bulge as continuously as possible with the hope of discovering transient microlensing amplification due to Earth-mass lenses. While transiting hot Jupiters would also be discovered, the primary aim here is the measurement of terrestrial mass planets and their incidence as a function of Galactocentric distance. Such a dataset would also give proper motion data, which constrains the mass and structure of the bulge, as well as the age of its stellar population (Kuijken and Rich, 2002). Proper motions effectively separate the foreground disk population from the bulge field stars (Fig. 4). Given the compelling science goals of SNAP and the planet search, the possibility of pairing the missions is worth consideration.

The bulge offers a great deal of secondary science. If the white dwarf cooling sequence method is proven in globular clusters, it may well be applied to get some constraints for the age and star formation history of the Galactic bulge. This will prove a most challenging goal, and will likely be feasible in fields well outside 1 kpc (that is, outside of the classical metal rich bulge). As infrared capability is a likely part of a SNAP mission, an ultra deep bulge exposure would almost certainly reach the end of the stellar hydrogen burning sequence, giving a mass function for normal stars (Zoccali et al., 2003). Because the disk and bulge populations are superposed, a measurement of the bulge luminosity function requires proper motion separation from the disk, more feasible if a wide field imager can address the problem with a study in a single field.

4.3. Local Group halos

The complexity of the M31 halo (Fig. 1; Ferguson et al., 2002; Ibata et al., 2001) presents the most compelling argument for how a wide field imaging mission could be a major boon to the study of stellar populations. Reaching the old main sequence turnoff at $V \sim 31$ while at the same time covering significant area would be a daunting challenge. The inner halo covers roughly 4 sq. deg.; depending on the focal plane geometry, this would take of order 20 pointings at 50 orbits/pointing – or 1/3 of a year of integration time. Considering a dedicated mission of a decade or more, such a program might actually be accomplished. A contiguous imaging survey, if extended to cover greater area, might also discover or rule out the presence of a large number of low luminosity satellites, predicted to be present in the current cold dark matter paradigm. Brown et al. (2003) obtained a deep ACS pointing in one M31 halo field 11 kpc distant on the minor axis. In such a complex stellar population, the AGB and HB give only sketchy indications of the age. In reality, there is little to constrain age differences for populations older than 5 Gyr. A distant satellite might have too few red giant members to have a measurable presence, while the number of subgiant and main sequence stars might be a factor of 100 greater. Thus, the goal of detecting the luminosity function of faint, distinct streams and companions is better served by a deep, high spatial resolution imaging survey.

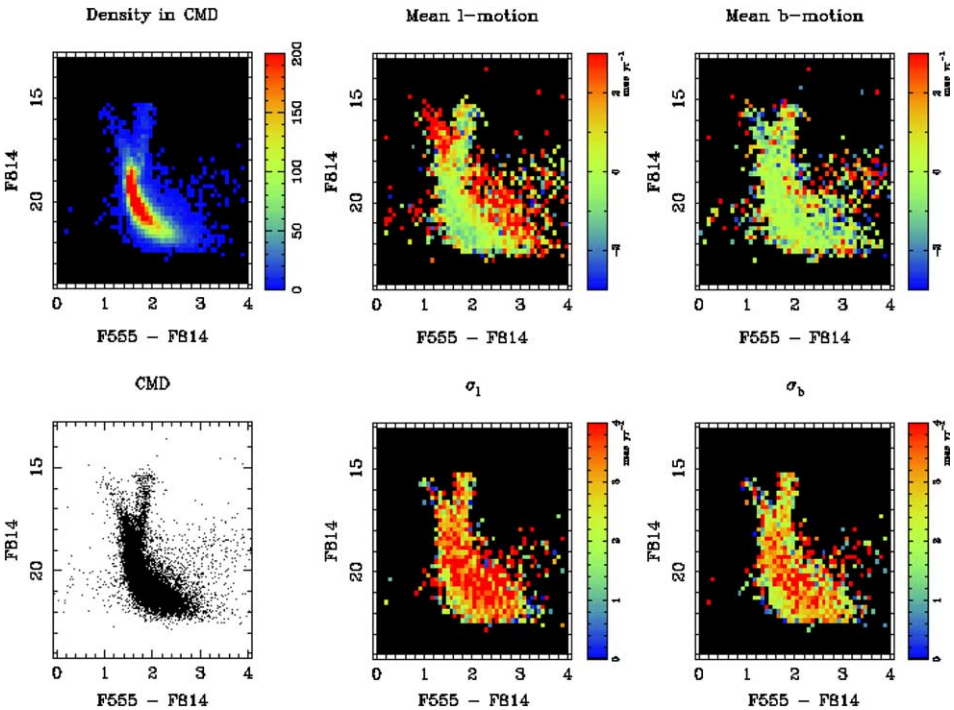

Fig. 4. Proper motion measurements can separate stellar populations in the Galaxy. The Galactic bulge field Sgr I ($l = 2$, $b = -2.6$) is cleanly separated from the foreground disk population in red, which has significant transverse velocity relative to the bulge field, due to the Sun's motion relative to the Galactic Center (Kuijken and Rich, 2002). This work shows that the Galactic bulge is dominated by a 12–13 Gyr old stellar population. (For interpretation of the references to colour in this figure legend, the reader is referred to the web version of this article.)

At present, we have an age constraint for one M31 globular cluster, GC 312 (Brown et al., 2004a,b). It is a compact metal rich cluster chosen for study because it is situated in the (Brown et al., 2003) deep halo field. Unfortunately, due to its compactness the uncertainty in the age is too great to settle the long running debate over whether the metal rich clusters and field stars are younger on the whole than the oldest halo stars. The analysis of 20 HST observations of M31 globular clusters (Rich et al., 2005) finds that the most metal poor globular clusters have a wide range in horizontal branch morphology and that the trend is distinctly different from that of the Milky Way (Fig. 5). The presence of the second parameter problem at such low metallicity raises the real possibility that the oldest, most metal poor stars in M31 are younger than the comparable Milky Way halo population. As opposed to measuring turnoff photometry for 1 or 2 clusters, a wide field imager could invest a long integration time on the study of several clusters, getting main sequence turnoff age constraints. The value of such a campaign has been raised greatly by a new set of techniques to obtain detailed chemical abundances and the mean red giant branch temperature from echelle spectroscopy of the integrated light (Bernstein and McWilliam, 2002). This information, combined with a deep color-magnitude diagram reaching the main sequence turnoff, would give age constraints sufficient to determine whether the halos of M31 and the Milky Way, two massive galaxies thought to have similar histories, do in fact differ in the ages of their oldest stars.

5. Beyond the Local Group

When their halos are considered, even galaxies as distant as 10–20 Mpc can cover an area on the

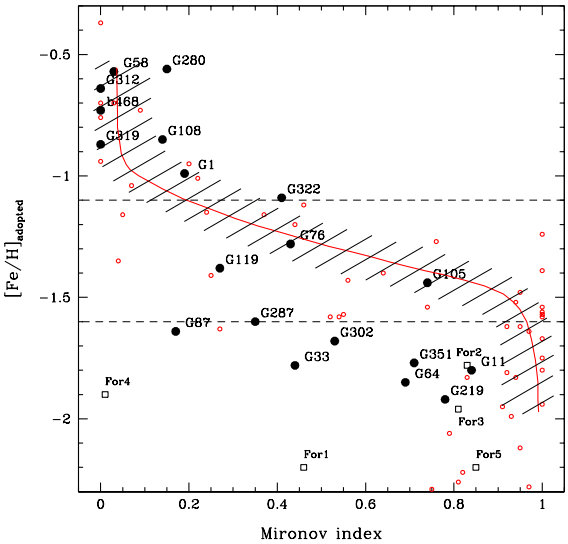

Fig. 5. Horizontal branch type from WFPC2/HST imaging, vs. [Fe/H] for M31 and Galactic (small points) globular clusters (Rich et al., 2005). Squares are clusters in the Fornax dwarf spheroidal galaxy. Notice that the M31 globular clusters exhibit a range in horizontal branch type (the second parameter problem) at [Fe/H] = – 1.6. This may be an indication that some of the M31 globular clusters are younger than those in the Galactic halo. Only a wide field imaging space-based survey can test whether this is true, by measuring the main sequence turnoff for a large sample of M31 globular clusters.

sky of 10–20′. Just as the properties of globular cluster systems have been the subject of wide ranging studies and important inferences on galaxy formation, the properties of stellar halo populations are now coming to the fore. The primary questions are how the metallicity and age distribution correlates with parent galaxy Hubble type and luminosity, and how widespread are low luminosity satellites, tidal streams, warped disks, debris fields, and other anomalies. The metal enriched winds of proto starbursts must have had a dramatic effect on scales of ∼1 Mpc in the intergalactic medium, and the fossil record of this period may well be recorded in the stellar halos.

The high spatial resolution and great sensitivity of the HST imagers has permitted the study of a few extragalactic halos. M31 was the first extragalactic halo to be studied and it was found to be have a broad, metal rich, abundance distribution – a contrast to the classical description of the Galactic halo.

Using Hubble and WFPC2, we have explored the stellar halo populations of other edge-on spiral and disk galaxies. We find a strong primary correlation between metallicity and the luminosity of the parent galaxy (Mouhcine et al., 2005). However, the Milky Way halo falls nearly 1 dex too metal poor, well below the trend (Fig. 6). At present, the field of view of WFPC2 (and also ACS) is too small to address the question of whether complex streams or features analogous to those seen in M31 by Ferguson et al. (2002) may be detected out to 10–20 Mpc. If one had the wide field of view and multi-wavelength capabilities of a SNAP-type mission, it would be possible to constrain the age distribution of halo stars (from the luminosity of AGB stars in the infrared) and to constrain better the metallicities from the shape of the red giant branch. The colors of the red giants could be compared to those of streams and satellites, and a truly

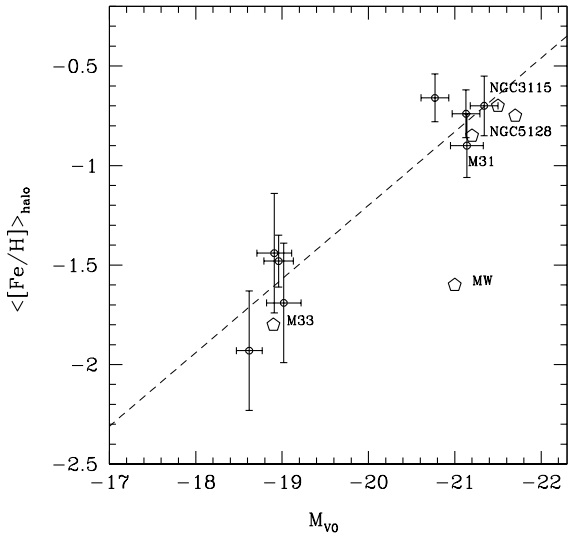

Fig. 6. Metallicity of stellar halo fields roughly 10 kpc off the Galactic disk, against total luminosity of the parent system. Most Galaxies in this plot are edge-on spirals and the metallicities are derived from the colors of the resolved red giants (Mouhcine et al., 2005). Notice that the Milky Way lies 1 dex below the general trend, perhaps indicating that the Galactic bulge has been less important than the debris of accreted satellites in forming the halo population. The halos of these nearby galaxies such as NGC 4565 actually subtend roughly 20′ on the sky and deep imaging from a wide field imager could reveal features such as streamers from disrupted satellites.

general picture of stellar halos and early galaxy evolution might begin to emerge. There is the tantalizing possibility of measuring actual main sequence turnoff ages for the first time over a wide range of the Hubble sequence, perhaps pushing as distant as the ellipticals of the Virgo cluster. Coupling these data with the properties of the associated globular cluster systems might give one of the most powerful scientific legacies of such a mission.

Any effort to understand galaxy formation and evolution is incomplete without including also detailed studies of the nearby Universe, as constraints and reality checks for any theory. A wide field imaging mission in space would make a critical contribution to this subject area, a contribution that could well rival in importance the goals of its primary mission.

Acknowledgements

R. Michael Rich acknowledges support from Space Telescope Science Institute funding under GO- 9436 and 9817. Rich further acknowledges support from NASA funding in support of the Galaxy Evolution Explorer, a Small Explorer mission.

References

Bennett, D.P., et al., 2004. AAS. 204, 1106.
Brown, T.M., Ferguson, H.C., Smith, E., Kimble, R.A., Sweigart, A.V., Renzini, A., Rich, R.M., VandenBerg, D.A., 2004a. ApJ 613, L125.
Brown, T.M., Ferguson, H.C., Smith, E., Kimble, R.A., Sweigart, A.V., Renzini, A., Rich, R.M., 2004b. AJ 127, 2738.
Brown, T.M., Ferguson, H.C., Smith, E., Kimble, R.A., Sweigart, A.V., Renzini, A., Rich, R.M., VandenBerg, D.A., 2003. ApJ 592, L17.
Ferguson, A.M.N., Irwin, M.J., Ibata, R.A., Lewis, G.F., Tanvir, N.R., 2002. AJ 124, 1452.
Hansen, B., 2004. Phys. Rep. 399, 1.
Hansen, B.M.S. et al., 2004. ApJS 155, 551.
Hansen, B.M.S. et al., 2002. ApJ 574, L155.
Hurley, J.R., Shara, M.M., 2003. ApJ 589, 179.
Ibata, R., Irwin, M., Lewis, G., Ferguson, A.M.N., Tanvir, N., 2001. Nature 412, 49.
Kuijken, K., Rich, R.M., 2002. AJ 124, 2054.
Mouhcine, M., Rich, R.M., Ferguson, H., Brown, T., Smith, E., 2005. ApJ (in press).
Bernstein, R.A., McWilliam, A., 2002. IAU Symposium 207, 739.
Oppenheimer, B.R., Hambly, N.C., Digby, A.P., Hodgkin, S.T., Saumon, D., 2001. Science 292, 698.
Reid, I.N., Sahu, K.C., Hawley, S.L., 2001. ApJ 559, 942.
Rich, R.M., 1998. ASP Conf. Ser. 133: Science With The NGST, p. 129.
Rich, R.M., Shara, M.M., Zurek, D., 2001. AJ 122, 842.
Rich, R.M., Cacciari, C., Federici, L., Fusi Pecci, F., Djorgovski, S.G., Freedman, W., 2005. AJ 129, 2670.
Salim, S., Rich, R.M., Hansen, B.M., Koopmans, L.V.E., Oppenheimer, B.R., Blandford, R.D., 2004. ApJ 601, 1075.
Saviane, I., Hibbard, J.E., Rich, R.M., 2004. AJ 127, 660.
Zoccali, M. et al., 2003. A&A 399, 931.

Available online at www.sciencedirect.com
SCIENCE DIRECT®
New Astronomy Reviews 49 (2005) 474–477
New Astronomy Reviews
www.elsevier.com/locate/newastrev

Star formation histories in the Local Group

Thomas M. Brown

Space Telescope Science Institute, 3700 San Martin Drive, Baltimore, MD 21218, USA

Available online 13 September 2005

Abstract

Deep color–magnitude diagrams extending to the main sequence provide the most direct measure of the detailed star formation history in a stellar population. With large investments of observing time, HST can obtain such data for populations out to 1 Mpc, but its field of view is extremely small in comparison to the size of Local Group galaxies. This limitation severely constrains our understanding of galaxy formation. For example, the largest galaxy in the Local Group, Andromeda, offers an ideal laboratory for studying the formation of large spiral galaxies, but the galaxy shows substructure on a variety of scales, presumably due to its violent merger history. Within its remaining lifetime, HST can only sample a few sight-lines through this complex galaxy. In contrast, a wide field imager could provide a map of Andromeda's halo, outer disk, and tidal streams, revealing the spatially-dependent star formation history in each structure. The same data would enable many secondary studies, such as the age variation in Andromeda's globular cluster system, gigantic samples of variable stars, and microlensing tracers of the galaxy's dark matter distribution.
© 2005 Elsevier B.V. All rights reserved.

Contents

1. Historical background 474
2. The advanced camera for surveys 475
3. The future: wide field imaging from space 476
References 477

1. Historical background

For more than 50 years (Sandage, 1953), a color–magnitude diagram (CMD) reaching the main sequence (MS) has been the most direct tool for measuring the star formation history in a stellar population. Much of that work focused on the ages of simple stellar populations, such as star clusters, within our own Galaxy. By the late 1980s, the leap in sensitivity and photometric pre-

E-mail address: tbrown@stsci.edu.

1387-6473/$ - see front matter © 2005 Elsevier B.V. All rights reserved.
doi:10.1016/j.newar.2005.08.025

cision offered by the widespread use of CCDs, coupled with advances in stellar evolution models, allowed accurate estimates for the ages of Galactic globular clusters (VandenBerg, 1988). In the 1990s, the launch of the Hubble Space Telescope (HST) and the subsequent installation of the Wide Field Planetary Camera 2 enabled the measurement of star formation histories in more complicated populations throughout the Local Group. Beyond the closest satellites of the Milky Way, these studies focused on the brighter and younger populations in dwarf galaxies (Dohm-Palmer et al., 2002).

2. The advanced camera for surveys

In 2001, the Advanced Camera for Surveys (ACS) was installed on HST, and its dramatic improvements in sensitivity, field of view, and sampling enabled dating of the oldest populations out to the edge of the Local Group. Extremely deep ACS imaging of Andromeda (M31) showed that its halo is surprisingly younger than our own (Brown et al., 2003), with over half of the halo younger than 11 Gyr, and with 30% of the population at intermediate ages of 6–8 Gyr (Fig. 1). The data from such long exposures are also useful for studying transient phenomena (e.g., microlensing, supernovae) and variable stars (Brown et al., 2004). Soon two more deep fields will be obtained in M31's outer disk and giant tidal stream. Because the ACS field is extremely small compared to the size of Local Group galaxies (e.g., the M31 halo is several degrees across), HST can only produce pencil-beam samples in each major component of a nearby galaxy. M31's complex substructure, seen in maps of its bright giant stars (Ferguson et al., 2002), cannot be sampled at this depth within the remaining HST lifetime.

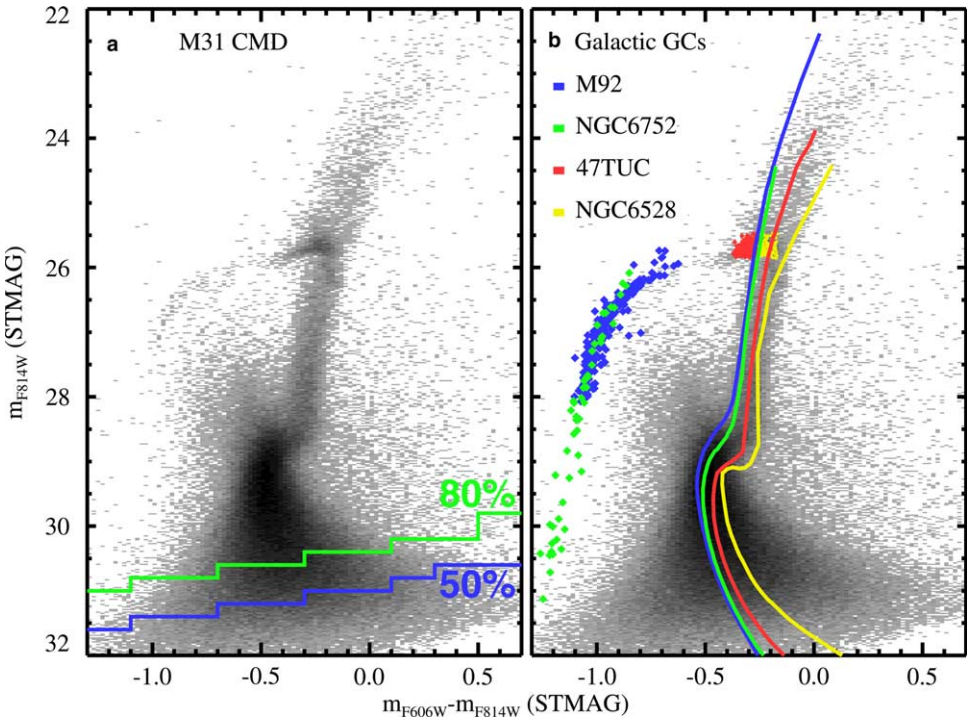

Fig. 1. Panel (a): the CMD of the M31 halo, as observed by ACS in the F606W (broad *V*) and F814W (*I*) bands (Brown et al., 2003), with completeness limits marked. Panel (b): comparison to the ACS observations of 4 Galactic globular clusters in the same bands. The relative MS turnoff luminosities demonstrate empirically that the M31 halo ranges from metal-rich stars at intermediate ages to metal-poor stars at old ages. Comparison to theoretical isochrones calibrated in the ACS bands also shows that over 50% of the M31 halo stars are at higher metallicity ([Fe/H] >-0.5) and younger ages (6–11 Gyr) than the stars in our own halo (Brown et al., 2003).

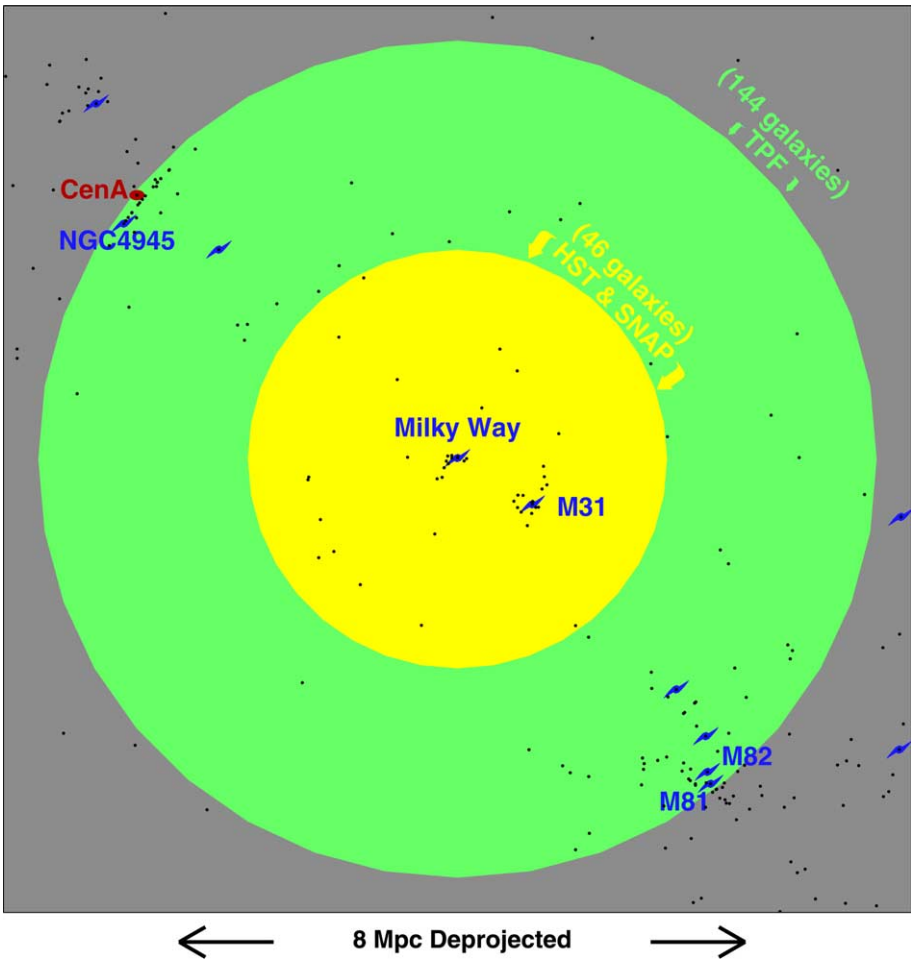

Fig. 2. A deprojected view of the galaxies in the local Universe (black points), assuming recent estimates of their distance and distribution (Karachentsev et al., 2004), showing the volume that can be surveyed down to an old (12 Gyr) MS turnoff with telescopes from various missions. Giant galaxies are marked by spiral and elliptical symbols. HST and SNAP can survey the Local Group, while TPF can reach nearly 4 Mpc, assuming 200 hours of observations per field in the F606W and F814W bands.

3. The future: wide field imaging from space

There are two near-term avenues for major advances in the study of star formation histories utilizing upcoming optical space missions (Fig. 2): the Supernova Acceleration Probe (SNAP) and the Terrestrial Planet Finder (TPF). The James Webb Space Telescope will also make progress, but its infrared bands do not provide as good a temperature lever for MS stars.

As an optical telescope with the sensitivity and sampling of HST, but with a much larger field of view, SNAP could map the star formation history in the outer disk and halo of large galaxies like M31 and M33. The observing program might consist of two stages: an exploratory stage, where shallow tiles across the galaxy provide secondary age diagnostics on the red giant branch and horizontal branch, and a deep followup stage, providing direct age diagnostics via MS photometry, sampling at a ≈20% fill factor. Current plans envision 0.1″ pixels; 0.05″ is better suited to surveys of the M31 outer disk, while larger pixels would be restrict this work to the halo outskirts. Its focal plane design (with many fixed filters) does not provide an efficient way to obtain two-band photom-

etry over large fields, but the additional bands would provide tighter population constraints.

The optical coronograph version of the TPF, with its 4×6 m aperture, will provide high-contrast, high-resolution imaging over tiny fields of view as its prime mission. However, a secondary instrument with a wide field of view could obtain MS photometry in galaxies nearly 4 Mpc away. Currently, we are limited to the study of the two giant galaxies in the Local Group (our own and Andromeda) plus a handful of smaller galaxies, but the volume of space that could be surveyed with TPF would include the Cen-A Group and the M81-M82 Group (Fig. 2), greatly expanding the sample of galaxies.

References

Brown, T.M., Ferguson, H.C., Smith, E., Kimble, R.A., Sweigart, A.V., Renzini, A., Rich, R.M., VandenBerg, D.A., 2003. Evidence for a significant intermediate-age population in the M31 halo from main sequence photometry. ApJ 592, L17–L20.

Brown, T.M., Ferguson, H.C., Smith, E., Kimble, R.A., Sweigart, A.V., Renzini, A., Rich, R.M., 2004. RR Lyrae stars in the Andromeda Halo from deep imaging with the Advanced Camera for Surveys. AJ 127, 2738–2752.

Dohm-Palmer, R.C., Skillman, E.D., Mateo, M., Saha, A., Dolphin, A., Tolstoy, E., Gallagher, J.S., Cole, A.A., 2002. Deep Hubble Space Telescope imaging of Sextans A. I. The spatially resolved recent star formation history. AJ 123, 813–831.

Ferguson, A.M.N., Irwin, M.J., Ibata, R.A., Lewis, G.F., Tanvir, N.R., 2002. Stellar substructure in the halo and outer disk of M31. AJ 124, 1452–1463.

Karachentsev, I.D., Karachentseva, V.E., Huchtmeier, W.K., Makarov, D.I., 2004. A catalog of neighboring galaxies. AJ 127, 2031–2068.

Sandage, A., 1953. The color–magnitude diagram for the globular cluster M 3. AJ 58, 62–75.

VandenBerg, D.A., 1988. Ages of Galactic globular clusters. In: Grindlay, J.E., Philip, A.G.D. (Eds.), Proceedings of the 126th Symposium of the IAU. Reidel, Dordrecht, pp. 107–120.

Available online at www.sciencedirect.com
SCIENCE DIRECT®
New Astronomy Reviews 49 (2005) 478–485
New Astronomy Reviews
www.elsevier.com/locate/newastrev

The Kepler Mission: A wide-field transit search for terrestrial planets ☆

Gibor Basri [a,*], William J. Borucki [b], David Koch [b]

[a] *University of California, Berkeley, CA, United States*
[b] *NASA Ames Research Center, Moffett Field, CA 94035, United States*

Available online 19 October 2005

Abstract

The Kepler Mission is a NASA Discovery mission which will continuously monitor the brightness of at least 100,000 main sequence stars, to detect the transits of terrestrial and larger planets. It is scheduled to be launched in 2007 into an Earth-trailing heliocentric orbit. It is a wide-field photometer with a Schmidt-type telescope and array of 42 CCDs covering the 100 square degree field-of-view. It has a 1-m aperture which enables a differential photometric precision of 2 parts in 100,000 for 12th magnitude solar-like stars over a 6.5-hour transit duration. It will continuously observe dwarf stars from 8th to 15th magnitude in the Cygnus constellation, for a period of four years, with a cadence of 4 measurements per hour. Hundreds of terrestrial planets should be detected if they are common around solar-type stars. Ground-based spectrometry of stars with planetary candidates will help eliminate false-positives, and determine stellar characteristics such as mass and metallicity. A null result would imply that terrestrial planets are rare.
© 2005 Published by Elsevier B.V.

Contents

1. Introduction . . . 479
2. The Kepler Mission . . . 479
   2.1. Photometer and spacecraft . . . 480
   2.2. Signal analysis . . . 480
   2.3. Selection of target stars and field-of-view . . . 481
3. Results from the mission . . . 481

☆ This project supported by NASA.
* Corresponding author.
E-mail address: basri@astro.berkeley.edu (G. Basri).

1387-6473/$ - see front matter © 2005 Published by Elsevier B.V.
doi:10.1016/j.newar.2005.08.026

3.1. Validation of planet detections . . . 483
3.2. Data release policy . . . 484
3.3. Guest observer program . . . 485
References . . . 485

1. Introduction

The Kepler mission is designed to discover hundreds of terrestrial planets in and near the habitable zone (HZ) around a wide variety of stars. Kepler was selected as NASA Discovery Mission #10 in December 2001. The PI is William Borucki, and Deputy PI is David Koch. Information on the rest of the team, and the mission, can be found at www.kepler.arc.nasa.gov. Rocky planets at orbital distances which allow liquid surface water are much more likely to harbor life than the gas giant planets that are now being discovered with the Doppler-velocity technique. Technology based on transit photometry can find smaller, Earth-like planets that are a factor of several hundred times less massive than Jupiter-like planets (Borucki and Summers, 1984).

Transits are a useful means of planetary detections because current technology allows detection of planets that are too small to be currently detectable by the Doppler method, astrometry, or ground-based interferometry. The method relies on the amount of stellar light that is blocked if a planet crosses the star as seen from here. The fractional blockage is just the ratio of the planet's area to the stellar area. A terrestrial planet causes a dip of only 10^{-4} in the star's light. Of course, the likelihood we will lie sufficiently close to the planetary orbital plane drops as the separation of the planet from its star increases. For true-Earth analogs, only about 0.5% of planets will be so aligned. This fraction rises to about 10% for planets with orbital periods of only a few days (like the already known "hot jupiters"). Because of this inefficiency, transit surveys must include large numbers of stars. The other problem is that the transit method only produces a signal during the actual transit (which typically lasts a few hours). There is thus a duty-cycle problem which also gets worse as the planetary separation gets larger.

For all the reasons above, a space-based transit survey is far superior. The photometric precision achievable without atmospheric interference and using space-based CCD differential photometry is up to the task. The telescope must be of sufficient aperture to collect adequate photon statistics on the faintest targets. It must also have a wide enough field-of-view (FOV) to obtain a statistically valid number of transits even with the inherent inefficiencies. Finally, a space-based photometer can have a duty cycle of nearly 100%, removing another of the main problems with ground-based surveys.

2. The Kepler Mission

The general scientific goal of the Kepler Mission is to explore the structure and diversity of planetary systems, with special emphasis on determining the frequency of Earth-size planets in the HZ of solar-like stars. This is achieved by surveying a large sample of stars to:

(1) Determine the frequency of Mars-sized and larger planets in or near the habitable zone of a wide variety of stellar spectral types.
(2) Determine the distributions of sizes and orbital semi-major axes of these planets.
(3) Estimate the frequency of planets orbiting multiple-star systems.
(4) Determine the distributions of semi-major axis, albedo, size, mass, and density of short period giant planets.

(5) Identify additional members of each photometrically discovered planetary system using complementary techniques.
(6) Determine the properties of those stars that harbor planetary systems.

2.1. Photometer and spacecraft

The photometer is based on a modified Schmidt telescope design that includes field flatteners near the focal plane. The corrector has a clear aperture of 0.95 m with a 1.4 m diameter F/1 primary. The optics are being built by Brashear. This aperture is sufficient to reduce the Poisson noise to the level required to obtain a 4σ detection for a single transit from an Earth-size planet transiting a 12th magnitude G2 dwarf. The brightness range of target stars is from R magnitudes 8–15 (fainter stars can be studied for closer-in planets). Only a single FOV is monitored during the entire mission, to avoid missing transits. The spacecraft is placed in an Earth-trailing heliocentric orbit by a Delta II 2925-10L launch vehicle. This orbit provides a benign thermal environment to maintain photometric precision. It also allows continuous viewing of the FOV for the entire mission without the Sun, Earth or Moon obtruding.

The focal plane is composed of forty-two 1024×2200 backside-illuminated E2V CCDs with 27 μm pixels. The detector focal plane is at prime focus and is cooled by heat pipes that carry the heat out to a radiator in the shadow of the spacecraft. The low-level electronics are placed immediately behind the focal plane. A four-vane spider supports the focal plane and its electronics and contains the power- and signal-cables and the heat pipes.

The spacecraft bus encloses the base of the photometer supports the solar panels for power and the communication, navigation, and power equipment. Several antennas with different frequency coverage and gain patterns are available for command uplink and data downlink. A steerable high-gain antenna operating at Ka band is used for high-speed data transfer to the Deep Space Network (DSN). It is the only movable part other than the ejectable cover and gyroscopes. Approximately 1 GByte/day of data are recorded and then transferred to the ground every few days when contact is made with the DSN. The spacecraft provides very stable pointing using four fine guidance sensors mounted in the photometer focal plane. Small thrusters are used to desaturate the momentum wheels. Sufficient expendables are carried to extend the mission to six years. Both the instrument and the spacecraft are being built by the Ball Aerospace and Technology Corporation (BATC) in Boulder, Colorado.

2.2. Signal analysis

To achieve the required photometric precision to find terrestrial-size planets, the photometer and the data analysis system must be designed to detect the very small changes in stellar flux that accompany the transits. The variability of the star, on time scales very different than that of the transits, is not a problem. Sharp images of the star field are not helpful because the PSF must be over-sampled and because a broad image profile reduces the sensitivity to image motion. The FWHM of point sources in Kepler images will be about 6″ (95% of the energy in a 3 pixel diameter). This provides the best estimates of image centroids that are used to reduce the systematic error due to image drift. The Kepler Mission approach is "differential relative photometry". In this approach;

(1) Target stars are always measured relative to the ensemble of similar stars on the same part of the same CCD and read out by the same amplifier.
(2) Only the time change of the ratio of the target star to the ensemble is of interest. Only decreases from a trend line based on a few times the transit duration are relevant (long-term stability of the trend is not required).
(3) Target star and ensemble stars are read out every three seconds to avoid drift and saturation
(4) Correction for systematic errors is critical (Jenkins, 2002).

Photometry is not done on the spacecraft. Instead, all of the pixels (6×6) associated with each

star image are telemetered to the ground for analysis. This choice allows many different approaches to be used to reduce systematic errors. Only data from pixels illuminated by pre-selected target stars are saved for transmission to Earth. Data for each pixel are co-added onboard to produce one brightness measurement per pixel per 15-min integration. Data for target stars that are monitored for p-mode analysis or transit shapes are recorded at a cadence of once per minute. Some background areas will also be continuously monitored.

At least three transits are required to show that the orbital period repeats to a precision of at least 10 ppm and at least a 7σ overall detection is required to validate any discovery. The threshold of 7σ is required to avoid false positives due to random noise. Planetary signatures exhibiting mean detection statistics of 7σ will be recognized 50% of the time. The recognition rate for planets exhibiting 8σ detection statistics increases to 84%. The mission lifetime of four years allows four transits to be observed so that 8σ detections can be obtained on true-Earth analogs.

Classical signal detection algorithms that whiten the stellar noise, fold the data to superimpose multiple transits, and apply matched filters are employed to search for the transit patterns down to the statistical noise limit (Jenkins, 2002). From measurements of the period, change in brightness and known stellar-type, the planetary size, the semi-major axis and the characteristic temperature of the planet can be determined.

2.3. Selection of target stars and field-of-view

Approximately 100,000 target stars must be monitored to get a statistically meaningful estimate of the frequency of terrestrial planets in the HZ of solar-like stars. A FOV centered on a galactic longitude of 70° and latitude of 6–12° satisfies both the constraint of a 55° sun-avoidance angle and provides a very rich star field. This FOV falls within the Cygnus constellation and results in looking a few hundred parsecs along the Orion spiral arm. (Fig. 1). The stellar population sampled is indistinguishable from the immediate solar neighborhood. In the 105 square degrees, there are half a million stars brighter than $R = 15$th magnitude. Studies are underway to classify all these stars (and fainter ones) and to choose the most appropriate 100,000 main-sequence stars as targets. The current approach is to use wide FOV ground-based telescopes with a color-filter system to identify both the luminosity class and spectral types and thereby enable the elimination of most giants and early spectral types from the target list. Such stars are too large to allow detection of terrestrial planets.

3. Results from the mission

After the mission ends, the results will be summarized as planetary frequencies for different sizes and separations of planets against different masses of stars. Because both the size and mass of the stars that are found to have planets will be determined by follow-up observations, the size of the planets and their orbital semi-major axes can be determined. If most stars have planets approximately the size of the Earth ($0.9 < R < 1.2$,) for example, then we should find approximately 25 planets at distances near 1 AU ($0.8 < a < 1.2$ AU). If stars often have planets 30% larger, then because such planets are more readily detected, and roughly 200 planets could be found for a semi-major axis near 1 AU. Planets twice the radius of the Earth (i.e., approximately 10 times the mass of the Earth) are readily detected even for large or dim stars so about 600 planets would be detected near 1 AU. Such planets are the potential cores required to start runaway gas accretion to make giant planets, so the number of giant planets already known suggests they should exist.

As the semi-major axis decreases, the expected number of discoveries rises very rapidly, for two reasons. The probability of a detection increases as the inverse of the orbital radius, and secondly the number of transits that occur during the mission lifetime increases. The detectability of transit patterns rapidly increase with the signal-to-noise ratio (SNR) and the SNR increases with the square root of the number of transits. At the value of the semi-major axis found for the "hot Jupiters" detected by the Doppler velocity technique, i.e.,

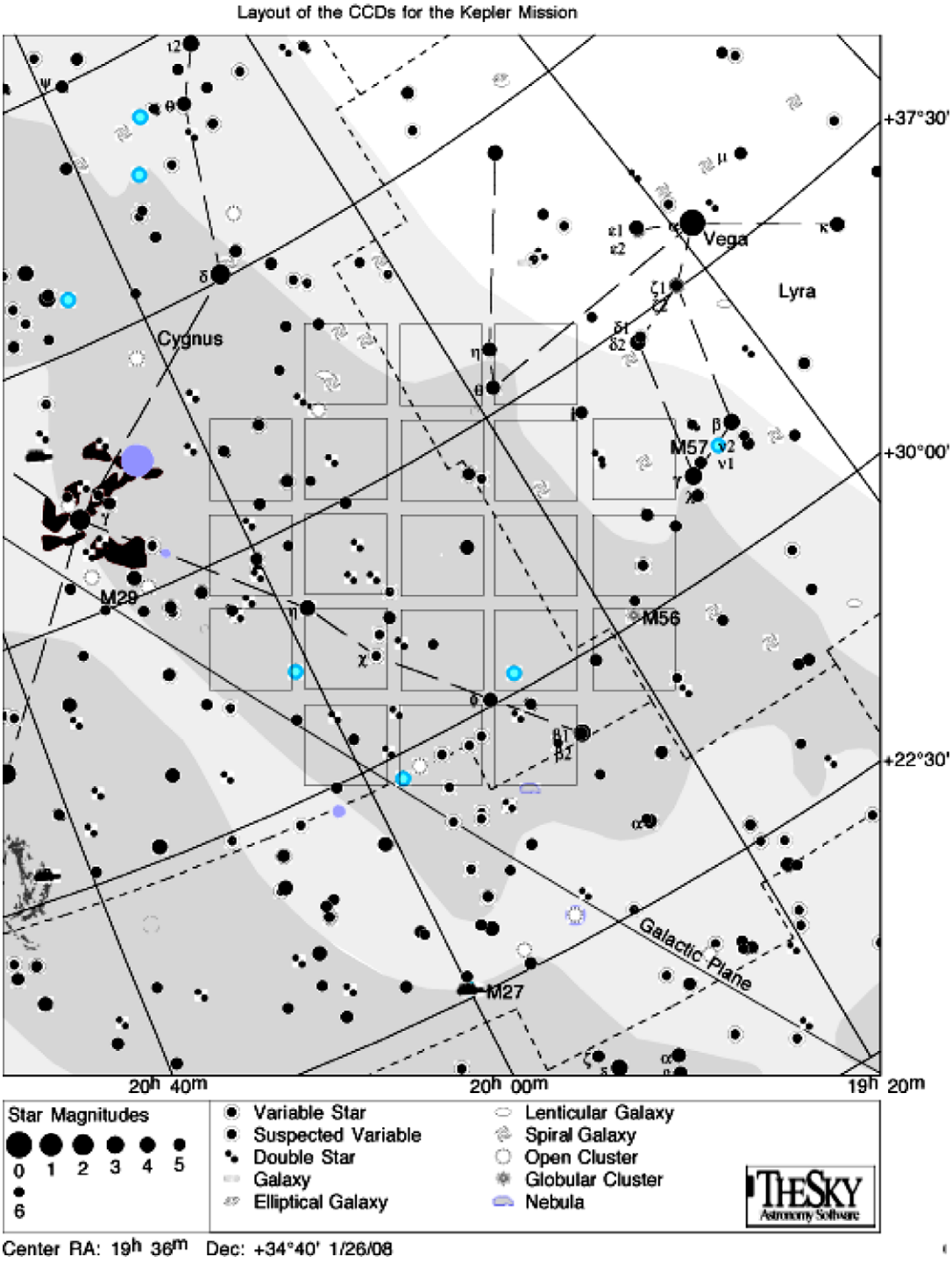

Fig. 1. The current Kepler FOV in the Cygnus constellation, looking along the Orion spiral arm. The field may be moved slightly further off the plane.

~ 0.05 AU, tens of thousands of planets could be found if they are common orbiting solar-like stars. Even if the planets are as small as Mars or Mercury, the number of transits that occur in such tight orbits during a four year mission will be so large (~ 400) that small planets should be found in profusion. For this reason, it will be closer-in planets that allow Kepler to provide a robust estimate of the number of terrestrial planets in the galaxy.

After two years of operation, the Kepler Mission should provide a good estimate of the frequency of terrestrial planets with orbital periods as long as six months (which covers the HZ for low-mass stars). Once the mission length reaches four years, a good estimate of that frequency will be obtained for planets in the HZ of solar-like stars. An extension to 6 years for the mission raises the number of expected detections by a factor of two at 1 AU and a factor of 3.5 at 2 AU. Of course, there is no reason to expect that all solar-like stars have planets, and therefore the actual detections are likely to fall well below the estimates above. Nonetheless, it is apparent that Kepler has the statistical sample to make null results meaningful. Knowledge of the frequency of Earth-sized planets is very helpful in providing an estimate of the number of stars that must be observed by the Darwin/TPF missions if they are to fulfill their goal of determining the atmospheric composition of such planets.

"Hot Jupiters" with orbits of less than seven days are also detectable by the periodic phase modulation of their reflected light, without requiring a transit (Borucki et al., 1997). Up to several hundred might be found that way. For the short-period giant planets that do transit, the planetary albedo can be calculated. Information on the scattering properties and phase-function of the planet's atmosphere can also be derived (Marley et al., 1999; Seager et al., 2000; Sudarsky et al., 2000).

3.1. Validation of planet detections

Stellar variability sets the limit to the minimum size of planet that can be detected. It reduces the signal detectability in two important ways;

(1) The variability introduces noise into the detection passband and thereby reduces the signal to noise ratio (SNR) and thus the statistical significance of transits.
(2) Because the flux of every target star is ratioed to the fluxes of many surrounding stars to reject common-mode instrument noise, variability of the stars used in the normalization introduces noise into the target star signal.

The second concern can be alleviated by measuring the variability of each star relative to an ensemble of others and then iteratively removing the noisiest from the list of comparison standards. To mitigate the effects of the first concern, stars must be chosen that have low variability.

Stellar variability in late-type main sequence stars is usually associated with the interplay of the convective layer and the internal magnetic field. Because the depth of the convective layer is a function of the spectral class of the star and because the activity level is higher when the star is rotating rapidly, the variability of solar-like main sequence stars is related to both their spectral class and rotation rate. Further, because the rotation rate decreases with age, the age of a star is an important variable. The age and rotation rate of the Sun are approximately 5 Gyr and 27 days, respectively. The age of the galaxy is about 12 Gyr and about 2/3 of the stars are older than the Sun and are expected to be at least as quiet as the Sun. That extrapolation is verified by observations with ground-based telescopes of the emission intensity of the calcium H and K lines. Finally, because the signal analysis uses strict variability as a strong filter, stellar phenomena will be enormously suppressed (Jenkins, 2002).

Before a candidate detection can be considered validated and the information released to the public, a rigorous process must be executed to ensure that it is not due to some other phenomenon (Jenkins et al., 2002). Public release of false-positives would reduce the credibility of mission results. Therefore to be considered a reliable detection the candidate planet detection must meet several requirements.

(1) The total SNR of the superimposed transits must exceed 7σ. This requirement prevents false positives produced by statistical noise when 8×1011 statistical tests are carried out on 105 stars for orbital periods from 1 to 700 days.
(2) At least three transits must be observed that demonstrate a period constant to 10 ppm. This test is independent of the previous test and demonstrates the presence of a highly periodic process. It essentially rules out mistaking stellar phenomenon for transits.
(3) The duration, depth, and shape of the light curve must be consistent. The duration must be consistent with Kepler's laws based on the orbital period. The depth must be consistent over all transits. A weaker requirement is that the shape must be consistent with the "U" shape of a planetary transit rather than the "V" shape of a grazing eclipse of a binary star. Clearly, low-amplitude transits are likely to be too noisy to make this distinction.
(4) The position of the centroid of the target star determined outside of the transits must be the same as that of the differential transit signal. If there is a significant change in position, the cause of the signal is likely to be an eclipsing star in the background.
(5) Radial velocity measurements must be conducted to demonstrate that the target star is not a stellar-mass eclipsing binary.
(6) High precision radial velocity measurements must be made to measure the mass of the companion (eliminate brown dwarfs) or provide an upper limit that is consistent with that of a small planet. These can also help eliminate diluted stellar systems (background or triple systems).
(7) High spatial resolution measurements must be made of the area immediately surrounding the target star to demonstrate that there is no background star in the aperture capable of producing a false-positive signal.

Ground-based Doppler spectroscopy and/or space-based astrometry with SIM can be used to detect additional massive companions in the systems, to better define the structure of each planetary system. The density of any giant planet detected by both photometry and either of the other methods can be calculated. Determination of the planet size, mass, semi-major axis, and stellar properties provides the properties needed for the validation and development of theoretical models of planetary structure.

White dwarf stars are about the size of the Earth and might be expected to produce a transit signal of similar magnitude. However, because of the gravitational lensing caused by their large-but-compact mass, the transits actually result in an increase in brightness (Sahu and Gilliland, 2003) and are thereby readily distinguished from those of a planet (it is also easy to eliminate them with Doppler spectroscopy). Jovian planets produce a transit signal of such high S/N and unique characteristics that even a single transit is unmistakable. It is possible that a few "true Jupiters" in large orbits could be found that way.

3.2. Data release policy

To avoid publication of false-positives, the series of ground-based observations described above must be made and analyzed to validate the discovery before any announcements are made. It is expected that several months will be required to obtain telescope time on suitable ground-based telescopes and make the observations with the usual time lost due to bad weather and to the limited seasonal observability of the FOV. Hence the data will not be released until several months have passed from the time that at least three transits with a combined SNR $<7\sigma$ have been detected. A partial analysis of the false-positive problem has been published (Brown, 2003).

For planets with short orbital periods, three or more transits will be seen within the first weeks and months of operation. Release of these data are expected by the end of the first year of operation. A downselect of targets due to unacceptable variability and reduced data transmission rates will result in tens of thousands of light curves being released to the community early in the mission as well. When data are released, both original

calibrated data for each target and the light curves generated by ensemble photometry will be provided so that all interested members of the scientific community can independently assess the reliability of the results.

3.3. Guest observer program

In addition to the primary observations described above, around 3000 target slots will be reserved for the general astrophysical community, to pursue science not covered by the Kepler mission. The photometric precision will allow observation of unprecedented detail of variable phenomena, and the lengthy uninterrupted coverage that is possible opens an equally spectacular new territory of parameter space. A list of reserved Kepler targets and a tool to determine whether other targets are on Kepler CCDs will accompany the first AO a few months before launch. It is anticipated that GO programs will last at least 3 months, but a few could last the entire mission. Some fast cadence (1 per minute) targets will also be supported.

References

Borucki, W.J., Summers, A.L., 1984. The photometric method of detecting other planetary systems. Icarus 58, 121–134.

Borucki, W.J., Koch, D.G., Dunham, E.W., Jenkins, J.M. 1997. The Kepler Mission: A mission to determine the frequency of inner planets near the habitable zone for a wide range of stars. In: Planets Beyond the Solar System and the Next Generation of Space Missions, ASP Conference Series, vol. 119, pp. 153–173.

Brown, T., 2003. Expected detection and false alarm rates for transiting jovian planets. ApJ 593, L125–L128.

Jenkins, J.M., 2002. The impact of stellar variability on the detectability of transiting terrestrial planets. ApJ 575, 493–501.

Jenkins, J.M., Caldwell, D.A., Borucki, W.J., 2002. Some tests to establish confidence in planets discovered by transit photometry. ApJ 564, 495–507.

Marley, M.S., Gelino, C., Stephens, D., Lunine, J.I., Freedman, R., 1999. Reflected spectra and albedos of extrasolar giant planets. I. Clear and cloudy atmospheres. ApJ 513, 879–893.

Sahu, K.C., Gilliland, R.L., 2003. Near-field microlensing and its effects on stellar transit observations by Kepler. ApJ 584, 1042–1052.

Seager, S., Whitney, B.A., Sasselov, D.D., 2000. Photometric light curves and polarization of close-in extrasolar giant planets. ApJ 540, 504–520.

Sudarsky, D., Burrows, A., Pinto, P., 2000. Albedo and reflection spectra of extrasolar giant planets. ApJ 538, 885–903.